Design and Modelling of Electronic Processing Circuits for Optical Code Division Multiple Access Communication Networks

A Thesis submitted for the degree of

Doctor of Philosophy (Ph.D)

Miguel Novais Pimenta

Communications and Information Systems Research Group
Department of Electrical and Electronic Engineering
University College London

September 2009

Statement of Originality

I, Miguel Pimenta, confirm that the work presented in this thesis is my own. Where information has been derived from other sources, I confirm that this has been indicated in the thesis.

Acknowledgments

I would like to sincerely thank Professor Izzat Darwazeh, my supervisor, for his valuable direction and support during this research. I would like to thank Izzat for being an excellent supervisor and a friend.

Much of the experimental work reported here was done at the University of Aveiro. I would like to express my gratitude to Professor Paulo Monteiro and Dr Miguel Madureira for sharing their expertise in distributed transversal filters and helping with the experimental setup; also, Professor Rogerio Nogueira and Carlos Marques for the fabrication of the Fibre Bragg Gratings and for useful comments about the experimental setup. I would like to thank Rui Morais and Pedro Teixeira for useful discussions about the implementation of Genetic Algorithms.

I have spent three months at CERN in Geneva during the spring of 2007. During my stay I was fortunate to work with Dr Paulo Moreira and learn the intricate details of CMOS IC design. Although the work done at CERN is not reported in this thesis, it may serve as the seed of interesting future work in this area. I would like to thank my colleagues at CERN's Microelectronics Research Group for making my stay in Geneva an enjoyable experience.

I am grateful to the Portuguese Foundation for Science and Technology FCT for awarding me a doctoral scholarship. I am also grateful to Professor Henrique Salgado, my undergraduate thesis supervisor, for introducing me to the area of optical communications and to Izzat's group at UCL.

Of course, I am grateful to my parents for their patience, support and *love*. I would also like to dedicate this work to the memory of Jorge and to Isabel.

Last but not least, I wish to thank the following: my friends for their constant support and encouragement; my colleagues in room 804 for making my life during my research enjoyable; Dr Richard Clegg for his valuable comments on the final draft of this thesis; Shila, for making me smile; finally, my sister Joana (because she asked me to).

Abstract

Code Division Multiple Access (CDMA) has been proposed for optical fibre networks to achieve high-speed connectivity, asynchronous operation and network control simplifications. Traditionally, all-optical devices have been proposed to encode, decode and process CDMA signals because the bandwidth in the optical medium is higher than electronic processing techniques. Today's advances in integrated circuit technologies coupled with bandwidth efficient circuit topologies, may provide robust alternatives for CDMA over fibre applications.

This thesis covers two areas of work. First, a new circuit for encoding and decoding incoherent CDMA signals in the electrical domain is proposed. This structure makes use of the high bandwidth of distributed amplifier-like topologies to achieve very wideband operation. As proof of concept, a distributed transversal filter was designed with a commercial available GaAs MMIC process; modelling results show feasibility of CDMA encoding/decoding at 40 GChip/s employing transistors with cut-off frequencies of 60 GHz. Limitations and potential practical applications of these design ideas are discussed.

The second part of the thesis focuses on the impact of the time skewing due to optical-fibre Group Velocity Difference in Wavelength-Hopping Time-Spreading (WHTS) Optical CDMA and the compensation of this impairment through electronic techniques. A new network model was created to assess the impact of such impairment in these systems. Conclusions about the time skewing impact on the auto and cross-correlation properties of the system are extracted. This model was employed to assess the use of an electronic distributed transversal filters as time skewing compensator in Optical CDMA networks.

Finally, an experimental setup of a WHTS Optical CDMA network was built to analyze the effect of time skewing and to assess the practical feasibility of its compensation with a distributed transversal filter. The Fiber Bragg Grating based system comprises 2.5 GBit/s transmission (20 GChip/s) with five wavelengths. Conclusions about the practical limitations are derived and presented.

Contents

List of Figures

List of Tables

List of Abbreviations

2D	Two Dimensional Codes
AC	Alternate Current
ADS	Advanced Design System
AlGaAs	Aluminium Gallium Arsenide
APH	Asymmetric Prime Hop
ASE	Amplified Spontaneous Emission
ATL	Artificial Transmission Line
BER	Bit Error Rate
BiCMOS	Bipolar Complementary Metal Oxide Semiconductor
CATV	Community Access Television
CCD-MF	Charge Coupled Device Matched Filter
CD	Chromatic Dispersion
CDMA	Code Division Multiple Access
CHPC	Carrier Hoping Prime Code
CMOS	Complementary Metal Oxide Semiconductor
CTD	Charge Transfer Device
DARPA	Defense Advanced Research Projects Agency
DC	Direct Current
DCF	Dispersion Compensating Fibre
DGD	Differential Group Delay
DMD	Differential Mode Delay
DSF	Dispersion Shifted Fibre
DTF	Distributed Transversal Filter
EDFA	Erbium Doped Fibre Amplifier
EM	Electro-Magnetic
EQC	Extended Quadratic Congruence
FBG	Fibre Bragg Grating
FEC	Forward Error Correction
FET	Field Effect Transistor
GA	Genetic Algorithms
GaAs	Gallium Arsenide

GVDiff	Group Velocity Difference
GVD	Group Velocity Dispersion
HEMT	High Electron Mobility Transistor
IC	Integrated Circuit
IM-DD	Intensity Modulation Direct Detection
InGaAs	Indium Gallium Arsenide
ISI	Inter Symbolic Interference
ITU	International Telecommunication Union
LAN	Local Area Network
LED	Light Emitting Device
LSI	Large Scale Integration
LTCC	Low Temperature Co-fired Ceramic
MAI	Multi-Access Interference
MEMS	Microelectromechanical Systems
MESFET	Metal-Semiconductor Field Effect Transistor
MIM	Metal Isolator Metal
MMF	Multi Mode Fibre
MMIC	Monolithic Microwave Integrated Circuit
MPC	Multi Pulses per Column
MPH	Modified Prime Hop
MPR	Multi Pulses per Row
NRZ	Non Return to Zero
OCDMA	Optical Code Division Multiple Access
OLT	Optical Line Terminator
ONA	Optical Network Analiser
ONU	Optical Network Unit
OOC	Optical Orthogonal Code
OOK	On Off Keying
OSNR	Optical Signal to Noise Ratio
PDF	Probability Density Function
PH	Prime-Hop
pHEMT	Pseudomorphic High Electron Mobility Transistor
PMD	Polarization Mode Dispersion
PON	Passive Optical Network

PSK	Phase Shifted Keying
RF	Radio Frequency
RS	Reed-Solomon
SAE	Spontaneous Amplified Emission
SCMA	Subcarrier Multiple Access
SI-FBG	Super Imposed Fibre Bragg Grating
SiGe	Silicon Germanium
SMF	Single Mode Fibre
TDM	Time Division Multiplexing
TDMA	Time Division Multiple Access
TF	Transversal Filter
TFF	Thin Film Filter
TL	Transmission Line
TOAD	Terahertz Optical Asymmetric Demultiplexer
WDM	Wavelength Division Multiplexing
WDMA	Wavelength Division Multiple Access
WHTS	Wavelength Hoping Time Spreading

Chapter 1

Introduction

Telecommunication networks play an exceedingly important role in a world where global communication has become an essential element of everyday life. Great technological demands on today's communications network are continuously created to respond to emerging applications such as data browsing and massive file transfer; multimedia communication, gaming and on-demand video; tele-working and tele-collaboration. It is clear that today's data rate delivery abilities are not going to be sufficient for future networks.

Optical systems have recently witnessed great advances and seem to be the solution to achieve such a tremendous throughput. Optical fibre has been the dominant transport technology for long-haul point to point communications for more than a decade and its importance is expected to rise. The maturity of the components and technologies achieved in long-haul has shifted the focus of optical networking research to short-haul metropolitan areas, local area and the access loop.

Amongst the techniques proposed to achieve multiple user access in short-haul networks, Code Division Multiple Access (CDMA) has received significant

enthusiasm. Code Division Multiple Access was first proposed in the context of Wireless Communications to achieve high-speed connectivity, asynchronous operation, increased security and immunity to multi-path fading [11]. In the 1980s, researchers started studying effective methods to transmit CDMA signals over optical fibres [5]. The vast majority of research work takes advantage of the enormous bandwidth of the optical medium by proposing all-optical encoders and decoders. Since the first proposal of Optical CDMA, over three decades ago [12], key research in this field has focused on finding reliable solutions to generate and detect CDMA signals, as well as finding methods to improve the performance of networks limited by physical parameters of the components and the transmission medium.

A possible alternative or complementary solution to all-optical CDMA implementations might come from electronics. The combination of ultra-fast analogue circuit design techniques such as the use of distributed topologies and modern integrated circuit processes with ever increasing speeds of operation, may provide the means to build circuits operating across higher frequency ranges. The bandwidth provided by such circuits might be enough to encode and decode CDMA signals at speeds that are attractive for optical fibre implementations. Moreover, electronic post-detection processing is a potential solution to ameliorate a specific problem associated with multi-wavelength Optical CDMA: the Group Velocity Dispersion (GVD) induced time skewing. This solution has traditionally been ignored as electrical signal processing is believed to be unable to cope with the ever increasing speed of Optical CDMA proposals. Researching such electronic means is the subject of studies of this thesis.

1.1 Motivation and Aims of the Work

This research explores electronic circuit techniques for applications in optical networks based on Code Division Multiple Access, namely encoding/decoding high-speed CDMA signals for transmission over fibre and the compensation of specific impairments existing in all-Optical CDMA networks using electronic post-detection signal processing. Encoding and decoding CDMA signals using distributed integrated circuit topologies was proposed in University College London with several limitations identified [13] [4]. Part of this thesis research aims to expand the work in [4] by finding efficient ways to encode/decode CDMA signals using distributed circuit principles.

A further aim of this research is to study compensation of GVD-induced time skewing in multi-wavelength Optical CDMA network. This is to be done through mathematical modelling, system design and experimental verification. Specifically, the aims of this research may be summarised in the following three points:

- Design multi Gbit/s encoding and decoding structures for CDMA signals in the electrical domain, using distributed integrated circuit topologies.
- Analyse the effect of GVD-induced time skewing in multi-wavelength Optical CDMA and develop solutions for its compensation.
- Demonstrate experimentally electronic post-detection signal processing in the context of multi-wavelength Optical CDMA networks.

1.2 Organisation of the Thesis

Following this introductory chapter a common structure is used throughout this thesis. Each chapter opens with an introductory part detailing its contents, and is concluded with a summary of the main contributions of the chapter. The exception is chapter 4, where merging the final summary with a discussion of the main findings was found to be more appropriate. The organisation of this thesis is as follows.

Chapter 2 provides an overview of Optical CDMA networks. The chapter commences with a discussion of the general aspects of Optical CDMA networks highlighting its main advantages over other multi-access schemes for short-haul optical networks. The chapter focuses on incoherent Optical CDMA approaches with brief references to coherent ones. Specifically, the chapter provides a description of incoherent time-domain and multi-wavelength Optical CDMA with emphasis on enabling technologies, code design, and advantages and limitations. Some significant work published in this area is summarised.

Chapter 3 is concerned with distributed circuit topologies for microwave and millimeter-wave applications. The chapter starts with a brief explanation of the advantages of the distributed approach over conventional circuits. The distributed amplifier and the distributed transversal filter structures are then analysed. Finally, an overview of the applications of distributed transversal filters in high-speed equalisation is presented.

Chapter 4 discusses the design of distributed transversal filters for generation/detection of high rate sequences for time-domain CDMA systems. It starts with a brief introduction to electronic CDMA encoding/decoding proposals including work done in University College London. The design of a new distributed

transversal filter (DTF) structure is discussed. The novelty of this design lies in its simplicity since the number of DTF stages is equal to the number of positive chips in the Optical CDMA codeword, and the delays between cells are implemented using simple LC-sections. The chapter describes the circuit design details including gain stages, specially designed delay lines and layout. The performance of circuit is analysed through scattering parameters (S-parameters) and transient response. A proposal of a distributed transversal filter with switchable delay lines, where time delays may be defined as multiples of the chip time is also discussed in this chapter. Finally, the last section before summary and discussion, deals with encoders and decoders for multi-wavelength CDMA signals for optical fibre transmission. The structures proposed are based on distributed transversal filter principles and the integrated circuit process is the same used for the time-domain CDMA approach. Pre-layout studies are presented, including S-parameters and transient analysis.

Chapter 5 discusses the impact of GVD-induced time skewing in Wavelength-Hopping Time-Spreading Optical CDMA networks. A brief review of the literature related to this topic is provided in the first section of the chapter. Following, the development of a new semi-analytical model, used to analyse the impact of time skewing in Optical CDMA networks is described in detail. Numerical results based on this model are presented for Prime-Hop Code and Bin Code, considering constant time skewing between wavelength channels and propagation in dispersion shifted fibre. A novel time skewing compensation scheme, based on electronic post-detection signal processing using a DTF in the front-end receiver is proposed. The optimisation routine to obtain the ideal filter coefficients is also described in detail. Finally, compensation results for Prime-Hop Code and Bin

Code are presented and critically assessed.

Chapter 6 is concerned with the design of a new experiment to demonstrate GVD-induced time skewing compensation in Optical CDMA networks. A Wavelength-Hopping Time-Spreading Optical CDMA network is designed and implemented based on specially designed Fibre Bragg Grating (FBG) arrays for encoding and decoding. The chapter describes the construction of new Optical CDMA codes, the fabrication of the FBG encoders/decoders and the experimental setup. The first part of the results is concerned with the analysis of the effect of time skewing in the Optical CDMA characteristics, namely its impact in the autocorrelation and cross-correlation characteristics of the received signals. Results are shown for propagation over Single Mode Fibre (emulating constant time skewing between wavelength channels) and Dispersion Shifted Fibre. The last section of the chapter is dedicated to the experimental study of the compensation scheme.

Chapter 7 concludes the thesis, with a brief discussion of its main findings followed by an outline of areas where further research may be appropriate.

1.3 Main Contributions

The contributions of this thesis are mainly in the use of electronics in Optical CDMA networks. This may be categorised in two main areas, with the contributions in each appearing as bullet points.

Generation and detection of CDMA signals for optical fibre applications

- A new topology for encoding and decoding high-speed CDMA signals for applications in short-haul optical fibre networks is introduced. The distributed topology gives its high-bandwidth characteristics. In the proposed approach,

the number of stages is equal to the number of positive chips in the code-word which represents very significant savings in terms of the number of the active cells of the DTF (compared with previously reported transversal filter architectures for CDMA encoding). Detailed full-model and electromagnetic simulation results suggest the adequacy of the techniques for 40 GChip/s CDMA generation and detection with a Monolithic Microwave Integrated Circuit (MMIC) process with a cut-off frequency of 60 GHz.

- New designs for the electronic generation and detection of two dimensional CDMA signals are presented. Preliminary results show the adequacy of such technique for 40 GChip/s operation and are in close agreement with theoretical predictions.

Compensation of time skewing in multi-wavelength Optical CDMA

- A new semi-analytical model for assessment of the impact of time skewing in multi-wavelength Optical CDMA networks is developed. The model has the advantages of avoiding the use of the computationally inefficient and impractical pure Monte-Carlo method. Instead, a relatively low number of bits is simulated (about 100,000) after which an approximation is used to capture Bit Error Rates of 10^{-12} and below. A mathematical proof of this approximation validity, for high number of simultaneous active users, is also derived. Conclusions about the impact of the time skewing in the auto and cross-correlations of the Optical CDMA system are depicted.

- A novel scheme for GVD-induced time skewing compensation in Optical CDMA networks is proposed. This scheme is based on the use of a distributed transversal filter embedded in the front-end receiver. This is the

first time that electronic post-detection processing is considered in the context of Optical CDMA networks. A new optimisation technique based on Genetic Algorithms is proposed for the estimation of the filter coefficients. The scheme proposed is verified through detailed modelling of practical network scenarios.

- An experimental setup to study the efficacy of the post-detection compensation scheme is designed and tested. The experiment uses Fibre Bragg Grating (FBG) technology to encode/decode Optical CDMA signals and an electronic MMIC Gallium Arsenide distributed transversal filter for post-detection compensation. Experimental results demonstrate the impact of time skewing on the characteristics of the Optical CDMA network and clearly show improvements on the detectability of the autocorrelation peak in presence of Multi-Access Interference.

1.4 List of Publications

The research work reported in this thesis and the above contributions have led so far to 11 publications and presentations at national and international conferences. These are listed in chronological order, below.

1. Pimenta, M. and Darwazeh, I. (2006), Distributed Transversal Filter for Encoding and Decoding unipolar CDMA signals, in 'Proc. of the London Communications Symposium LCS'06', London, UK, pp. 65-69.

2. Pimenta, M. and Darwazeh, I. (2006), Novel Encoder and Correlator for Optical Code Division Multiple Access Networks, in 'Proc. of IEEE Lasers

and Electro-Optics Society Annual Meeting LEOS2008', Montreal, Canada, pp. 422-423.

3. Pimenta, M. and Darwazeh, I. (2007), Optical fibre CDMA for access and local area networks, Invited Contribution, in 'Proc. 6th International Conference on Information, Communications and Signal Processing ICICS'07', Singapore, pp. 1-4.

4. Pimenta, M. and Darwazeh, I. (2007), System and Circuit Design for Time-Wavelength Optical CDMA Networks, Invited Contribution, in 'Proc. 9th International Conference on Transparent Optical Networks ICTON'07', Rome, Italy, pp. 126-126.

5. Pimenta, M. and Darwazeh, I. (2008), Mitigation of Group Velocity Dispersion in optical CDMA networks using electronics, in 'Proc. of the IEEE/LEOS Summer Topical Meetings', Acapulco, Mexico, pp. 157-158.

6. Pimenta, M. and Darwazeh, I. (2008), Electronic signal processing for Optical Code Division Multiple Access Networks, in 'Proc. 6th International Symposium on Communication Systems, Networks and Digital Signal Processing CNSDSP', Invited Contribution, Graz, Austria, pp. 740-742.

7. Pimenta, M. and Darwazeh, I. (2008), Performance Modeling of Optical Code Division Multiple Access Networks Impaired by Group Velocity Dispersion, in 'Proc. IEEE Global Telecommunications Conference GLOBECOM', New Orleans, USA, pp. 1-5.

8. Pimenta, M. and Darwazeh, I. (2009), Experimental Demonstration of Electronic Compensation in Optical CDMA Networks, in 'Proc. of the IEEE/LEOS

Summer Topical Meeting', Newport, USA, paper TuA3.3.

9. Pimenta, M. and Darwazeh, I. (2009), Electronic Processing for Generation and Detection of Multi GBit/s CDMA over fibre, in 'Proc. 14th OptoElectronics and Communications Conference OECC'09', Invited Contribution, Hong Kong.

10. Pimenta, M. and Darwazeh, I. (2009), Distributed Transversal Filters for GVD Compensation in Multi-Wavelength Optical CDMA Networks, in 'Proc. of the London Communications Symposium LCS'09', London, UK.

11. Pimenta, M. and Darwazeh, I. (2009), Circuit Design Proposal for Multi-GBit/s CDMA over Fibre using Distributed Topologies, in 'Proc. of 9th International Symposium on Communications and Information Technology', Seoul, South Korea.

Chapter 2

Optical Code Division Multiple Access

Code Division Multiple Access was first proposed for Wireless Communications applications to achieve high-speed connectivity, asynchronous operation, increased security and immunity to multi-path fading [11] [14]. Developments in optical networks have led to growing interest on the adoption of this technique in the optical domain to develop new generations of access and Local Area Networks [15] [12] [5].

This chapter presents a short overview of Optical CDMA systems. It commences with an introduction to Optical CDMA where the main advantages of this technique are highlighted in comparison to its alternative optical multi-access techniques: Wavelength Division Multiple Access (WDMA), Time Division Multiple Access (TDMA) and Sub-Carrier Multiple Access (SCMA). In general, the Optical CDMA systems proposed can be classified in two main categories: incoherent and coherent. This thesis deals solely with incoherent Optical CDMA and therefore a detailed explanation of such systems is provided. Designs rely-

ing on incoherent optical techniques use data encoding in the temporal domain (direct sequence encoding), spectral domain (spectral encoding) or a mixture of both (two dimensional encoding). Codes, enabling technologies, advantages and limitations are emphasized with special attention given to temporal domain and two dimensional encoding because these techniques are used in this research.

2.1 General Aspects of Optical CDMA Networks

The success of long-haul fibre optical networks shifted the focus of optical networking research to short-haul metropolitan areas, local area and the access loop. In fact, the use of multi-access optical fiber networks, such as Local Area Networks (LANs) and Passive Optical Networks (PONs) in the access loop, plays an essential role in modern telecommunication networks. Essentially, four techniques have been established to provide shared access to the optical transmission medium. These are:

1. *Time Division Multiple Access (TDMA)*, where each user is assigned a specific transmission time slot. This technique has received the most attention for broadband access networks because it is suited for high speed data transmission and makes use of the digital processing capacity of existing circuits [16]. A TDMA system divides the transmission time in discrete time slots and each user is granted exclusive access to the medium during these periods. This effectively means that all users need to be synchronized to a common central clock reference. This is particularly difficult (and potentially costly) in PONs because complex ranging protocols to sense the distance from each user to the central node need to be employed [16].

2. *Wavelength Division Multiple Access (WDMA)* where each user is assigned a specific wavelength. This technique provides a powerful solution for multi-access because it creates a virtual point-to-point topology in physical point-to-multipoint or multipoint-to-multipoint topologies. As with TDMA, this technique benefits from the maturity of electrical multiplexing and optical transmission gained in backbone networks [17]. However, it is the most costly due to the requirements in wavelength-selective functions. Moreover, the use of WDMA in LANs requires a large amount of dynamic coordination (pre-transmission) between nodes which wastes bandwidth that could be used for data transmission. [18].

3. *Sub-Carrier Multiple Access (SCMA)* where each user is assigned with an electrical sub-carrier. This technique is not commonly deployed for all-fibre access and local area networks due to high requirements on the electronics in the user's equipment and the potential degrading effect of beat noise [16]. SCMA has been proposed and used in specific applications such as hybrid fibre-coax networks to carry broadcast community access television (CATV) channels [19].

4. *Optical Code Division Multiple Access (OCDMA)* where a wavelength or a set of wavelengths are asynchronously shared in time. In other words, signals from different users can overlap in time and wavelength.

Optical code division multiple access was proposed in the 1980s to combine the large bandwidth provided by the optical fiber with the advantages of the code division techniques already popular in the satellite and mobile radio communications [20] [12]. In particular, this technique was recognized to be more suited for

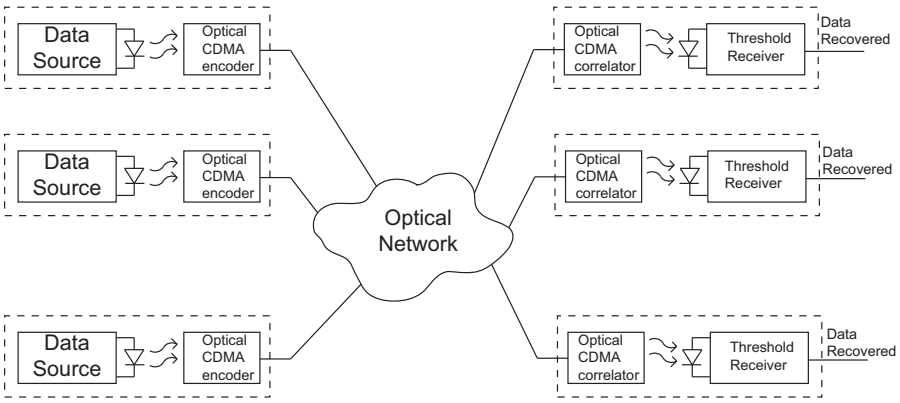

Figure 2.1: Block diagram of a typical Optical CDMA network.

the bursty traffic pattern of LANs than the traditional synchronous multiplexing schemes such as TDMA, which dedicate a portion of a channel to each user [18]. More recently, the advantages of Optical CDMA in the context of access networks have been studied [17] [15]. The number of groups and projects dedicated to Optical CDMA have increased in the recent years [1], including a multi-million dollar program by Defense Advanced Research Projects Agency (DARPA) [21]. However, to the author's knowledge, no commercial networks based on this technique exist.

The most common Optical CDMA architecture proposed in the literature is the passive star network shown in figure 2.1 [8]. Nodes in the network are simply connected through a passive NxN star coupler. Single mode star couplers as large as 32x32 are commercially available and the number of users can be further increased by adding optical combiners in each input of the coupler. Each user is assigned with a unique code in the network and the encoding function is reconfigured according to the sequence of the intended node receiver. The receiver detects the information by correlation, i.e., the decoder should be able to generate an autocorrelation peak when its unique code is received and reject

[1] See discussion and references in the first chapter of the reference [5].

any other code. The amplitude of the autocorrelation peak is extracted by a threshold device. The dominant source of noise in Optical CDMA is normally the crosstalk between users, which is named Multi-Access Interference (MAI). The performance of the system depends on the mathematical design of codewords so that the contribution of MAI can be minimized.

One of the main features of CDMA systems is the **asynchronous access** to the medium. In fact, Optical CDMA is a "tell-and-go" access strategy [22] in which the user can share the medium by transmitting information concurrently. Some synchronous Optical CDMA systems have been proposed [23] [24] [25] [26] and their role in specific applications such as networks with users transmitting information in scheduled patterns should not be neglected. In general however, the synchronization of the network increases the complexity of the system.

The **"soft capacity degradation"** is often referred as another important advantage of Optical CDMA [15] [9] [27]. This effectively means that if a new user starts transmitting information, the overall performance is degraded but no blocking occurs for this user (or any other user). In TDMA and WDMA, the respective limited number of time slots and wavelengths results in channel blocking.

Optical CDMA offers the possibility of **differentiated services** at the physical layer [15] [28] [17] [29]. In fact, the use of multi-rate Optical CDMA codes allows the definition of different traffic classes at the physical layer; transmissions with lower bitrate requirements can be allocated with longer codewords while reserving codewords with shorter lengths for prime users.

The **inherent security** associated with Optical CDMA is another important advantage of networks based on this technique [30]. The main idea is that, as users transmit data simultaneously and share the channel, it is nearly impossible

to detect comprehensive information without knowing the coding scheme. This situation contrasts with the conventional WDM system where isolating a channel and access the information can be straightforward. The implementation of Optical CDMA systems as an alternative to traditional digital encryption systems has been explored [31]. However, it should be pointed out that having a "code" associated with each user does not imply that the information is encrypted.

Optical CDMA coding can be done incoherently via optical intensity modulation or coherently via optical field modulation. Coherent approaches use short broadband pulses where optical phase is manipulated in the encoding and decoding process. On the other hand, incoherent approaches rely on power summation rather than manipulation of the optical field. Coherent approaches can be further divided in spectral phase coded [32] [33] and temporal phase coded [34] [35], depending on whether wavelength slots within one pulse are manipulated or several ultra-short pulses are spread in time to form the codeword. The incoherent systems can be implemented in one dimensional fashion, either time or wavelength, or a combination of both: 2D multi-wavelength Optical CDMA. Table 2.1 provides a short overview on some crucial aspects of the five Optical CDMA techniques proposed in the literature.

Regarding coherent coding, time spread coding comprises a long sequence of phase-shifted keyed (PSK) pulses [41] while spectral-phase coding employs phase shifts to the spectral components of a pulse. Normally, binary modulation is used, i.e., no phase shift or a 180 degrees phase shift is applied to the time/spectral slot. One of the main advantages of coherent Optical CDMA is that it allows the use of bipolar codes. As will be explained in section 2.2.1 below, truly orthogonal codes cannot be achieved with conventional time-domain incoherent optical codes

Table 2.1: Comparison of five Optical CDMA systems (adapted with modifications from [7]).

	Incoherent			Coherent	
Characteristic	Time	Wavelength	2D	Time	Wavelength
MAI	High	Medium	Medium	Low	Low
Beat Noise [a]	High	Medium	Medium	V. High	V. High
Spectral efficiency	Low	Low	Medium	Medium	Low
Data Rate	250 M	622 M	5 G	10 G	10 G
Chip Rate	6.6 G	-	115 G	200 G	-
Number of users	4	7	8	8	32
Reference	[36]	[37]	[38]	[39]	[40]

[a] In [7] Wang considers beat noise to have low impact in temporal incoherent systems and medium in 2D. However, the impact of beat noise is generally found to be higher for time domain systems [9].

which gives rise to lower spectral efficiency. Coherent optical systems can have the advantages of the common CDMA techniques in wireless environments allowing the use of truly orthogonal codes. However, coherent beat noise was found to be particularly detrimental in such optical systems [7] [42]; coherent beat noise occurs when the correctly decoded signal temporally overlaps with Multiple-Access Interference (MAI) from other users. Therefore, the vast majority of coherent Optical CDMA experimental demonstrations rely on some sort of synchronisation [7]; from complete bit synchronization [32] to time slot assignment within the bit [43]. As explained before, a major strength of Optical CDMA when compared to TDMA is the possibility to transmit information asynchronously. In the research presented in this thesis, asynchronous Optical CDMA based on incoherent systems will be considered.

2.2 Incoherent Optical CDMA Systems

Despite the fast progress of optical communication technologies over the past two decades, IM-DD (intensity modulation - direct detection) schemes used in the first generation of optical networks, still have the central role in today's networks. This is mainly due to the huge bandwidth of the optical fibres, the improvements in their loss characteristics, the introduction of the erbium-doped fibre amplifiers and the technical problems associated with the implementation of coherent fibre optic systems [44]. Therefore, a great deal of the Optical CDMA systems proposed in the literature rely on incoherent encoding, decoding and transmission of data. Incoherent Optical CDMA may be classified in three categories:

1. Direct Sequence/Temporal Encoding,
2. Spectral Amplitude Encoding,
3. Two Dimensional (2D) Multi-Wavelength Encoding.

2.2.1 Direct Sequence/Temporal Encoding

Direct sequence was the first Optical CDMA encoding scheme to be proposed in the literature. The two technical papers [12] [45] published in the late 80s, considered to be first to establish the field of Optical CDMA, both proposed incoherent temporal encoding. Conceptually, in its simplest form, encoding is achieved by dividing the bit period into N temporal chips. Each receiver is assigned with a sequence of chips that constitutes a unique code in the network. The transmitter broadcasts the sequence of the intended receiver for data bit "1" and when the bit is "0" no power is transmitted. Decoding is essentially an intensity correlation process, giving rise to a autocorrelation peak when the correct sequence

is applied and rejecting any other sequence as background interference signal. The autocorrelation peak is detected using threshold devices.

When Optical CDMA was first proposed, CDMA codes had been extensively studied in the context of satellite and mobile radio communications. However, these codes could not be applied in incoherent Optical CDMA due to the lack of "negative" signal components in the optical domain. For example, the unipolar version of Gold codes [46] were unacceptable for incoherent optical processing due to their large cross-correlation variance [12]. This motivated intensive research in suitable codes for incoherent asynchronous Optical CDMA which became one of the most important topics in the area. A family of codes specifically designed for use in these networks was proposed in 1989: the Optical Orthogonal Codes (OOC) [8] [45].

A (N,w,λ_a,λ_c) OOC is a family of (0,1) codes with length N and weight w, where the normalised autocorrelation side-lobes and the cross-correlation function are less than or equal to λ_a and λ_c, respectively (both are natural numbers). The weight of the code is effectively the number of "1s" in the codeword, and these may also be called "positive" chips. The autocorrelation constraint results from the asynchronous operation requirements since high central values and low side-lobes are required for detection of the autocorrelation peak without help of system synchronization. The Multi-Access Interference comprises the sum of the cross-correlations and, therefore, it is key to minimize λ_c. According to these definitions, the Optical Orthogonal Code (denoted as C) should have the following properties:

1. Autocorrelation constraint: For any codeword $X = [x_0,x_1,\ldots,x_{N-1}] \in C$:

$$\sum_{t=0}^{N-1} x_t x_{t\oplus\tau} \leq \lambda_a \tag{2.1}$$

for any integer $\tau \in [1, N-1]$, where $x_t \in \{0,1\}$ and $\oplus$ is the operator addition modulo N.

2. Cross-correlation constraint: For any codeword $X = [x_0,x_1,...,x_{N-1}] \in C$ and $Y = [y_0,y_1,...,y_{N-1}] \in C$, we have:

$$\sum_{t=0}^{N-1} x_t y_{t\oplus\tau} \leq \lambda_c \tag{2.2}$$

for $X \neq Y$ and any integer $\tau \in [1, N-1]$, where $x_t, y_t \in \{0,1\}$.

The maximum number of codes that satisfy the auto and cross-correlation constraints for a specific number of users is normally referred as the cardinality of the code and denoted as S. Therefore, S is the maximum number of users that a network can support. In [8], the upper-bound of S for $\lambda_a = \lambda_c = \lambda$ was derived to be:

$$S(N, w, \lambda) \leq \frac{(N-1)(N-2)...(N-\lambda)}{w(w-1)...(w-\lambda)} \tag{2.3}$$

with $w(w-1) \leq N-1$. More specifically, the cardinality of a code (N,w,1,1) can be written as:

$$S \leq \frac{N-1}{w(w-1)}. \tag{2.4}$$

Table 2.2 illustrates the increase of the code length with the number of users in the network for Optical Orthogonal Codes with unitary auto and cross-correlation. The length of the code is N and numbers in brackets represent the position of the binary ones in the codeword. For example, for a network with five users and three active chips, the minimum code length is 31 chips. It is clear from table 2.2 and equation 2.4 that one of the main problems of OOCs is the low number of codewords (and therefore users) supported. Allowing the cross-correlation constraint

Table 2.2: Optimal (N,3,1,1) codes [8].

N	Optimal (N,3,1,1) codes						
7	(0,1,3)						
13	(0,1,4)	(0,2,7)					
19	(0,1,5)	(0,2,8)	(0,3,10)				
25	(0,1,6)	(0,2,9)	(0,3,11)	(0,4,13)			
31	(0,1,7)	(0,2,11)	(0,3,15)	(0,4,14)	(0,5,13)		
37	(0,1,11)	(0,2,9)	(0,3,17)	(0,4,12)	(0,5,18)	(0,6,12)	
43	(0,1,19)	(0,2,22)	(0,3,15)	(0,4,13)	(0,5,16)	(0,6,14)	(0,7,17)

to be higher than one, the number of codewords may be increased at the expense of higher Multi-Access Interference.

Prime Code [47] allow higher number of subscribers when compared to OCC (N,w,1,1). In fact, a Prime Code with the number of active chips equal to a prime number p, has codewords with length p^2; the cross-correlation constraint is two and the number of network subscribers is p. Comparing with Gold codes (which have cardinality equal to N + 2, where N is the length of the code), the cardinality of the Prime Code is small. In addition, Prime Code have very high autocorrelation side-lobes (normalized amplitude p-1). This makes the clock recovery extremely difficult which limits the interest in such codes for asynchronous operations [48]. This motivated research for codes such as Extended Quadratic Congruence (EQC) which have autocorrelation constraint one and cross-correlation less than two (such as Prime Code). The main drawback of EQC is that the code length is almost twice as the Prime Code ($p(2p-1)$) which, for a given bandwidth, reduces the potential bitrate by a half.

A significant example of the early temporal encoding schemes is presented in [12]. This design uses optical delay lines to encode and decode the Optical CDMA signal, as shown in figure 2.2. For the encoder, the delay lines are set to

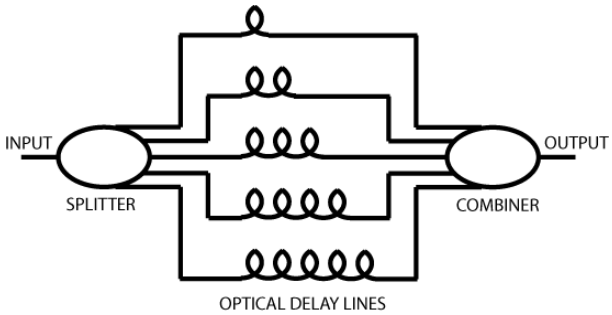

Figure 2.2: Scheme using optical delay lines for encoding and decoding time-domain incoherent Optical CDMA.

provide time delays that are a multiple of the chip time according to the codeword. The receiver is essentially the same structure, however, for the same codeword, the time delays are defined in a complementary fashion.

A major drawback of the structure shown in figure 2.2 is the heavy power loss in the optical splitters [49]. Considering that an OOC with weight w is being used, the signal is divided in w parts in the receiver, then is divided by the number of total allowable users in the star network N_{max} and then another w times in the receiver. This effectively means that the original pulse is divided by $N_{max}w^2$. Moreover, designs relying on optical delay lines suffer from lack of tunability since it is impossible to achieve very accurate variable time delays for high speeds with the existing techniques [50]. Further, time-domain Optical CDMA systems are sensitive to beat noise in the receiver [9].

Because encoding and decoding are performed in the optical domain, the electronic processing is reduced to comparison with a decision threshold, an operation that can be implemented at relatively high-speeds. However, it should be noted that the use of a passive correlation receiver requires electronic circuitry operating at chip-rate [49].

2.2.2 Spectral Amplitude Encoding

Spectral Amplitude Encoding (SAE Optical CDMA) is implemented by spectral decomposition of the frequency contents of a broadband light source followed by spacial filtering with an amplitude mask. The filtering function defines a unique code that identifies the user in the network. The incoherent nature of this technique allows the use of simple intensity direct-detection receivers and low cost low-coherence light sources. Zaccarin and Kavehrad [51] proposed a SAE Optical CDMA system based on a bulk optical system. In this proposal, the light coming from a directly modulated LED (Amplitude Shift Keying) is passed through a uniform grating that spatially disperse its spectral components. The amplitude mask is chosen according to the codeword of the user and other uniform grating is used to recombine the signal. The receiver comprises two spectral filters and photodetectors in balanced configuration. Unfortunately, this technique is prone to have small mismatches in the orientation of the mirrors, lenses and the amplitude mask which gives rise to unacceptable performance degradation. Therefore, this system is virtually impossible to implement in real networks.

A more realistic approach relies on the use of Fibre Bragg Gratings (FBGs). Both linear arrays of FBGs [52] and superimposed Fibre Bragg Gratings (SI-FBGs) [53] have been proposed as SAE Optical CDMA encoders and decoders. The former option gives rise to encoders and decoders that can be dynamically reconfigured because each FBG can be individually tuned using localized thermal devices or applied strain. However, the physical separation of the gratings gives rise to temporal delays between the reflected components that have to be compensated with other array of FBGs as shown in the figure 2.3. The SI-FBGs avoids this problem since all the gratings have the same physical location. The

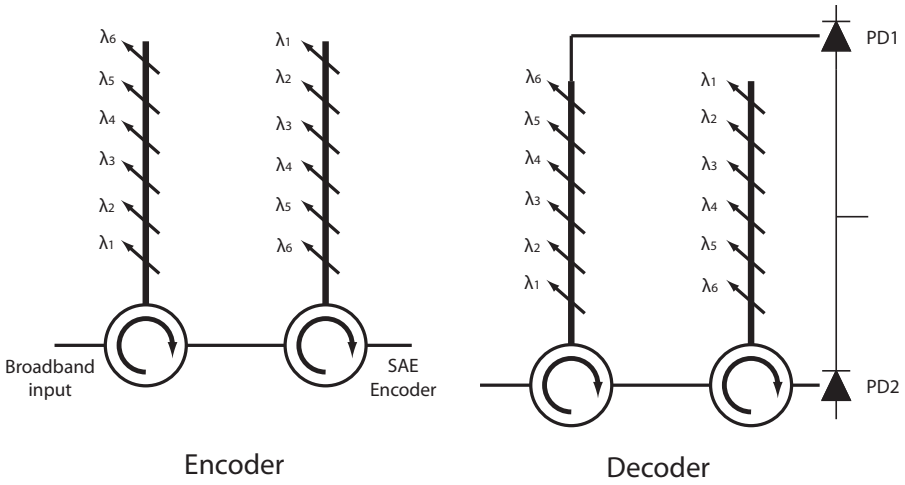

Figure 2.3: SAE Optical CDMA encoder and decoder based on linear array of FBGs.

main drawback of this solution is that thermal and strain adjustments in the grating will affect all the structure giving rise to uniform shifts to longer or shorter wavelengths. Therefore, the tunability of this device is very limited.

Despite the incoherent nature of SAE Optical CDMA, it is possible to design codes so that truly orthogonal transmission is achieved [52] [54] [55]. For example, Hadamard codes have been proposed for such purpose [55]. A Hadamard Code is obtained by selecting as codes the rows of a Hadamard matrix. It is well known that an (N x N) Hadamard matrix of 1s and 0s has the property that any row differs from any other row in exactly N/2 positions. All rows except one contains N/2 zeros and N/2 ones. The cardinality of such codes is N-1.

2.2.3 Two Dimensional (2D) Multi-Wavelength Encoding

The techniques presented in the sections 2.2.1 and 2.2.2 have the intrinsic limitation of comprising only one dimension. In the case of temporal encoding, for a large number of users, the network design demands long codewords which, for a given chiprate, reduces the bitrate. Moreover, the number of network subscribers

is severely limited by the cardinality of the codes. In the spectral amplitude encoding technique, the size of the codeword is limited by the number of spectral bins in the network.

With a two dimensional code, both time and wavelength are used to define the position of the active chips in the codeword. Since the active code chips are dispersed throughout several wavelengths and the cross-correlation is defined in the time domain, the Multi-Access Interference is reduced. Moreover, in order to achieve certain values of auto and cross-correlation, one have more flexibility in the code design with two dimensional codes than with the one dimensional spectral or temporal codes. Overall, since the code dimension is given by the product of the number of time slots and the spectral bins, the number of codes with good correlation properties is larger when compared to Direct Sequence Optical CDMA. This can be used either to increase the bitrate or to reduce the chip rate, reducing the complexity of the system.

Similarly to one dimensional codes, the efficiency of the networks based on multi-wavelength Optical CDMA greatly depends on the codes employed. Since the mid 1990s, code design for multi-wavelength Optical CDMA systems has been established as a subject across many different disciplines including information theory [56] [57] [58]. In [56], Tancesvski and Andonovic introduced a family of codes based on Prime-Hop sequences. These codes present a needle-shaped autocorrelation function with zero sidelobes and a cross-correlation of at most one, which makes them suited for truly asynchronous operation. The authors present theoretical results for different network scenarios for varying number of simultaneous users with $BER \leq 10^{-9}$. Prime-Hop Code belong to a code subclass named "Wavelength-Hopping Time-Spreading" because each wavelength presents

Table 2.3: Two-dimensional Time and Wavelength Codes (adapted from [9]).

Code	Length	Wavelengths	Weight	Reference
Prime-Hop (PH)	p^2	p	p	[56]
CHPC	p	w	w	[60]
Asymmetric PH (APH)	p_1^2	$p_2 > p_1$	p_1	[61]
Modified PH (MPH)	p^2	p	$(p+1)/2$	[62]
Bin Code	w	n	w	[57]

a maximum of one active chip. Codes with multiple pulse per wavelength - also called Multiple Pulses per Row (MPR) - have also been proposed in the literature but those cannot be implemented with linear arrays of Fibre Bragg Grating (FBGs) [59], as will be explained in detail in section 4.7. Table 2.3 summarizes the characteristics of some codes proposed in the literature for multi-wavelength Optical CDMA systems. p, p_1 and p_2 are prime numbers while n and w may be any positive integer number.

Multi-Access Interference is normally assumed to be the dominant source of performance degradation in 2D multi-wavelength Optical CDMA. Therefore, the negative effect of thermal and shot noise as well as the Poisson characteristics of the optical direct detection are generally not considered. The receiver's clock is normally assumed to be already synchronized with the transmitter. Although users are intended to transmit information asynchronously, most of the theoretical performance analysis considered chip synchronism for mathematical convenience; this assumption has been proved to provide a lower bound on the system performance [45].

The incoherent nature of multi-wavelength Optical CDMA systems and the assumptions described in the previous paragraph dictate that errors can only occur when the accumulative MAI exceeds the threshold level transforming a "zero"

into a "one" [59]. This effectively means that, for a network with N simultaneous active users, the cross-correlation pulses from (N-1) interfering users builds up to a level higher than the decision threshold. The hit probability q describes the overall probability that a pulse of a particular user hits one pulse of the desired user. Considering Prime-Hop Code [56] and regarding that the cross-correlation constraint of such codes is one and that the number of wavelengths is the prime number p, the hit probability is given by

$$q = \frac{p}{2L} \tag{2.5}$$

where the factor 1/2 accounts for equiprobable binary data transmission and L is the code length equal to p^2. The interference between (N-1) users and the desired one is given by a binomial distribution where $P_I(I = i)$ denotes probability of i interfering users

$$P_I(I = i) = \binom{N-1}{i} q^i (1-q)^{N-1-i}, i = 0, 1, ..., N-1. \tag{2.6}$$

The probability of bit error, P_e, is defined as

$$\begin{aligned} P_e(exact) &= P_I(i \geq TH \mid b_0 = 0) \cdot P_r(b_0 = 0) \\ &+ P_I(i < TH \mid b_0 = 1) \cdot P_r(b_0 = 1) \end{aligned} \tag{2.7}$$

where TH is the threshold level and b_0 is the transmitted symbol.

Since Optical CDMA with incoherent signal processing is a positive system and assuming that Multi-Access Interference (MAI) is the dominant source of noise, errors can only occur when the MAI exceeds the threshold level transforming a

"zero" into a "one". In positive systems there is no interference cancellation or autocorrelation peak reduction (due to interference) and all signal components add as positive real numbers. Therefore:

$$P_e = \frac{1}{2}\sum_{i=TH}^{\infty} P_I(I=i) \tag{2.8}$$

where the factor 1/2 stands for equiprobable symbol transmission.

Substituting 2.6 into 2.8, and considering that the ideal threshold for the MAI limited case is the amplitude of the autocorrelation peak q, the system error probability is:

$$P_e = \frac{1}{2}\sum_{i=q}^{N-1}\binom{N-1}{i}(\frac{p}{2L})^i(1-\frac{p}{2L})^{N-1-i}. \tag{2.9}$$

This analysis assumes the chip pulses to be non-return zero (NRZ). An adjustment factor θ is commonly added to reflect other optical pulse shapes. In such case, the error probability will be

$$P_e = \frac{1}{2}\sum_{i=q}^{N-1}\binom{N-1}{i}(\frac{p}{2L\theta})^i(1-\frac{p}{2L\theta})^{N-1-i}. \tag{2.10}$$

For example, $\theta = 2$ is the value commonly assumed for Gaussian pulses [9]. Figure 2.4 plots the BER of the system for different families of Prime-Hop Code, for NRZ and Gaussian pulses. It is evident that there is soft capacity performance degradation, referred to in the beginning of this chapter. Moreover, the figure shows that the impact of the pulse shape is significant on the system performance.

As explained in the previous section, a linear array of Fibre Bragg Gratings can be used to encode and decode SAE Optical CDMA. However, the physical separation of the gratings introduces a time delay that is required to be compensated

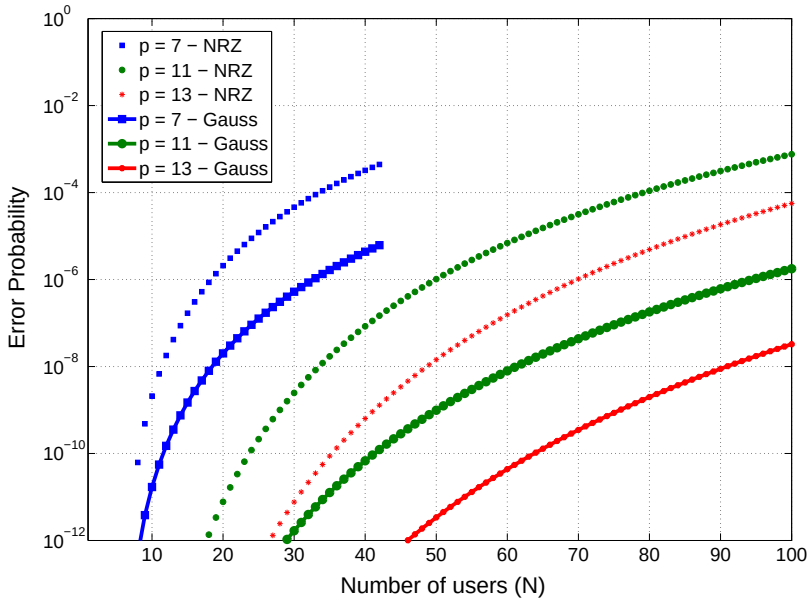

Figure 2.4: Bit Error Rate for 2D Optical CDMA network based on Prime-Hop Code (from equation 2.10 - NRZ: $\theta = 1$; Gaussian: $\theta = 2$).

by another linear array of Fibre Bragg Gratings. In time-wavelength coding, the physical distance between the FBGs can be set to provide a round trip delay time equal to the chip time or its multiples [63] [1] [64].

Figure 2.5 shows an example of a time-wavelength encoder. The light source should be able to generate a spectrally broad pulse when the user sends information bit '1'. The FBGs of the array are individually tuned for different spectral components of the broadband pulse. Therefore, each spectral component is reflected with a different time delay. As illustrated in figure 2.6, two consecutive FBGs with reflection in the wavelengths λ_1 and λ_3 will appear with a delay of a chip time in the output of the decoder. The physical distance between two consecutive gratings is set to be:

$$d = \frac{c.T_{chip}}{2.n} \tag{2.11}$$

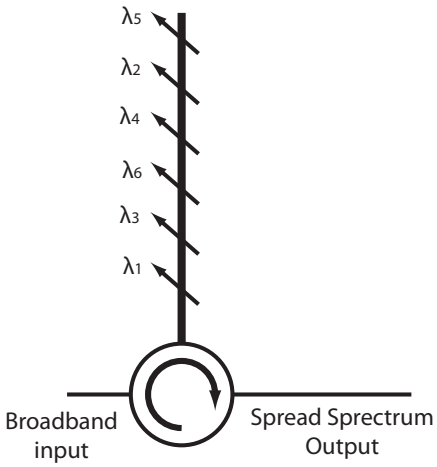

Figure 2.5: Time-Wavelength encoder/decoder based on linear array of FBGs.

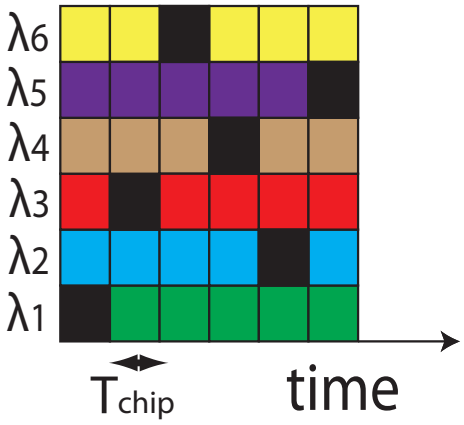

Figure 2.6: Time-Wavelength matrix generated by the encoder of figure 2.5.

where c is the speed of light in vacuum, T_{chip} is the chip time and n is the refractive index of the fibre.

In the receiver, a similar structure is used with the reflective peaks of the array of the FBGs chosen in a reverse manner to that of the encoder. When the correct codeword is applied, an autocorrelation peak is generated because the reflected spectral components are delayed so that all of them coincide temporally at the output of the decoder. If the input sequence does not match the decoder, the spectral components are re-scrambled below the threshold limit of the decoder.

Researchers from University of Laval proposed an Optical CDMA system [1] [65] based on FBG arrays (figure 2.7). The Optical codes were constructed according to the algorithm described by Bin [57]; these codes have received attention from the academic community for Optical CDMA applications and are suited for FBG implementation but it should be noted that their cardinality is low (equal to the number of wavelengths), which limits their practical interest [66].

This group described in [65] a system that comprises codes with 8 active chips (and therefore arrays with 8 FBGs), 8 time slots and 30 wavelengths. Piezo-

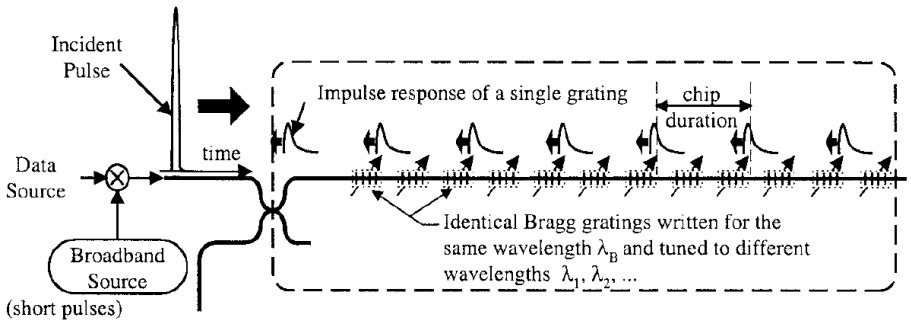

Figure 2.7: Time-wavelength Optical CDMA encoder based on FBG array [1]. The decoder is the same structure as the encoder with the wavelengths in the reverse order.

electric devices are used to individually tune the central wavelength of each FBG by locally stretching the fibre. The reflectivity and bandwidth of the individual gratings is reported to be 13 dB and 20 GHz, respectively. The amplified spontaneous emission (ASE) of an erbium-doped fibre amplifier (EDFA) is used as a broadband light source. Imperfections in the matching of the encoder/decoder delays, limited bandwidth of the gratings and residual dispersion in the link (Single Mode Fibre and Dispersion Compensating Fibre) were presented as responsible for the autocorrelation peak broadening from 105 ps to 161 ps. The system has a chip duration of 150 ps and transmits information at 860 MBit/s; this corresponds to the round-trip delay between adjacent FBGs of 1.15 ns.

Wada and co-workers [63] at Communications Research Laboratory, Japan, built a prototype with the same encoding principles to implement Prime-Hop Code [56]. The proof of concept prototype operates at 2.5 GBit/s, chip time of 35 ps and FBGs with reflection bandwidth of 3 nm. The originality of this proposal is in the use of chirped FBG instead of uniform; therefore, each reflected wavelength occupies a duration longer than the bit period but this elongation is compensated in the decoder whose FBGs have the opposite chirp.

Another highly active Optical CDMA group from University of Princeton pro-

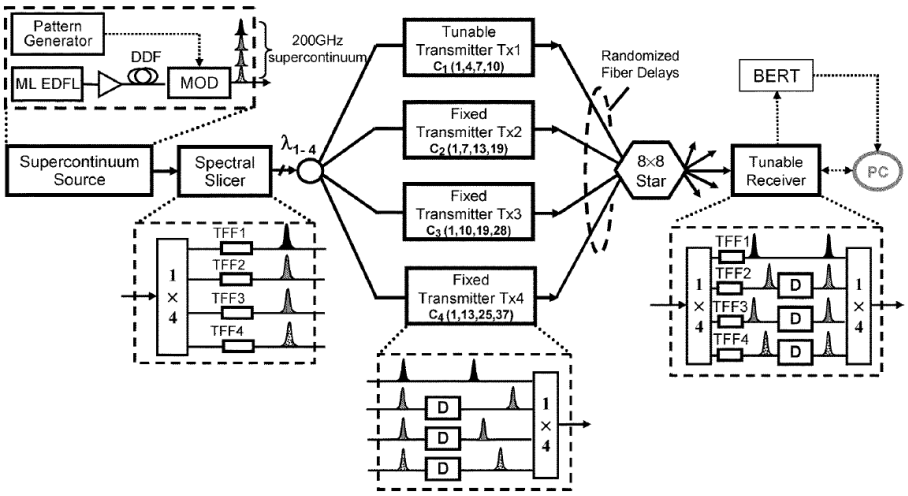

Figure 2.8: Schematic of the 2D Optical CDMA network testbed [2].

poses a different approach for encoding/decoding Wavelength-Hopping Time-Spreading systems. The work described in [2] is a significant example of the preferred encoding/decoding technology used by this group: Thin-Film Filters (TFFs) cascaded by parallel optical delay lines. Figure 2.8 shows the basic structure. Pulses from a super-continuum source are split and filtered with TFFs; these are optical bandpass filters [67] that can be tuned using piezo-electric effect. While in FBG arrays the chip rate is limited to the spacing between FBGs, this limitation does not exist in this system. However, it should be noted that the Princeton system is very inefficient in terms of optical power because high losses occur in the splitter and also in the TFFs because the energy outside the passband is lost.

As discussed before, the main source of errors in multi-wavelength Optical CDMA systems is the Multi-Access Interference caused by the summation of the cross-correlation functions of the active network users. All-optical techniques to minimise the impact of MAI have been explored, with the most significant being optical time gating [68] and optical thresholding [69] [70]. In optical time gating,

a optical clock train is used to open the switching window of an optical gate, which results on rejection of MAI noise that falls outside that detection window. This technique has two major drawbacks:

1. The receiver is required to be perfectly synchronized with the autocorrelation peaks. Note that the system does not need to be globally synchronized but optical clock recovery is required. In [68], a technique for synchronization with the autocorrelation peak is proposed; in the initial setup period (before data communication starts), the receiver continuously sweeps the optical gate control signal to discover the presence of the autocorrelation peak. This can be a lengthly process and its implementation is complex.

2. Time gating relies on the use of complex and lossy devices such as Terahertz Optical Asymmetric Demultiplexer (TOAD).

The optical thresholder is a nonlinear device that allows high intensity autocorrelation peaks to pass to the photoreceiver while reducing the lower-intensity MAI [70]. The main advantage of this technique (compared with optical gating) is that the system does not need optical clock recovery. Moreover, a TOAD with simpler structure (without control signal) can be utilized but the structure can still be considered complex and lossy for use in practical low-cost Optical CDMA networks.

Beat Noise may be a significant source of noise in 2D multi-wavelength systems [71] although not as important as in direct sequence time domain Optical CDMA. This is because the beating between chip pulses in different wavelengths falls outside the electrical bandwidth of the receiver. For such reason, the effect of beat noise is only significant when chip clashes in the same wavelength channels occur.

Experimental results indicated that beat noise can introduce 10 dB power penalty at a BER of 10^{-9} for a single interferer [9]. Time gating is a potential solution to alleviate this effect because it reduces the intensity of MAI and therefore the beat noise.

Wavelength dependent group velocity variation, inducing temporal skewing of the different wavelength components, has been identified as a major impairment in multi-wavelength Optical CDMA systems[2] [6] [72] [73]. In fact, the detection of a given codeword is an incoherent process that relies on the temporal distance among chips transmitted on different wavelengths . The impact of the optical fibre Group Velocity Difference (GVDiff) in multi-wavelength Optical CDMA systems is the main topic addressed in chapters 5 and 6 and therefore detailed analysis of this effect will be described in the chapter 5.

2.3 Summary

This chapter provides an overview of Optical CDMA with emphasis on incoherent systems and processing techniques. A brief introduction to the main advantages of the technique is provided. Time-domain encoding was first proposed for high-speed Optical CDMA systems. These systems can be encoded/decoded with passive structures based on optical delay lines and achieve asynchronous access to the network. Time-domain Optical CDMA systems require long sequences with sparse active chips to achieve acceptable bit-error rates. Spectral Amplitude Encoding was also briefly introduced although this technique will not be considered further in this thesis.

[2] In this thesis we term this "temporal skewing" as **Group Velocity Difference (GVDiff) induced time skewing**, which is more accurate than what is termed in some of the literature as dispersion-induced time skewing (see for example [72].)

Finally, time-wavelength Optical CDMA systems were discussed as an alternative to time-domain Optical CDMA. These systems provide higher code design flexibility and achieve higher transmission speeds for the same chiprates. A review of significant experimental demonstrations of this technique were presented namely the ones based on Fibre Bragg Grating arrays and Thin Film Filters with optical delays lines. All-optical techniques to eliminate MAI and beat noise such optical time gating and optical thresholding were introduced; these techniques still present major drawbacks such as high power losses, complexity and cost.

In conclusion, this brief introductory chapter shows that the increased research activities in Optical CDMA are leading to several systems and techniques of different practicabilities. Chapters 5 and 6 deal with the analysis and compensation of Group Velocity Dispersion in multi-wavelength Optical CDMA systems such as the ones described in this chapter. Chapter 4 will consider specifically the techniques used to generate and detect CDMA signals using electronic circuits based on distributed principles, which are the subject of the following chapter.

Chapter 3

Distributed Circuit Design

The concept of distributed topologies was developed for the first time by Percival in the context vacuum tubes [74]. Percival realized that cascaded amplifiers become inefficient as the gain of each stage becomes close to unity, i.e., when the bandwidth is a key requirement and active devices need to operate close to the limit of their gain-bandwidth product. Percival suggested that it is more efficient to combine the outputs of the tubes in an additive fashion so that the total gain is proportional to the number of tubes. Since Percival's patent, the evolution of electronics allows the application of this idea in the solid-state circuits - the distributed circuit design.

This chapter starts with a brief description of the issues that high-speed integrated communications circuits face today, emphasising the need for development of distributed circuits. One section is dedicated to the mechanism that allows the high frequency operation of the distributed circuits, namely, the integration of the input and output capacitances of the active devices in the so called artificial transmission lines (ATLs). The following sections are dedicated to the theoretical analysis of the distributed amplifiers and distributed transversal filters.

The last section is devoted to applications of distributed transversal filters in high-speed communication systems, particularly optical networks. The section provides an overview on the literature related with this topic with special emphasis in enabling technologies and circuit design aspects.

3.1 Conventional Circuit Limitations in High-Speed Communications

The capacity of a communications network is greatly dependent on the performance of the integrated circuits. Both in wireless systems (e.g., mobile phones) and wired applications (e.g., optical fibre communications), integrated circuits used on the network nodes limit its overall throughput. According to Shannon, the founder of modern information theory, the maximum bitrate achievable is directly proportional to the channel bandwidth. Therefore, increasing the bandwidth of the system components and allowing them to operate at higher frequencies is one of the most important goals for telecommunications engineers.

However, conventional integrated circuit design comprise intrinsic limitations in terms of exploring the capacities of the integrated circuit (IC) technologies employed. The most significant parameters of an IC process is the cut-off frequency of the transistors f_T - the frequency at which the current gain of the transistor drops to one. Although some IC processes have a very high f_T, conventional circuits rarely operate at frequencies higher than one third of this value [75] [76]. Two main reasons contribute for this behaviour. First, the vast majority of the modern IC amplifiers use negative feedback effectively operating in a closed loop. While making the design more resistant to parameter variations, the closed loop

operation demands very high open loop gain. Even when open loop operation is acceptable, higher gains usually improve the noise behaviour and the power efficiency. Secondly, parasitic components associated with the passive devices such as capacitors and inductors become a limitation at high frequencies.

Generally speaking, conventional analogue circuit design rely on the "divide-and-conquer" approach. This means that simple blocks are cascaded to perform more complex functions. The designer can optimise the blocks individually and then connect them to form a single signal-bearing path through which the information is processed. This approach led to significant progress in this field because it enables the circuit designer to think in the system design without worrying about the behaviour of each transistor. However, since all blocks have different characteristics, it is very difficult to avoid the "weakest-link" situation, i.e., one node that limits the overall performance of the system and the overall bandwidth of a circuit is lower than that of the lowest sub-circuit bandwidth. Further bandwidth limitation would exist in cascade circuits due to capacitive loading of successive stages. A solution to avoid these two effects is to distribute the gain of the constituent parts and make use of the capacitive loading. This is discussed in the sections below.

3.2 Artificial Transmission Lines

In order to understand the principles behind the distributed amplifying circuits, it is important to introduce the concept of artificial transmission line (ATL). The model presented here offers a good outline of the characteristics of distributed circuits and is a good starting point for their design. Artificial Transmission Lines

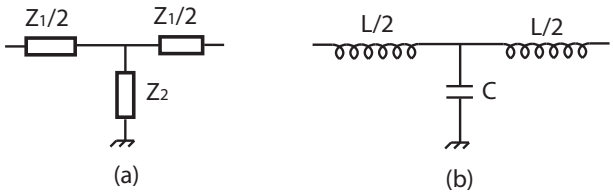

Figure 3.1: A scheme of T-section (a) General form (b) LC network.

differ from Real Transmission Lines in the fact that an ATL is composed of lumped elements associated with active devices and interconnecting inductances (usually synthesized by short transmission lines or spiral inductors).

An ATL can be modeled as a ladder of reciprocal low pass T-sections as the one shown in figure 3.1. The image impedance of the structure can be calculated through the short circuit impedance (Z_{sc}) and open circuit impedance (Z_{oc})

$$Z_{0T} = \sqrt{Z_{oc} \times Z_{sc}} = \sqrt{\frac{Z_1^2 + 4Z_1Z_2}{2Z_1 + 4Z_2} \times \frac{Z_1 + 2Z_2}{2}} \tag{3.1}$$

$$Z_{0T} = \sqrt{Z_1Z_2} \times \sqrt{1 + \frac{Z_1}{4Z_2}}. \tag{3.2}$$

Considering figure 3.1(b), where $Z_1 = j\omega L$ and $Z_2 = \frac{1}{j\omega C}$ the image impedance is given by

$$Z_{0T} = \sqrt{\frac{L}{C}} \times \sqrt{1 - \omega^2 \frac{LC}{4}}. \tag{3.3}$$

Based on this equation we can define the characteristic impedance Z_0 and the angular critical frequency ω_c

$$Z_0 = \sqrt{\frac{L}{C}} \quad , \qquad \omega_c = \frac{2}{\sqrt{LC}}. \tag{3.4}$$

The equation 3.3 can now be rewritten as follows

$$Z_{0T} = Z_0 \times \sqrt{1 - \frac{\omega^2}{\omega_c^2}}. \tag{3.5}$$

It is clear from equation 3.5 that the image impedance of the structure is approximately constant and asymptotically approximates the characteristic impedance of the line for $\omega < \omega_c$.

Therefore, it is possible to build an artificial transmission line by connecting several of those structures and terminating them with a resistive load whose value is equal to the characteristic impedance of the line. According to transmission line propagation theory, a signal travels down the line with constant characteristic impedance without reflections and is then absorbed by the matched resistor [77] [78].

3.3 Distributed Amplification

The concept of distributed circuit design is introduced by considering the basic distributed amplifier shown in figure 3.2. It is possible to identify two artificial transmission lines composed by the transistor capacitances and the inductors connecting them. The input signal travels down the input line which is terminated by a resistor with the value of the characteristic impedance of the line. Therefore, the signal should be completely absorbed by this resistor. As the signal travels along the input line, it is amplified in turn by each transistor, giving rise to several appropriately delayed copies that will add up at the output of the device. As result, each stage will equally contribute for the amplification. The low-frequency gain of such structure may be easily derived as a function of the transmission line

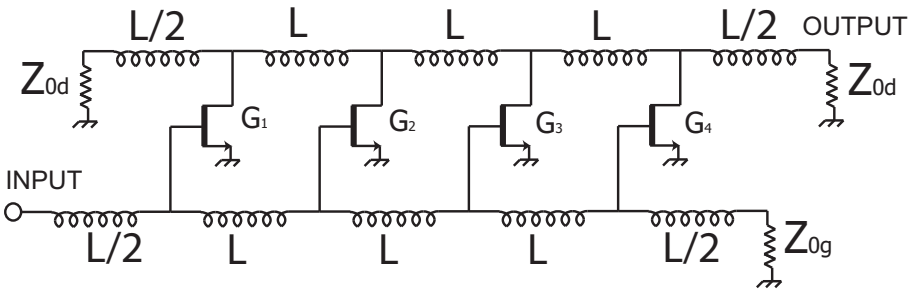

Figure 3.2: Conventional Distributed Amplifier.

parameters and the transistors' transconductance g_m [1] as:

$$A_v = \frac{N.g_m.Z_{0d}.L}{2} \tag{3.7}$$

where N is the number of the distributed amplifier stages, Z_{0d} is the characteristic impedance of the drain line and L is the end-to-end loss of the artificial transmission line. The factor 1/2 is due to the fact that the drain line is terminated at each end with a resistor; for low-frequency gain calculations, these two resistors are effectively in parallel.

The high frequency operation of the distributed amplifier is achieved by absorbing the parasitic components in an artificial transmission line. Let us consider the small signal model of a generic field effect transistor (FET) illustrated in fig-

[1] g_m is a function of the semiconductor process used and the transistor dimensions. For silicon g_m of a field-effect transistor operating in saturation mode is given by the following equation [79]:

$$g_m = \mu_n C_{ox} \frac{W}{L}(V_{GS} - V_t)(1 + \lambda V_{GS}) \tag{3.6}$$

where μ_n is the electron mobility, C_{ox} is the capacitance per unit area of the parallel-plate capacitor formed by the gate electrode and the channel, W and L are the width and length of the channels region, respectively, V_{GS} is the bias gate-to-source voltage, V_t is the threshold voltage of the transistor, λ is the channel length modulation and V_{GS} is the drain-to-source voltage. For epitaxial HEMT processes, g_m is a more complex function of the active (epitaxial) layer geometric and electrical characteristics and of the transistor's dimensions and bias [80]. For HEMT processes g_m is normally given by the manufacturers as a simple measurement based function of the gate width and number of fingers [10].

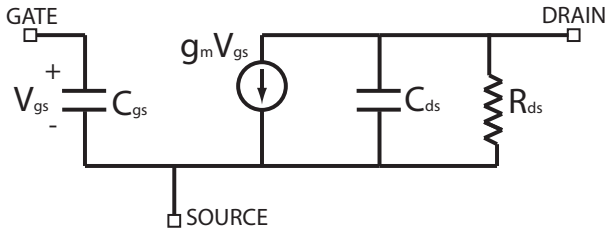

Figure 3.3: Basic small-signal model of a Field Effect Transistor (FET) with additional parasitic components.

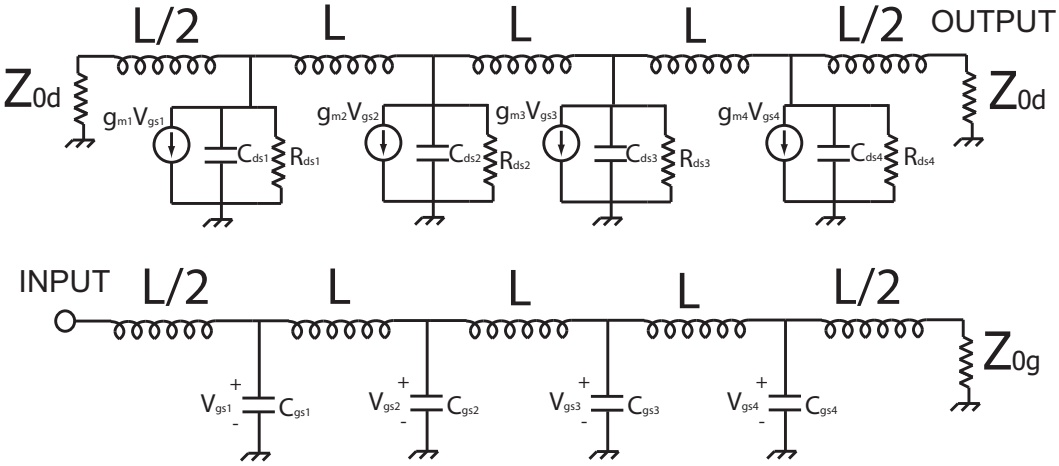

Figure 3.4: Small-signal equivalent circuit of FET-based distributed amplifier ATLs.

ure 3.3. If we replace each of the transistors of figure 3.2 by this model, the distributed amplifier may be represented by two transmission line circuits coupled by the transconductance of the transistors (figure 3.4).

The strict trade-off between gain and bandwidth in the conventional structures is more relaxed for distributed topologies. In fact, even when the transistors are individually working in sub-unity gain region, the additive nature of the distributed amplifier allows it to provide gain. Therefore, unlike conventional structures, the distributed amplifier can theoretically operate at frequencies higher than the cut-off frequency of any individual transistor.

As mentioned before, both gate and drain lines can be seen as artificial trans-

mission lines based on reciprocal LC-sections. If the inductances are chosen so that the value of the characteristic impedance given by equation 3.4 is constant for all sections and the line is terminated with a resistor with the value of the characteristic impedance, then the line is adapted. In other words, when a signal comprising frequencies within the passband $\omega < \omega_c$ of the ATL is applied, no reflections should arise and the signal is absorbed by the resistor on the other end.

3.4 Distributed Transversal Filter

Transversal filters have an important role in the equalisation of telephone lines in order to increase their data transfer capabilities [81]. Telephone lines were originally designed to accommodate analogue transmission of audio signals with relatively low bandwidth (normally from 300 Hz to 4 KHz). The use of transversal filters as equalizers allows the transmission of digital signals at high transmission rates. Other applications include the frequency equalisation of magnetic hard drives with the goal of increasing the storage capacity and reading velocity. In fact, analog transversal filters present several advantages compared with their digital implementation such as equalisation at higher speeds, less power consumption and no quantisation noise.

More recently, the potential of analogue transversal filters have been studied for applications in high-speed communication systems such as optical networks with the main goal of increasing the capacity of the channel and the distance of transmission. This subject will be presented in detail in the section 3.5.

The classical transversal filter structure is presented in figure 3.5. The filter comprises N delay sections each one providing a delay τ_i, forming a delay line with

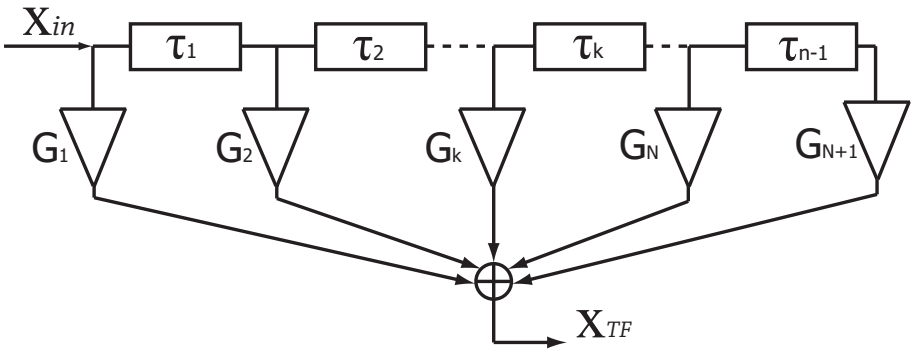

Figure 3.5: Block diagram of the conventional Transversal Filter (TF).

total delay of $\sum \tau_i$. As the signal travels down the line, the signal x_{in} is sampled in the input of each gain stage and multiplied by the respective coefficient. The delayed inputs are multiplied by a factor G_k and then summed together. The time domain response of such structure is given by [82]

$$x_{TF}(t) = \sum_{k=1}^{N+1} G_k x_{in}(t - \sum_{i=0}^{k-1} \tau_i). \tag{3.8}$$

By applying the Fourier transform to the equation 3.8, the transfer function in the frequency domain becomes:

$$H_{TF}(\omega) = \sum_{k=1}^{N+1} G_k e^{-j\omega \sum_{i=0}^{k-1} \tau_i}. \tag{3.9}$$

The implementation of this structure for low frequencies is relatively straight forward and have been widely used. However, as the frequency increases, two main problems arise. First, the complexity of the multiplication and specially the adding stages increase. Second, the delays introduced by the interconnections between elements become significant when compared to the delay sections [83].

Therefore, it is crucial to find a structure that performs similarly to the transver-

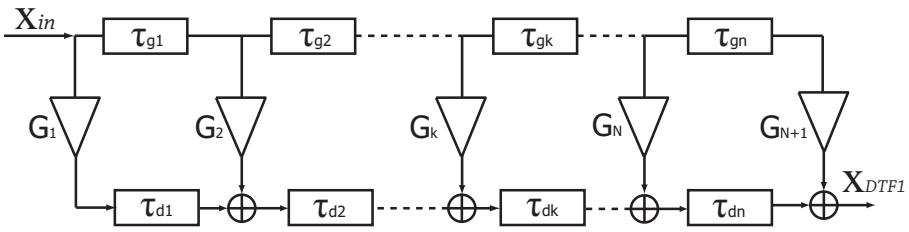

Figure 3.6: Block diagram of the Distributed Transversal Filter (DTF) in forward-mode operation.

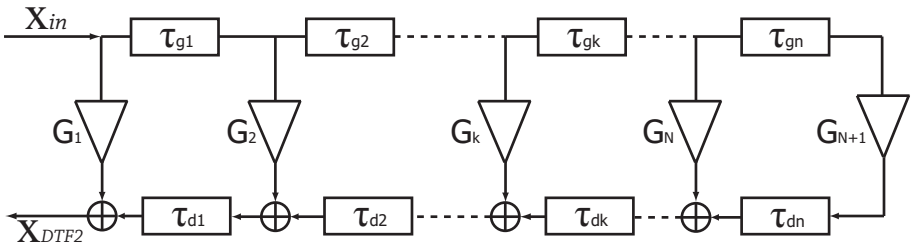

Figure 3.7: Block diagram of the Distributed Transversal Filter (DTF) in reverse-mode operation.

sal filter while being suitable for high-speed operation. This could be done using distributed principles for transversal filter implementation - the distributed transversal filter. Such structure is analyzed in [82] where the authors demonstrated that the distributed amplifier and the transversal filter are functionally equivalent topologies. By allowing the distributed structure to have different phase velocities and gains, input signals can be amplified and delayed in a similar way to transversal filters.

Two alternative approaches have been proposed for the distributed transversal filter: the forward-mode DTF (figure 3.6) and the reverse-mode DTF (figure 3.7). The output of the forward-mode DTF is taken from the opposite side of the input, i.e., next to the output of the last tap. This is similar to the distributed amplifier and therefore, this topology is often referred as "distributed amplifier-like". However, the distributed amplifier requires the gate and drain line phase velocities to be equal so that the pulses amplified by the active stages add-up

in phase in the output. This is not the case of the distributed transversal filter where the lines are deliberately designed with different phase velocities to perform a prescribed transfer function.

Alternatively, the output can be taken from from the input's side - the reverse-mode DTF (figure 3.7). This operation mode is preferable when the transversal filter requires delays per stages that are larger than the sum of the intrinsic delays provided by gate and drain lines.

The output signal of the structure represented in figure 3.6 (DTF in forward-mode operation) is given by

$$x_{DTF1}(t) = \sum_{k=1}^{N+1} G_k x_{in}(t - \sum_{i=0}^{k-1} \tau_{gi} - \sum_{j=k}^{N} \tau_{dj}). \tag{3.10}$$

The transfer function of the structure is obtained by applying a Fourier:

$$H_{DTF1}(\omega) = \sum_{k=1}^{N+1} G_k e^{-j\omega \sum_{i=0}^{k-1} \tau_{gi} + \sum_{j=k}^{N} \tau_{dj}}. \tag{3.11}$$

Equations 3.11 and 3.9 are equivalent if the following equation is verified:

$$\sum_{i=0}^{k-1} \tau_i = \sum_{i=0}^{k-1} \tau_{gi} + \sum_{j=k}^{N} \tau_{dj}. \tag{3.12}$$

Expanding the equation for all k between 1 and N+1, we obtain N+1 equations, with solutions given by

$$\tau_k = \tau_{gk} - \tau_{dk}. \tag{3.13}$$

The time domain response of the reverse-mode operation DTF is given by

$$x_{DTF2}(t) = \sum_{k=1}^{N+1} G_k x_{in}(t - \sum_{i=0}^{k-1} (\tau_{gi} + \tau_{di})). \tag{3.14}$$

Similarly, its frequency transfer function is given by

$$H_{DTF2}(\omega) = \sum_{k=1}^{N+1} G_k e^{-j\omega\left(\sum_{i=0}^{k-1}\tau_{gi}+\tau_{di}\right)}. \tag{3.15}$$

Equations 3.11 and 3.15 are equivalent if the following proposition is true:

$$\sum_{i=0}^{k-1}\tau_i = \sum_{i=0}^{k-1}(\tau_{gi}+\tau_{di}) \tag{3.16}$$

which corresponds to

$$\tau_k = \tau_{gk} + \tau_{dk}. \tag{3.17}$$

From equation 3.13, one can conclude that the traditional transversal filter structure is functionally equivalent to the forward-mode distributed transversal filter because, if the stage delay of the former is made equal to the stage differential delay of the latter, they perform the same transfer function. Similarly, equation 3.17 shows the equivalence between the traditional transversal filter and the DTF in reverse-mode operation; in this case, the transversal filter stage delay is made equal to the sum of the delays per section of the input and output lines.

3.5 Applications in High-Speed Communication Systems

Optical networks operating at 10 GBit/s and beyond are implemented and represent a significant share of the total communications traffic nowadays. This ever increasing speed in the optical domain, requires the electronic circuitry associated with the optical transmitters and receivers to operate at increasing frequencies.

The high-bandwidth characteristics of the distributed circuit topologies makes them increasingly attractive for application such as external modulation drivers [84] [85] and front-end receiver amplification [86] [87] [88]. Because the work reported in this thesis is mainly concerned with the design of distributed transversal filters for optical networks, this section provides an overview of the relevant proposals in this area. Some results about backplane equalisation are also provided due to similarities with optical compensation proposals (in fact, some groups address equalisation of inter-modal dispersion in optical links and backplane equalisation in the same paper [89]). The description here provided focuses mainly on circuit design issues and enabling technologies.

3.5.1 Distributed Transversal Filter for High-Speed Equalisation

In long-haul optical communication systems, bit rates and maximum achievable transmission distances are limited by intersymbolic interference (ISI) due to the transmission impairments in the optical medium. Pulse distortion can degrade the bit error rate to values that are not acceptable for telecommunications. Among the impairments contributing to pulse distortion in a long-haul lightwave system, chromatic dispersion (CD) is normally the dominant. CD is often claimed to be easily compensated with inexpensive static all-optical techniques such as the use of Dispersion Compensating Fibre (DCFs) [90]. Therefore, the majority of active research groups working on electronic dispersion compensation for long-haul optical systems focus on Polarisation Mode Dispersion (PMD) because it comprises random fluctuations due to its dependence on external environmental factors [91] [92]. In this case, the adaptability of the electrical dispersion

compensator represents a major advantage over static optical methods. Results considering the simultaneous electronic compensation of PMD and CD have also been reported [90] [93].

Another important area of research is the electronic compensation of high-speed transmission over legacy systems such as short-reach optical links [94] [95] [89]. In fact, it is economically attractive to use the large number of installed Multi-Mode Fibres (MMF) for transmission of signals exceeding 5-10 Gb/s. However, transmission rates beyond a few Gb/s are limited by Differential Modal Dispersion (DMD) which results from the excitation of multiple modes in the MMF. Since different modes propagate with different velocities, they arrive at the receiver at different times, pulse spreading and increased error rates. Distributed transversal filters have been explored to compensate such impairment.

Finally, several research groups have presented work related with the equalisation of electrical backplane transmission. In fact, the presence of open-ended vias at the linecard-backplane interface and crosstalk interference can cause undesirable reflections and can severally degrade the signal [89]. Distributed transversal filters have been proposed to compensate such impairments.

In the 1990s, a group from University of Wales (Bangor) proposed a variation of the distributed amplifier structure in order to include pulse shaping capabilities [96]. The distributed amplifier operated as transversal filter by comprising unequal delays in the gate and drain lines and different tap gains to obtain a prescribed transfer function. In this case, the gain coefficients were optimized so that the response of the filter provided a raised cosine shape. The group started using distributed transversal filters operating in the forward-mode topology [96] [82] but later changed to the reverse-mode topology [97] [98]. Simulations and exper-

imental results showed suitability for 10 Gb/s operation [96] [98] with a MESFET Gallium Arsenide (GaAs) process with $f_T = 20$ GHz. The group showed simulation results for 40 Gb/s operation with a 40-GHz High Electron Mobility Transistor (HEMT) MMIC process [82]. The expected (full-model) circuit response showed near-ideal behaviour up to 35 GHz, which is sufficient for 40 Gb/s operation.

Freundorfer and coworkers proposed MMIC transversal filters based on distributed topologies to compensate fibre impairments for 5 and 10 Gb/s optical transmission systems, namely chirp and chromatic dispersion [99] [100] [101]. The distributed transversal filter uses five taps with intrinsic delay equal to 25 ps each. In [99], the group proposed a structure based on cascode stages and therefore allowing only positive tap weights. A major improvement was introduced in 2000, with the use of Gilbert cells allowing the positive and negative tap weights [100]. This enabled a more flexible definition of the circuit response with a higher range of scenarios that the filter could compensate. The authors refer that this improvement enabled the device to operate with no DC gain.

The work of Prof. Hajimiri (California Institute of Technology) focused on compensation of Differential Mode Dispersion (DMD) in multi-mode fibres [102] [94] [103]. The main goal is the utilisation of the huge installed base of such fibre for high speed communications systems (10 Gb/s). Results show improvements in the bit error rate from about 10^{-5} to less than 10^{-12}. The proposed structures are intended to be used on its own or as a part of more advanced equalizer architectures, such as decision-feedback equalizers.

In terms of circuit design, this group uses a commercially available 0.18 μm SiGe BiCMOS process with $f_T = 120$ GHz. Differential topology is used; the authors justify this option by difficulties in the definition of the ac path to ground

due to lossy and poorly modelled substrate. The differential architecture ensures a virtual local ground within each stage and each section of the delay lines, since fundamental components of differential ac currents cancel each other. The delay lines comprise spiral inductors and Metal-Isolator-Metal (MIM) capacitors. Gilbert cells are used as transversal filter stages.

A group from Georgia Institute of Technology worked in compensation techniques for high-speed transmission over legacy systems such as short-reach optics and electrical backplanes [95] [89] [104]. The authors have used several processes with main emphasis on $0.18\mu m$ CMOS [95] but with results reported with $0.25\mu m$ BiCMOS [89] [104]. The distributed circuit presented in [95] is designed for compensation of DMD at 10 Gb/s but, unlike the design presented by Hajimiri in [102], the currents of the output cells are summed together and therefore the distributed principles are only applied to the input line. Gilbert cells were used to provide positive and negative cell gains. The implementation of the delay lines is done through passive spiral inductors and MIM capacitors and also with active delay lines with active peaking for extended bandwidth operation. A comparison between these two techniques is provided in [95], where the latter technique was found to give rise to more compact ICs. A delay locked loop was used in the design employing active delay lines in order to compensate performance variations detected in the process corners.

Haznesci and Voinigescu [105] proposed the first distributed transversal filter for operation above 40 Gb/s. Results showed backplane equalisation at 40 Gb/s and 49 Gb/s. A 7-tap filter was built with a $0.18\mu m$ Silicon Germanium BiCMOS process with transistors of 160 GHz cut-off frequency. Delay lines were implemented with microstrip delay lines with the nominal delay per section being 6.75

ps. Gain stages were implemented with Gilbert cells.

The work from a group lead by Professor Antony Carusone (University of Toronto) has received much attention due to their "bandwidth efficient" designs [106] [107] [108]. In fact, this group proposed a number of filters based on distributed principles whose upper limit bandwidth is very close to the cut-off frequency of the active devices. The work focused mainly on the compensation of first-order polarisation mode dispersion (differential group delay) in optical systems. The group uses differential configurations but avoids the use of Gilbert cells because the internal nodes of such structures would introduce poles that would reduce the bandwidth of the device. The proposed devices are suitable for 40 Gb/s equalisation with a CMOS 0.18μm process with f_T of only 45 GHz.

In a series of recent demonstrations, researchers from University of Aveiro in Portugal used transversal filters based on distributed principles to overcome fibre impairments in high-speed optical transmission systems [76] [90] [109] [91] [110]. Specifically, the proposed optical systems achieved high tolerance to Group Velocity Dispersion and Differential Group Delay (DGD - first order PMD) by simultaneously using electronic dispersion compensation techniques and Optical Single Side Band (OSSB) transmission, a modulation known for its high tolerance to fibre impairments [111] [112]. The DTF provided equalisation of both GVD and DGD; it is claimed that DGD is more difficult to compensate due to random fluctuations with time and therefore the electrical tunability is specially suited to compensate this impairment because the gain coefficients can be adapted to changing conditions of the optical link in real time [91].

The distributed approach is used for the transversal filter implementation; this approach is claimed to be advantageous when the upper limit of the passband

is required to be 0.3 or 0.4 times higher than the unity gain frequency of the active devices. The DTF uses Gilbert cells and is implemented with a 0.13 μm Gallium Arsenide HEMT process. The unity gain frequency of the active devices is about 100 GHz and the bandwidth of the device is about 35 GHz. While the distributed approach is still justified for such bandwidths, it should be noted that higher operation bandwidth *to* transistor cut-off frequency ratios have been achieved in the literature. One possible reason is the use of Gilbert cells whose internal nodes (not connected to an artificial transmission lines) may include poles that degrade the high-frequency response [106].

The group experimentally showed that 408 ps/nm of GVD or 18 ps of DGD could be compensated separately with an optical signal-to-noise ratio (OSNR) penalty of 1.3-dB. The simultaneous effect of 12.3 ps of DGD and 374 ps/nm of GVD could also be compensated with less than 2-dB of OSNR penalty [90].

Table 3.1 shows a summary of the distributed transversal filters described in this section. In addition, work related with encoding and decoding CDMA signals with distributed transversal filter is included (these designs will be described in detail in the following chapter). The figure of merit (sixth column) represents the ratio between the intended operation bitrate to the cut-off frequency of the active devices of the process (f_T).

Table 3.1: Distributed Transversal Filters proposed in the literature

Group	Year	Ref.	Bitrate (Gbit/s)	f_T (GHz)	Figure of merit (%)	Apps	IC process	Performance
Bangor University	1993	[113]	10	20	50	Pulse shaping	GaAs MESFET	NA
Manchester + UCL	1997	[114]	40	40	100	Pulse shaping	GaAs HEMT	NA
Queen's University	2000	[100]	10	20	50	Chromatic Dispersion	NORTEL GaAs 0.8 μm MESFET	NA ??
Caltech	2003	[102]	10	120	8.3	DMD in MMF	0.18 μm BiCMOS	BER from 10^{-5} to 10^{-10}
Georgia Tech.	2005	[95]	10	-	NA	DMD in MMF	0.18 μm CMOS	"Majority of ISI is removed"
University Toronto	2004	[105]	49	160	11.8	PMD	0.18 μm SiGe BiCMOS	Improvements in eye opening
University Toronto	2006	[106]	40	45	88	PMD	0.18 μm CMOS	Final BER 10^{-13} @ 30 GHz Final BER 10^{-10} @ 40 GHz
University Aveiro	2007	[90]	40	100	40	PMD + CD	0.13 μm pHEMT GaAs	12 ps of DGD + 272 ps/nm of GVD
University College London	2005	[3]	40	60	67	CDMA	0.2 μm pHEMT GaAs	code length = 7 Gain -15 dB
University College London (this work)	**2009**	**[115] [116]**	**40**	**60**	**67**	**CDMA**	**0.2 μm pHEMT GaAs**	**code length = 10 Gain -5 dB**

3.6 Summary

This chapter provides an overview of distributed circuit for high-speed optical networks. The chapter highlights the main principles behind the distributed circuit design followed by a discussion of the mechanism allowing for the high-bandwidth characteristics of such circuits: the use of artificial transmission lines. The distributed amplifier is discussed since, although this structure is not used in its "pure" form in the research work reported in this thesis, it is heavily used in distributed IC circuits and it is tipped to be the structure of choice for front-end receivers operating in 60 Gbit/s systems and beyond. A study of the distributed transversal filter is provided, with the analysis of its two main operation modes: reverse-mode and forward-mode.

Importantly, this chapter provides a comprehensive literature review of the applications of distributed transversal filters in high-speed equalisation. In fact, many groups worldwide are realising that the flexibility of electrical signal processing associated with the superior bandwidth characteristics of the distributed circuit topologies, allows the compensation of fibre impairments at unprecedented bitrates. This is already allowing faster and more reliable optical communication networks.

Chapter 4

Electronic Encoders and Correlators for CDMA over Fibre

In the previous chapter, transversal filters based on the distributed principles were discussed for applications in high-speed communication networks. These structures provide a flexible solution to overcome optical fibre impairments by appropriate choice of gains and delays to perform a prescribed transfer function.

In this chapter, the use of the transversal filter based on distributed principles is discussed for encoding/decoding high-speed CDMA signals for optical fibre links. It begins with an introduction to the topic where relevant proposals of electronic CDMA over fibre are presented. This chapter deals with encoding and decoding of unipolar codes; the potential advantages of encoding such signals are highlighted. The circuit design idea and the main principles that would allow the implementation of high-speed unipolar CDMA signals with a Monolithic Microwave Integrated Circuit (MMIC) process are then presented. For concept verification and study of the practical feasibility of the circuit design ideas, a three-stage distributed transversal filter was designed with a commercially avail-

able GaAs pHEMT $0.2\mu m$ process. Details about circuit design are provided in section 4.4. The expected performance of the circuit is then analyzed through full circuit model and electromagnetic simulations. A section with a potential improvement that would allow flexibility in the CDMA codeword selection is then presented. Section 4.7 describes preliminary studies about a potential implementation of 2D time-wavelength CDMA signals over fibre in the electronic domain. The chapter is concluded with a discussion of the technical limitations of the designed circuits and its potential applications.

4.1 Electronic Encoding/Decoding for CDMA over Fibre

There are two different ways of implementing time domain CDMA in Optical Networks. One way is performing encoding and decoding in the electrical domain [64] [117]. This effectively means that electronic baseband CDMA signals are converted to the optical domain for transmission and then back to the electrical domain for decoding. The second way is to perform encoding and decoding in the optical domain as presented in chapter 2.

In electronic baseband CDMA transmission, there are electronic bottlenecks both at the encoder and the decoder. In fact, the bandwidth available in the optical medium is known to be much higher than the bandwidth of electronic detection and processing techniques [49]. All-Optical CDMA explores receiver structures with minimum electronic processing; these are normally limited to integration and comparison to a threshold which can be implemented in the electronic domain at relatively high speeds [49].

In 1985, Tamura and colleagues [117] explored the transmission of electronic baseband CDMA signals over fibre. Charge Transfer Devices (CTDs) were used to encode and decode Gold Sequences. The experimental demonstration comprises six active users but the transmission rates were very modest (20 KBit/s and 2.53 MChip/s). The transmitter sends an unipolar version of the bipolar codeword, i.e., the sequence (+1, -1) becomes (+1, 0). Although the paper does not have any explicit reference to the transformation from the "positive" optical signal to the electrical domain, the bipolar received signal $Y(t)$ is related to its unipolar version $X(t)$ through the expression [48] [118]:

$$Y(t) = 2X(t) - N \tag{4.1}$$

where N is the number of simultaneous active users in the network. Users should be able to access the medium asynchronously.

In a series of recent demonstrations, researchers from the Japanese company Oki Electric Industry Co. demonstrated CDMA transmission over PON for 2 GChip/s [119] [120] [121]. The electronic encoder used conventional digital Large Scale Integration (LSI) circuits. The decoder was an analog Charge Coupled Device Matched Filter (CCD-MF), which is claimed to eliminate the need for an expensive high-speed analog-to-digital converter and digital matched filter [121]. As in the previous case, the analog CCD-MF provided positive and negative gains with the number of stages equal to the number of chips. However, the system is still limited to relatively low speeds when compared to Optical CDMA demonstrations (2 GChip/s and 62.5 MBit/s). Moreover, this system requires global synchronisation to minimize the interference between users. Each Optical Network Unit (ONU) has a tunable delay circuit in the transmitter to adjust send-timing (this

part is not described in the paper). The Optical Line Terminator (OLT) controls the delay to achieve global synchronisation as in TDM-PON system [122].

Another group from the University of Cambridge proposed a similar approach for operation at 18 GChip/s [123] [124] [125]. This group used an analogue transversal filter with eight stages for encoding and decoding baseband CDMA signals based on Gold Codes. Two users (matching and interferer) are multiplexed in the electrical domain, and this signal modulates a 1312 nm distributed feedback laser through a Mach-Zehnder optical modulator. Regarding network synchronisation, the authors clarified that "It would be necessary to impose synchronisation for optimum performance. Asynchronous operation is not likely to be possible if several users are allowed to transmit simultaneously - the multiple access interference would be excessive, especially with short codes" [126]. The group also reported to be working on synchronisation schemes, with the aim of achieving simpler stage synchronisation than in TDM-PON systems.

The use of the distributed transversal filter for generation and detection of high speed sequences was proposed at University College London [13]. The main idea was to take advantage of the good high-frequency characteristics of the distributed topologies to design integrated circuits operating at speeds close to the cut-off frequency of the IC process. Distributed Transversal Filters can be implemented as a Monolithic Microwave Integrated Circuit (MMIC) avoiding optical losses usually featured in optical matched filters. The proposed structures were intended to be used in Fiber-Optic Code Division Multiple Access systems such as the one shown in figure 4.1. Integrated circuits were designed with a 60 GHz GaAs process for 40 GChip/s [3].

This concept gave rise to the topology shown in the figure 4.2 which was

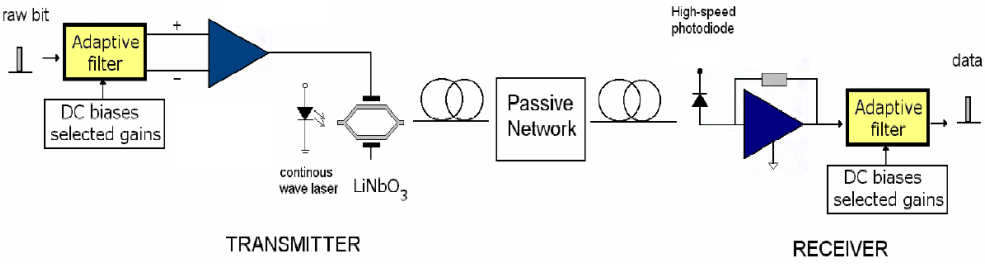

Figure 4.1: Transmitter and receiver for non-coherent CDMA over fibre encoding and decoding (figure taken from [3]).

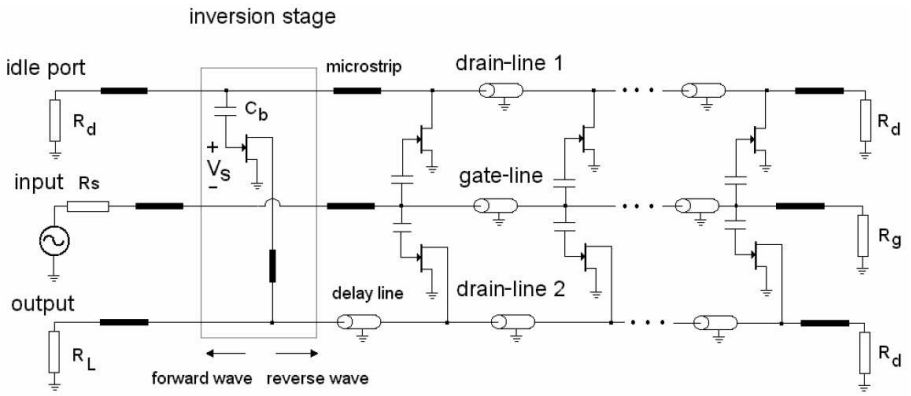

Figure 4.2: Dual-drain line transversal filter (figure taken from [3]).

named dual-drain line transversal filter. It consists of N-distributed cells, delay lines between filter sections and an inverter as output stage. The principles described in the previous chapter are employed here since the cell design effectively absorbs the parasitic capacitance of the active devices in a single input (gate) line and two drain lines. Detailed analysis of the design is provided in [3]. This structure presents major drawbacks that compromise its applicability in practical CDMA over fibre applications. Firstly, each stage of the distributed transversal filter is required to provide positive and negative gains. Traditionally, this increases the complexity of the integrated circuit when compared with designs providing positive gains only. Distributed transversal filters relying on positive gains have been proposed with simple common-source [82] and cascode stages [99], while the

first MMIC distributed transversal filter suitable for reception of bipolar signals was proposed by Lee and Freundorfer [100] and employed Gilbert cells. In the case of the dual drain lines transversal filter, increased complexity is reflected on the use of three ATLs and an additional inverter.

Secondly, processing bipolar CDMA signals requires the number of transversal filter stages to be equal to the number of chips in the time domain CDMA codeword. This gives rise to a high number of stages which is one of the main limitations for high-speed distributed topologies design [4] [127]; in fact, each artificial transmission line segment formed by the active stage and microstrip line induces dispersion which limits the number of stages. A structure requiring lower number of active stages would solve these problems and would reduce the power consumption of the circuit.

Finally, structures allowing positive and negative tap gain control perform poorly in terms of gains when compared to conventional positive tap implementations. For example, the dual-line transversal filter shown in figure 4.2 effectively attenuates the input signal by more than 15 dB. In fact, to maintain low capacitance of the input line, the gains of the transversal filter stages must be kept low; this is achieved both by choosing small transistors and defining bias conditions that led to low transconductance. Figures 4.3(a) and 4.3(b) show the temporal response of the circuit in figure 4.2 with an input pulse of 10 mV [4]. The amplitude of each chip is reduced to 0.6-0.9 mV. Structures with higher gains are required to relax the requirement of the front-end transimpedance amplifier. Due to the limitations described above and the fact that the dual-line approach does not present strong potential for improvement due to dispersion in lines and integrated circuit size constraints, the research reported in this thesis took a different

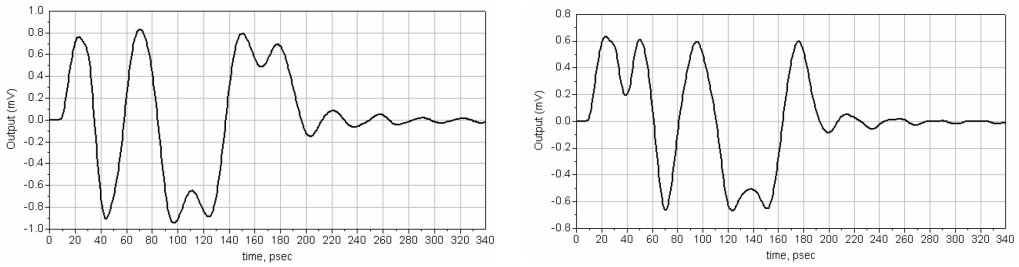

(a) Temporal response of the filter to a single pulse tuned to the sequence (+1,-1,+1,-1,-1,+1,+1) (figure taken from [3])

(b) Temporal response of the filter to a single pulse tuned to the sequence (+1,+1,-1,+1,-1,-1,+1) (figure taken from [3])

Figure 4.3: Temporal response of the filter of figure 4.2 [4].

approach for encoding/decoding CDMA in electrical domain. This chapter deals with encoding and decoding unipolar signals in the electrical domain rather than employing bipolar sequences. From integrated circuit design point of view, the main advantages of this new technique are the following:

1. Traditional encoding/decoding of bipolar codes requires the number of transversal filter stages to be equal to the number of CDMA chips; in the unipolar approach this number is only required to be equal to the number of active chips is the codeword. The delay between stages is performed with electronic delay lines (LC-sections) that can be designed to have better propagation characteristics than the artificial transmission lines formed by the active stages and the microstrip lines.

2. Each stage is only required to provide positive gains. Therefore, a simpler structure more suited for high-speed communications such as cascode stage is used.

3. Simplifications in the circuit structure enable the overall gain performance of the distributed transversal filter to be improved.

4.2 Design Concept

In a time-domain Optical CDMA network, each user is assigned a unique binary unipolar sequence with length n and the weight w; each element of this sequence is called a chip. To describe a mathematically tractable and specific (0,1) sequence, we define the vector $\mathbf{c} = (c_1, c_2, \ldots, c_k, \ldots, c_w)$ with $c_{k+1} > c_k$ and $c_k < n$ for all k, where each element represents the position of a "positive" chip relative to the beginning of the sequence (with 0 being the location at the start of the sequence). For example, if the user sequence is "10010100", the vector $\mathbf{c}$ is (0,3,5), $n = 8$ and $w = 3$. The user transmits data bit "one" by sending the sequence assigned to the intended user in the time T_{bit} ($T_{chip} = \frac{T_{bit}}{n}$) and transmits nothing for bit zero [45].

The encoder of the unipolar CDMA system generates a unipolar sequence when a pulse $x_{in}(t)$ with width T_{chip} is applied. Therefore, the time-domain response of the encoder may be represented as:

$$x_{ENC}(t) = \sum_{k=1}^{w} x_{in}(t - c_k T_{chip}). \tag{4.2}$$

The frequency-domain transfer function can be obtained by applying the Fourier transform to (4.2):

$$H_{ENC}(\omega) = \sum_{k=1}^{w} e^{-j\omega c_k T_{chip}}. \tag{4.3}$$

Conversely, the unipolar CDMA decoder should be able to generate an autocorrelation peak whose amplitude is proportional to the number of "positive" chips, when the correct sequence is applied. To achieve this, the time-domain

output response of the decoder is given by:

$$x_{DEC}(t) = \sum_{k=1}^{w} x_{in}(t - (c_w - c_{w-k+1})T_{chip}). \tag{4.4}$$

The correspondent frequency-domain transfer function can be derived from the previous equation through Fourier transform:

$$H_{DEC}(\omega) = \sum_{k=1}^{w} e^{-j\omega(c_w - c_{w-k+1})T_{chip}}. \tag{4.5}$$

The transversal filter is an attractive structure to encode and decode unipolar sequences. The desired temporal response of the system is achieved by adjusting the time delays between stages to multiples of T_{chip}, depending on the distance between positive chips in the codeword. The reverse-mode distributed transversal filter topology represented in Figure 4.4 is an ideal candidate to perform this function because:

1. This structure is suitable for Monolithic Microwave Integration with commercially available transistor processes.

2. It is suitable for very high-speed applications due to its distributed topology. As seen in the previous chapter, the transistor parasitic capacitances are absorbed in artificial transmission lines so that the circuit may operate at frequencies close to the transistors cut-off frequency.

3. Compared with the forward-mode topology, the reverse-mode distributed transversal filter gives rise to higher electronic delays; in fact, the delay per stage in the reverse-mode topology comprises the sum of the gate and drain ATL delays. This is desirable in this application since large delays (multiple

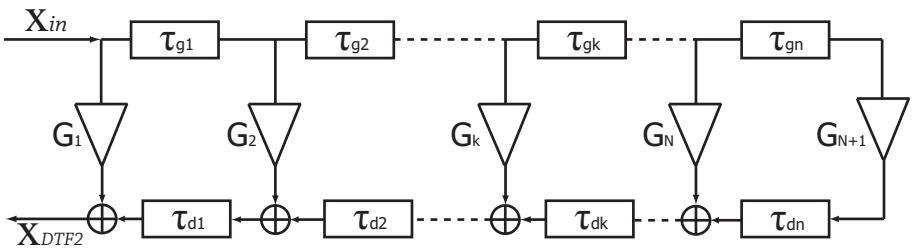

Figure 4.4: Block diagram of the Distributed Transversal Filter (DTF) in reverse-mode operation.

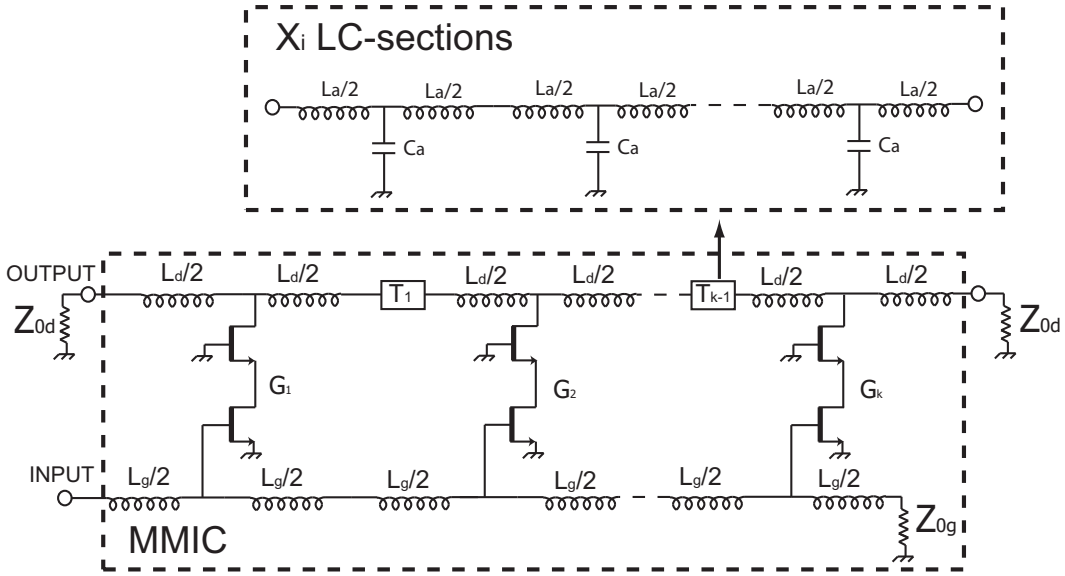

Figure 4.5: Schematic of the circuit implementation (bias not shown).

to the chip time) have to be implemented.

The Distributed Transversal Filter (DTF) can be implemented as a Monolithic Microwave Integrated Circuit (MMIC) as shown in figure 4.5. For such purpose, the number of amplifier stages is equal to the sequence weight w and the delay between stages is a multiple of the time T_{chip}, depending on the distance between positive chips in the codeword. The gain blocks may be implemented with a transistor amplifier configuration (in this example, two transistors in cascode configuration are used); Artificial Transmission Lines (ATLs) comprising the intrinsic capacitances of the amplifier stages and inductors are used in the gate and

drain lines to absorb the transistor capacitances and to provide a part of the delay required for the CDMA codeword implementation. As shown in figure 4.5, additional delay can be obtained by cascading X_i LC-sections. The transfer function of this circuit is given by [99]:

$$H_{DTF}(\omega) = \frac{V_{out}}{V_{in}} = -\frac{1}{2} Z_{0d} e^{-j\omega \frac{1}{2}(\tau_d + \tau_g)} \times \sum_{k=1}^{w} g m_k e^{-j\omega[(k-1)(\tau_d+\tau_g)+\sum_{i=1}^{k-1}\tau_{a,i}]} \tag{4.6}$$

where $\tau_g = \sqrt{L_g C_g}$, $\tau_d = \sqrt{L_d C_d}$ and $\tau_{a,i} = X_i\sqrt{L_a C_a}$ are the gate-line, drain-line and additional LC-section intrinsic delays respectively; gm_k is the k^{th} gain block transconductance and Z_{0d} is the drain-line termination. For simplicity and without loss of generality, the first exponential can be ignored since it is a fixed time shift of the filter response. Therefore, the simplified transfer function is:

$$H_{DTF}(\omega) = -\frac{1}{2} Z_{0d} \sum_{k=1}^{w} g m_k e^{-j\omega[(k-1)(\tau_d+\tau_g)+\sum_{i=1}^{k-1}\tau_{a,i}]}. \tag{4.7}$$

From the above, the voltage gain per stage takes the value G_k given by

$$|G_k| = \frac{1}{2} Z_{0d} g m_k. \tag{4.8}$$

To derive the requirements for the DTF to operate as an encoder or a decoder, we consider the generalized frequency responses and the respective circuit transfer function. For the encoder, the necessary condition can be derived by equating the time argument of the phase expressions of equations (4.3) and (4.7):

$$(k-1)(\tau_d + \tau_g) + \sum_{i=1}^{k-1} \tau_{a,i} = c_k T_{chip}. \tag{4.9}$$

For calculation of circuit parameters, we replace τ_d, τ_g and $\tau_{a,k}$ by their respective circuit element values. This defines the equivalent total delay, from input to output of a circuit containing k stages as:

$$(k-1)(\sqrt{L_d C_d} + \sqrt{L_g C_g}) + \sum_{i=1}^{k-1} X_i \sqrt{L_a C_a} = c_k T_{chip}. \tag{4.10}$$

A key circuit design parameter is the interstage delay, i.e., the delay between each two adjacent gain stages. For all k = *1,2,...w-1*, and taking stages k and $k+1$, the following condition must be satisfied:

$$[k-(k-1)](\sqrt{L_d C_d} + \sqrt{L_g C_g}) + \sum_{i=1}^{k} X_i \sqrt{L_a C_a} - \\ - \sum_{i=1}^{k-1} X_i \sqrt{L_a C_a} = (c_{k+1} - c_k) T_{chip}. \tag{4.11}$$

By considering the two summations, the above equation simplifies to:

$$\sqrt{L_d C_d} + \sqrt{L_g C_g} + X_k \sqrt{L_a C_a} = (c_{k+1} - c_k) T_{chip}. \tag{4.12}$$

Similar derivations can be done for the case of the decoder by considering equations (4.5) and (4.7), to give the decoder design equation:

$$\sqrt{L_d C_d} + \sqrt{L_g C_g} + X_k \sqrt{L_a C_a} = (c_{w-k+1} - c_{w-k}) T_{chip}. \tag{4.13}$$

From the above it is clear that, for a given codeword, the encoder and decoder have effectively the same circuit structure but with the time delays between stages T_k and T_{w-k+1} swapped for every k integer and $k \leq \frac{n}{2}$. In other words, the same circuit structure can be used either as encoder for a specific sequence or a matched

filter of its reciprocal. The design technique discussed here is applied and further explored in the specific design example given in sections 4.4 of this chapter.

4.3 MMIC Process Description

The selection of a specific integrated circuit technology is mainly determined by the bandwidth requirements of a given application. CDMA over fibre takes advantage of the high bandwidth provided by the optical medium, to deliver information at high bit rates. In this work we will consider operation at 40 GChip/s. As pointed out in chapter 2, all-optical CDMA encoders and decoders have been proposed because the bandwidth of these devices is much higher than what can be achieved using electronics. However, recent advances in integrated circuits allow to encode and decode CDMA signals in the electrical domain at rates approaching those of all-optical proposals.

For our application, Gallium Arsenide (GaAs) was the material of choice for the Microwave Monolithic Integrated Circuit (MMIC) design. Compared to MMICs based on silicon, GaAs devices are faster mainly due to the larger low-field electron mobility and lower saturation field [128]. Moreover, GaAs gives rise to passive elements with better characteristics; this is due to the fact that Gallium Arsenide can be made semi-insulating (with bulk resistivity of the order of 10^6 Ω) which reduces the parasitic capacitances associated with passive elements. This improves the high frequency response of such devices.

A High Electron Mobility Transistor (HEMT) process was chosen to implement the encoders and decoders. HEMT devices have larger transconductance and better figure of merits when compared to other integrated circuit technolo-

gies [129] [130]. Moreover, the input impedance of the HEMTs are essentially capacitive which make them more suitable to build artificial transmission lines; this advantage is more evident when compared with bipolar transistors where the input impedance are predominantly resistive [131], resulting in ATLs with poorer matching. A distinct feature of the transistors employed in this work is the active layer based on AlGaAs/InGaAs/GaAs system which introduce a lattice constant different from the GaAs semiconductor substrate. Therefore, the process used falls in the sub-category of pseudomorphic-HEMT (pHEMT).

In this research , a commercially available GaAs MMIC process named ED02AH is used; the process was developed by OMMIC, a foundry company associated with the group Philips [10]. This is a $0.2\mu m$ pHEMT process comprising active and passive components characterised up to 60 GHz, which is sufficient for 40 GChip/s operation. The thickness of the semi-isolating GaAs substrate is $100\mu m$. The process includes depletion and enhancement mode transistors with threshold voltages of -0.9 V and 0.225 V, respectively[1]. On-chip resistors can be made either using the GaAs active layer (non etched) or using a thin film metal layer (NiCr). Two types of MIM capacitors, using the Si_3N_4 layer and the $Si_3N_4 + SiO_2$ layer can be implemented. Metal plated via holes through the substrate are used to reduce parasitic inductances to ground. Other features of the process include three metalisation layer, dielectric layers and a mesa layer that enable the implementation of the active devices and different passive components.

[1] In the research reported in this thesis, only depletion mode transistors were used.

Table 4.1: Characteristic of the ED02AH process [10]

f_T	60 GHz
V_t (depletion mode HEMT)	-0.9 V
V_t (enhancement mode HEMT)	0.225 V
Gate length (L)	0.2 μm
Substrate resistivity	$> 10^7$ Ohms.cm
g_m[a]	51 mS

[a]Based on depletion mode transistors with 4x20 μm, $V_{GS} = 0$ V and $V_{DS} = 3$ V.

4.4 Circuit Design

This section presents the circuit design of the distributed transversal filter for CDMA encoding/decoding applications. Detailed analysis of the gain stages, artificial transmission lines, additional delay lines as well as considerations about the layout with ED02AH are provided. By means of example, the structure was tuned to encode the codeword '1001010000'; as explained before, this structure can act as a decoder/matched filter for its reciprocal sequence '1010010000'[2].

4.4.1 Gain Stages Design Methodology

The transversal filter active stages are designed using two pseudomorphic HEMTs in cascode configuration as shown in figure 4.6. This topology is preferred over the basic common-source configuration mainly due to its higher output resistance. As shown in table 4.2, the pHEMT output resistance (Rds) is relatively low especially when compared to silicon process transistors (normally higher than several kilo-ohms). Since in the distributed transversal structures the outputs of the stages are effectively connected in parallel, the gain of the amplifier may be severely reduced.

[2]The reciprocal sequence is obtained by reversing the bit order of the original sequence. When the final sequence begins with zeros, these are normally shifted to the end of the sequence so that it starts with a positive chip

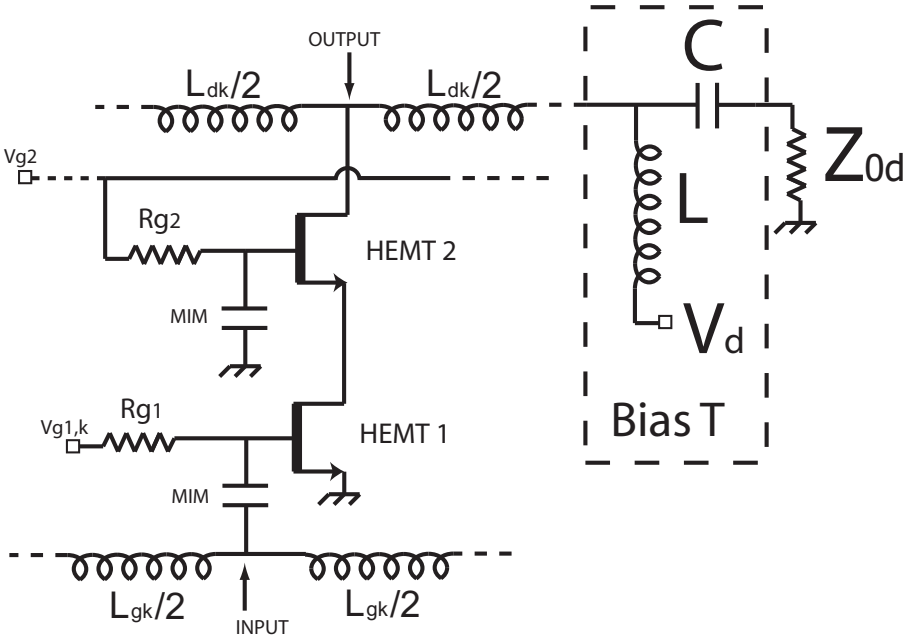

Figure 4.6: Cascode circuit diagram.

The cascode configuration results in a significant increase of the output resistance of each stage which results in increased stage and overall gain. The cascode stage also presents lower input capacitance giving rise to improved bandwidth due to reduced Miller effect [132]. However, this advantage is not as significant as in conventional multi-stage amplifier topologies because the stage gains are very modest in distributed topologies.

Figure 4.6 also displays the details of the DC bias circuitry. The gain of each amplifier is set through the gate voltage of the common-source transistor of the cascode amplifier. There is a single input DC voltage for all common gate transistors with a value of 3 V. A bias T is used to provide the DC voltage of the drain line which is set to be 6 V.

Capacitive coupling was used to connect the input of the cascode amplifier stage to the gate line. This technique was first proposed in the context of power distributed amplifiers [133] to improve the input power handling of the device and

Table 4.2: Intrinsic parameters of the pHEMT ($4 \times 20\mu m$. VDS=3 V, VGS=0 V).

$R_{gs} = 1.7\Omega$	$C_{gs} = 84.5fF$
$R_{ds} = 320\Omega$	$C_{ds} = 19.6fF$
$R_{gd} = 13\Omega$	$C_{gd} = 14.9fF$

then in broadband distributed amplifiers for high rate optical-fibre data transmission systems, satellite and radar applications [134] with the intent of achieving higher bandwidth operation. Capacitive coupling is simply achieved by the insertion of a capacitor between the gate line and the gate of the common-source transistor. The primary purpose of the use of capacitive coupling in our design is to bias the common-source transistors independently. Moreover, the bandwidth of the circuit is improved because the effective input capacitance of the transversal filter stage is reduced. However, this comes at the expense of gain reduction since the added capacitor will form a capacitive voltage divider with the input capacitance of the transistor, resulting in a proportional fraction of the signal on the input line appearing at the gate of the common-source transistor.

The choice of the transistor dimensions and the value of the DC blocking capacitor is mainly determined according to bandwidth requirements. In this design it was decided that the input capacitance of the cascode stage should not exceed 100 fF and the DC blocking capacitor should not reduce the gain by more than one third. The equivalent small-signal model of the pHEMTs is shown in figure 4.7. Table 4.2 and 4.3 show, respectively, the intrinsic and extrinsic parameters of the device with $4 \times 20\mu m$ width gate fingers, for the "reference" bias conditions $V_{gs} = 0V$ and $V_{ds} = 3V$. The transconductance of a device with such characteristics and bias is 51 mS.

A simplified transistor model was considered as first approach for small-signal

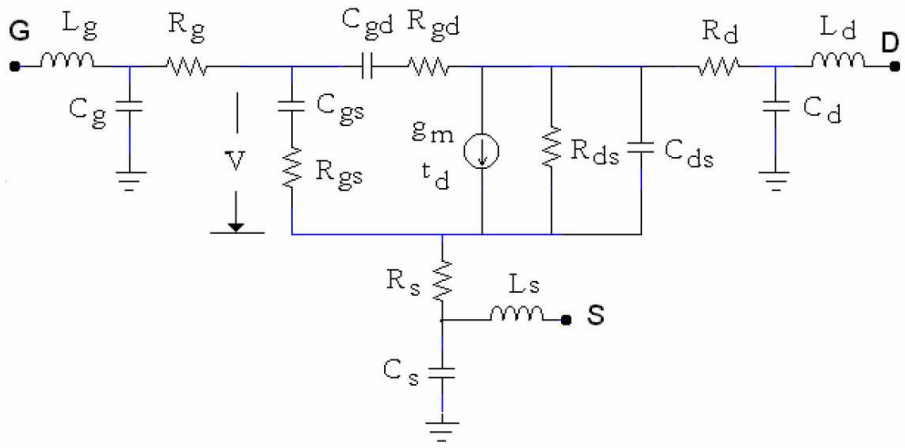

Figure 4.7: Small-signal pHEMT model.

Table 4.3: Extrinsic parameters of the pHETM ($4 \times 20\mu m$. VDS=3 V, VGS=0 V).

$R_s = 6.75\Omega$	$C_s = 4.1fF$	$L_s = 13.5pH$
$R_d = 0.27\Omega$	$C_d = 2.7fF$	$L_d = 13.6pH$
$R_g = 1.1\Omega$	$C_g = 6fF$	$L_g = 13.6pH$

gain calculations. The input capacitance of the cascode is taken to be approximately equal the sum of C_{gs} and C_{gd}. The DC blocking capacitor is placed in series with the input capacitance of the cascode and therefore, the input capacitance of the whole stage can be expressed as

$$C_{in} = \frac{C_{DC}(C_{gs} + C_{gd})}{C_{DC} + (C_{gs} + C_{gd})}. \tag{4.14}$$

The gain of the cascode cell at low-frequencies can be calculated by considering the simplified hybrid π model as shown in figure 4.8. Such structure presents a voltage gain given by the following expression:

$$G_{Cas} = \left|\frac{V_{out}}{V_{in}}\right| = \left(g_{m1} + \frac{1}{R_{ds2}}\right)(R_{ds1}||R_{in2})\,(g_{m2}R_{ds2} + 1)\left(\frac{R_L}{R_L + R_{ds2}}\right) \tag{4.15}$$

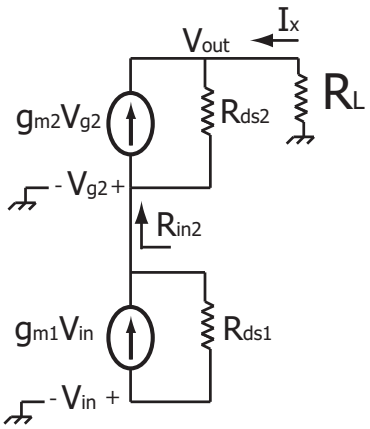

Figure 4.8: Small signal circuit of the cascode cell for gain calculation.

where the symbol || represents parallel resistors and R_{in2} is:

$$R_{in2} = \frac{1}{g_{m2} + \frac{1}{R_{ds2}}}. \tag{4.16}$$

However, this gain does not take in account the effect of the DC blocking capacitor (C_{DC}). The voltage in the input of the cascode stage (after the DC blocking capacitor) is multiplied by the following quantity

$$M = \frac{C_{DC}}{C_{DC} + C_{in}}. \tag{4.17}$$

The output resistance of the cascode stage can be expressed as

$$R_{out} = \frac{V_{out}}{I_x} = (R_{ds1} + R_{ds2})(1 + g_{m2}(R_{ds1}||R_{ds2})). \tag{4.18}$$

The gain control of the cells is achieved by adjusting the bias voltage of the common source transistor. Table 4.4 shows the characteristics of gain and input capacitance of the cascode stages. Here a 25 Ω (two 50 Ω loads in parallel) resistor was assumed as a load resistor. Note that the value of M is always

Table 4.4: Characteristics of the cascode stages for different bias voltages.

V_{g1} (V)	M	C_{in} (fF)	G_{Cas} (dB)	G_{Stage} (dB)	R_{out} (K Ω)
-0.5	0.74	51.4	-9.02	-11.6	9.4
-0.3	0.68	62.3	-1.18	-4.44	5.9
-0.1	0.67	66.1	1.2	-2.36	5.7
0.1	0.67	66.5	1.92	-1.78	6.0

greater than 2/3.

Figure 4.9 shows the final layout of the cascode cell. It comprises two pHEMTs with $4 \times 20\mu m$ width fingers. The grounding is done through via-holes with dimensions $120\mu m \times 120\mu m$. The DC blocking capacitor (200 fF) associated with the common-source stage is a Metal-Isolator-Metal (MIM) Si3N4+SiO2 capacitor. These devices are fabricated using the 150 nm Silicon Nitride layer and the 850 nm Silicon dioxide layer between the first metal (BE) and the interconnection metal (IN) [10]. The capacitance is a function of the area ($W1 \times W2$) of the capacitor and its perimeter ($2 \times (W1 + W1)$) where W1 and W2 are the dimensions of the capacitor. The capacitor used to ground the common-gate stage is designed using the 150nm Silicon Nitride layer between the first layer metal (BE) and the top electrode metal (TE); therefore, these structures yield higher capacitive values per unit area. This capacitor should be much higher than the intrinsic gate-source capacitance of the common-gate transistor to guarantee that no small-signal voltage drop occurs across this capacitor. Considering that C_{gs} is 84 fF, the capacitor was chosen to have 1 pF resulting in a drop better than 8 %.

Finally, given the exceptionally high input resistance of the pHEMTs used, the values of the bias resistors is non critical, as far as bias is concerned. Such resistors have to be chosen according to low cut-off frequency, noise and geometric considerations. Appropriate values are in the kΩ range and the values used were 7000Ω

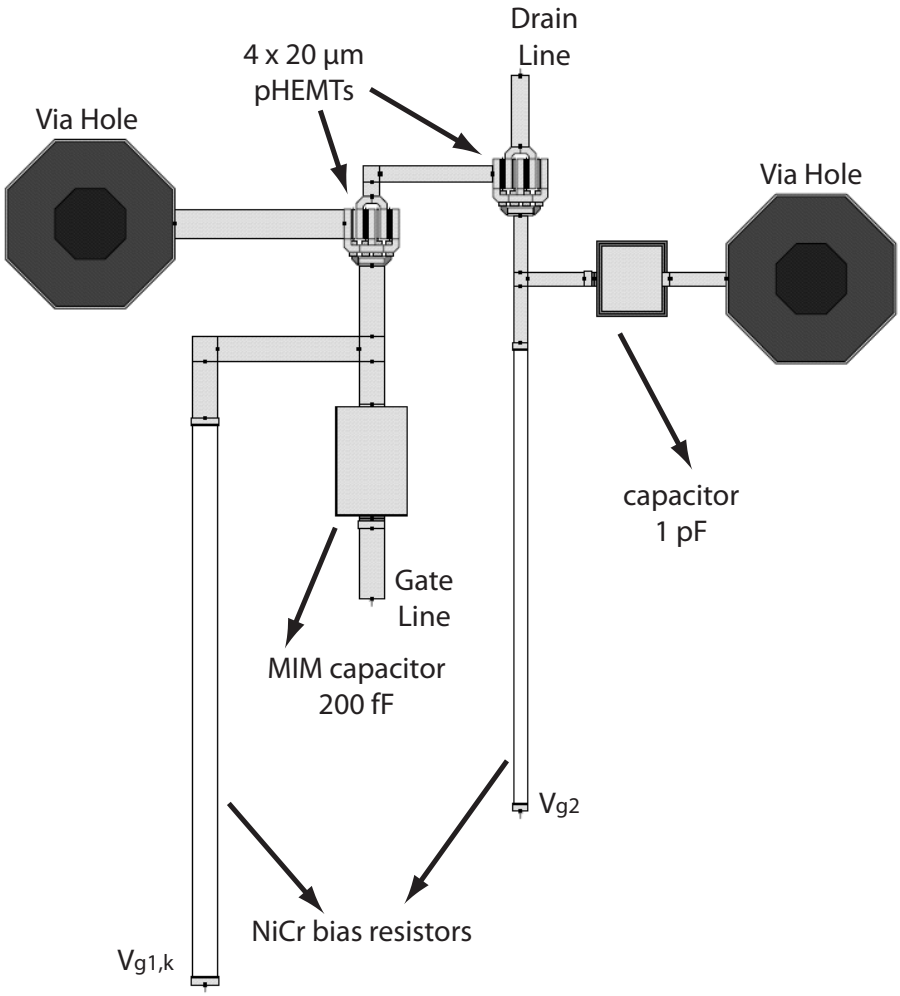

Figure 4.9: Layout of the cascode cell.

and 4500Ω for the common-source and common-gate transistors, respectively. These were designed as nichrome (NiCr) strips with $10\mu m$ and $18\mu m$ width.

4.4.2 ATLs Design Considerations

Keeping in mind that the main challenge of this particular DTF topology is the implementation of large interstage delays, the gate line was designed with two main goals:

1. To have large intrinsic delay.

2. To provide linear phase (or flat group delay) across operation frequencies.

The gate line design is a compromise between dimensions and characteristics with the aim of maximizing the group delay and minimizing the pulse broadening. As shown in the cascode cell design above, the overall input capacitance (C_{in}) per stage does not exceed 70 fF. As a design goal, the group delay was chosen to be 10 ps per stage (effectively providing 40 % of a chip period) and the width of the microstrip lines were chosen to be $30\mu m$. Through Agilent's Linecalc^{TM} simulation tool, the characteristic impedance of the $30\mu m$ delay line was calculated to be 65Ω while its the group delay was found to be approximately 0.95 ps per $100\mu m$. This corresponds to intrinsic capacitance and inductance per section of $\Delta C_{30\mu m} = 15\text{fF}/100\mu m$ and $\Delta L_{30\mu m} = 65\text{pH}/100\mu m$, respectively. Therefore, as a first approximation, the length of the gate inductors can be calculated through the following equation:

$$Z_{0g} = \sqrt{\frac{\Delta L_{30\mu m} L_i}{\Delta C_{30\mu m} L_i + C_{in}}} \tag{4.19}$$

where L_i is the length of the gate microstrip line that forms one ATL section. The equation gives the length of the microstrip line to be $640\mu m$, and further

circuit optimisation yields a final length of $800\mu m$. Figure 4.10 shows the gate line group delay characteristics and the scattering parameter $S21$. It shows that the group delay has minimal variation from near DC to 31 GHz. It should be noted that the line has resonant behaviour at 34 GHz which leads to negative group delay. The study of the meaning of negative group delay is outside the aim of this thesis but it has been analyzed before in the context of complex circuits [135] [136] and has also been identified in distributed structures [96] [91]. A closer look into the characteristics of the microstrip line gives a hint for the source of this characteristic. In fact, the microstrip line with $30\mu m$ width and $800\mu m$ length can only be considered to approximate an inductor for frequencies lower than 30 GHz. This can be confirmed by simulations with results shown in figure 4.11 where the $S21$ characteristics of this microstrip line are contrasted to those of an ideal inductor.

The high group delay of the gate line has a direct impact on its cut-off frequency and would lead to minor distortion; however, the negative group delay is not expected to lead to significant signal distortion. This can be verified by studies of propagating pulse behavior as below.

The pulse propagation in the gate line can be seen in figure 4.12, "measured" at the inputs of each of the three transversal filter stages (taken from full simulation of the full design shown in figure 4.20). The input signal is a Gaussian pulse with 25 ps width at 1/e intensity point; the measured pulse widths at the input of stages 1, 2 and 3 are 26.2 ps, 28.5 ps and 31 ps, respectively. These values show minimal pulse spreading and are suitable for 40 GChip/s transmission, as for the worst spread pulse, less than 10 % inter chip interference would result. This favourably compares to recently reported work [123], of the highest speed elec-

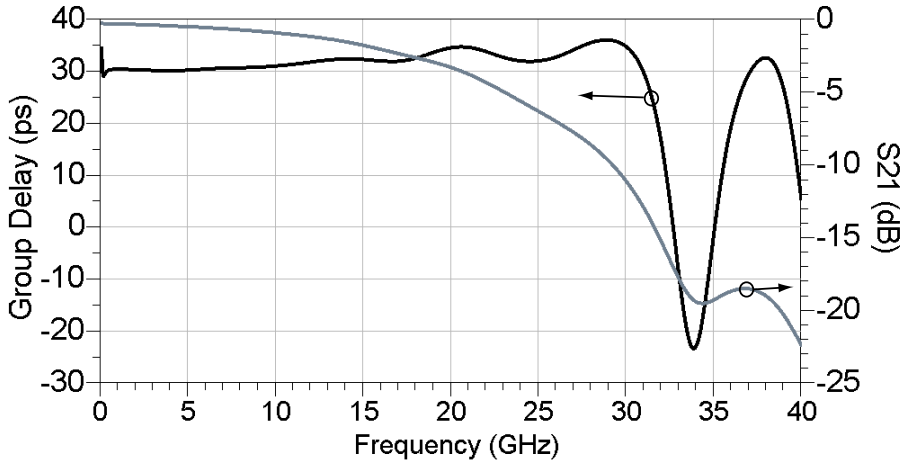

Figure 4.10: Group delay characteristics of the gate line.

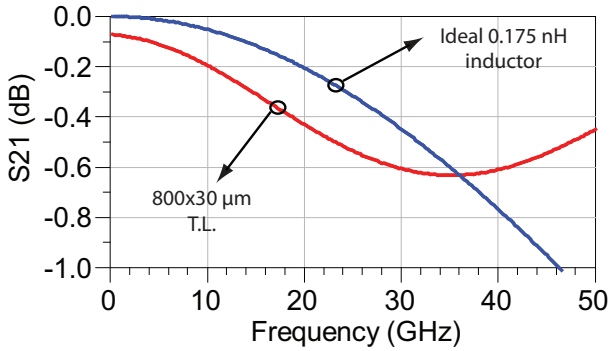

Figure 4.11: Group delay characteristics of the gate line.

tronic CDMA over fibre demonstration to date, where the bandwidth limitation of the non-distributed transversal filter results in severe pulse broadening so that the width of the final pulse exceeds 80 ps for a 18.1 GChip/s system.

The drain line was designed following similar principles. To guarantee uniformity in the line, the microstrip line width was chosen to be equal to the additional delay lines, i.e., 20 μm. The output capacitance of the active stage is approximately equal to C_{ds} which is 19.6 fH. Therefore, the following equation is required to be meet:

$$Z_{0d} = \sqrt{\frac{\Delta L_{20\mu m} L_i}{\Delta C_{20\mu m} L_i + C_{ds}}} \tag{4.20}$$

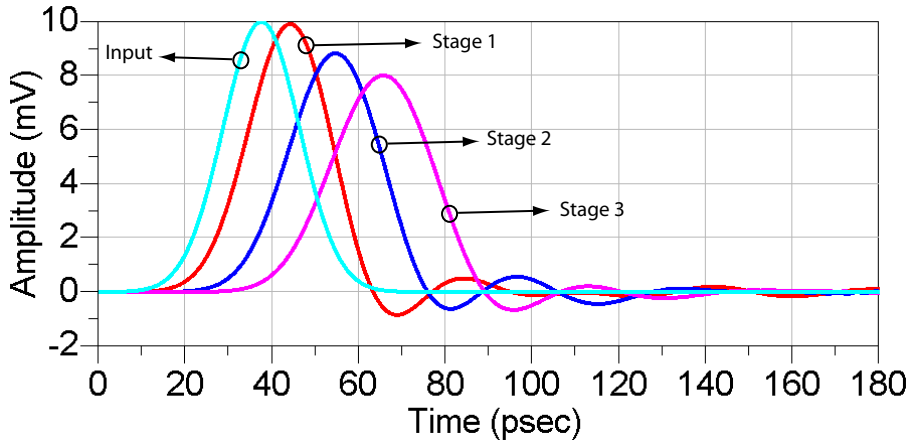

Figure 4.12: Temporal response of the gate line.

Table 4.5: Characteristics of the gate and drain transmission lines.

$W_g = 30\mu m$	$L_g/2 = 400\mu m$
$W_d = 20\mu m$	$L_d/2 = 90\mu m$

with $\Delta C_{20\mu m} = 13.8\text{fF}/100\mu m$ and $\Delta L_{20\mu m} = 72\text{pH}/100\mu m$. From equation 4.20, the length of the microstrip line is initially calculated to be $131\mu m$. Further optimisation of the time domain response yields a length of $180\mu m$.

4.4.3 Additional Delay Lines

One of the main requirements of the MMIC DTF topology for CDMA over fibre purposes is the large interstage delays. For example, in distributed amplifiers, delay lines are implemented for the purpose of equalising small differences between the phase velocities of the gate and drain lines. For high frequency operation this rarely exceeds few picoseconds. On the other hand, this particular DTF design should provide interstage delays that are multiples of the chip time and with constant group delay over the device frequency of operation. Since the chip time is 25

ps for 40 GChip/s operation, interstage delays of 50 ps and 75 ps have to be implemented for the codeword '1001010000'.

The delay could be implemented using matched microstrip transmission lines (i.e. with characteristic impedance equal to that of the drain ATL), taking advantage of the flat group delay provided by such structures. However, such technique would result in lines with excessive length and width. To save integrated circuit area, extra delay may be achieved by using LC-sections [102] [106] [76]. These can be constructed as Metal-Isolator-Metal (MIM) capacitors and thin microstrip lines. In order to avoid reflections in the drain line, their characteristic impedance $Z_{0a} = \sqrt{\frac{L_a}{C_a}}$ is set to 50Ω. The number of LC-elements X_k in each delay section T_k depends on the trade-off between the size occupied by the structures in the integrated circuit and the cut-off frequency of the additional delay lines which is given by [77]:

$$f_{ca} = \frac{1}{\pi\sqrt{L_a C_a}}. \tag{4.21}$$

Microstrip lines of 20 μm width were chosen to implement the LC-sections. The characteristic impedance of a 20 μm line was calculated with Agilent's Linecalc^{TM} ($Z_{0,20\mu m} = 72\ \Omega$); the intrinsic group delay is approximately 1 ps/100 μm. Therefore, the intrinsic capacitance and inductance per unit length are respectively $\Delta C_{20\mu m} = 13.8\text{fF}/100\mu m$ and $\Delta L_{20\mu m} = 72\text{pH}/100\mu m$. Under such circumstances, the characteristic impedance and time delay of the additional lines are given by the following equations:

$$Z_{0d} = \sqrt{\frac{\Delta L_{20\mu m} L_i}{\Delta C_{20\mu m} L_i + C_{ADD}}} \tag{4.22}$$

$$t_d = \sqrt{\Delta L_{20\mu m} L_i (\Delta C_{20\mu m} L_i + C_{ADD})} \tag{4.23}$$

where C_{ADD} is the capacitance of the additional Metal-Isolator-Metal (MIM) capacitor and L_i is the length of the microstrip line for each LC-section. The above equations can be re-written to express the relation between C_{ADD} and the length of the microstrip line L_i:

$$C_{ADD} = \frac{\Delta L_{20\mu m} L_i - Z_{0d}^2 \Delta C_{20\mu m} L_i}{Z_{0d}^2} \tag{4.24}$$

$$C_{ADD} = \frac{t_d^2 - \Delta L_{20\mu m} \Delta C_{20\mu m} L_i^2}{\Delta L_{20\mu m} L_i}. \tag{4.25}$$

A simple graphical solution to design the matched delay lines was devised as depicted in Figure 4.13. For a given drain line characteristic impedance ($Z_{0d} = 50\Omega$ in this circuit), a line with combinations of additional capacitance and microstrip line length can be drawn (equation 4.24). Each point in this line corresponds to an intrinsic delay of the LC-section. The microstrip length and additional capacitance values are determined at the intercept of the characteristic impedance line and a specific time delay curve (equation 4.25).

Because a large number of LC-section are placed in series to provide the prescribed delay, it is essential to design each LC-section with low losses and flat group delay. Therefore, the theoretical cut-off frequency of each delay line is chosen to be higher than the frequency of interest. In this case, the delay lines were designed to provide approximately 6.2 ps delay (per section); this corresponds to:

$$f_{ca} = \frac{1}{\pi \times 6.2 \times 10^{-12}} = 51.3\text{GHz}. \tag{4.26}$$

From equations 4.24 and 4.25, the values of microstrip length and capacitance are calculated to be $L_i = 430\ \mu m$ and $C_{ADD} = 62$ fF. For 40 GChip/s operation,

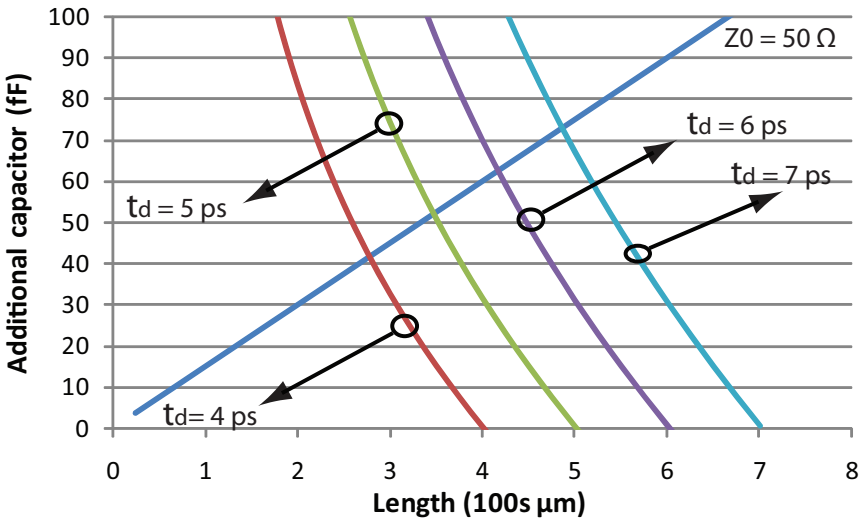

Figure 4.13: Design of delay lines.

the chip duration is 25 ps and therefore, for the considered sequence, delays of 75 ps and 50 ps are required between stages one and two, and stages two and three, respectively. Considering the intrinsic delays of gate and drain artificial transmission lines, T_1 requires ten LC-sections and T_2 six sections.

Figures 4.14 and 4.15 present the layout of the additional delays inserted in the drain line. These were divided into three structures for modelling and optimisation convenience. Structure 1 was designed to provide approximately 25 ps delay; it is present in both interstage delays sections and comprises four LC-sections. Structure 2 is designed for 36 ps (6 LC-sections) while structure 3 provides 11 ps (2 LC-sections). Individual optimisation processes were carried out, to achieve flat group delay and hence minimum pulse distortion and ripple. This resulted in structures 1 and 3 using 50 fF capacitors while structure 2 uses 60 fF capacitors with longer microstrip lines. The group delay characteristics and gain parameters of such structures were modelled using the electromagnetic simulator MOMENTUM^{TM}, a three dimensional planar simulator in ADS^{TM}.

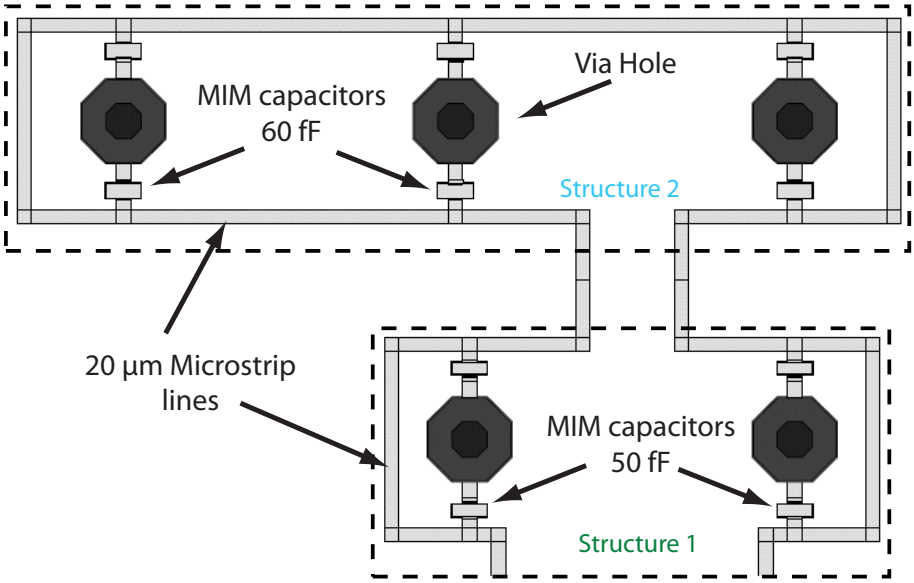

Figure 4.14: Delay lines between stages one and two (ten LC-sections).

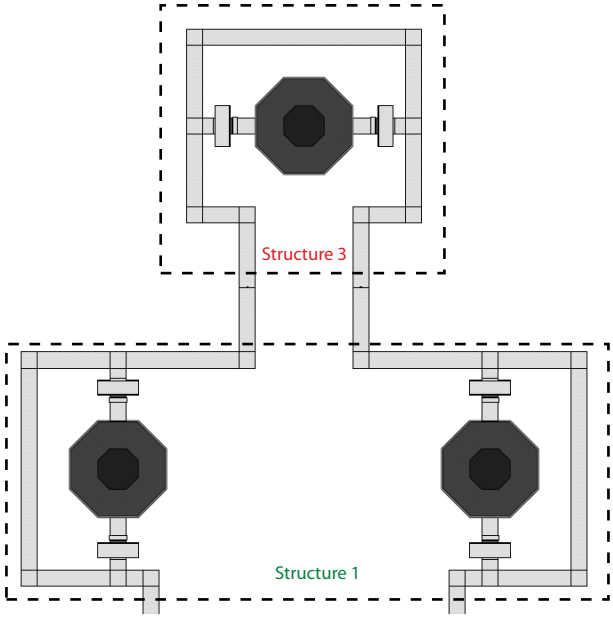

Figure 4.15: Delay lines between stages two and three (six LC-sections).

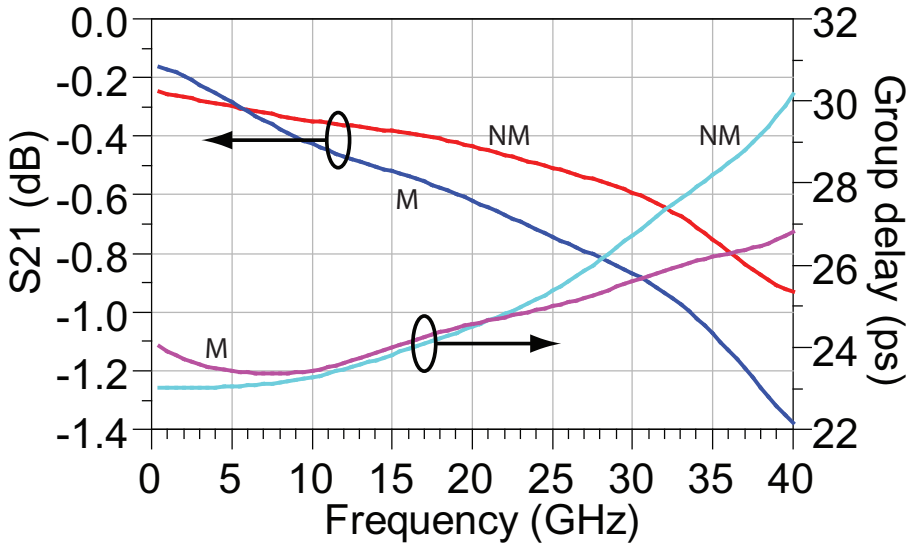

Figure 4.16: Group delay and $S21$ of the structure 1 (figure 4.14) - simulation including momentum (M) and excluding momentum (NM).

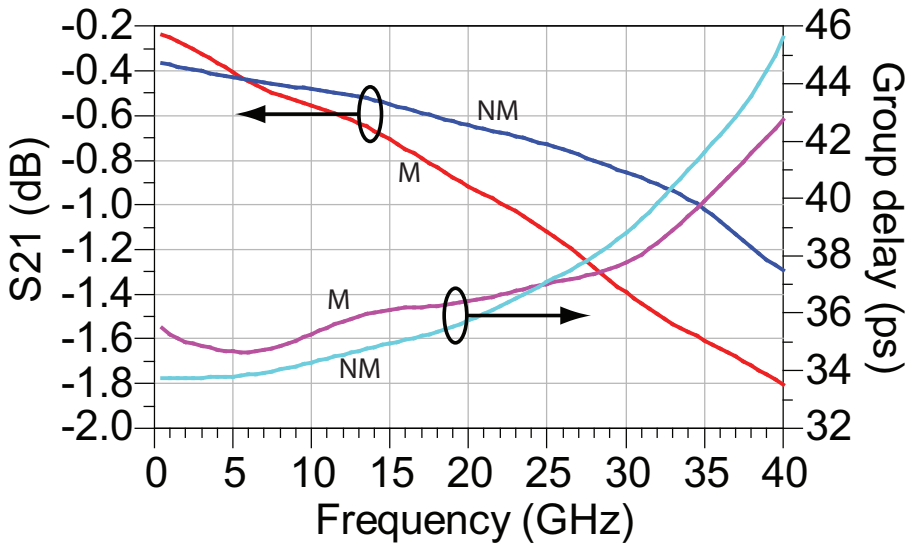

Figure 4.17: Group delay and $S21$ of the structure 2 (figure 4.14) - simulation including momentum (M) and excluding momentum (NM).

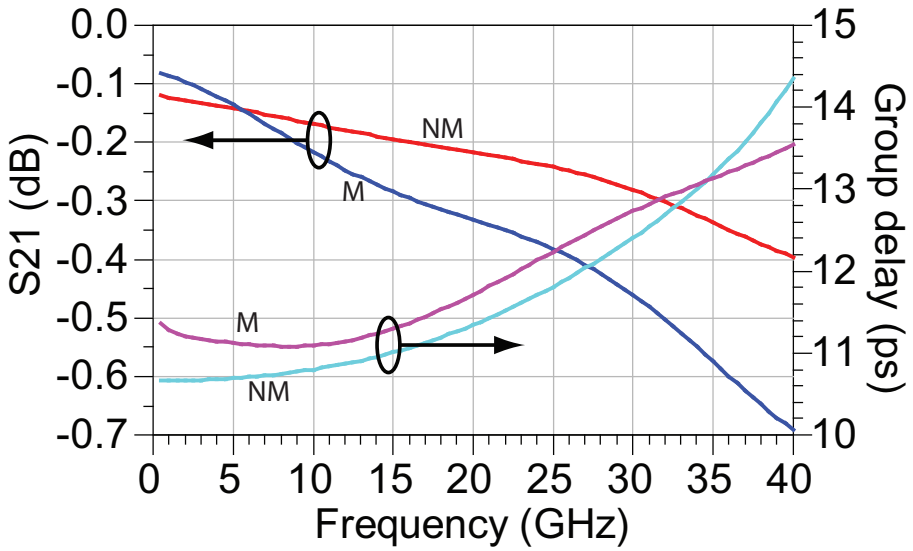

Figure 4.18: Group delay and S21 of the structure 3 (figure 4.15)- simulation including momentum (M) and excluding momentum (NM).

Table 4.6: Characteristics of the delay lines.

	Delay (20 GHz)	Delay variation (0-40 GHz)	Attenuation (30 GHz)
Structure 1	24.8	±7%	0.9
Structure 2	36.2	±9.5%	1.4
Structure 3	11.6	±9%	0.45

Figures 4.16, 4.17 and 4.18 show the expected $S21$ parameter of the three delay structures used in the MMIC design and their group delay characteristics; the graphs show circuit simulation results and full electromagnetic results accounting for coupling among the different MMIC elements, i.e., simulations with and without MOMENTUM. Results indicate differences in the expected behavior of parameter $S21$, especially at high frequencies. Considering that for 40 GChip/s signaling most of the spectral energy is concentrated within 30 GHz bandwidth, the intrinsic losses of the structures were maintained below 0.9 dB, 1.4 dB and 0.45 dB, respectively. Table 4.6 summarizes the characteristics of the structures.

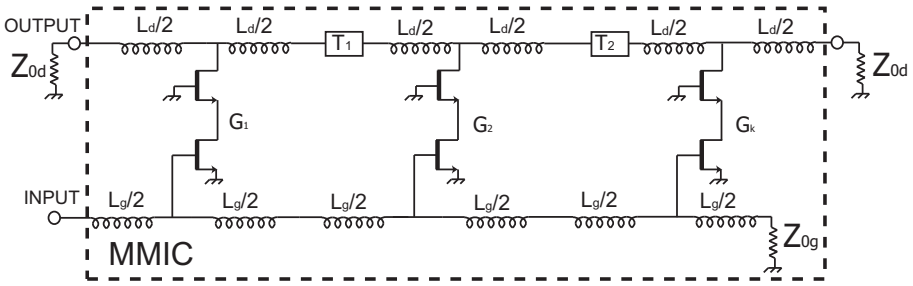

Figure 4.19: MMIC Distributed Transversal Filter (Bias circuitry not shown).

4.4.4 DTF Layout Considerations

Figure 4.19 shows the circuit of the Distributed Transversal Filter (DTF). Since the codeword comprises three positive chips, the device has three active stages and therefore two interstage delay elements as described in section 4.4.3.

Since both drain and gate lines are lossy, there is need to compensate it by adjustments on the gain of the active devices. This problem is particularly critical in the Distributed Transversal Filter operating in the reverse-mode topology because, while the pulse amplified for the first stage of the DTF will immediately appear in the output, the input signal of the response amplified by the last stage will travel all the gate and drain lines. Therefore, the gain of the last stage should be larger than the first stage. The optimized values for the gate voltage of the common-source transistor of the cascode were found to be $V_{gs1} = -0.45V$, $V_{gs2} = -0.3V$ and $V_{gs3} = 0.1V$.

Figure 4.20 presents the layout of the 3-stage Distributed Transversal Filter. The chip size is $3000\mu m \times 1700\mu m$, within the range recommended by the foundry design rules. In the bottom of the pad frame, the gate line runs horizontally and is capacitively coupled with the cascode stages. The microstrip transmission line that runs alongside the gate line is the DC Bias line of the common-gate transistor (3V); the connection between this line and the gate of the transistors is made

through thin NiCr resistor (vertical lines). The top of the frame is dominated by the drain line comprising the delay sections. The gate line is terminated with an on-chip 50 Ω NiCr resistor.

The grounding of the integrated circuit is made through 21 via holes, used in the LC sections, RF pads and bias circuitry. The size of such structures is $120\mu m \times 120\mu m$ and, according to the process design rules, the minimum distance between via-holes is $200\mu m$.

RF probe pads (which also may be used as bond pads for a packaged MMIC) have a Ground-Signal-Ground structure, with a central RF pad and two adjacent pads grounded through via holes; these were added to fulfill the requirements of conventional testing equipment. Three RF ports are employed: input and output ports and a port for termination of the drain line. External drain line termination will be used to avoid excessive on-chip power dissipation. The power dissipation of this topology is 210 mW with a current intake of 35 mA for the three cascode stages.

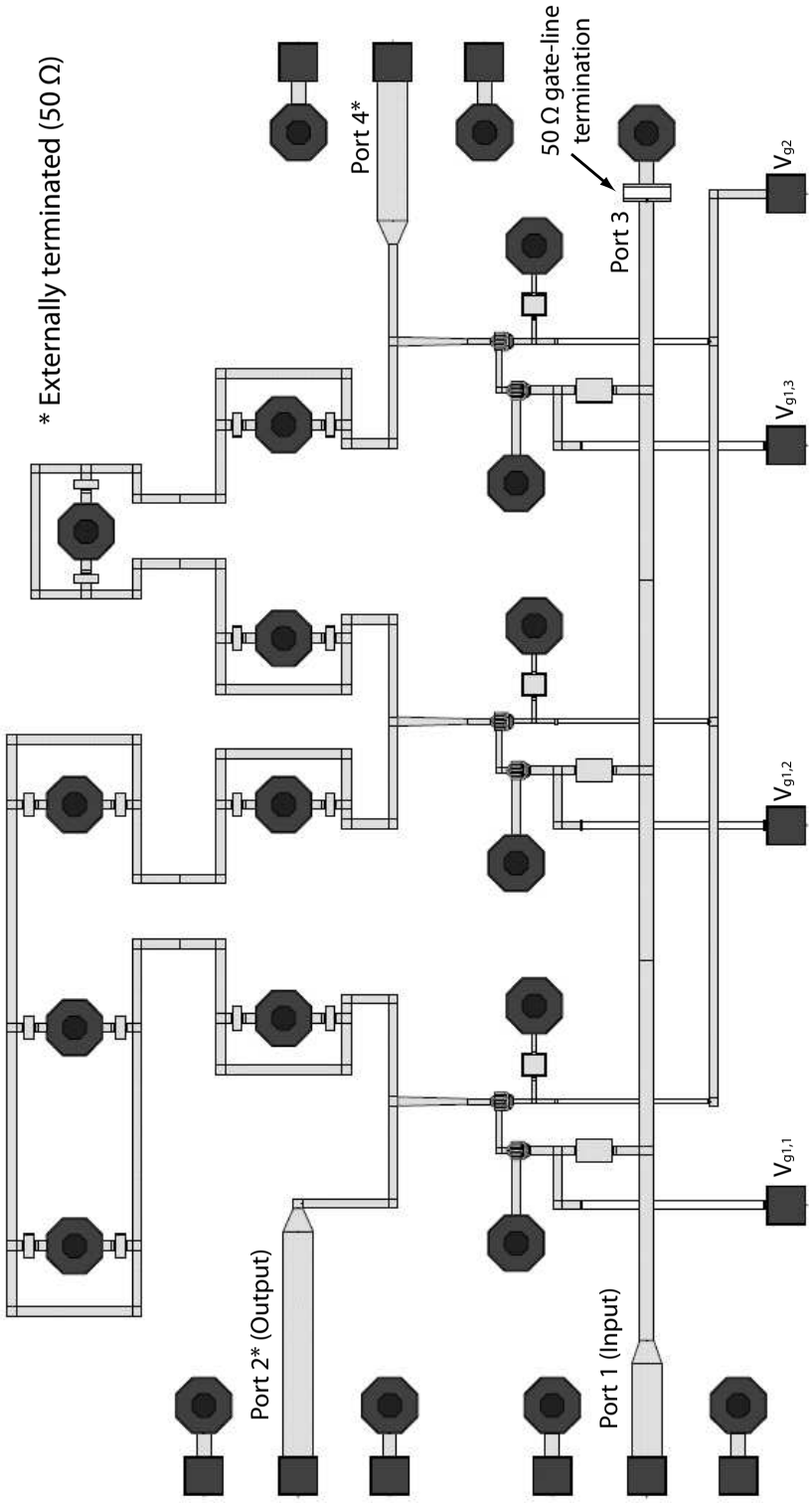

Figure 4.20: Layout of the MMIC Distributed Transversal Filter.

4.5 Performance of the MMIC Distributed Transversal Filter

The performance of the MMIC Distributed Transversal Filter is assessed through a study of its scattering parameters and temporal response.

4.5.1 Frequency Analysis

The behavior of the Distributed Transversal Filter in the frequency domain is essential to assess its capability to operate at high chip rates (40 GChip/s). The traditional scattering parameters are used to characterize microwave behavior. Problems such parasitic couplings, impedance mismatch, undesired reflections in the loads can be identified by analyzing such parameters.

Gain parameters

The gain parameter $S21$ is shown in figure 4.21. The ideal response plotted in grey was obtained by considering the Fourier transform of the ideal transversal filter which is given by:

$$H_F(\omega) = G_{max} \sum_{k=1}^{w} e^{-j\omega\tau_k} \tag{4.27}$$

with $\tau_1 = 0$, $\tau_2 = 75ps$ and $\tau_3 = 125ps$.

Figure 4.21 shows good agreement between theoretical and full model simulated response. The peaks and nulls of the frequency response are coincident up to 30 GHz where the dispersive effect of the lines moves the peaks and nulls to lower values than the ideal, resulting in minor divergence from the theoretical response.

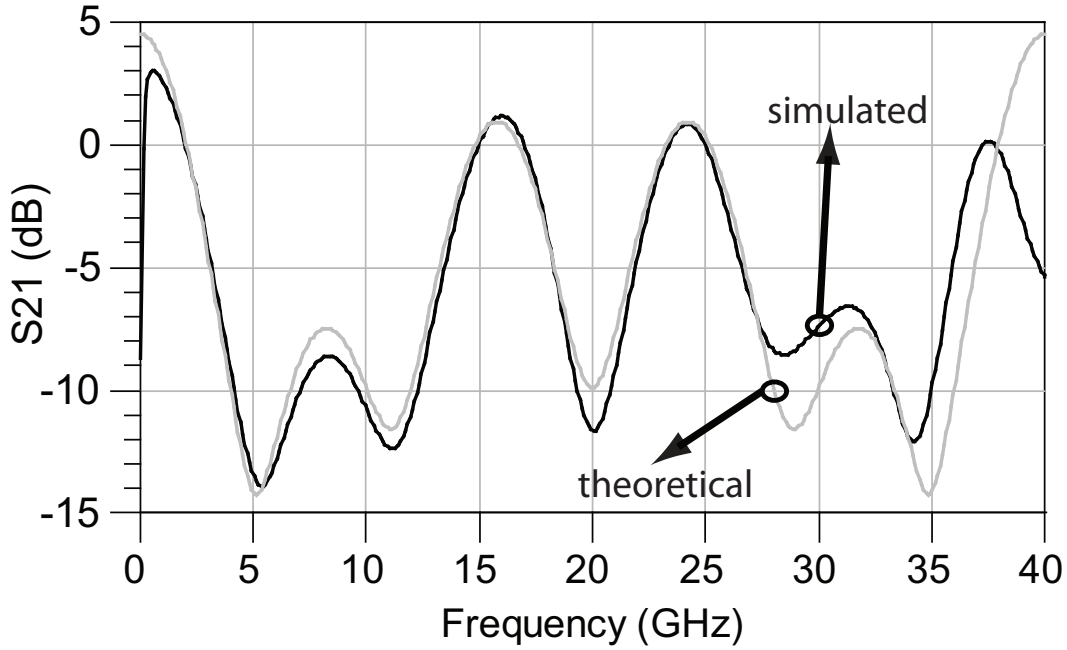

Figure 4.21: Gain parameter $S21$: theoretical (grey line) and simulated (black line).

Input and output port reflection parameters

The input port reflection parameter $S11$ is essential to assess the matching of the gate line. This is important since undesired reflections on this line will be amplified by all stages and distort the output. Similarly, the output port reflection parameter $S22$ is an indicator of the matching of the drain line.

In this design $S11$ was maintained below -10 dB up to 32 GHz while $S22$ is below -10 dB for almost all the bandwidth considered except for the frequencies between 27 and 31 GHz where it reaches a maximum of -8 dB.

The better behavior of $S11$ at low frequencies can be explained by the fact that the gate line is thicker (30 μm while the drain line is 20 μm) and shorter (approximately 2.5 mm for the gate line and 5 mm for the drain line), and therefore has lower losses than those of the drain line. At higher frequencies, the effect of the artificial transmission lines formed by the transistor parasitic capacitance and

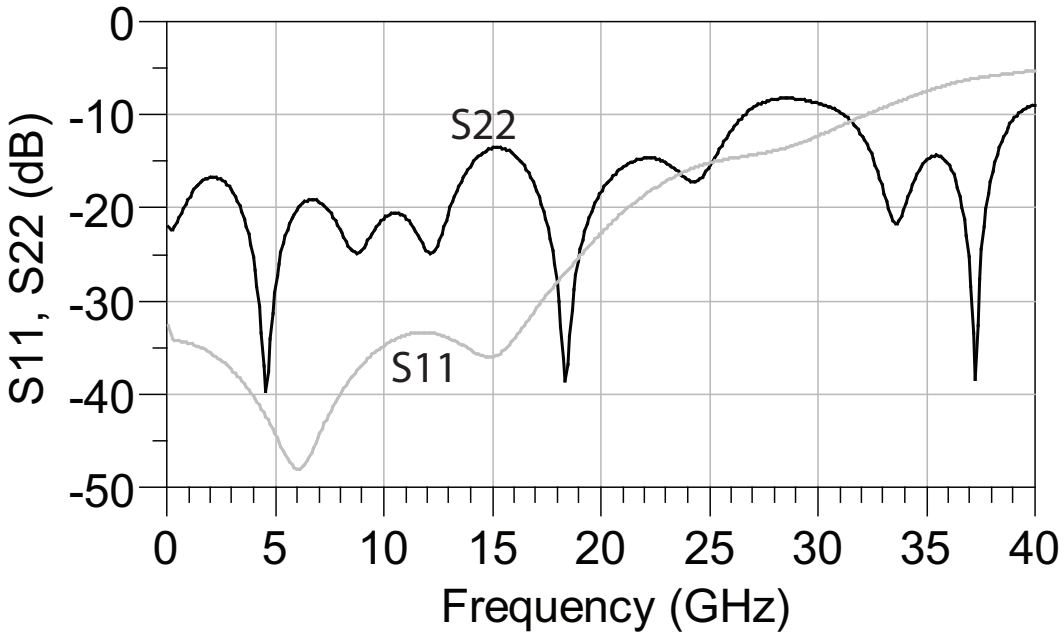

Figure 4.22: Input port reflection parameter $S11$ (grey line) and output port reflection parameter $S22$ (black line).

the microstrip inductor is dominant; since both lines are designed to have 50 Ω characteristic impedance, the higher input capacitance of each cascode stage, (relative to the lower output capacitance C_{ds}), results in a gate line with a lower cut-off frequency than that of the drain line, and therefore degraded $S11$ at high frequency. Nevertheless, the values obtained show suitability of operation at 40 Gchip/s.

Reverse transmission parameters

The Distributed Transversal Filter was designed considering the cascode stages as unilateral elements, i.e., no feedback is considered from the drain to the input gate line. Ideally, a perturbation in the drain line should not affect the input gate line. However, leakage in the transistors and other elements of the circuit, creates current paths between the output and input. The parameter $S12$ presented in

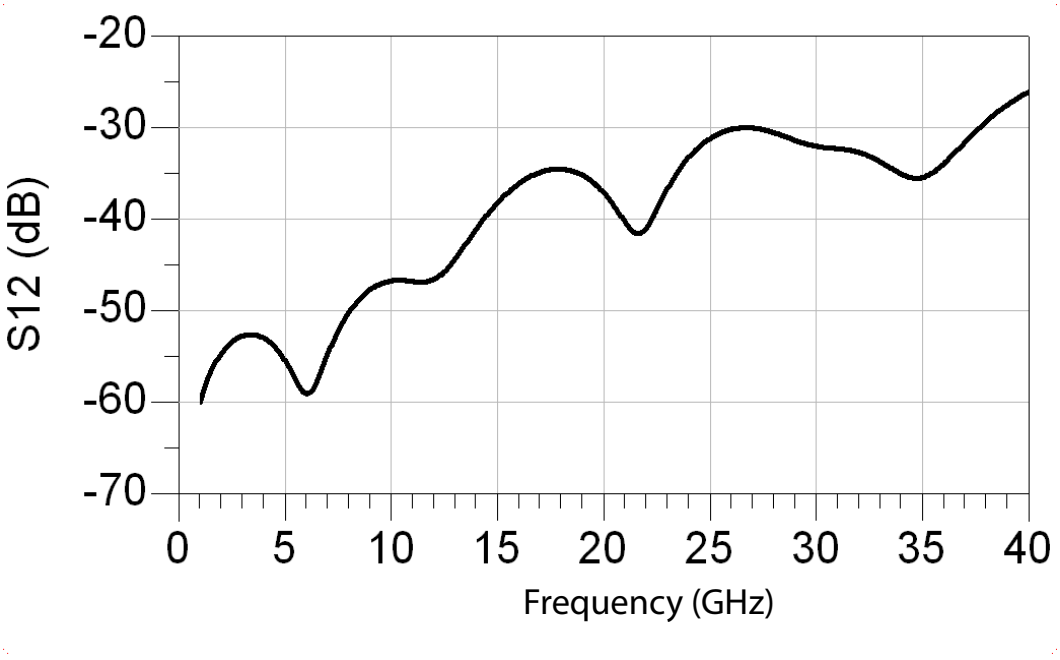

Figure 4.23: Reverse transmission parameter $S12$.

figure 4.23 is an indicator of the isolation of the output of the circuit. The isolation of the output was maintained below -30 dB until 38 GHz.

4.5.2 Temporal Analysis

The Distributed Transversal Filter described above is designed to satisfy a specific temporal response for high-speed encoding/decoding of a specific CDMA codeword. For this reason, the optimisation of the distributed circuit was mainly determined by the adjustment of the pulse response to the target response given by the equation:

$$x_{ENC}(t) = \sum_{k=1}^{w} G_k x_{in}(t - \tau_k). \tag{4.28}$$

Figure 4.24 shows the temporal response of the encoder for the sequence '1001010000' with single gaussian impulse with 1/e width of 25 ps and peak amplitude of 10 mV. Figure 4.24(a) shows the temporal response of the device

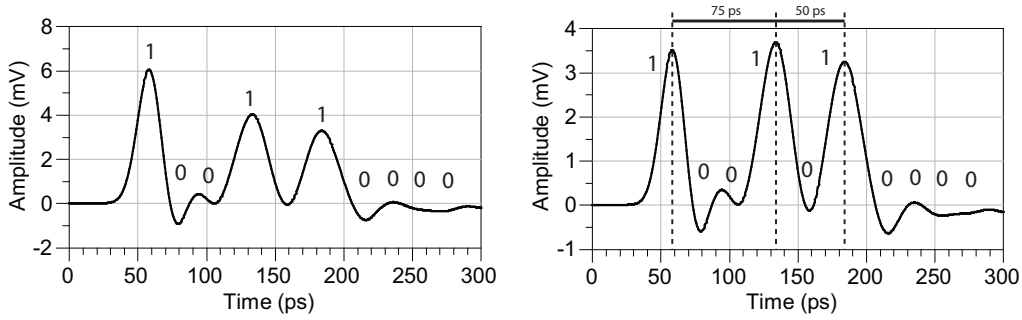

(a) Constant stage gains $V_{gs} = 0$ (b) Optimized stage gains

Figure 4.24: Temporal response of the encoder for the codeword "1001010000".

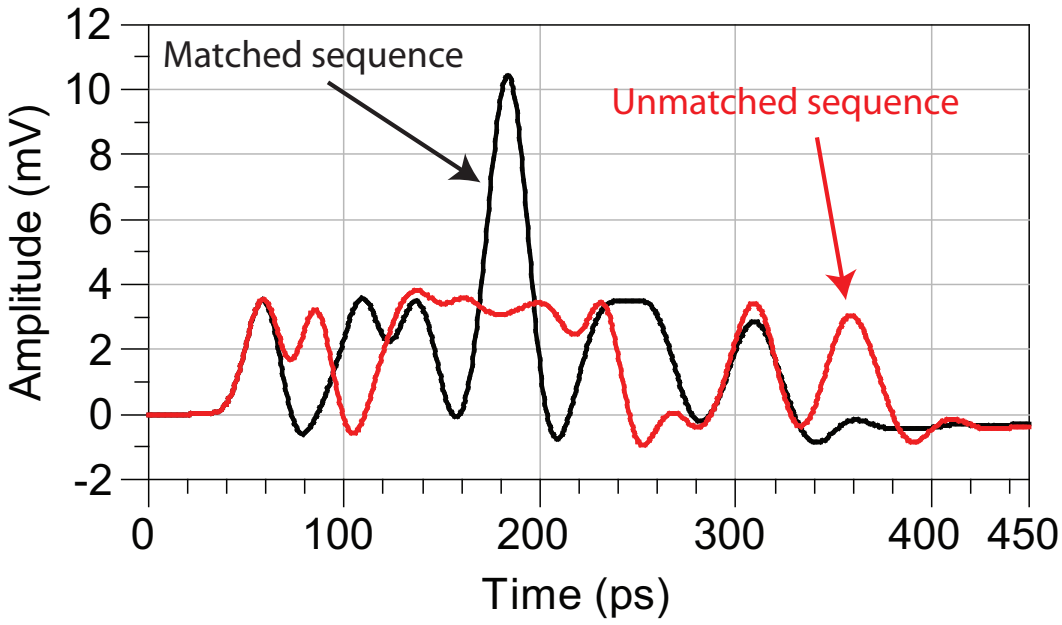

Figure 4.25: Temporal response of the correlator with the matched input sequence "1010010000" (black line) and the unmatched input sequence "1100000100" (red line).

with all stages under the same bias conditions ($V_{gs} = 0V$). This effectively means that drain and gate line attenuations are not compensated. This results in the most delayed chip (c_2 in this example) having half of the amplitude of the first chip (c_0). In a real CDMA over fibre network this would be an undesirable effect because the basic principle of these networks dictates that all chips in the codeword contribute with same amount of energy for the auto-correlation peak.

Figure 4.24(b) shows the distributed transversal filter with the gains adjusted to compensate line losses. The gate voltages were optimized to $V_{g1,1} = -0.45$, $V_{g1,2} = -0.3$ and $V_{g1,3} = 0.1V$. The figure also shows pulse broadening of 17 % and 30 % for the second and third pulses in relation to the first pulse. In fact, this is one of the main problem associated with this design; the reverse-mode topology associated with large interstage delays makes impossible to achieve constant pulse widths in the output. The chips amplified by the first stage have always narrower widths, as they suffer less line dispersion.

The same structure was tested as a correlator for the matched sequence "1010010000" and for an unmatched sequence "1100000100". The results presented in figure 4.25 indicate that the designed distributed transversal filter can operate as unipolar CDMA decoder. In fact, when the correct sequence is applied, an autocorrelation peak is generated with amplitude of **2.92** times the autocorrelation sidelobes. Note that an in an ideal correlator this ratio is three. Moreover, the DTF shows good characteristics in terms of rejection of an a unmatched codeword; the autocorrelation peak to maximum cross-correlation level is **2.74** (the ideal would yield three). These results show the appropriateness of the design technique and that it is possible to translate a theoretical/ideal design into a MMIC with less than 10 % error.

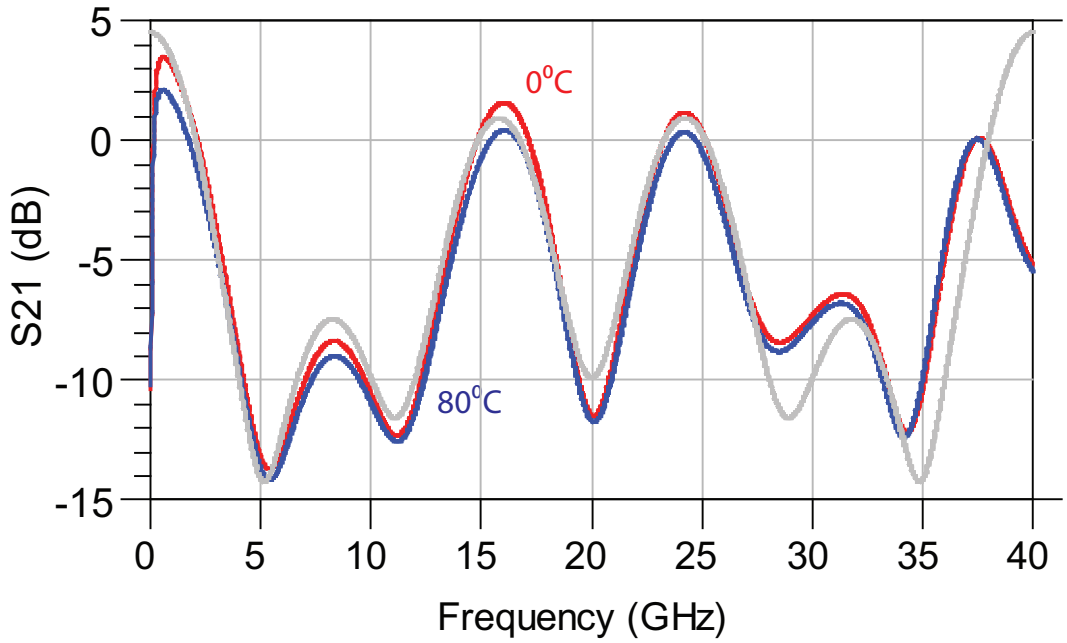

Figure 4.26: Gain parameter $S21$: theoretical (grey line) and simulated (black lines) for 0°C and 80°C.

4.5.3 Temperature Variation Studies

The thermal conductivity of Gallium Arsenide is about one third of that of the silicon [137] and therefore, circuits based on Gallium Arsenide are generally more tolerant to temperature variation than silicon CMOS circuits. Nevertheless, there are variations in the circuit performance that ougth to be considered. The results presented in the previous sections use a reference temperature of 27°C; in this section, simulation results for 0°C and 80°C will be shown.

Figure 4.26 shows the variation of the S-parameters with temperature. Note that there are differences particularly in the low frequency gain. The consequence of this is shown in figure 4.27, where the temporal response of the encoder is plotted. The amplitude of the signal is reduced by less than 7% for 80°C when compared with 0°C. Such minor variations can easily be compensated adjusting the bias of the transistors.

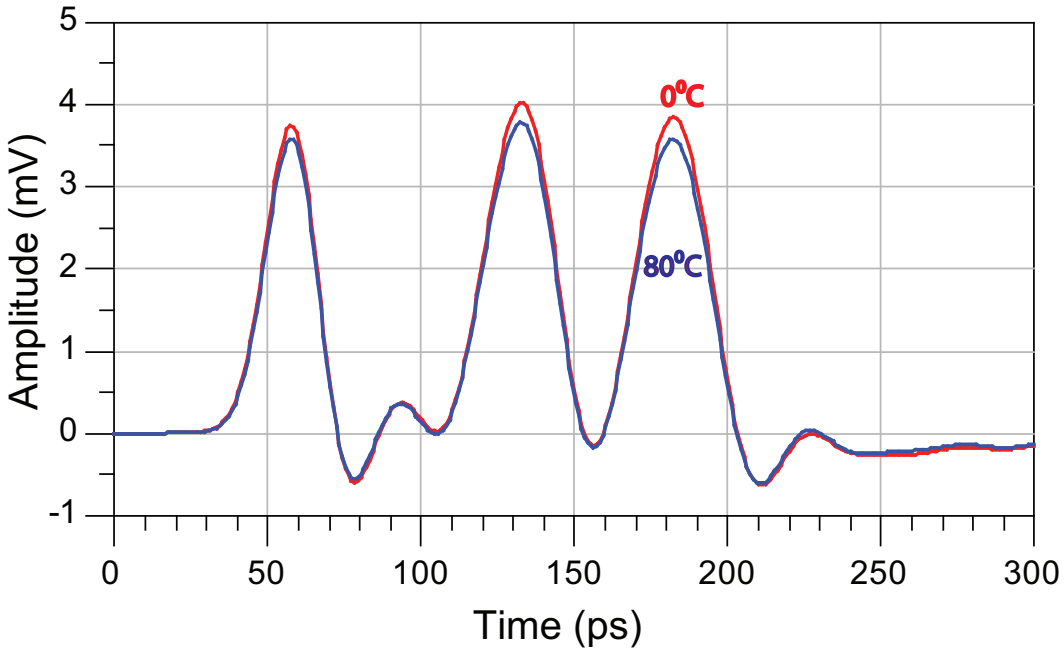

Figure 4.27: Temporal response of the encoder for the codeword "1001010000" for 0°C and 80°C.

4.5.4 Mismatch Variation

In this particular process, the variability of the capacitors is particularly high when compared to other circuit components; in fact, the wafer to wafer capacitor standard deviation is 4% while the stadard deviation within the same wafer is 0.4%[3]. Studies on variance of the capacitor values are included here, with the extreme assumption of wafer to wafer variation. The capacitors of the LC-sections are varied 5%. Figure 4.28 and 4.29 show the S-parameters and temporal response variation with capacitor values, respectivelly.

The variability of the transistor width is also considered in figures 4.30 and 4.31. For a range of variability of ±10%, it gives rise to less than 10% difference in the chip amplitude. It should be noted that the ±10% is an extreme indicator and is taken here in the absence of variation parameters in the design manual [10]

[3] NiCr resistor variation is 0.1% within the same wafer and other metal variations are stated as "negligected" in the design manual [10]

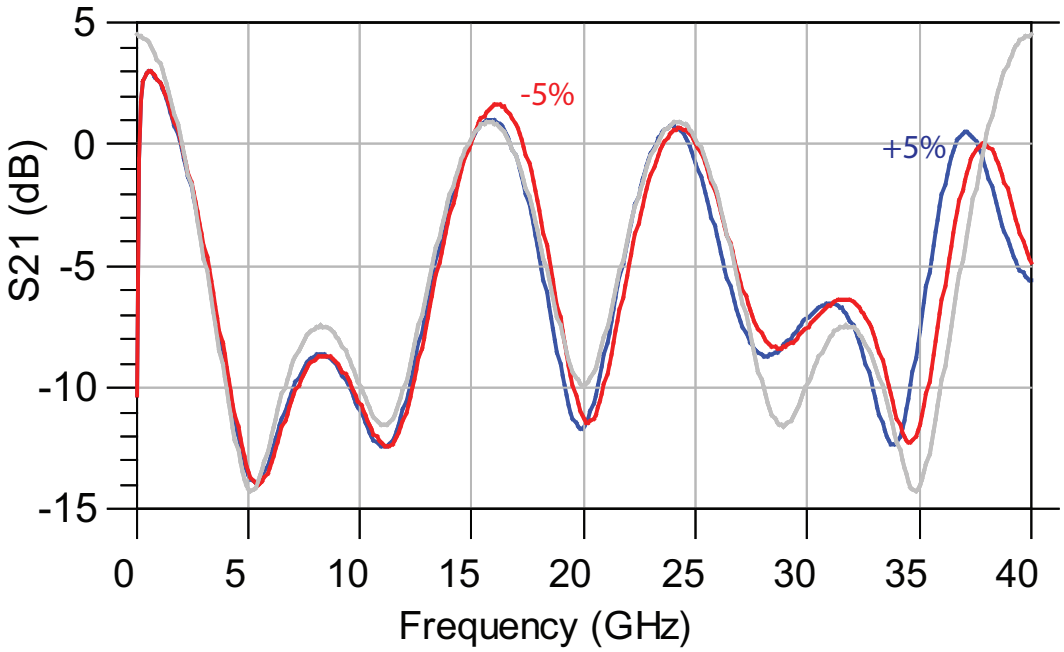

Figure 4.28: Gain parameter $S21$: for +5% and -5% in variation of the capacitors.

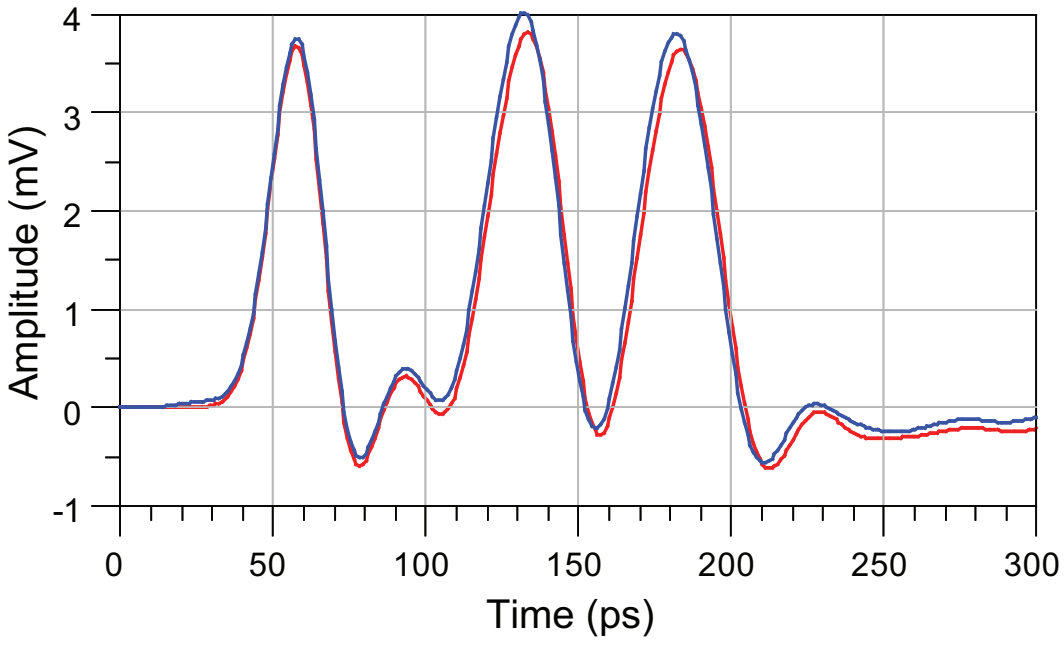

Figure 4.29: Temporal response of the encoder for the codeword "1001010000" for +5% and -5% in variation of the capacitors.

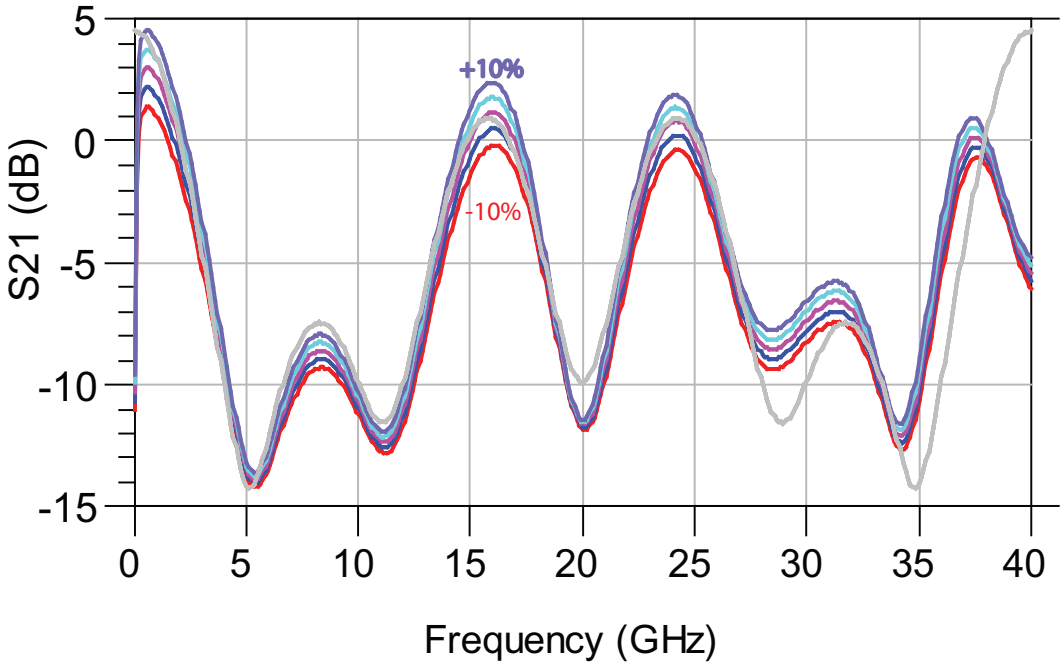

Figure 4.30: Gain parameter $S21$: for +10% and -10% in variation of the transistor dimensions (width).

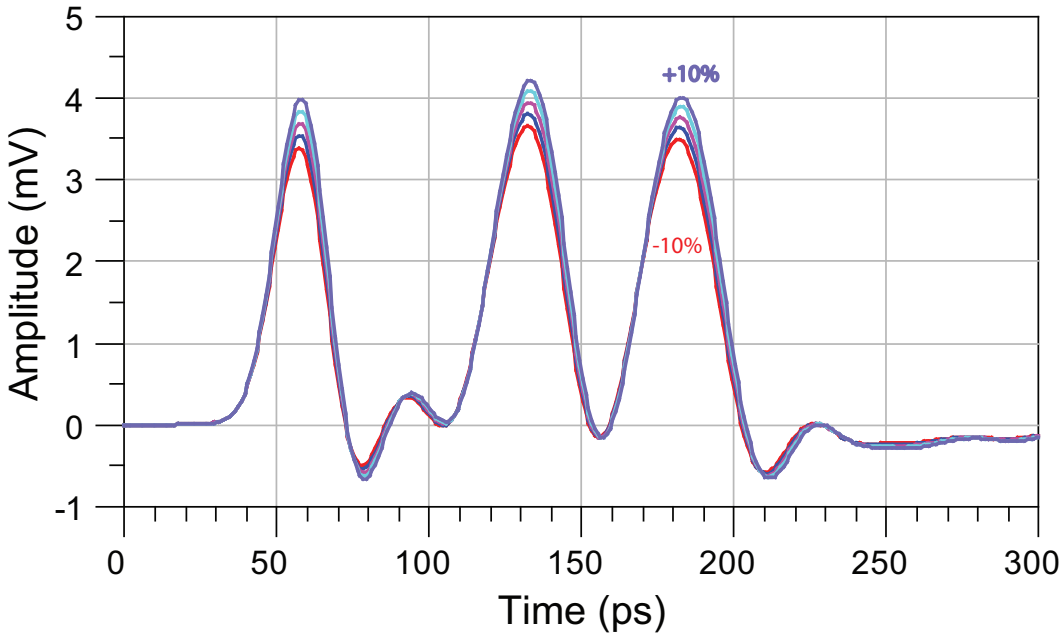

Figure 4.31: Temporal response of the encoder for the codeword "1001010000" for +10% and -10% in variation of the transistor dimensions (width).

and to illustrate the robustness of the proposed design.

4.5.5 Noise Considerations

Using ADS, the circuit noise figure, as well as the input and output noise spectral densities were simulated, taking into consideration the thermal noise generated by the resistive components and the combined thermal and shot noise components in the active devices. The simulation results for the noise figure are shown in 4.32. The noise figure is higher than what is generally found in distributed amplifiers mainly due to the lower gain provided by this structure [138] [139]. Moreover, distributed amplifiers require additional delays to "phase-match" the input and output lines. Such phase matching requires only short delay lines and results in increased gain and gain flatness. In the CDMA encoder/decoder distributed transversal filter, the large interstage delays required, to enforce the encoding/decoding functions and thereby create a deliberate phase mismatch, necessitate the use of extra inductors and capacitors which help create the required frequency response but result in increased losses.

The total noise input and output power spectral densities, in dBW/Hz, are shown in figure 4.33. It is worth noting the unusual characteristics of the noise behaviour where the output noise is occasionally lower than the input noise. This is attributed to the fact that the filter analysed here has attenuation peaks in its frequency response as is evident in the amplifier gain responce, depicted in figure 4.21 above. Figures 4.34(a) and 4.34(a) show the input noise current spectral density (in $pA/\sqrt{Hz}$) and the output noise voltage spectral density (in $nV/\sqrt{Hz}$). These figures are useful for predicting the minimum input signal levels. By numerical integration, over the DC to 40 GHz frequency range, the total input

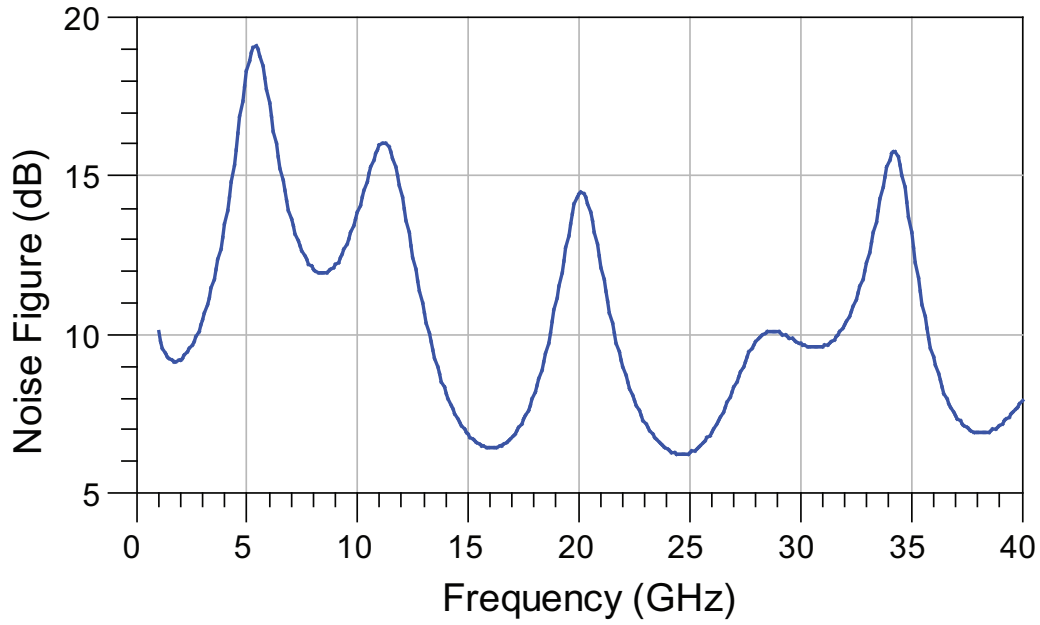

Figure 4.32: Noise figure.

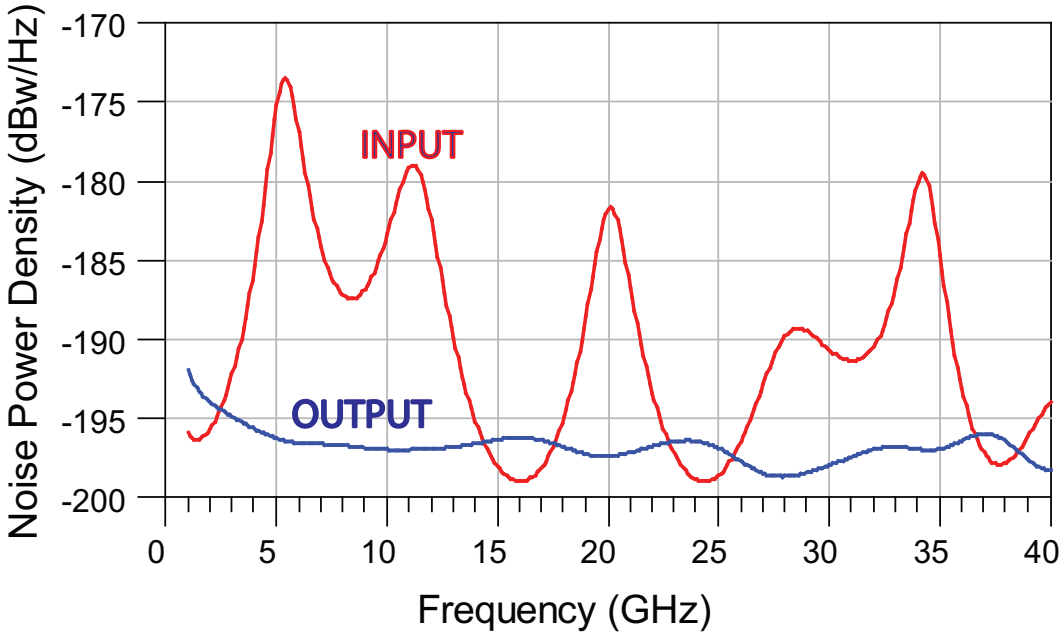

Figure 4.33: Noise power density.

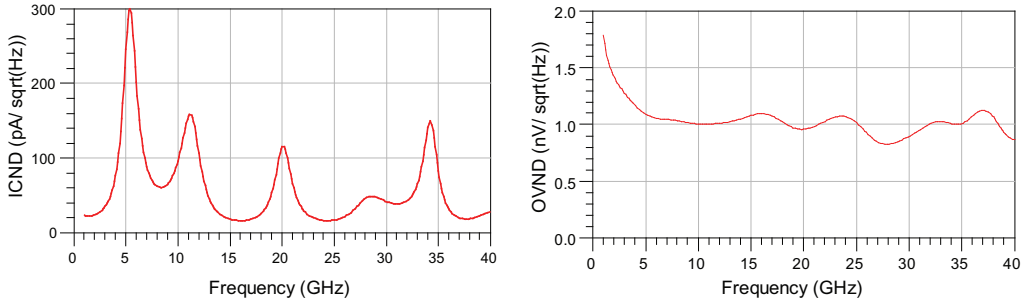

(a) Input Current Noise Density (pA/$\sqrt{Hz}$) (b) Output Voltage Noise Density (nV/$\sqrt{Hz}$)

Figure 4.34: Input Current Noise Density and Output Voltage Noise Density.

rms noise current and total output rms noise voltage are obtained to be 15.7 μA and 213 μV, respectively. The input noise current indicates that for chip error rates below 10^{-9}, the peak chip power required must be at least 12 times the rms noise-responsivity ratio [140] which, for a responsivity of 1 A/W, will be equal to 188 μW or -7 dBm. Again, these figures are higher than what would be expected from traditional distributed amplifier of a similar frequency operating range but without the encoding/decoding function [114]. Despite the high noise expected for the design, the input signal levels required for low error rate operation are easily achievable in local area networks, even without the use of optical amplifiers.

4.6 DTF with Switchable Delays

The structure presented in the previous chapter served as proof of concept for high-speed encoding/decoding of unipolar CDMA signals in the electronic domain. However, in contrast to the electronic devices of [4] [119] [124], this structure presents a major limitation that compromises its practical application: the device is designed to encode a specific codeword and decode its reciprocal and therefore is not flexible in terms of code selection. This motivated research in structures that allow reconfiguration for a range of CDMA codewords.

One possible solution could be the introduction of variable delay elements between gain stages; this can be done with switching devices able to turn on and off delay sections, so that the total delay between stages may be reconfigured as an integer multiple of the chip time. The switching time of these devices does not have to be particularly fast because it is intended to transmit/receive the same codeword for long periods of time; however, these devices are required to have low insertion losses in the ON state and high isolation for the OFF state.

Microelectromechanical systems (MEMS) switches are promising devices to perform this role. Devices operating from DC to 40 GHz with an insertion loss of 0.1 dB and isolation of 30 dB at 40 GHz have been reported [141]. The fabrication technology is versatile in terms of the substrate mainly due to the low temperature of the thin films deposited atop the substrate. Therefore, Gallium Arsenide, epitaxial Gallium Arsenide, silicon and quartz substrates were considered suitable for integration with this technology [141].

Moreover, MEMS switches found practical applications in broadband true time delays [142] and, more importantly for the sake of this thesis, it proved to be suitable for integration with GaAs pHEMT MMIC processes with minimal modifications in the fabrication process [143] [144]. However, to the author's knowledge, there are no commercial GaAs processes that include devices with such characteristics.

Another possible approach relies on the use of transistor switches. The basic common-base/gate configuration enables the use of a transistor as a switch. Although the insertion loss and isolation are worse than those of a MEMS switch, this solution can be easily implemented with an integrated circuit process.

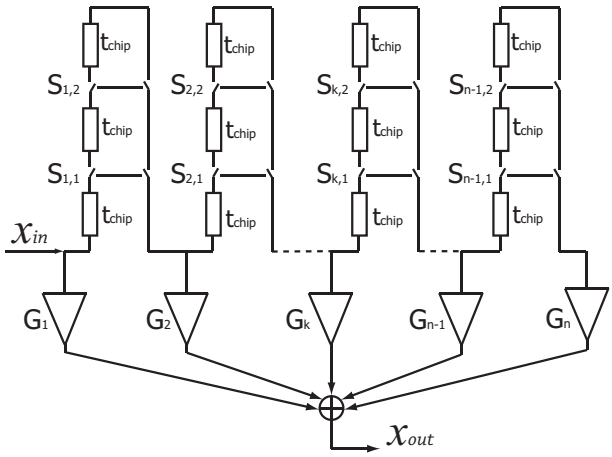

Figure 4.35: Transversal filter with switchable delays.

4.6.1 Concept

Figure 4.35 shows the block diagram of the transversal filter with switchable delays. The signal $S_{k,n}$ activates two switches and this results in a T_{chip} increase in the delay. For example, if the switch $S_{1,1}$ is activated and $S_{1,2}$ deactivated, the delay between stages one and two is $2 \times T_{chip}$. (50 ps for 40 GChip/s signaling). Note that the transversal filter can be implemented in a distributed form as presented in the previous sections.

4.6.2 Design with MMIC Process (ED02AH)

The Distributed Transversal Filter with switchable delays can be designed by replacing the additional delay sections T_1 and T_2 designed in the section 4.4.3 (figures 4.14 and 4.15) with the structure in figure 4.36.

The switching circuit operates as follows:

- When $V_B = 0V$ and $\overline{V_B} = -3V$, T1 and T2 are opened and T3 is closed. The signal path is open (low-impedance) to the following delay section,

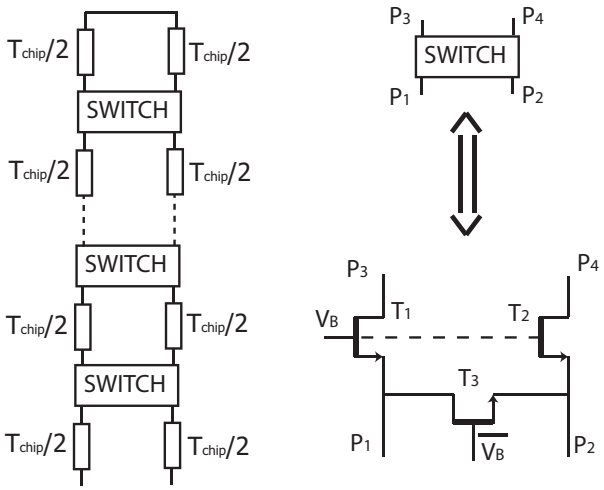

Figure 4.36: Transistor switch topology.

adding 25 ps to the inter-stage delay.

- When $V_B = -3V$ and $\overline{V_B} = 0V$, T1 and T2 are closed and T3 is opened. Therefore, the switching element creates a low impedance path between the two input lines and isolates the remaining delay sections.

A study of the practical feasibility of this approach was carried out through a circuit design exercise using the same MMIC process as that of the DTF design. The dimensions of the transistor switches were chosen considering the isolation of the OFF state ($V_B = -3V$) and insertion loss in the ON state ($V_B = 0V$). This is the main design trade-off, since a large transistor provides low insertion loss but that comes at expense of higher capacitance in the OFF state and higher leakage current. On the other hand, a small transistor gives rise to high resistance in the ON state. After optimisation, three four-finger pHEMTs were used; the width of each finger is chosen to be $20\mu m$. Figure 4.37 shows the proposed layout of the switch.

The characteristics of the four port switch are analyzed through the scattering

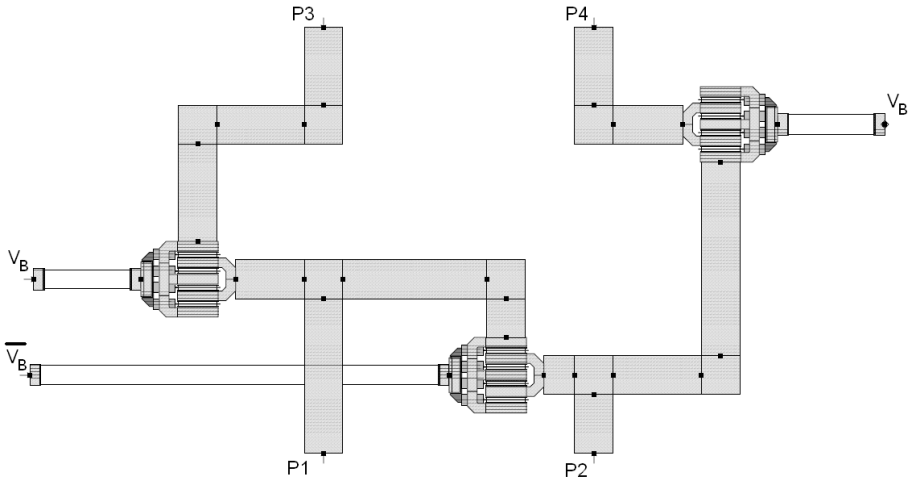

Figure 4.37: Possible MMIC layout of the switch with transistor implementation.

parameters $S11$, $S21$, $S31$ for both values of the control voltage V_B. Figure 4.38(a), 4.38(b) and 4.38(c) show the S-parameters of the switch when the $V_B = 0V$ and $\overline{V_B} = -3V$ and 4.38(d), 4.38(e) and 4.38(f) for the other state of the switch $V_B = -3V$ and $\overline{V_B} = 0V$.

Preliminary studies of the implementation of the DTF with such structures were not successful. The attenuation in the drain line produced by the switches could not be compensated by adjustments in the gain of the amplifier stages. For example, when $V_B = 0\ V$, the electronic signal will pass through port 1 to 3 and then from 4 to 2. The accumulated attenuation in both paths is 4dB for only one section. A DTF with such switches gives rise to an unacceptable temporal response.

The practical implementation of such design ideas requires the use of switches with insertion losses in the order of very few tenths of a dB. Moreover, this topology requires that all inter-stage delay elements include a number of T_{chip} delay elements equal to the maximum distance between ones in any CDMA codeword. This can impose an important limitation in terms of the circuit size. For exam-

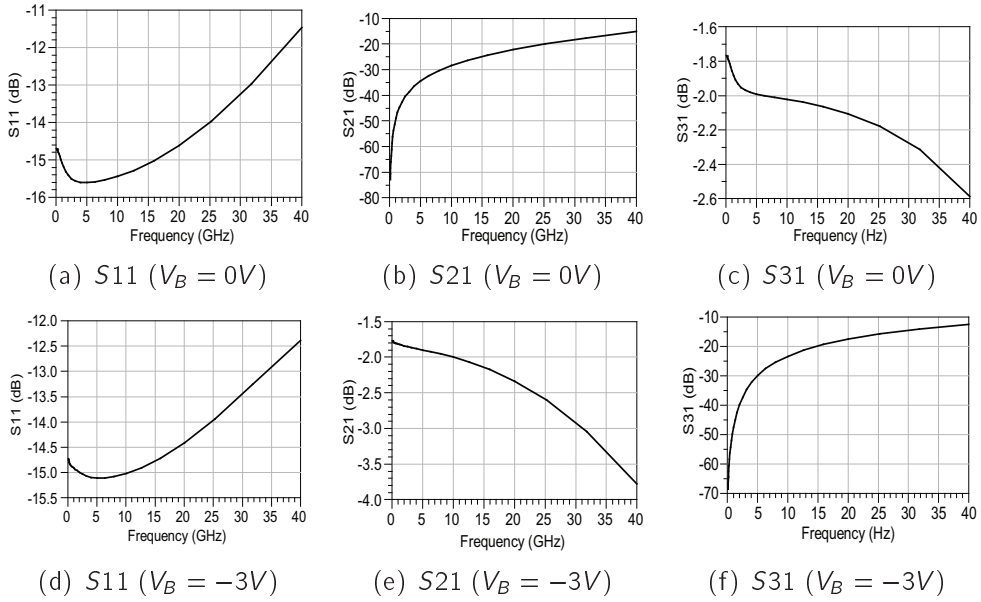

(a) $S11$ ($V_B = 0V$) (b) $S21$ ($V_B = 0V$) (c) $S31$ ($V_B = 0V$)

(d) $S11$ ($V_B = -3V$) (e) $S21$ ($V_B = -3V$) (f) $S31$ ($V_B = -3V$)

Figure 4.38: Scattering parameters of the transistor switch ((a-c) - ON state; (d-f) - OFF state).

ple, the 25 ps element designed in section 4.4.3 (structure 1) has dimensions $900\mu m \times 450\mu m$. Considering that foundry rules do not allow integrated circuits with dimensions exceeding $4500\mu m \times 4500\mu m$ and that the DTF, switches and connection pads occupy at least half of the circuit area, no more than 25 delay sections could be employed in the circuit.

4.7 Time-Wavelength Electronic Encoders and Correlators

In the previous sections, wideband distributed transversal filters for multi-GBit/s applications were proposed. Appropriate selection of the gains and delays enables our designs to operate as time-domain CDMA encoders and decoders. However, there are two main limitations associated with this solution.

Firstly, there is an intrinsic problem associated with time-domain incoherent

Optical CDMA. As explained in the chapter 2, a network supporting high number of users demands codewords with high number of chips. Since the length of the codeword is inversely proportional to the bitrate, these networks tend to have very low spectral efficiencies.

The second problem is associated with practical limitations in the circuit design. In fact, the distributed transversal filter is based on artificial transmission lines and additional delay lines which are dispersive and lossy, as seen in the section 4.5.2. In order to keep the propagation characteristics within reasonable limits, the number of stages and delay elements is limited.

These two limitations led the investigation in structures capable of encoding and decoding time-wavelength Optical CDMA codes. Traditionally, all-optical devices have been used to encode and decode time-wavelength CDMA signals with special emphasis in techniques relying on the use of Fibre Bragg Gratings arrays [1] [63] [64]. These structures are claimed to provide cost-effective and flexible solutions to perform such functions [5].

However, there are several drawbacks associated with all-optical proposals and FBG based solutions in particular. Unlike electronic integrated circuits, there are not many commercial applications for FBGs and therefore the fixed costs involved in their manufacturing cannot be shared among different users/applications. Note that the costs involved in the individual manufacturing of a Fibre Bragg Grating array are not particularly high because it only requires photo-sensitive fibre which, although more expensive than standard single mode fibre or dispersion shifted fibre, is still cheap. However, printing FBGs requires very precise lasers and instrumentation. Therefore, the costs involved in building a dedicated facility to fabricate FBGs could compromise its commercial viability.

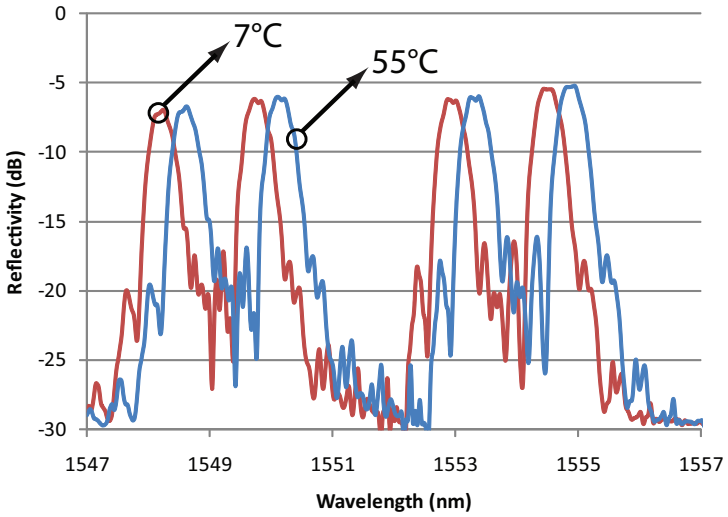

Figure 4.39: FBG array variation with temperature.

Moreover, Fibre Bragg Gratings are very susceptible to environmental variations such as physical stress and temperature. These characteristics may be advantageous as they allow individual tuning of the Fibre Bragg Gratings [1] but can also be a serious drawback in environments where strict control of physical stress and temperature are not possible. For example, figure 4.39 shows the experimental results of the temperature variation of a Fibre Bragg Grating array for Optical CDMA encoding/decoding designed for use in the experiments described in chapter 6. A variation of about 0.4 nm in the peak reflectance is clear for a temperature variation from 7°C and 55°C.

This section proposes a new concept of encoding/decoding time-wavelength CDMA signals in the electrical rather than in optical domain. The design philosophy is based on the same distributed principles, but the structures have multiple inputs for the receiver and multiple outputs for the transmitter.

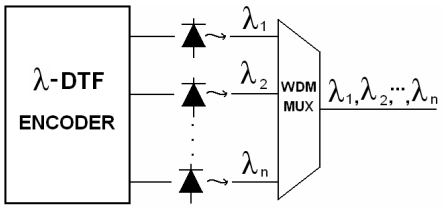

Figure 4.40: Multi-wavelength Optical CDMA transmitter.

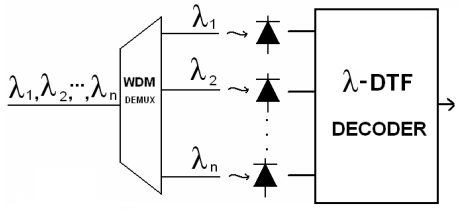

Figure 4.41: Multi-wavelength Optical CDMA receiver.

4.7.1 Design Concept

Figures 4.40 and 4.41 show schematics of the Optical CDMA transmitter and receiver, respectively. While in the previous sections (time-domain CDMA) the encoder and decoder used similar electronic structures, the transmitter and the receiver topologies for time-wavelength CDMA possess substantial differences. The encoder of the Optical CDMA system generates a fast unipolar sequence in each output when a pulse of width T_{chip} is applied; each sequence modulates an optical transmitter device. The correlator should be able to generate a correlation peak whose amplitude is proportional to the total number of "positive" chips, when matching sequences are applied in each of the device inputs.

We define a (λ,n,w) code as a family of time-wavelength unipolar codes with λ wavelengths, each containing a temporal sequence with chip length n and weight (i.e. number of "positive" chips) w per wavelength. Note that w is different from what is referred to as the "weight of the code" which is equal to the product $\lambda \times w$ and which, for a time-domain optical orthogonal code, described the code figure of merit. Each CDMA user is assigned a codeword defined by the following $\lambda \times w$ matrix:

$$\begin{pmatrix} a_{1,1} & a_{1,2} & \dots & a_{1,k} & \dots & a_{1,w} \\ a_{2,1} & a_{2,2} & \dots & a_{2,k} & \dots & a_{2,w} \\ \dots & \dots & \dots & \dots & \dots & \dots \\ a_{j,1} & a_{j,2} & \dots & a_{j,k} & \dots & a_{j,w} \\ \dots & \dots & \dots & \dots & \dots & \dots \\ a_{\lambda,1} & a_{\lambda,2} & \dots & a_{\lambda,k} & \dots & a_{\lambda,w} \end{pmatrix}$$

with $a_{j,k+1} > a_{j,k}$ and $a_{j,k} < n$ where each element of the array is the position of a "positive" chip in the sequence j. The user transmits data bit "one" by sending its λ sequences (each represented in a row of the matrix) in the time T_{bit} ($T_{bit} = n\ T_{chip}$).

The designs proposed in this thesis are based on the use of single input multiple output DTF for the encoder, and multiple input single output DTF structures for the decoder. In all cases the DTF is designed with unit delay elements of T_{chip} or its integer multiples. The basic design ideas are described below.

Encoder

For simplicity, figure 4.42 shows the CDMA encoder for only two wavelengths. The encoder comprises two distributed transversal filters sharing a common input line (gate line for transistor implementations). In a more generalized case, λ drain lines may share the common gate line. The delay per section is defined as the sum of delays in the input and the output lines: $t_{j,k} = t_{gk} + t_{dj,k}$.

The encoder of the Optical CDMA system generates two fast unipolar sequences in each output, each will be used to modulate a separate optical source, when a pulse with width T_{chip} is applied. In order to achieve this, the delay of

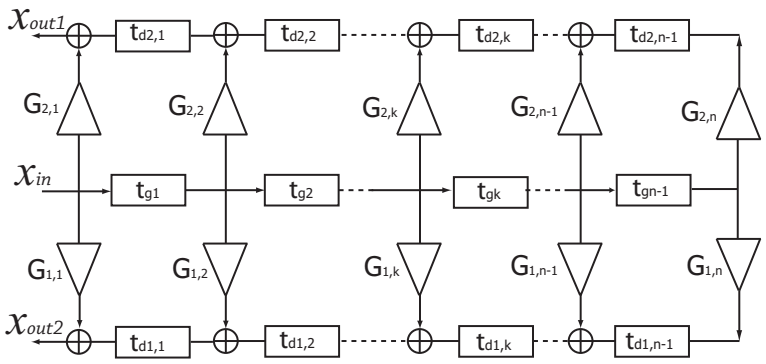

Figure 4.42: Block diagram of the 2D time-wavelength encoder.

each stage of the DTF is defined as follows:

$$t_{j,k} = (a_{j,k+1} - a_{j,k})T_{chip}. \tag{4.29}$$

Hence, the time-domain response of the encoder for each sequence j may be represented as:

$$x_{out_j}(t) = \sum_{k=1}^{w} G_{j,k}x_{in}(t - (a_{j,k} - a_{j,1})T_{chip}). \tag{4.30}$$

Correlator

The correlator is designed to generate an autocorrelation peak whose amplitude is proportional to the total number of "positive" chips when the two correct sequences (received on two different wavelengths) are applied, to each of its inputs. As shown in figure 4.43, the topology comprises two distributed transversal filters sharing a common output line (drain line for transistor implementations). In the generalized case, λ gate lines share the common drain line. The delay of each stage of the DTF is defined as follows:

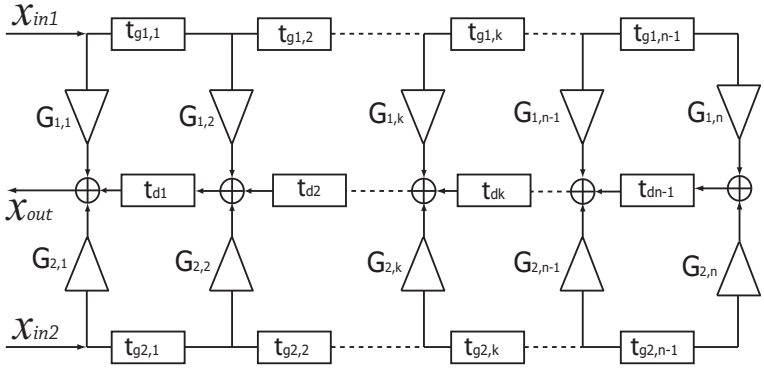

Figure 4.43: Block diagram of the 2D time-wavelength correlator.

$$\tau_{j,k} = (a_{j,w-k+1} - a_{j,w-k})T_{chip}. \tag{4.31}$$

Hence, the time-domain output response of the decoder is given by:

$$x_{out}(t) = \sum_{j=1}^{\lambda} \sum_{k=1}^{w} G_{j,k} x_{in_k}(t - (a_{j,w} - a_{j,w-k-1})T_{chip}). \tag{4.32}$$

4.7.2 Circuit Design Considerations

The time-wavelength encoders and correlators were designed with the ED02AH pHEMT process used for the time domain distributed transversal filter presented in the previous sections. The structures here presented are a generalisation of the one dimensional structure based on the same distributed principles. For concept verification purposes, structures with two wavelengths are designed.

Figure 4.44 shows the simplified circuit diagram of the encoder for two independent outputs, enabling the driving of two separate light emitting devices transmitting at different wavelengths. Two cascode stages are connected to the same point in the gate line which means that the capacitance is twice of that of a single cascode stage. Therefore, the combination of inductances L_g and

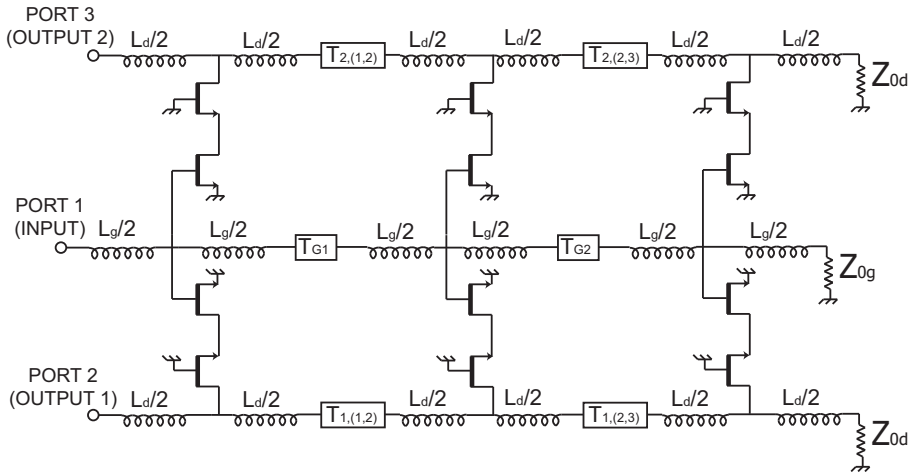

Figure 4.44: Schematic of the 2D time-wavelength MMIC Encoder (bias circuit not shown).

the combined input capacitances of two cascode stages ($2C_{in}$) forms an artificial transmission line (ATL) with characteristic impedance $Z_{0g} = \sqrt{\frac{L_g}{2C_{in}}}$. Similarly, $Z_{0d} = \sqrt{\frac{L_d}{C_{out}}}$ is the characteristic impedance of the drain line formed by the inductance L_d and the output capacitance of the cascode. In this design both characteristic impedances are set to be equal to 50Ω.

Figure 4.45 shows the simplified circuit diagram of the correlator for two independent inputs (corresponding to two separate optical carriers and two detectors). In this structure, the outputs of all cascode stages are connected to a single output line. This shared output artificial transmission line has a characteristic impedance of $Z_{0d} = \sqrt{\frac{L_d}{2C_{out}}}$. The characteristic impedance of the gate lines, formed by the inductance L_g and the output capacitance of the cascode, is $Z_{0g} = \sqrt{\frac{L_g}{C_{in}}}$. Similar to the encoder the characteristic impedances are set to be equal to 50Ω.

Additional inter-stage delay elements have to be inserted in the gate and drain lines so as to satisfy the temporal response criteria. In the encoder, the additional delays associated with the gate line (T_{G1} and T_{G2} in the figure 4.44) are designed to achieve one chip delay time, i.e., their group delay is the difference between

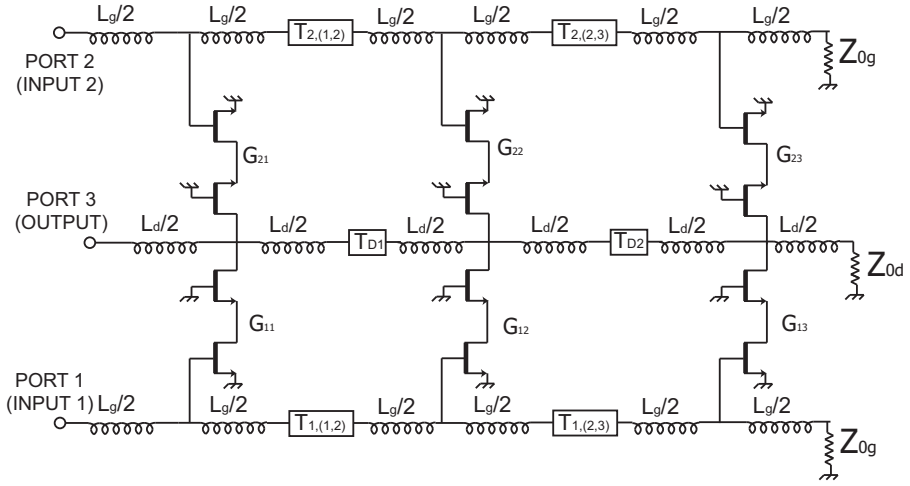

Figure 4.45: Schematic of the 2D time-wavelength MMIC Correlator (bias circuit not shown).

the sum of the intrinsic delays of the gate and drain artificial transmission lines, and T_{chip}:

$$T_G = T_{G1} = T_{G2} = T_{chip} - \sqrt{2L_gC_{in}} - \sqrt{L_dC_{out}}. \tag{4.33}$$

Therefore, T_{G1} and T_{G2} are independent of the codeword that is being encoded. The additional delays in the gate line are integer multiples of T_{chip} chosen according to the number of zeros between consecutive ones in the Optical CDMA codeword. In the correlator, the drain line additional delays are used to implement the difference between the ATLs intrinsic delay and T_{chip} while the delays associated with the codewords are implemented in the gate line:

$$T_D = T_{D1} = T_{D2} = T_{chip} - \sqrt{2L_dC_{out}} - \sqrt{L_gC_{in}}. \tag{4.34}$$

These additional inter-stage delay elements could be implemented using matched microstrip transmission lines (i.e. with characteristic impedance equal to that of the drain ATL), taking advantage of the flat group delay provided by such structures. Alternatively, it is possible to build an artificial transmission line by peri-

odically placing additional capacitors in a microstrip line with high characteristic impedance, the option taken in section 4.4.3. This provides reasonable time delays and chip area at the expense of slight signal distortion. As the system was designed, it became clear that it would not be possible to fit the layout in the $4.5 \times 4.5\text{mm}^2$ maximum allowed circuit dimensions. Therefore, the results presented in this section correspond to pre-layout simulations. The gain stages were designed as cascode stages with full foundry model but with ideal links connecting the transistors (unlike in the single wavelength design described earlier in this chapter). In these designs, microstrip transmission lines with $Z_0 = 50\Omega$ were used to implement the additional delays.

4.7.3 Results

The results were obtained through pre-layout full device and circuit level simulations for 40 GChip/s. The characteristics of all elements are taken in account but, since the layout was not implemented, the electromagnetic losses due to the geometry of the integrated circuit are not considered, unlike for the integrated circuit presented in the previous sections. Therefore, the results presented here should be interpreted as proof-of-concept rather than final expected results.

Encoder

Figure 4.46 shows the temporal response of the two outputs of the encoder. Output 1 is tuned for the sequence '10001001' and output 2 corresponds to the sequence '10001100'. The input is modeled as a Gaussian pulse with 25 ps at the 1/e amplitude point and 10 mV peak amplitude.

The simulated gain parameter $S21$ is compared to the theoretical projections in

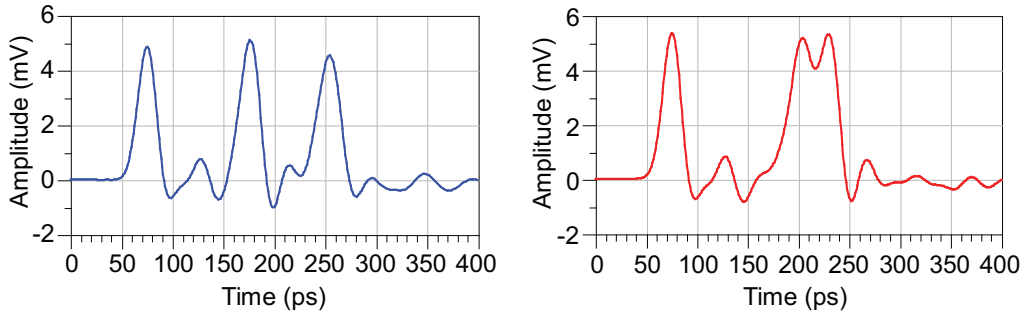

(a) Encoder output 1 - sequence "10001001" (b) Encoder output 2 - sequence "10000110"

Figure 4.46: Temporal response of the 2D time-wavelength MMIC encoder.

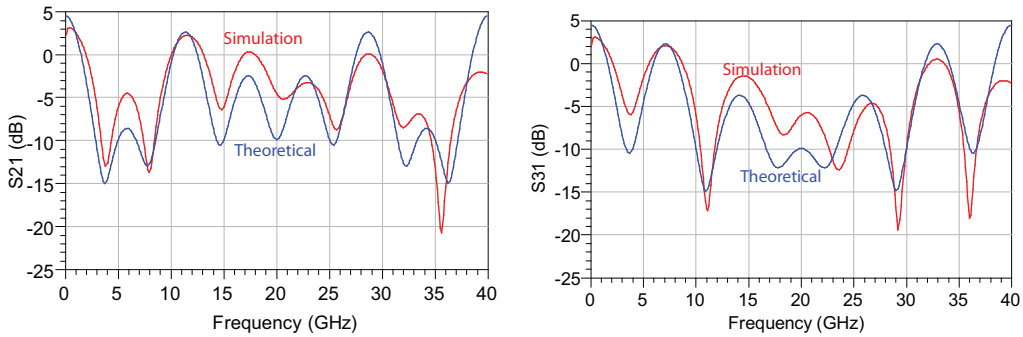

(a) Encoder output 1 - sequence "10001001" (b) Encoder output 2 - sequence "10000110"

Figure 4.47: Frequency response of the 2D time-wavelength MMIC encoder.

figures 4.47(a) and 4.47(b) for the outputs 1 and 2, respectively. The theoretical response of each input is effectively the frequency response of each transversal filter which is:

$$H_F(\omega) = G_{max} \sum_{k=1}^{w} e^{-j\omega\tau_k}. \tag{4.35}$$

For the output 1 the delay parameters are $\tau_1 = 0$, $\tau_2 = 100ps$ and $\tau_3 = 175ps$. For the output 2 they are $\tau_1 = 0$, $\tau_2 = 125ps$ and $\tau_3 = 150ps$.

The temporal responses in figure 4.46 present a maximum ripple of 12 %; this exceeds the ripple obtained in the time domain designs. This is particularly concerning since the modelling results here presented do not include electromagnetic (MOMENTUM^{TM}) simulations and uses adapted microstrip lines instead of

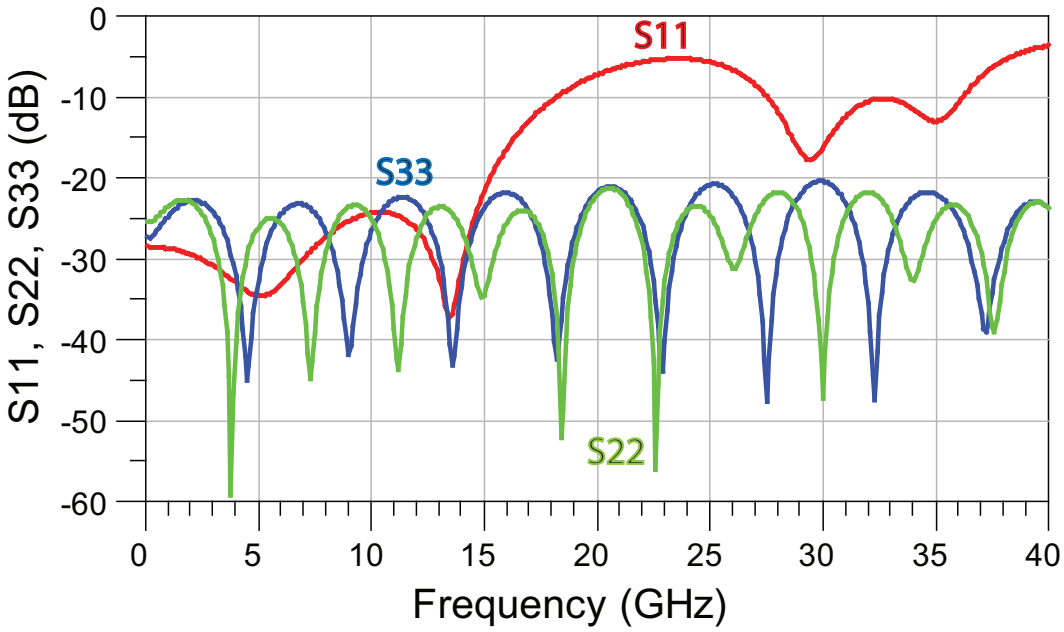

Figure 4.48: Input and output reflection parameters of the encoder.

LC-sections for designing the additional delay elements.

A study of the S-parameters, shown in Figure 4.48, helps understanding the source of such behavior. This figure shows the results of the reflection parameters of the circuit. It is possible to see that the parameter $S11$ is much worse than the one presented in the previous time-domain CDMA design depicted in figure 4.22. This is due to the higher capacitance associated with the gate line that is double that of a single transversal filter stage. In fact, this is one of the main limitation associated with the time-wavelength CDMA encoder proposed in this section. The capacitance of each ATL section increases proportionally with the number of wavelengths in the system, which compromises the propagation characteristics in the gate line and therefore the overall performance of the circuit.

Figure 4.48 also shows good propagation characteristics of the drain lines that remain below 20 dB from DC to 40 GHz. Note however that it is predictable that using LC-section and considering EM losses of such structures, the characteristics

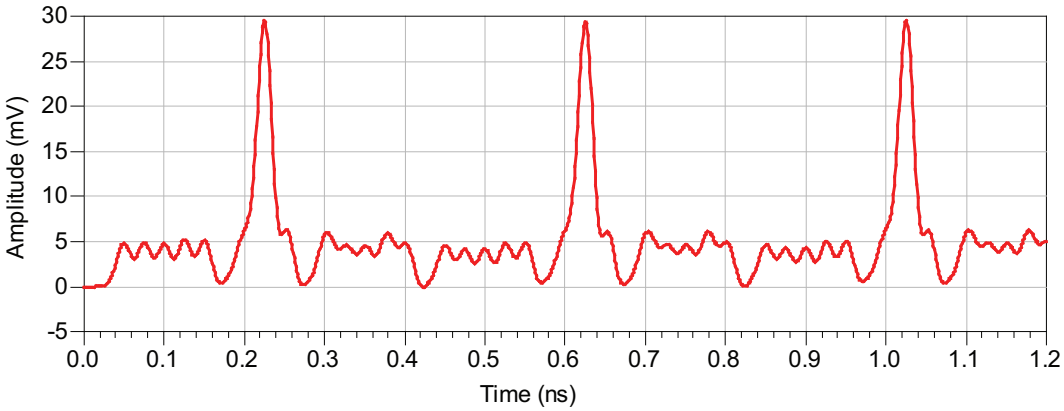

Figure 4.49: Temporal response of the MMIC correlator with matching input sequences "11000010" and "10010001".

of such lines could be degraded.

Correlator

Figure 4.49 presents the temporal response of the correlator with matching sequences applied at the inputs - "11000010" at input 1 and "10010001" at the input 2. Each chip is a Gaussian pulse with 25 ps width at 1/e amplitude point and 10 mV peak amplitude. The response comprises three consecutive bits using guard time equal to the length of the codeword, as done in [58].

Figure 4.50 shows the simulated gain parameters compared with theoretical /ideal predictions. These are obtained through the equation 4.35, by considering two transversal filter sharing a common output line. The delays considered for such transversal filter are the reciprocal of the sequences that they are intended to decode. Therefore, for input 1, the delays are $\tau_1 = 0$, $\tau_2 = 25$ ps and $\tau_3 = 150$ ps while for the input 2 they are $\tau_1 = 0$, $\tau_2 = 75$ ps and $\tau_3 = 175$ ps.

From figure 4.49 one can see that the correlation peak has 29.6 mV amplitude for input chips with 10 mV. Since the level of the autocorrelation sidelobes generated in the correlation process is 5.9 mV, the figure of merit of the correlator

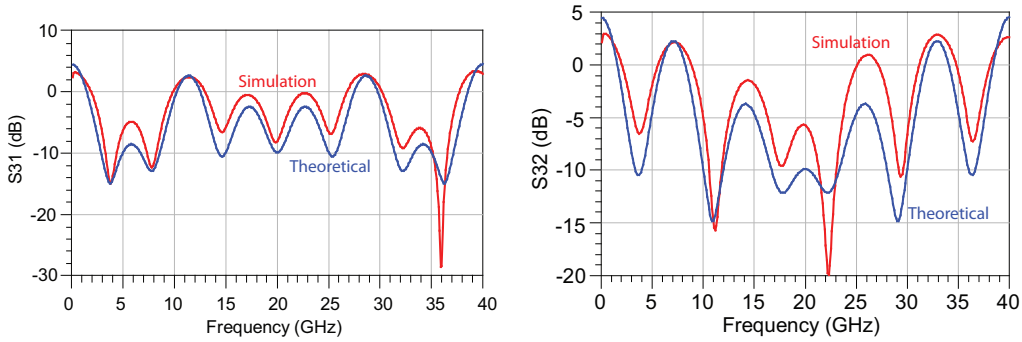

(a) Correlator input 1 (b) Correlator input 2

Figure 4.50: Frequency response of the 2D time-wavelength MMIC correlator.

is approximately five; the ideal correlator would achieve a figure of merit of six which is the total weight of the code (two wavelengths each with w=3).

Figure 4.51 shows the reflection parameters of the input and output ports of the 2D time-wavelength correlator. Unlike the encoder, all parameters are below -10 dB for the frequency range of DC to 40 GHz. In fact, the correlator has better reflection characteristics than the encoder. The reason is attributed to the fact that, for the encoder, two transversal filters share a common gate line whilst the decoder's two transversal filters share a drain line. Since the ATL gate capacitance is always higher than the capacitance associated with the drain ATL, it is more difficult to match the gate line, especially across a wide range of frequencies. For example, in this design, even using capacitive coupling technique, the input capacitance of the cascode stages was found to be between 50 and 70 fF. The output capacitance is 20 fF. This gives more flexibility in the design of the correlator than in the encoder. The figure also shows that the drain line has worse characteristics throughout frequency range from DC to 40 GHz. It is also interesting to note that, although both output ports have good reflection behaviour, $S11$ and $S22$ have slight differences. This is due to the fact that each section of the line decodes a different code and therefore employs different delay

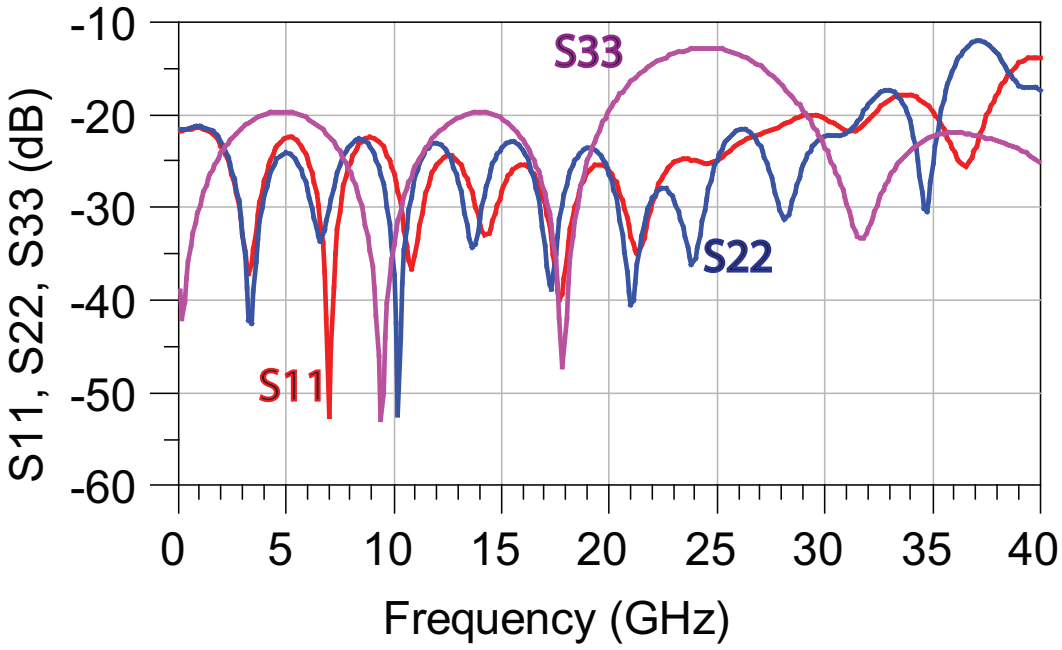

Figure 4.51: Input and output reflection parameters of the correlator.

elements leading to different responses.

4.8 Discussion and Summary

This chapter presented new electronic circuit concepts for high-speed CDMA over fibre. Analytical and simulation studies are reported showing the suitability of the novel distributed topologies to encode and decode CDMA signals at higher speeds than previous proposals. By means of example, the circuit ideas were tested with a GaAs process employing transistors with a cut-off frequency of 60 GHz; the results proved suitability for 40 GChip/s operation. The main challenge of the structure is the implementation of the delays in the electronic domain; in this case, nineteen LC-sections and six ATL sections were used to implement a total delay of 125 ps. To the best of the author's knowledge, the designs discussed in this chapter present the largest delay in a single distributed transversal filter operating in the 10s of

Gbit/s regime (see section 3.5.1 in the previous chapter). The work presented in this chapter gave rise to several publications in conference proceedings including regular papers [115] [145] [146] and invited contributions [147] [148] [149] [116].

The Distributed Transversal Filter could be employed in unipolar CDMA asynchronous systems. In fact, simulation results shows feasibility for encoding these signals; they also show ability to generate a correlation peak with presence of a matching sequence and rejection of the unmatched sequences. The DTF satisfied both time and frequency characteristics according to prescribed temporal responses and showed little performance variability with changes in temperature and process parameters, thereby validating our concept and the design techniques followed.

However, there are some problems with such an approach that compromise its practical application. The first issue is related to the time domain Optical CDMA technique itself. As explained in chapter 2, the transmission of unipolar CDMA signals requires a very high number of chips leading to low spectral efficiencies and low cardinalities. For such reason, Optical CDMA review papers often cite coherent approaches and time-wavelength incoherent approaches as the most promising candidates to develop practical Optical CDMA applications [7]. This issue is independent of whether the encoding and decoding unipolar signals are performed in the optical or electrical domains.

Another problem is related with technical issues in the Distributed Transversal Filter design. Distributed topologies have limits in terms of the number of stages and delay sections that can be implemented with reasonable pulse broadening. This is even more serious impairment in a Distributed Transversal Filter operating in the reverse mode topology because of the electrical path that each amplified

pulse faces. Broadly speaking, the fraction of the output response amplified by the first stage immediately appears in the output while the fraction amplified by the last stage will have the commulative dispersion of all components in the drain and gate lines. In this design, the optimized response leads to 17 and 30 % braodening of the second and third pulses when compared to the first. Moreover, the attenuation in the lines can be compensated by adjusting the gains in the transversal filter stages but this is done by reducing the gain of the first stage to values much below its maximum. This leads to circuits effectivelly attenuating the input signal, which may require front-end transconductance amplifiers with very high gains.

The comparison of the unipolar and bipolar CDMA signals performance may give some insight on these limitations. For example, following the analysis in [5], the error probability for asynchronous transmission with bipolar Gold Codes and unipolar Prime Codes is given by the expressions:

$$P_{GC} = \theta\left(\sqrt{\frac{2L}{K-1}}\right) \tag{4.36}$$

$$P_{PC} = \theta\left(\sqrt{\frac{3L}{5(K-1)}}\right) \tag{4.37}$$

where K is the number of simultaneous active users, L is the length of the code and $\theta(x)$ is the unit-normal cumulative distribution defined as:

$$\theta(x) = \frac{1}{\sqrt{2\pi}} \int_{-\infty}^{x} \exp\left(\frac{-y^2}{2}\right)\, dy. \tag{4.38}$$

Figure 4.52 shows that the performance of Gold Codes is better than the Prime-Hop codes for the families of codes with comparable lengths. It shows

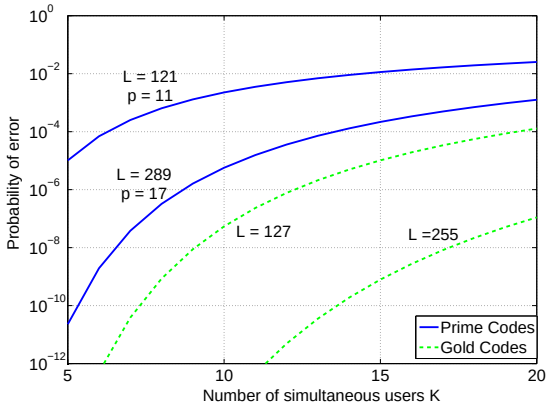

Figure 4.52: Error probability versus number of simultaneous users for Gold and Prime Codes (adapted from [5]).

that even for relatively modest bit error rates and a low number of asynchronous users, the number of stages and additional delay lines required are large. For example, if we consider 5 subscribers with a BER $= 10^{-5}$, a prime code with p=11 has to be used which means that a transversal filter with 11 stages and a total delay equal to 121 times T_{chip} would have to be implemented. With the techniques described in this chapter and the semiconductor processes currently available this is clearly impractical. Moreover, unipolar CDMA signals suffer from very low cardinalities which limits the number of network subscribers. As seen in chapter 2, the cardinality of Prime codes is $\sqrt{L}$ while Gold Codes allow $L-2$ codes.

Next, the possibility of building structures allowing flexibility in the codeword selection was explored in this chapter, as opposed to distributed transversal filters that are codeword specific. Preliminary studies with transistor switches failed to provide an acceptable response mainly due to high insertion losses when the switch is open. In fact, losses in the order of 2 dB were suffered by each transistor which is too high for integration within the transversal filter. The integrations of MEMS

devices featuring lower losses seems to be a promising future technique, alas the integration with commercial high-speed integrated circuit processes is currently unavailable.

The limitation associated with the Distributed Transversal Filter design for time domain CDMA led to our study in structures that could encode and detect 2D time-wavelength Optical CDMA signals in the electronic domain. These designs could be an alternative to traditional all-optical devices that suffers from large optical losses, susceptibility to environmental factors (for example, variations in temperature and strain) and cannot encode all types of codewords. The only optical component necessary in the transmitter/receivers are WDM multiplexers and demultiplexers; these are mature due to their widespread use in long-haul optical communications. Results described in this thesis are preliminary and should be interpreted as proof-of-concept rather than final expected results. In fact, it was impossible to fit the designs within the foundry maximum allowed IC size and therefore only full-device schematic results are shown. Further, the 2D time-wavelength designs discussed here were limited to two wavelength systems. For multi-wavelength systems, there is obviously a limitation in the potential implementation as multi-dimensional circuits would be required. Such may well be possible in future technologies such as hybrid structures and Low Temperature Co-fired Ceramic (LTCC) technology [150].

The practical application of such design ideas is dependent upon the efficient construction of electronic delay lines. In fact, these have to occupy less space and provide constant group delay over the frequency of operation of the device. For example, in [95] active electronic delay lines are proposed for the use in distributed topologies. These include a delay locked loop to provide accurate delays [95].

Active delay lines lead to compact IC designs and therefore can be an alternative to analogue passive delay lines. The main concern is that the operation speed is significantly lower than analog LC-delay lines, and therefore unable to catch up with the ever increasing speed of Optical CDMA proposals.

It is believed that this chapter not only contributes with alternative approaches for the implementation of high speed CDMA encoding and decoding, but also presents novel circuit design techniques of high speed distributed structures. The designs presented in this chapter, despite the limitations discussed, may well find applications beyond optical CDMA, with the ever increasing developments in integrated circuit processes and technologies.

Chapter 5

Group Velocity Difference in Wavelength-Hopping Time-Spreading Optical CDMA: Modelling and Compensation

This chapter starts with a brief overview on the problem of time skewing in multi-wavelength Optical CDMA networks. Next, a section is devoted to the description of a semi-analytical model developed to analyse the effect of time skewing in Optical CDMA networks. This model provides a good estimation of the network performance while avoiding the use of pure Monte-Carlo simulations, which are inefficient in terms of computational time. Section 5.3 describes the application of the model to two codes presented in the literature: Bin Code and Prime-Hop Code. The performance is first analysed for constant time skewing between adjacent wavelength channels; this allows us to extract conclusions about the behaviour of the system with single mode fibres as transmission medium. The

performance is then analysed for Dispersion Shifted Fibres (section 5.4).

Section 5.5 presents the electronic post-detection scheme proposed for compensation of time skewing in Wavelength-Hopping Time-Spreading Optical CDMA systems. This section describes the modifications to the model presented in section 5.2 to accommodate the transversal filter and details about the optimisation algorithms used to estimate the optimum transversal filter coefficients are provided.

Results for Bin Code are presented in detail in section 5.6 where conclusions about the performance of the proposed scheme are derived. A subsection about Prime-Hop Code results is also presented although this is briefer because some of the conclusions derived for Bin Code would be redundant. A summary of the main findings is provided in the end of the chapter.

5.1 GVDiff-induced Time Skewing in Multi-Wavelength Optical CDMA

In the late 80s, networks operating in the third communication window (wavelengths in the 1.55 μm vicinity) started to be deployed to achieve longer span due to its lower attenuation when compared with the 1.3 μm communication window. The advent of high performance Erbium Doped Fibre Amplifiers (EDFAs), optimised for 1.55 μm, reinforced it as the most suitable window for high bit rate optical communication systems. However, as the bit rates increased, chromatic dispersion caused by the optical fibre Group Velocity Dispersion (GVD) started to become the major transmission limiting factor.

Chromatic dispersion has been acknowledge as the major impairment in high

speed ligthwave communication systems. For pulse transmission, each optical pulse comprises a range of wavelength components traveling at different velocities; this causes the so called dispersion induced pulse broadening. Consequently, signals in adjacent bit periods overlap and errors arise due to Inter Symbol Interference (ISI) [151].

High chromatic dispersion of Single Mode Fibre (SMF) at 1.55 μm motivated the development of Dispersion-Shifted Fibres (DSF). The refractive index profile of such fibre is manipulated so that the zero dispersion point is moved from the natural 1.30 μm in silica to fall within the 1.55 μm communication window. These fibres provide increased tolerance to chromatic dispersion. However, when used in multichannel systems, dispersion-shifted fibres suffer from nonlinear effects such as four-wave mixing which may cause intermodulation of independent signals [140].

In ultrahigh-speed optical transmission systems of more than 100 Gb/s, the effect of the positive dispersion slope (third-order dispersion) of 1.55 μm Dispersion Shifted Fibres is also a factor limiting the transmission distance [152]. This dispersion slope causes pulse waveform distortion, especially trailing ripple, which also causes Inter Symbolic Interference (ISI).

In multi-wavelength optical systems, group velocity difference results in induced time skewing among different wavelength channels. In fact, pulses undergo different delays and such differences are mainly determined by their channel central wavelength. Time skewing is not an issue in conventional WDM systems since the information of a single wavelength channel is independent of others. However, there are optical applications requiring precise synchronism between the wavelength channels. For example, in bit parallel optical systems, the bit skew caused by group delays of the different transmission wavelengths has been identi-

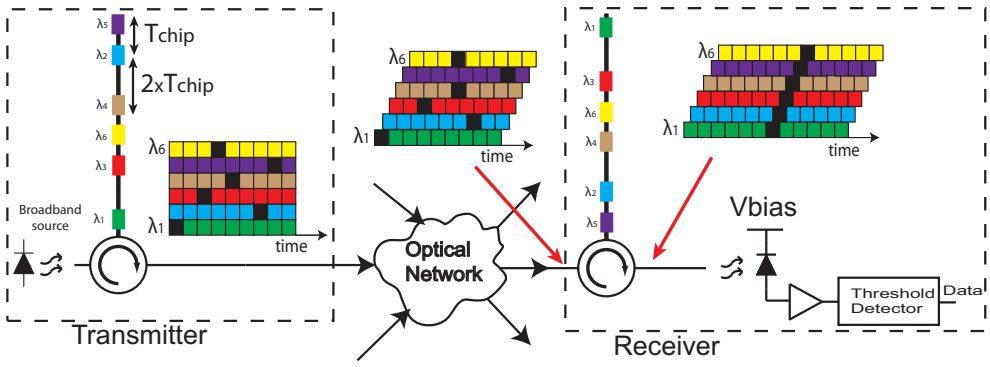

Figure 5.1: Impact of GVD in Optical CDMA networks.

fied as a main impairment [153] [154].

Time skewing has been identified as a major impairment in multi-wavelength Optical CDMA systems. This effect can be seen in figure 5.1. In fact, the detection of a given codeword is an incoherent process that relies on the temporal distance among chips transmitted on different wavelengths. Distortion of received code patterns results when the network induces relative temporal shifting between the wavelengths, giving rise to errors in the receiver. The impact of the optical fibre Group Velocity Dispersion (GVD) in multi-wavelength Optical CDMA systems has been addressed by several research groups, where the resulting time skewing between the different λ channels (as opposed to pulse broadening) is the key factor affecting performance [6] [72] [73].

Zuo and colleagues [6] identified GVDiff-induced temporal skewing as the major impairment in WHTS Optical CDMA systems. The authors developed a theoretical model including a third order approximation of the Group Velocity Dispersion. The results are mainly qualitative and no BER analysis is provided. Standard Single Mode Fibre (SMF) is considered an unsuitable medium for WHTS Optical CDMA systems because the transmission distance is limited to less than 1 km for the cases studied, a distance that the authors considered insufficient. It also

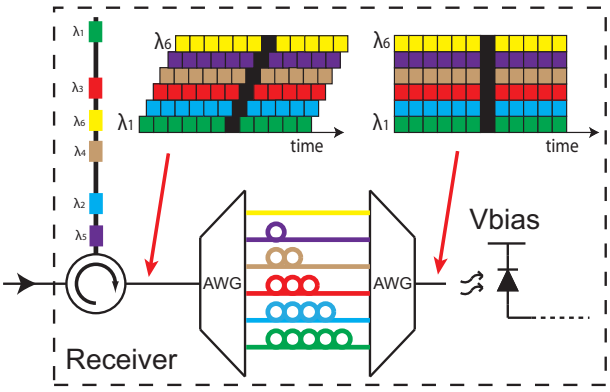

Figure 5.2: GVD compensation structure proposed in [6].

describes a compensation scheme that comprises two arrayed waveguide gratings and delay lines as presented in figure 5.2. Although this device can theoretically fully compensate time skewing, there are practical implementation issues to take in consideration, namely:

1. Cost and complexity,

2. Lack of tunability - with the existing techniques, it is difficult to fabricate accurate tunable delay lines [50].

Ng and colleagues [72] presented in 2002 an important paper dealing with the same topic. In this approach, all signals are ON-OFF keyed (OOK), non-return to zero (NRZ) format with ideal rectangular-shaped temporal pulses. The paper assumes that the mean and variance of Multi-Access Interference is proportional to the number of interferes; this assumption is not always accurate as seen in [60]. The paper proposes a solution to alleviate this problem which relies on code pattern pre-skewing. With traditional optical encoding techniques, this could only be achieved with tunable delay lines. For example, using FBG arrays, the ability to change the physical distance between FBGs would have to be introduced.

Similar conclusions were reached by Sahin and Willner in [73] where time skew-

ing was found to be the dominant source of performance degradation in multi-wavelength Optical CDMA. Results are limited to codes with 3 wavelengths and 7 temporal chips, and details about the modelling methodology are scarce in this 2-page abstract. To the author's knowledge this work has not been published elsewhere.

5.2 Modelling Methodology

The goal of the model presented in this section is to analyse the effect of time skewing between wavelength channels in Wavelength-Hopping Time-Spreading (WHTS) Optical CDMA systems. Assessment of the BER performance degradation resulting from GVDiff-induced time skewing is essential to select the appropriate set of codes and propagation medium, and to assess the need for compensation schemes at the expense of increasing system complexity. Moreover, the model will be used to assess the performance of the compensation scheme proposed in the section 5.5.

The model uses a passive star network as reference topology (figure 5.3). Users transmit information in a fully asynchronous fashion (both chip and bit asynchronous) and are multiplexed in the central passive node. The correlation is then performed for a specific user in the network and, as usual in WHTS networks with incoherent signal processing, the user sends its Wavelength-Hopping Time-Spreading sequence for information bit "one" and no power for bit "zero".

In general, a Wavelength-Hopping Time-Spreading codeword of the user k, comprising q wavelengths, L time slots and the weight w (i.e. number of "positive" chips), may be represented by the vector $c_k(i)$ with q elements; each element

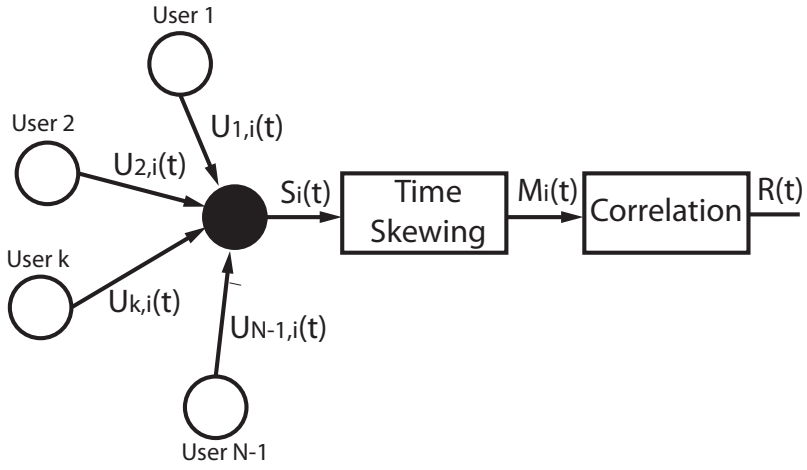

Figure 5.3: Optical CDMA model diagram with a star network as reference topology.

represents the position of the "positive" chip in the wavelength i. Therefore, the value of each entry of $c_k(i)$ can be either an integer value from 0 to $L-1$, or the symbol $\otimes$, which stands for absence of "positive" chip in the wavelength i. The signature of the user k is the sum of q time sequences (one for each wavelength of the system). For the wavelength i, this may be described by the equation:

$$Sig_{k,i}(t) = \begin{cases} \Psi(t - c_k(i)T_{chip}), & c_k(i) \neq \otimes \\ 0, & c_k(i) = \otimes \end{cases} \tag{5.1}$$

where T_{chip} is the chip period and $\Psi(t)$ is the chip signal as a function of time. A common assumption in systems encoded and decoded with Fibre Bragg Gratings [1] is to mathematically model the optical pulse from the broad-band light source as a Dirac function $\delta(t)$ and the reflectivity of the gratings with an apodization profile of Gaussian [6]. Therefore, the chip signal has a Gaussian shape and can be described by:

$$\Psi(t) = \exp\left(-\frac{t^2}{2\rho^2}\right) \tag{5.2}$$

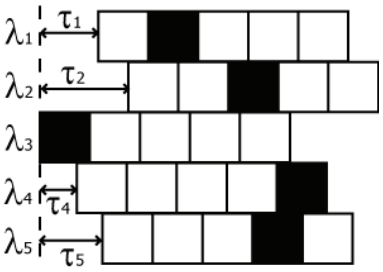

Figure 5.4: Induced time skewing in WHTS Optical CDMA systems - black squares represent chip "one".

where ρ is 1/4 of the pulse width at $1/e^2$ intensity point.

For modelling convenience, the information of user k is translated into a vector p with each element being the temporal position of a bit "one". Considering that user k sends B_k bits "one", the temporal transmission on wavelength i is described as:

$$U_{k,i}(t) = \begin{cases} \sum_{a=1}^{B_k} \Psi(t - c_k(i)T_{chip} - p(a)), & c_k(i) \neq \otimes \\ 0, & c_k(i) = \otimes \end{cases} \tag{5.3}$$

At a specific wavelength i, the signals of all interfering users are incoherently summed in the central node as follows:

$$S_i(t) = \sum_{k=1}^{N-1} U_{k,i}(t) \tag{5.4}$$

where N is the number of simultaneous active users in the network.

Dispersion induces time skewing between wavelength channels of the WHTS Optical CDMA system. Therefore, a vector τ_i may be defined as the relative induced time skewing of the wavelength i (figure 5.4). The wavelength with the least induced time skewing is taken as a reference (λ_3 in the example of figure 5.4). For each wavelength i, this may be mathematically modeled as:

$$M_i(t) = S_i(t - \tau_i). \tag{5.5}$$

At the receiver, incoherent correlation is performed for user N:

$$R(t) = \sum_{i=1}^{q} \gamma(c_N(i)) M_i(t - (L - c_N(i))T_{chip}) \tag{5.6}$$

where $\gamma(x) = 0$ for $x = \otimes$, and $\gamma(x) = 1$ for other x value.

The next step is the calculation of the threshold level. Incoherent WHTS Optical CDMA systems, where Multi-Access Interference (MAI) is the dominant source of errors, belong to a class known as "positive systems" [155]. In positive systems there is no interference cancellation or autocorrelation peak reduction (due to interference) and all signal components add as positive real numbers[1]. Under such conditions, errors can only occur when the MAI exceeds the threshold level transforming a "zero" into a "one" and therefore the ideal setting for the threshold is the peak amplitude of the autocorrelation function of the code [59]. This effectively means that the reduction in the autocorrelation peak due to GVDiff-induced time skewing introduces errors. Considering the induced time skewing and for the specific user k, the autocorrelation function $A(t)_k$ can be simply represented by the following equation:

$$A(t)_k = \sum_{i=0}^{q} \gamma(c_k(i)) \Psi(t - \tau_i). \tag{5.7}$$

Therefore, the threshold value is derived to be:

$$TH_k = \max_t(A(t)_k) = \max_t \left(\sum_{i=0}^{q} \gamma(c_k(i)) \Psi(t - \tau_i) \right). \tag{5.8}$$

If the system is under no influence of time skewing (i.e. $\tau_i = 0$, for all i), the

[1] This is, of course, not the case for coherent Optical CDMA systems where field amplitude is added vectorially.

threshold level is equal to the weight of the code. Moreover, equation 5.8 shows that apart from the induced time skewing, the threshold level can also depend on the specific codeword that the receiver is decoding. This is an aspect to consider with codes in which the number of wavelengths q is higher than the number of "positive" chips w (such as One-Coincidence Code described in [57]). The threshold level is constant for all the codewords in codes such as Prime-Hop [156] where $q = w$.

The performance of the Optical CDMA system is commonly analysed through BER. The exact BER of these systems considering MAI as a dominant source of noise is defined as

$$BER(exact) = P_r(Z \geq TH \mid b_0 = 0) \cdot P_r(b_0 = 0)$$
$$+P_r(Z < TH \mid b_0 = 1) \cdot P_r(b_0 = 1) \tag{5.9}$$

where Z is the maximum amplitude of MAI over single bit period window, TH_k is the threshold level for the user k, and b_0 is the transmitted symbol. The second term of equation 5.9 is zero because an error occurs only when the cumulative MAI at a particular user, which is actually receiving a data bit zero, is over the decision threshold [60]. Therefore, the probability of error when $b_0 = 1$ is zero. Considering a binary system with equiprobable symbol occurrence, the error rate arising from the first term is

$$BER(exact) = \frac{1}{2} \int_{TH}^{+\infty} P(Z)\, dx \tag{5.10}$$

where $P(Z)$ is the probability density function of the Z parameter.

Note that BER analysis in chapter 2 assumes that synchronisation has already

been achieved and that Multi-Access Interference is assessed at the sampling point. In this work, we assume fully asynchronous system using a simple threshold detector. For modelling purposes, errors are assumed to occur when MAI exceeds the threshold at any point in the bit period. Therefore, the BER values presented in this chapter are effectively a worst case scenario, and represent a lower bound in the system performance.

The model extracts the maximum MAI over single bit period windows (Z) from the vector $R(t)$ (equation 5.6). Such values could be used to estimate the BER through Monte-Carlo simulation, i.e., by comparing them to the threshold level and calculating the number of errors over the total bits. However, the high number of computational steps involved and the high number of samples per bit required, make the application of Monte Carlo simulations impractical. Instead, Z values may be used to estimate the bit error rate through studies of their distribution.

The MAI Probability Density Function (PDF) can be proved to follow a Gaussian distribution through application of the Central Limit Theorem. As seen before, the Optical CDMA signal after detection $R(t)$ is the sum of cross-correlation function of the active network users. The maximum MAI value (Z) over a bit period T_{bit} can be defined as

$$Z = \max_{t}(R(t))_{[0,T_{bit}]} = R(t_{max})_{[0,T_{bit}]},\ t_{max} \in [0, T_{bit}]. \tag{5.11}$$

From each cross-correlation function, there will be only one pulse (or no pulse) contributing to the amplitude at $R(t_{max})$. Because the system is asynchronous, the relative delay between any two cross-correlation functions is a random variable. Therefore, the temporal distance between the center of the contributing pulse of the cross-correlation i and t_{max} is assumed to be a random uniformly distributed

variable. It is possible to define the distance between the central time of the nearest pulse of the cross-correlation function of user i as

$$t_{ni} = t_{ci} - t_{max} \tag{5.12}$$

where t_{ni} is a random variable with probability density function uniformly distributed on the interval [-T_{chip},T_{chip}].

Therefore, recalling the Gaussian pulse shape as defined in equation 5.2, the cross-correlation functions with one pulse falling in the interval [$t_{max} - T_{chip}, t_{max} + T_{chip}$] contribute to the amplitude Z with the quantity

$$X_i = exp\left(\frac{t_{ni}^2}{2\sigma_f^2}\right). \tag{5.13}$$

The Central Limit Theorem states that the sum of a sufficiently large number of identically distributed independent random variables, with finite mean and variance, approximately follows a normal distribution [157]. In fact, Z is defined as:

$$Z = \sum_i X_i. \tag{5.14}$$

Since X_i are identically distributed independent random variables, Z satisfies the criteria for application of the Central Limit Theorem. Therefore, the probability density function of Z approximates a Gaussian (normal) distribution:

$$P(Z) = \frac{1}{\sigma\sqrt{2\pi}} exp\left(-\frac{(x-\mu)^2}{2\sigma^2}\right). \tag{5.15}$$

This approximation is valid when a large number of cross-correlation functions are interfering, i.e., the Optical CDMA network has a large number of simultaneous

active users. The Gaussian distribution mean (μ) and standard deviation (σ) are calculated through analysis of the vector $R(t)$. The model gives:

$$\mu = \frac{1}{N_{bits}} \sum_{j=1}^{N_{bits}} z_j \tag{5.16}$$

$$\sigma = \sqrt{\frac{1}{N_{bits}} \sum_{j=1}^{N_{bits}} (z_j - \mu)^2} \tag{5.17}$$

where z_j are the values of Z for each bit period j.

Finally, the Bit Error Rate of the Optical CDMA system is approximated by:

$$BER_k = \frac{1}{2\sigma\sqrt{2\pi}} \int_{TH_k}^{+\infty} exp\left(-\frac{(x-\mu)^2}{2\sigma^2}\right) dx. \tag{5.18}$$

In terms of commutative error function, the Bit Error Rate of the system may be expressed as:

$$BER_k = \frac{1}{4}\text{erfc}\left(\frac{TH_k - \mu}{\sqrt{2}\sigma}\right). \tag{5.19}$$

Another important aspect of this model is how to define the temporal data transmission of each user. The system is designed to be fully asynchronous, i.e., the active users are both bit frame and chip asynchronous. Note that an user is considered active if it is continuously transmitting information in the simulation time without breaks. For any two active users, the time difference between two bit frames τ_R (see figure 5.5) is completely uncorrelated; hence, τ_R should be a random variable with uniform distribution in the interval $[0, T_{bit}/2]$.

The solution to approximate the behaviour described in the previous paragraph is to transmit a number of bits N_{burst} separated by a random idle time with uniform distribution in the interval $[0, t_{rand}]$. If the simulation has an infinite number

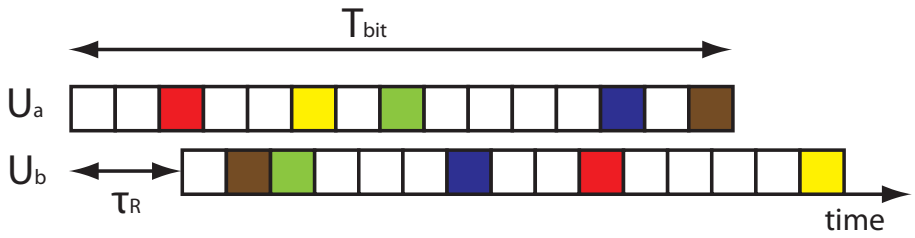

Figure 5.5: Two codes from user a and user b arriving at the star with temporal difference τ_R (each color represents one wavelength).

of bits, the value t_{rand} may be defined as an arbitrarily small quantity. In practice, simulations with limited number of bits requires t_{rand} to be carefully chosen considering the following trade-off:

1. t_{rand} should be small enough so that the user can be considered active. In this model, it is assumed that the user is active when it transmits data at least for 99% of the simulation time. The percentage of active time P_{active} for any user is defined as:

$$P_{active} = \frac{T_{bit} \times N_{burst}}{T_{bit} \times N_{burst} + \frac{1}{2} t_{rand}}. \tag{5.20}$$

2. t_{rand} should be large enough so that τ_R closely approximates a random variable with uniform distribution considering the total simulation time. This assumption is tested for each scenario considered, as shown in the beginning of the next section.

5.3 Impact of Time Skewing on WHTS Optical CDMA Performance

As seen in chapter 2, research on codes for WHTS Optical CDMA is a very active area in the field of information theory and there are probably hundreds of different codes that could be selected in this work (see [5] especially the discussion in chapter 1 where a part of the 525 references provided are related to WHTS Optical CDMA codes). Each code is distinguished by its unique combination of autocorrelation and cross-correlation characteristics, and different dimensions. In this chapter, we consider two sets of codes described the literature: Prime-Hop (PH) Code [156] and One-Coincidence Code described in [57] by Bin, which will be referred henceforth as Bin Code. The characteristics of the particular code families selected are represented in table 5.1. These codes are selected for the following studies for the reason that their wavelengths $\times$ time slots products are of the same order but differently distributed. Bin Code has a large number of wavelength slots and low number of time slots while Prime-Hop Code has the opposite characteristics. Bin Code, although not optimum for Optical CDMA due to their low cardinality [1], have been widely used for laboratory experiments [65] and served as the base for the development of other codes that achieve higher cardinalities [66]. Prime-Hop Code and its multiple variants (see table 2.3 in chapter 2) have been proposed for practical Optical CDMA implementations and were implemented in laboratory demonstrations [63]. The use of these two sets of codes allow comparison of the effects of time skewing on system parameters. The system is simulated for 40 GChip/s. Effectively, the studies in this chapter are indicative and not exhaustive.

Table 5.1: Characteristics of the WHTS Optical CDMA codes.

Code	Weight	Wavelengths	Time Slots	Code Dim
Bin [57]	12	29	12	$29 \times 12 = 348$
PH [156]	7	7	49	$7 \times 49 = 343$

Table 5.2: Model parameters.

	Prime-Hop	Bin
N_{burst}	6	6
t_{rand}	$5 \times T_{chip}$	T_{chip}
P_{active}	99.16%	99.31%

For each code, the model parameters N_{burst} and t_{rand} were selected according to the trade-off described in the end of the previous section. Table 5.2 shows N_{burst}, t_{rand} and P_{active} calculated as in equation 5.20.

Figure 5.6(a) and 5.6(b) show the histograms of the temporal distance between the start of two bit frames (τ_R) for Prime-Hop and Bin Code, respectively. They show the distribution of τ_R in a 100,000 bit simulation, which was the value chosen in this section. It can be seen that distribution is approximately uniform in the period $[0, T_{bit}/2]$ for both codes.

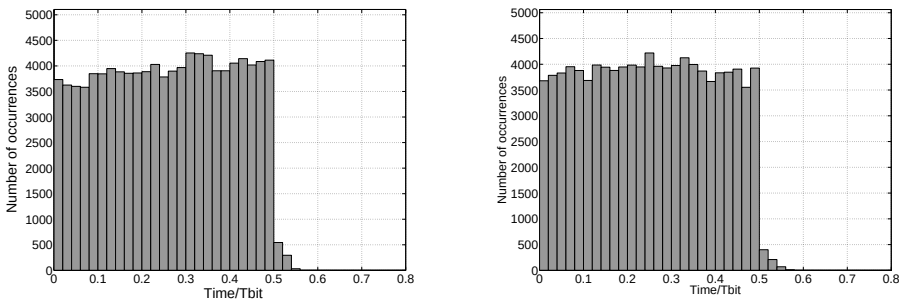

(a) Prime-Hop Code (b) Bin Code

Figure 5.6: Histogram of τ_R for a simulation with 100,000 bits (simulation parameters of table 5.2).

5.3.1 Constant Time Skewing with Prime-Hop Code

The performance of the WHTS Optical CDMA network is first studied considering constant time skewing between adjacent wavelength channels. This is approximately the time skewing regime provided by standard single mode fibres as the effect of dispersion slope can be disregarded. The time skewing as defined in equation 5.5 may be expressed as a function of the time skewing between wavelength channels ΔT as follows:

$$\tau_i = i.|\Delta T|, i = 0, 1, 2, ..., q-1 \tag{5.21}$$

where q is the number of wavelengths of the system. The impact of time skewing on the autocorrelation peak is studied for different values of pulse width, considering the chip pulse with Gaussian shape. The width of the pulse is measured at $1/e^2$ intensity point and, for simplicity, will be referred to as pulse width throughout this chapter.

Figure 5.7 shows the degradation of the autocorrelation peak due to time skewing for four different values of pulse width: 25 ps, 20 ps, 15 ps and 10 ps. These represent 100 %, 80 %, 60 % and 40 % of the chip time T_{chip}, respectively. In each graph, a sweep in the time skewing between adjacent wavelengths is performed from 0 to 7.5 ps with steps of 1.5 ps.

The first conclusion to extract from the graphs is that the autocorrelation peak amplitude is independent of the pulse width when no time skewing is present in the system; however, as the time skewing builds up, the pulse width strongly influences this value. For example, for 25 ps pulse width, the autocorrelation peak amplitude is halved with 4.5 ps of time skewing between wavelength channels

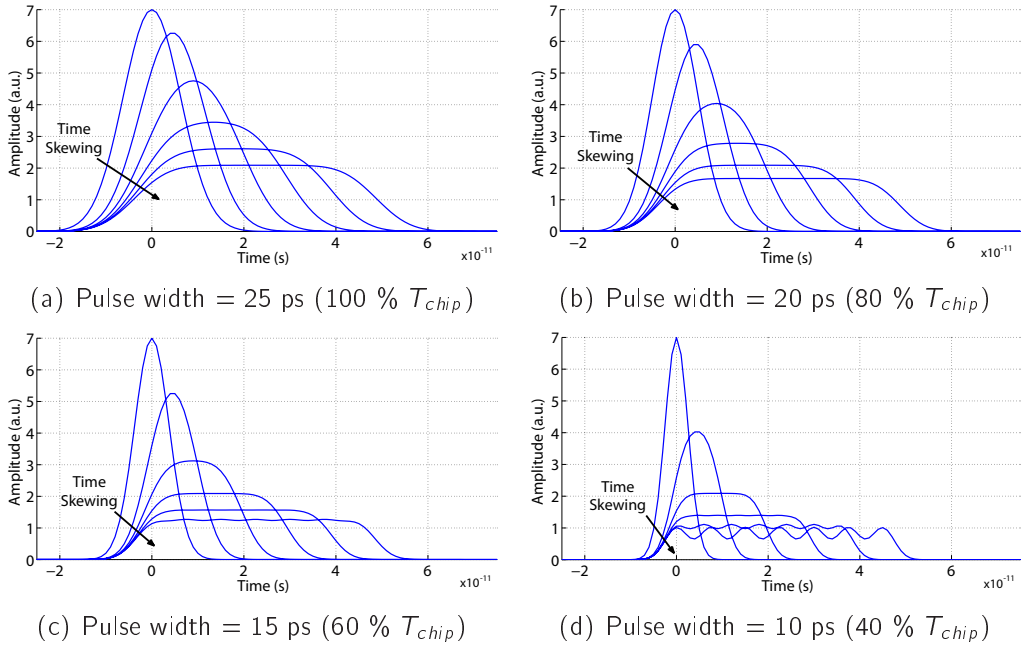

(a) Pulse width = 25 ps (100 % T_{chip}) (b) Pulse width = 20 ps (80 % T_{chip})

(c) Pulse width = 15 ps (60 % T_{chip}) (d) Pulse width = 10 ps (40 % T_{chip})

Figure 5.7: Autocorrelation peak degradation due to time skewing - time skewing between adjacent wavelengths varies from 0 to 7.5 ps (1.5 ps steps).

whereas with 10 ps width this value drops to 1.5 ps. This effect becomes clearer in figure 5.8 where the autocorrelation peak amplitude is plotted against the time skewing between adjacent wavelengths for different pulse width regimes.

Multi-Access Interference (MAI) comprises the sum of the cross-correlation functions of the active network users, and it is simulated according to the model described in section 5.2. Time skewing influences MAI because it affects the cross-correlation characteristics of the code. Figure 5.9 shows an illustrative example of the time skewing impact on the cross correlation function, where Codeword 1 (C1) and Codeword 2 (C2) are optically orthogonal codewords (normalised cross-correlation constraint equal to one).

The illustration on the top of the figure 5.9 shows the codeword 1 being decoded with a matching correlation receiver. As expected, an autocorrelation peak with amplitude equal to the code weight (three in this case) is generated.

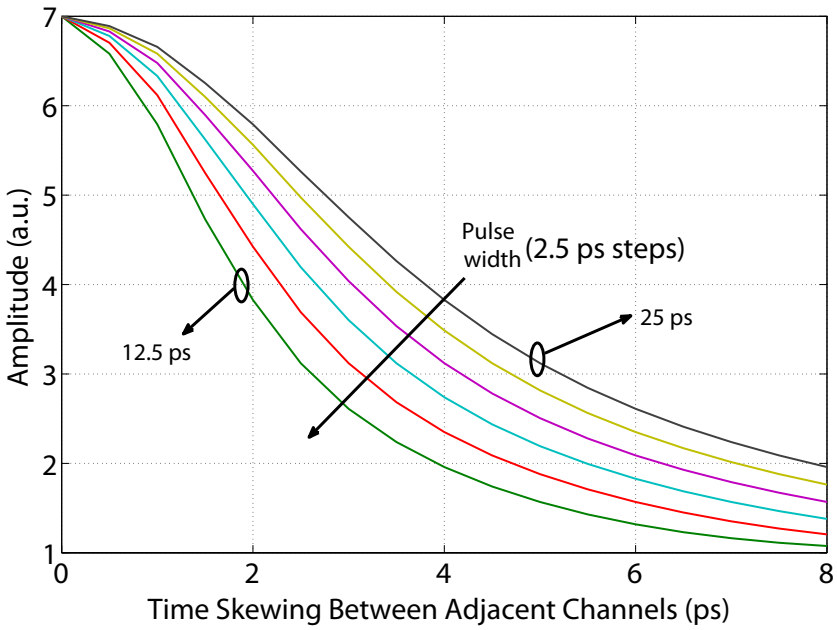

Figure 5.8: Autocorrelation peak amplitude vs. time skewing for PH codes(pulse width varies from T_{chip} to 50 % T_{chip}).

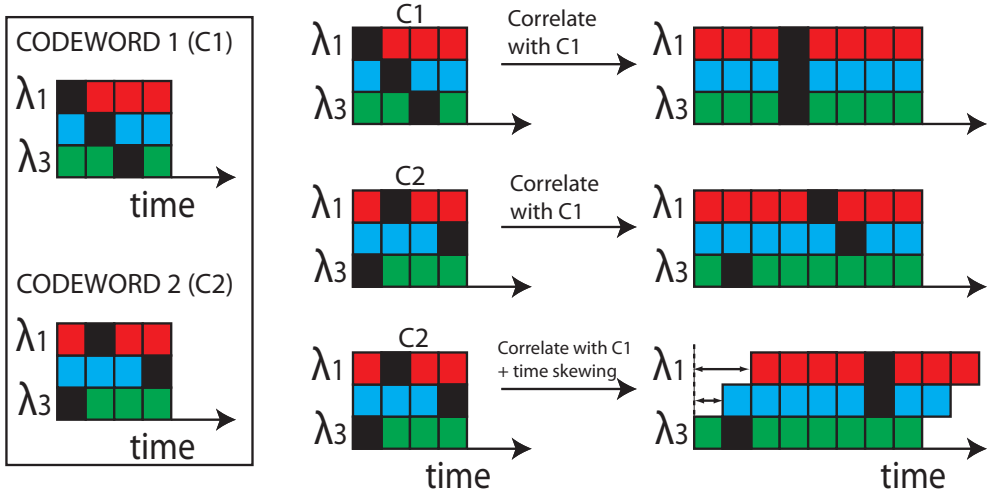

Figure 5.9: Impact of time skewing in the cross-correlation of an Optical CDMA system.

The schematic in the middle shows the result of the same correlation receiver with the codeword 2 at its input. One can observe that there are no clashes among chips in different wavelengths; this codeword satisfies the optical orthogonality condition of normalised cross-correlation constraint equal to one. Time skewing may induce chips to coincide in time and therefore the optical orthogonality of the codes may be violated. This scenario is shown on the bottom schematic of figure 5.9, where there is a clash in the time position seven.

The impact of time skewing on the Multi-Access interference strongly depends on the code structure. This effect could be studied through detailed mathematical modelling of the stochastic behavior of the MAI versus different levels of time skewing or by Monte Carlo simulations. The first requires rigorous mathematical analysis, which is unnecessary and beyond the scope of this thesis whilst pure Monte-Carlo studies would require very large simulation time. Alternatively, a semi-analytical approach described in the previous section was developed, based on numerical computation of the MAI and followed by statistical modelling and approximation. This yields a computationally efficient technique that is deemed appropriate for the purpose of this study. Figure 5.10 shows the expected values of the simulated MAI amplitude as a function of the time skewing. The standard deviations of the MAI are represented using error bars. Results show 15 and 25 active simultaneous users in the network. Figure 5.10 shows a slight increase of both mean value and standard deviation of MAI [2].

From figures 5.8 and 5.10, one can conclude that time skewing impacts substantially the autocorrelation peak but only slightly the MAI amplitude. For our

[2]Note that the BER calculations that will be presented in this chapter include the time skewing effect on the reduction of the autocorrelation peak through reduction in threshold level and also the effect on cross-correlation through the increase on the mean and standard deviation of MAI.

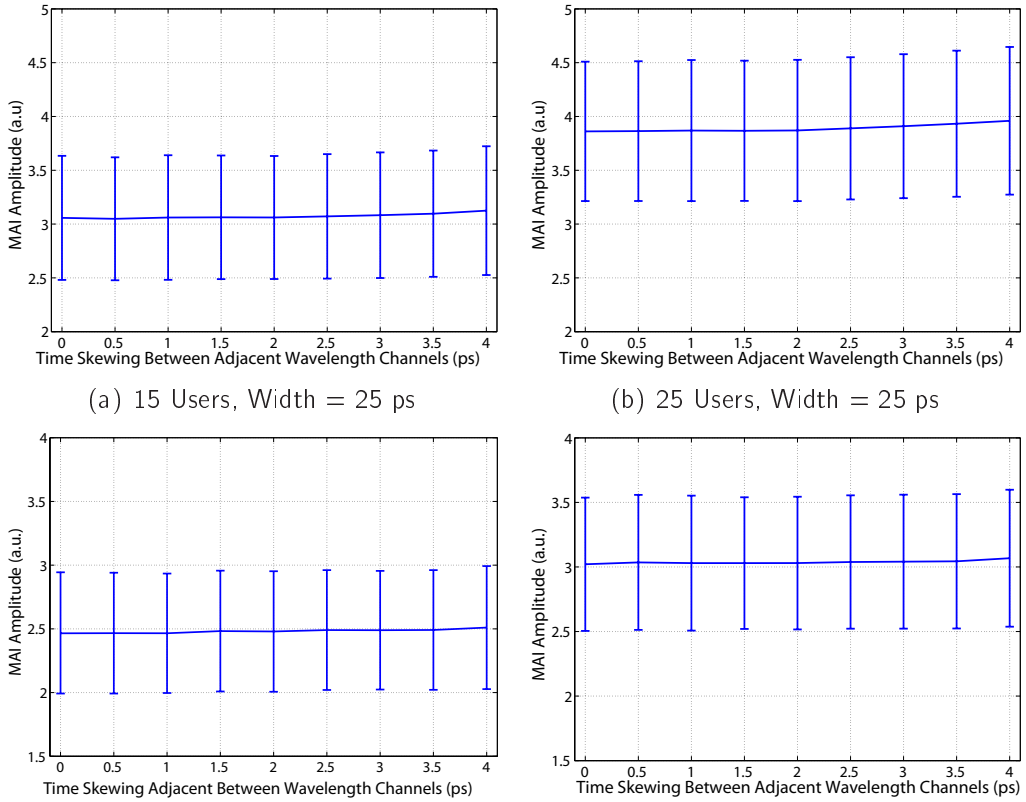

(a) 15 Users, Width = 25 ps

(b) 25 Users, Width = 25 ps

(c) 15 Users, Width = 12.5 ps

(d) 25 Users, Width = 12.5 ps

Figure 5.10: Mean and Standard Deviation of the Multi-Access Interference for Prime-Hop Code (error bars indicate standard deviation).

example, the autocorrelation peak amplitude is reduced to almost half with 4 ps of time skewing between adjacent wavelength channels (considering the 25 ps width case); the same amount of time skewing gives rise to an increase in the MAI amplitude of less than 5%. This topic will be developed in the end of this section.

Figure 5.11 shows the histograms of the MAI values obtained by simulation compared to their Gaussian approximation. These histogram clearly show that the accuracy of the Gaussian distribution increases with the number of simultaneous active users in the network. Note that the figure 5.11(a) corresponds to the worst case considered in this thesis as the network comprises only 10 users.

As one can see from the histograms, the Gaussian curve (black lines) provides

a good approximation for the considered scenarios. This approximation can be further improved by acknowledging that the MAI values of interest for BER calculation are the ones close to threshold level. Therefore, it is possible to "fold" the Gaussian across its mean point (ignoring the left part of the histogram) and effectively approach the values above the mean MAI value with a Gaussian curve. This folded-Gaussian approximation is shown in red in the histograms of figure 5.11.

Modelling results are summarised in Bit Error Rate (BER) plots as a function of time skewing between adjacent wavelength channels. For Prime-Hop Code, 10, 15, 20 and 25 active simultaneous active users are considered. According to the study carried out in [158], the use of Forward Error Correction (FEC) such as Reed-Soloman RS(255,239) allows error free transmission with Pre-FEC BER of 2.9×10^{-4}. This value will be used as a reference for error free transmission.

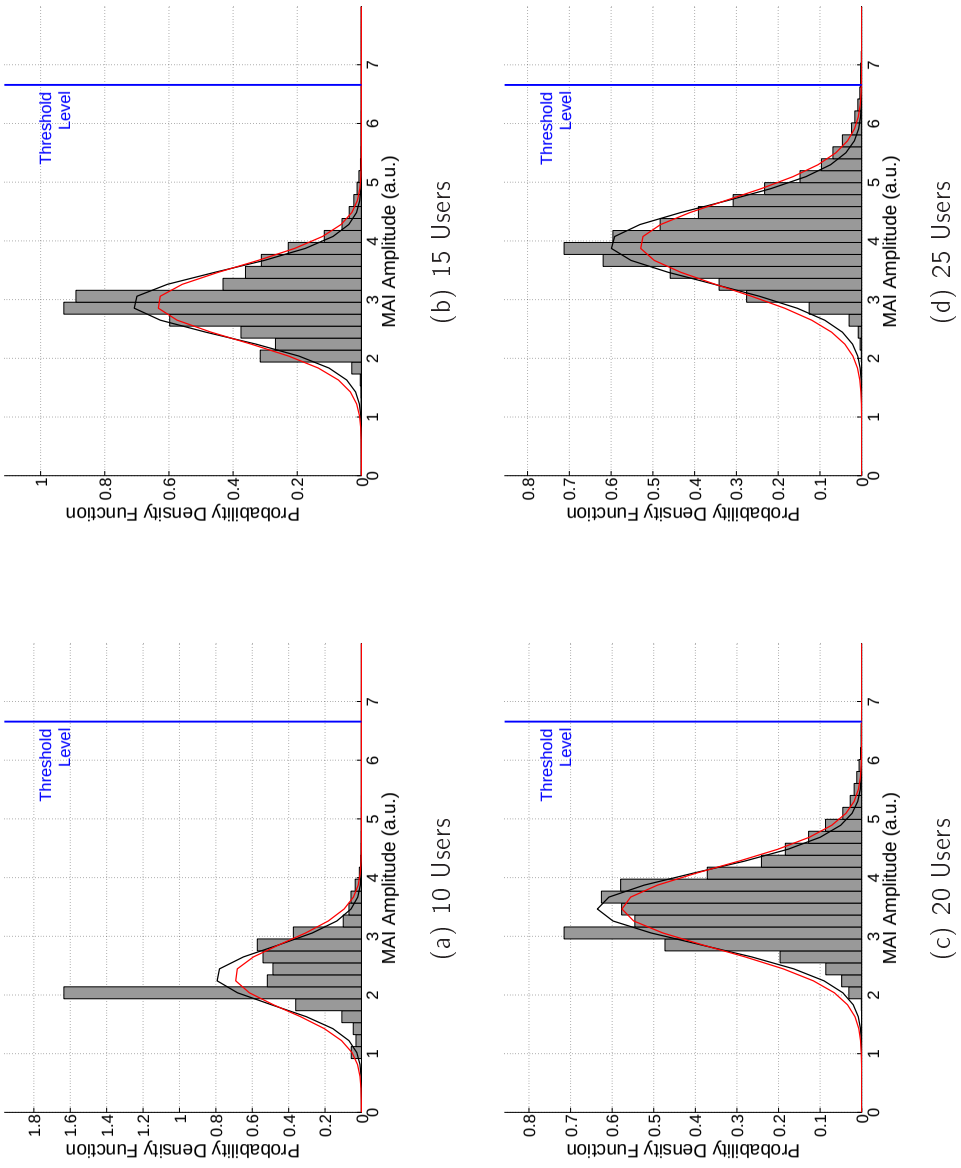

Figure 5.11: MAI probability density functions with Gaussian and folded-Gaussian approximations for PH Code(black and red lines, respectively) - time skewing between wavelengths is 1ps.

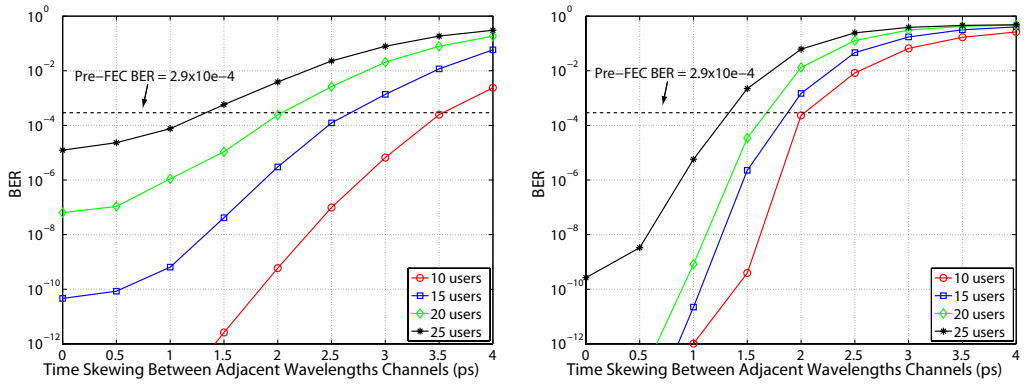

(a) Pulse width = 25 ps (b) Pulse width = 12.5 ps

Figure 5.12: BER as a function of time skewing between adjacent wavelengths for Prime-Hop Code.

Figure 5.12 shows the BER plots for Prime-Hop Code. As expected, for low time skewing values, the system performs better with lower pulse widths. For higher values of time skewing however, the autocorrelation peak reduction is more intense (see figure 5.7), and the system performs better with higher values of pulse width. For example, the system based on 12.5 ps width pulses with 20 users gives better output below 1.4 ps of time skewing between adjacent wavelength channels, when compared with the system based on 25 ps pulse width.

Figure 5.12 provides evidence that time skewing is a serious impairment in WHTS Optical CDMA system. An important conclusion is that the standard single mode fibre (SMF) is not a convenient transmission medium for WHTS Optical CDMA systems. In fact, a standard SMF presents a dispersion of 16 ps/nm/km; using conventional channel spacing (100 GHz), the time skewing between adjacent wavelengths exceeds 12 ps/km. Even for the most favorable scenario studied (Prime-Hop Code with 10 simultaneous users) the time skewing between adjacent wavelengths cannot exceed 3.5 ps (with Pre-FEC BER of 2.9×10^{-4}). Therefore, the transmission distance would be limited to 290 meters.

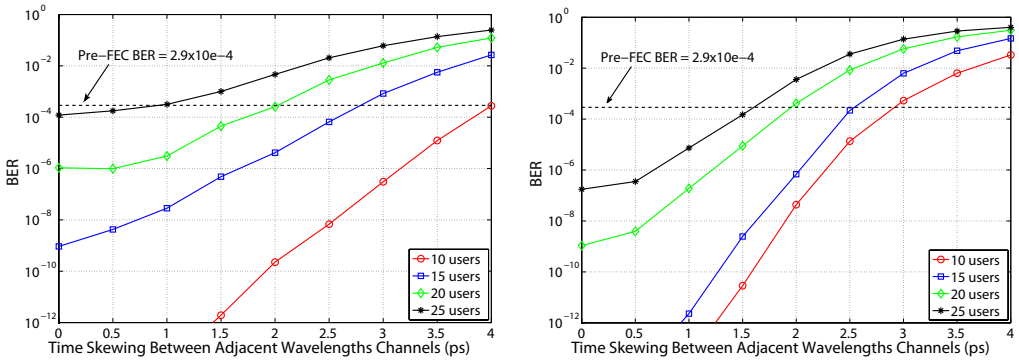

(a) Pulse width = 25 ps (b) Pulse width = 12.5 ps

Figure 5.13: BER as a function of time skewing between adjacent wavelengths for Prime-Hop Code - including electronic bandwidth limitation.

The results presented so far, while considering Gaussian pulses that are obviously limited in their frequency spectrum, have not included the effect of the bandwidth limitation of the electronic part of the receiver. For more realistic modelling, this effect is included in the BER results presented in figure 5.13. Several low pass-filters have been proposed in the literature to model the bandwidth limitation of the receiver; these include Bessel filters of several orders [159] [76] [160] and Butterworth filters [161]. In this project, a low-pass third order Bessel filter of 40 GHz bandwidth (equal to the chiprate) is adopted. In terms of the model described in section 5.2, the only modifications are that time vectors $R(t)$ and $R(t)_{AUTO}$ (equations 5.6 and 5.7, respectively) are passed through a third order low-pass Bessel filter before further processing. This is done with a Matlab built-in function.

Results show that the bandwidth limitation impact is higher for the system based on 12.5 ps pulses than that of 25 ps. This is expected as the frequency components of narrower Gaussian pulses are extended to the higher end of spectrum. Results also show degradation of the BER for low values of induced time skewing. In fact, the sharp autocorrelation peak is spread and its amplitude is

Table 5.3: Impact of auto and cross-correlation in the BER of the Optical CDMA system (PH codes).

TS (ps)		Users			
		10	15	20	25
0	BER	8.57×10^{-17}	4.61×10^{-11}	6.35×10^{-8}	1.23×10^{-5}
2	BER	5.96×10^{-10}	3.00×10^{-6}	2.40×10^{-4}	3.9×10^{-2}
	BER_A	3.62×10^{-10}	1.88×10^{-6}	1.43×10^{-4}	3.60×10^{-2}
	BER_M	1.91×10^{-16}	1.09×10^{-10}	1.24×10^{-7}	1.43×10^{-5}
4	BER	2.40×10^{-2}	5.83×10^{-2}	1.84×10^{-1}	3.03×10^{-1}
	BER_A	2.20×10^{-2}	4.05×10^{-2}	1.49×10^{-1}	2.83×10^{-1}
	BER_M	8.94×10^{-17}	1.67×10^{-9}	8.55×10^{-7}	4.22×10^{-5}

reduced; this causes a reduction of the threshold level and consequently a rise in the BER. The opposite effect happens when the time skewing is high. In this case, the autocorrelation peak is already time spread due to the effect of time skewing and therefore the BER is decreased due to the "integration" effect of the low-pass filter.

As shown throughout this section, time skewing has a detrimental effect on both the autocorrelation peak and Multi-Access Interference of the Optical CDMA network. Table 5.3 shows the separate performance impact of autocorrelation peak degradation and MAI increase. For each scenario, comprising a number of users and time skewing regime, three BERs are calculated:

1. BER - System global Bit Error Rate including both effects. These are the values presented in figure 5.12.

2. BER_A - System BER including the autocorrelation peak degradation only. This value is obtained considering the threshold level as described in equation 5.8, but using the values of MAI mean and standard deviation as extracted

from the simulation with no time skewing.

3. BER_M - System BER including only the degradation in Multi-Access Interference. This value is obtained by ignoring the effect of time skewing in the autocorrelation peak, i.e., setting the threshold equal to the code weight.

The main conclusion to take from table 5.3 is that the time skewing effect on the autocorrelation peak is clearly the main cause of performance degradation in WHTS Optical CDMA system. In fact, the values on the rows BER and BER_A are very close, while the time skewing impact on Multi-Access Interference (BER_M) is responsible for a much smaller number of errors.

5.3.2 Constant Time Skewing with Bin Code

The selected Bin Code family presents a significant difference when compared with Prime-Hop: the number of wavelengths is higher than the code weight whereas in Prime-Hop, these numbers are equal. The immediate consequence is that the time skewing effect in the autocorrelation peak is no longer independent of the codeword selected. Therefore, the following assumptions used for Prime-Hop Code are not valid for Bin Code:

$$TH = TH_k \Longrightarrow BER = BER_k. \tag{5.22}$$

For modelling purposes, the threshold level was calculated for all active users in the network, and its average value was used in the BER calculation

$$TH_{av} = \frac{1}{N}\sum_{k=1}^{N} TH_k \Longrightarrow BER = \frac{1}{2\sigma\sqrt{2\pi}} \int_{TH_{av}}^{+\infty} exp\left(-\frac{(x-\mu)^2}{2\sigma^2}\right) dx. \tag{5.23}$$

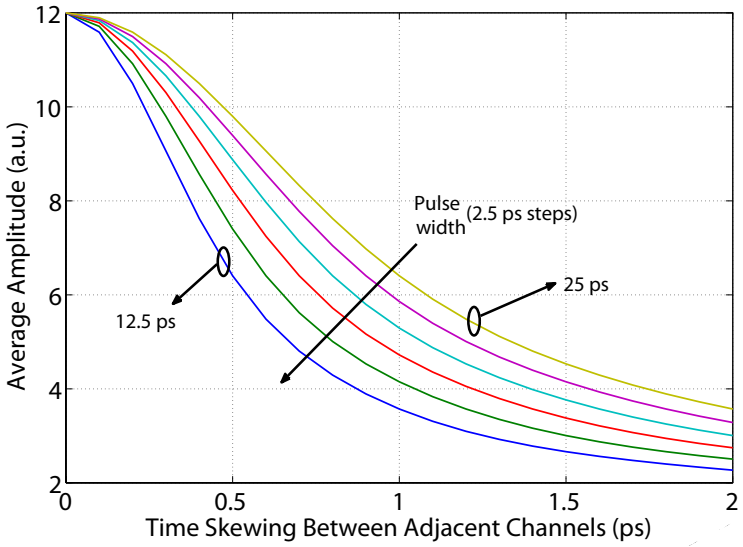

Figure 5.14: Autocorrelation peak amplitude vs. time skewing for Bin Code (pulse width varies from T_{chip} to 50 % T_{chip}).

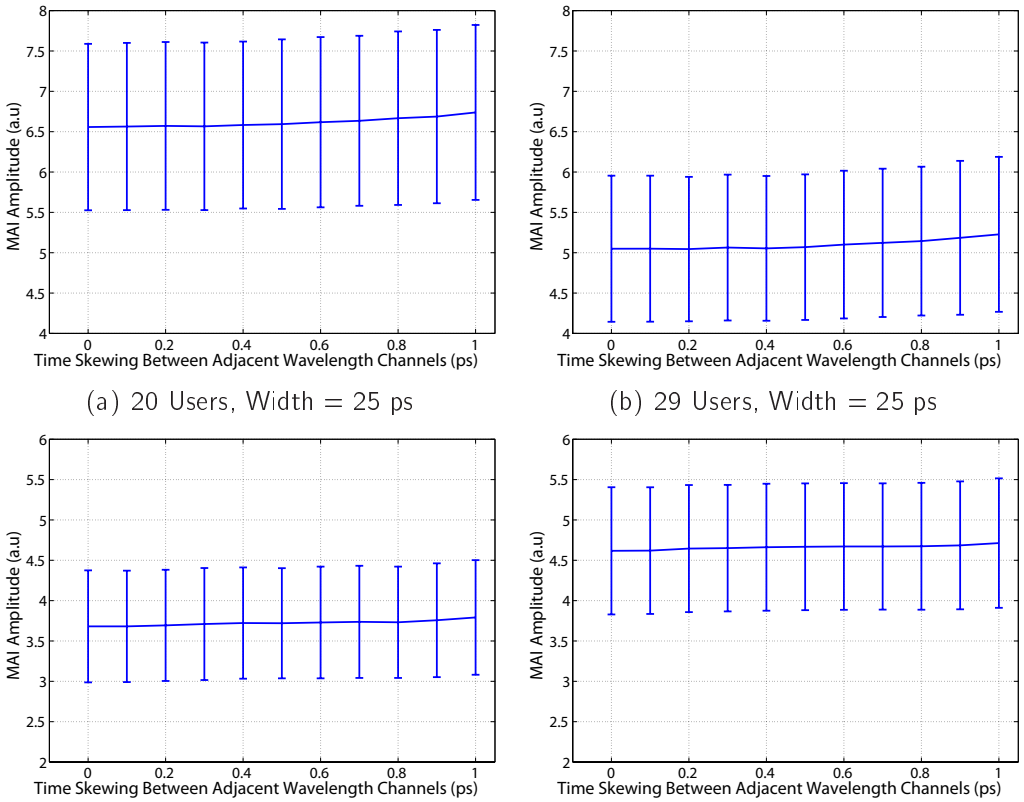

(a) 20 Users, Width = 25 ps

(b) 29 Users, Width = 25 ps

(c) 20 Users, Width = 12.5 ps

(d) 29 Users, Width = 12.5 ps

Figure 5.15: Mean and Standard Deviation of the Multi-Access Interference for Bin Code (error bars indicate standard deviation).

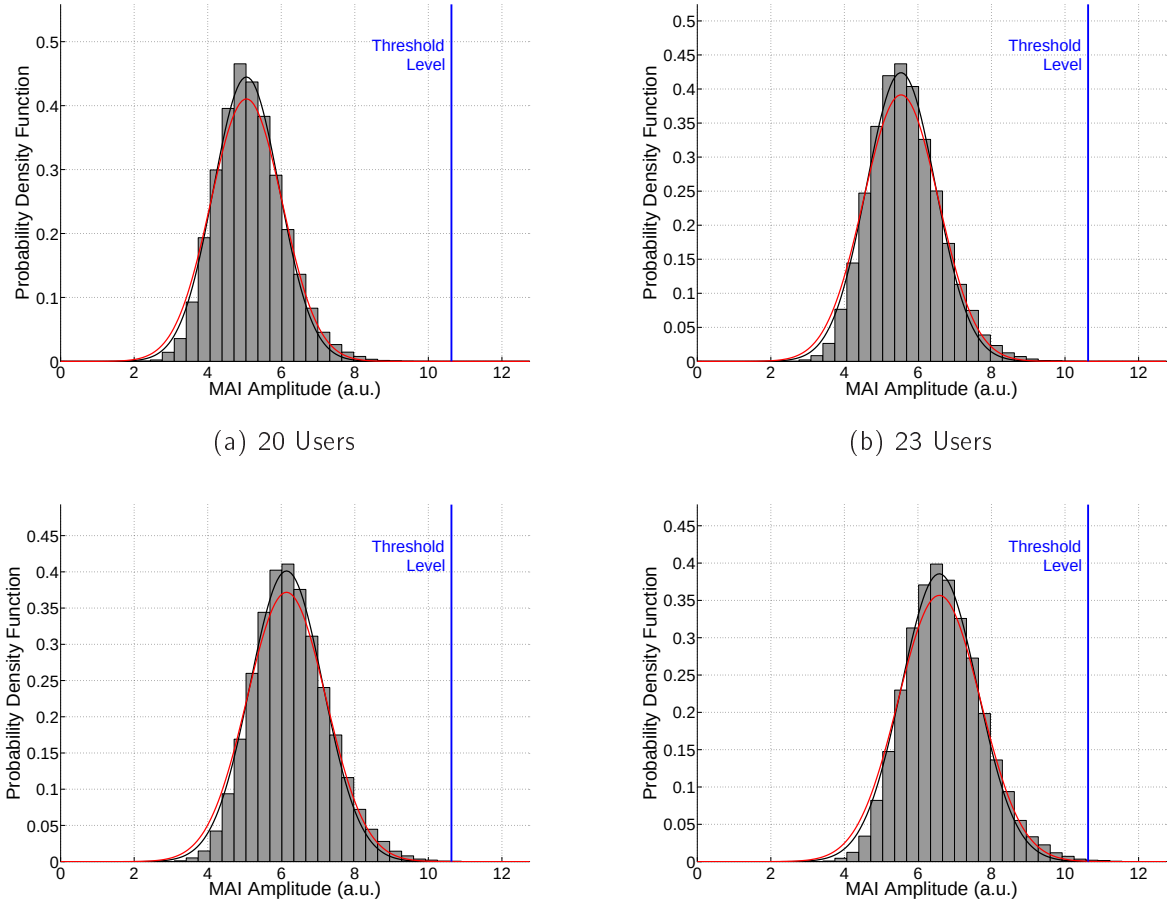

(a) 20 Users

(b) 23 Users

(c) 26 Users

(d) 29 Users

Figure 5.16: MAI probability density functions with Gaussian and folded-Gaussian approximations for Bin Code (black and red lines, respectively) - time skewing between wavelengths is 0.4 ps.

Figure 5.14 shows the average autocorrelation peak amplitude plotted against the time skewing between adjacent wavelengths for different pulse width regimes. These values were obtained by averaging the autocorrelation peak amplitude of all 29 codewords belonging to this code family. As expected, the higher number of wavelengths in the Bin Code results that the time skewing impact is more severe for Bin than PH codes. For example, comparing systems based on 25 ps pulse widths, the autocorrelation peak amplitude is reduced to half with 1.1 ps of time skewing between adjacent wavelength channels while for Prime-Hop Code this happens after 4 ps.

Figure 5.15 shows the expected values of the simulated MAI amplitude as a function of the time skewing with the standard deviation represented using error bars; as with the Prime-Hop Code, there is a trend on increasing both parameters.

Figure 5.16 presents the histograms of the Multi-Access Interference obtained by simulation and their Gaussian approximations similar to the ones obtained for Prime-Hop Code (figure 5.11). Comparing Prime-Hop and Bin Code, one can conclude that the Gaussian approximation fits better the latter for the same number of users. From the discussion in section 5.2 and particularly from equation 5.14, we learn that the application of the Central Limit Theorem depends on the number of chips contributing for the Z value. It is clear that this number is higher for Bin Code. In fact, the cross-correlation function of Prime-Hop Code comprises 7 chips in a bit frame of 49 temporal chip positions (ratio = 0.142). For Bin Code, the number of chips in a cross-correlation function is variable; it depends on the number of active wavelengths of the interfering user that match the active wavelengths of the receiver. The probability of an active wavelength of the interfering users matching the receiver is given by the number of active wavelengths divided

by the total number of wavelengths in the system, i.e., 12/29. Because the interferer has 12 active chips, the average number of chips in a cross-correlation function is 12 × 12 / 29 which is 4.96. Since the number of temporal chips for Bin Code is only 12 (ratio = 0.413), the "density" of chips is higher for Bin than for PH codes; therefore, the Gaussian curve provides a better approximation for Bin Code.

Figure 5.17 shows the BER of the network as a function of the time skewing between adjacent wavelengths channels using Bin Code. Four curves were plotted for 20, 23, 26 and 29 active simultaneous users. The graphs show that Bin Code have lower tolerance to time skewing than Prime-Hop Code. This could be predicted as the number of wavelengths is higher. For example, for 20 active users, only 0.7 ps time skewing can be allowed for error free transmission as opposed to 2.5 ps for Prime-Hop (both with 25ps pulse width). As in Bin Code, results including the electronic bandwidth limitation of the receiver are provided (figure 5.18).

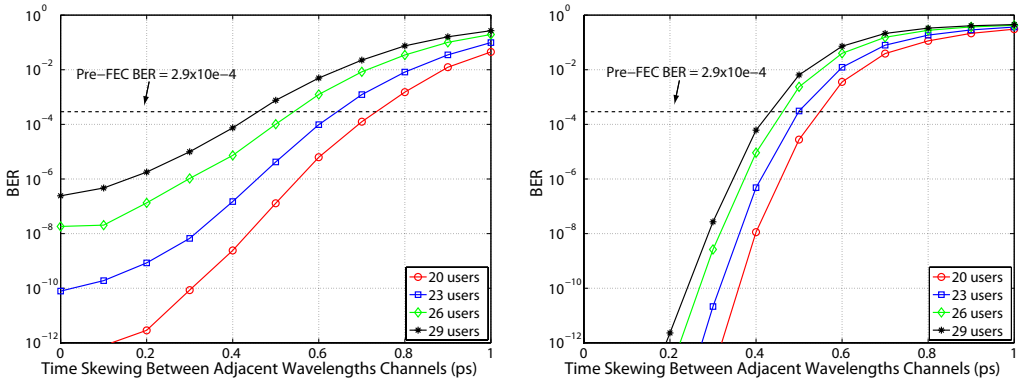

(a) Pulse width = 25 ps (b) Pulse width = 12.5 ps

Figure 5.17: BER as a function of time skewing between adjacent wavelengths for Bin Code.

The results for separate performance impact of autocorrelation peak degradation and MAI increase are shown in table 5.4. These results confirm the conclusion

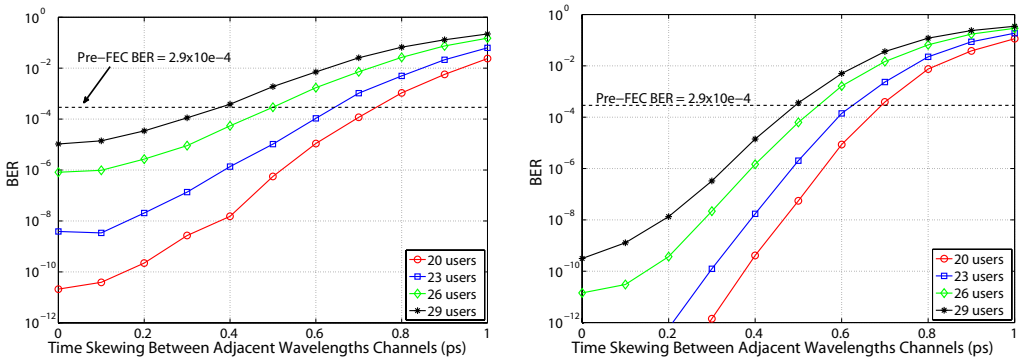

(a) Pulse width = 25 ps (b) Pulse width = 12.5 ps

Figure 5.18: BER as a function of time skewing between adjacent wavelengths for Bin Code - including electronic bandwidth limitation.

Table 5.4: Impact of auto and cross-correlation in the BER of the Optical CDMA system (Bin Code).

TS (ps)		Users			
		20	23	26	29
0	BER	2.59×10^{-13}	7.86×10^{-11}	1.83×10^{-8}	2.42×10^{-7}
0.5	BER	1.29×10^{-7}	4.20×10^{-6}	1.01×10^{-4}	7.61×10^{-4}
	BER_A	1.09×10^{-7}	3.79×10^{-6}	1.07×10^{-4}	5.21×10^{-4}
	BER_M	3.40×10^{-13}	8.91×10^{-11}	1.51×10^{-8}	5.48×10^{-7}
1	BER	4.47×10^{-2}	9.86×10^{-2}	1.95×10^{-1}	2.69×10^{-1}
	BER_A	2.56×10^{-2}	7.10×10^{-2}	1.65×10^{-1}	2.34×10^{-1}
	BER_M	1.92×10^{-11}	2.11×10^{-9}	1.54×10^{-7}	2.22×10^{-6}

obtained for Prime-Hop Code (table 5.3), i.e., the degradation of autocorrelation peak is clearly dominant when compared with the cross-correlation impact of time skewing.

5.4 Propagation in Dispersion Shifted Fibre

So far in this chapter, the study of the time skewing effect was limited to constant time skewing between adjacent wavelength channels. These results were used to

Table 5.5: Wavelength ranges for 100 GHz spacings.

Code	Wavelengths	Wavelength ranges
Bin [57]	29	1536.61 - 1558.98
PH [156]	7	1545.32 - 1550.12

extract conclusions about the unsuitability of the Single Mode Fibre as transmission medium. Dispersion Shifted Fibres (DSF) have been described as a convenient support for Optical CDMA Networks [6]. For this reason, the BER performance is analysed in a realistic propagation scenario over a commercially available DSF fibre with zero-dispersion wavelength at 1547.58 nm and a dispersion slope of 0.06811 ps/nm^2/km. Standard ITU wavelengths with 100 GHz spacing are used with the central wavelength of the system chosen to be the nearest ITU wavelength to the zero-dispersion of the fibre (1547.72 nm). The wavelength ranges for each code are displayed in the table 5.5. For the sake of simplicity and without loss of generality, the attenuation in the fibre is not considered.

In a real star network, the distances between users and the central node of the network are generally variable. In order to model such variation, the simulation considers the distance between the receiver and the matching transmitter as d and the distance between this receiver and any other transmitter as a Gaussian random variable with mean value d and standard deviation of 10% of d. This emulates a more realistic scenario but the difference in results was found to be insignificant. This can be simply acknowledged by considering tables 5.3 and 5.4 where the impact of time skewing in autocorrelation was found to be significantly higher than the impact in cross-correlation. Variable distances between the receiver and interfeering users would only change the amount of time skewing affecting individual cross-correlation functions and therefore its impact is not relevant.

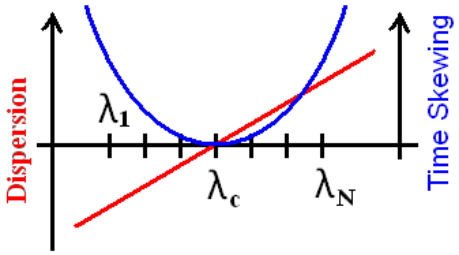

Figure 5.19: DSF fibre dispersion and time skewing profile.

Note that the vector of time skewing delays (τ_i) may be easily calculated by considering that, for a wavelength λ, the time skewing per unit length relative to the DSF zero-dispersion wavelength is

$$\tau(\lambda) = \frac{S}{2}(\lambda - \lambda_{ZD})^2 \tag{5.24}$$

where λ_{ZD} is the zero-dispersion wavelength of the fibre and S the dispersion slope. Note that the time skewing between two adjacent wavelengths is not constant as shown in figure 5.19. In such conditions the time skewing vector, as expressed in equation 5.5, may be defined as follows:

$$\tau_i = \tau(\lambda_i) - \min_i(\tau(\lambda_i)). \tag{5.25}$$

The Bit Error Rate is plotted against the transmission length in the DSF fibre for Bin (figure 5.20) and Prime-Hop Codes (figure 5.21). The trade-offs involved in the selection of a specific code are presented in the table 5.6.

Bin Code allows network operation at bitrates four times higher than the Prime-Hop Code based network, for the same chiprate but this comes at the expense of optical bandwidth as shown in table 5.6. Without considering the effect of dispersion, the network can support either 21 active simultaneous users with a

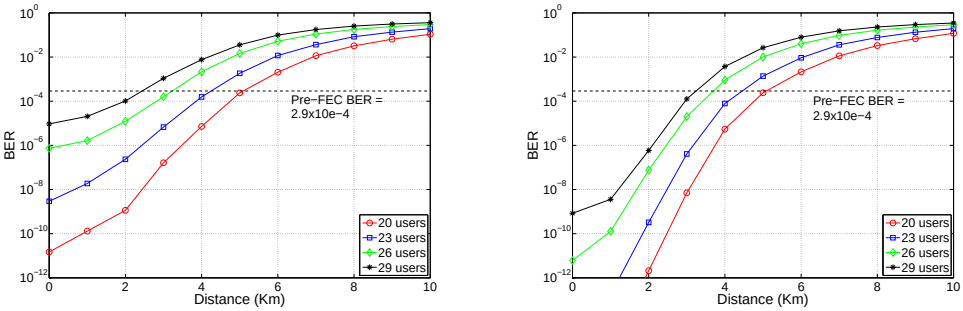

(a) Pulse width = 25 ps (b) Pulse width = 12.5 ps

Figure 5.20: BER as a function of DSF transmission length for Bin Code.

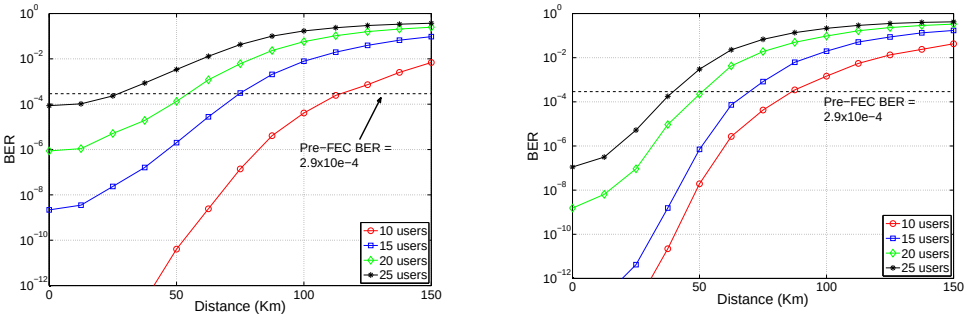

(a) Pulse width = 25 ps (b) Pulse width = 12.5 ps

Figure 5.21: BER as a function of DSF transmission length for Prime-Hop Code.

BER of 10^{-10} with Bin Code or only 14 users with Prime-Hop (with 25 ps pulse width). In this scenario, 12.5 ps pulse widths allow a higher number of users: 18 users for Prime-Hop Code and 27 users for Bin Code. Comparing Bin and PH codes for identical initial conditions ($BER = 10^{-10}$ at 0 km), the propagation in DSF fibre with FEC is limited to 4.5 km with Bin Code, while PH Code allows error free operation up to 70 km. Comparing the systems for equal number of users (20), PH codes allows longer transmission propagation than Prime-Hop Code.

While Single Mode Fibre was found to be unsuitable for multi-wavelength Optical CDMA transmission, the discussion above proves time skewing is a very relevant impairment when DSF is used. In fact, the sharp degradation of BER performance with distance, especially in Bin Code, hints that schemes to compen-

Table 5.6: Comparison between Bin and Prime-Hop Code @ 40 GChip/s.

Code	**Bin [57]**		**PH [156]**	
Pulse width	25 ps	12.5 ps	25 ps	12.5 ps
Bitrate	3.33 GBit/s		816 MBit/s	
Number wavelengths	29		7	
Optical Bandwidth	22.37 nm		4.8 nm	
Max. no. users[a]	21	27	14	19
Max. distance[b]	$\backsim 4.5km$	$\backsim 3.5km$	$\backsim 70km$	$\backsim 60km$
Max. distance (20 users)[c]	$\backsim 5km$	$\backsim 5km$	$\backsim 60km$	$\backsim 50km$

[a] Number of users for 10^{-10} BER with no time skewing (back-to-back).
[b] Maximum distance for the number of users in [1] using FEC.
[c] Maximum distance for 20 users using FEC.

sate residual dispersion are required in WHTS Optical CDMA networks.

5.5 Transversal Filter in Optical CDMA Compensation

As shown in chapter 3, analogue transversal filters have been proposed for Optical Communication networks. The adaptability and simplicity of such a device provides the means to overcome fatal transmission impairments like Chromatic Dispersion (CD), Polarisation Mode Dispersion (PMD), inter-modal dispersion in multi-mode fibres and other nonidealities in the optical link. However, analogue electrical signal processing has never been proposed in the context of Optical CDMA networks.

Electronic post-detection processing is a potential solution to mitigate the Optical CDMA performance degradation due to time skewing. In fact, the auto-correlation to Multi-Access Interference (MAI) ratio of the Optical CDMA system

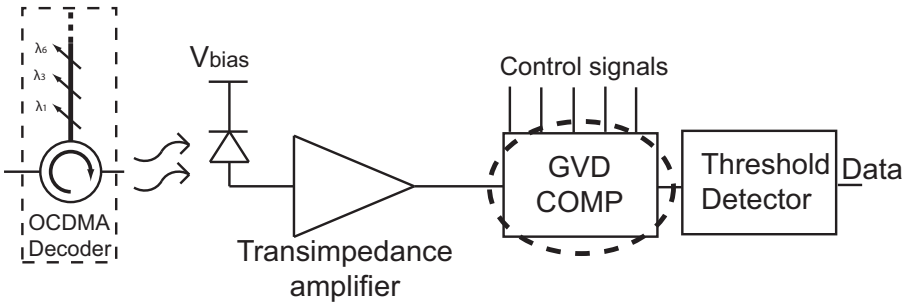

Figure 5.22: Optical CDMA receiver with GVD compensation.

can be improved (and therefore the BER can be reduced) through electronic signal processing. The remaining part of this chapter provides a study on the limitations and performance enhancement that such proposal may provide.

The structure of the proposed Optical CDMA receiver is shown in figure 5.22. The Optical CDMA signal is decoded in the optical domain using traditional methods (for example, an array of Fibre Bragg Gratings [1]) after which it is received with a photodetector. The compensator is a transversal filter with the temporal response described by equation 5.26.

$$x_{outTF}(t) = \sum_{j=0}^{N-1} G_j x_{in}(t - jT) \tag{5.26}$$

where N is the number of stages of the transversal filter, T is the temporal spacing between transversal filter taps, G_j is the gain coefficient of the stage j.

5.5.1 Model Description

Figure 5.23 shows the complete simulation model used in this section. The model is similar to the one used in section 5.2 but also includes the transversal filter for time skewing compensation.

The first step is the calculation of the threshold level. Following the same

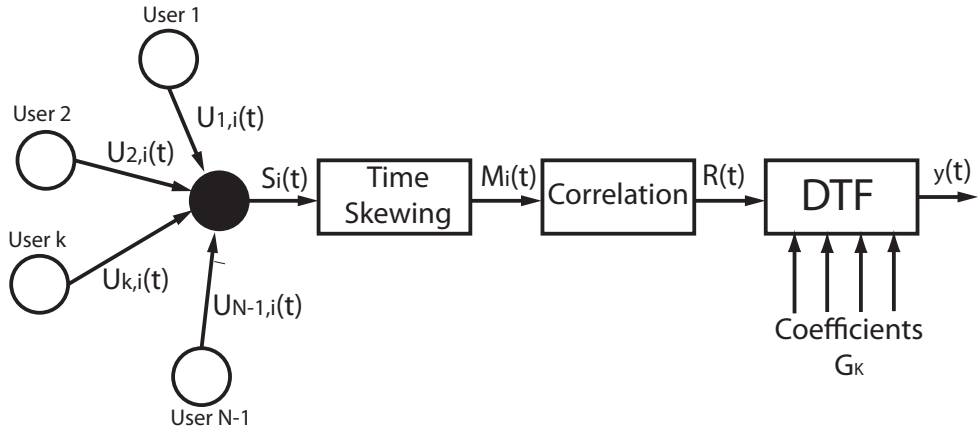

Figure 5.23: Modelling diagram of a star Optical CDMA system including a Distributed Transversal Filter.

methodology presented in section 5.2, the intensity of the optical field in the photodetector when only the correct user is in the network $(A(t)_k)$ is given by:

$$A(t)_k = \sum_{i=0}^{q} \gamma(c_k(i))\Psi(t-\tau_i). \tag{5.27}$$

Considering equations 5.26 and 5.27, the output of the transversal filter is given by the expression

$$A(t)_{CP_k} = \sum_{j=0}^{N-1}\sum_{i=0}^{q} G_j\gamma(c_k(i))\Psi(t-jT-\tau_i). \tag{5.28}$$

As explained in section 5.2, the ideal setting for the threshold is the amplitude of the autocorrelation peak of the code. Therefore:

$$TH_{CP_k} = \max_t(A(t)_{CP_k}) = \max\left(\sum_{j=0}^{N-1}\sum_{i=0}^{q} G_j\gamma(c_k(i))\Psi(t-jT-\tau_i)\right). \tag{5.29}$$

The transversal filter temporal response is formed as a linear combination of the voltages taken from uniformly spaced taps in a non dispersive delay line. For

this reason, the impact of the transversal filter in the Multi-Access Interference (MAI) depends on the relative position of the cross-correlations of different users, which is a random process. Therefore, the statistical distribution of the MAI with presence of the transversal filter is analysed with a model similar to the one presented in the section 5.2. Recalling equation 5.6 in section 5.2, $R(t)$ is given by:

$$R(t) = \sum_{i=1}^{q} \gamma(c_N(i)) M_i(t - (L - c_N(i))T_{chip}). \tag{5.30}$$

From equations 5.26 and 5.30, $y(t)$ is given by:

$$y(t) = \sum_{j=0}^{N-1} \sum_{i=1}^{q} \gamma(c_N(i)) M_i(t - jT - (L - c_N(i))T_{chip}). \tag{5.31}$$

The Gaussian distribution mean (μ) and standard deviation (σ) are calculated through analysis of the vector $y(t)$ following the procedure presented in the section 5.2 and the Bit Error Rate of the system calculated as follows

$$BER_k = \frac{1}{2\sigma\sqrt{2\pi}} \int_{TH_{CPk}}^{+\infty} \exp\left(-\frac{(x-\mu)^2}{2\sigma^2}\right) dx. \tag{5.32}$$

5.5.2 Transversal Filter Optimisation

For each network scenario (comprising a time skewing regime and a number of active users), there is combination of the transversal filter coefficients G_j that maximise the performance of the system. This ideal combination is determined through optimisation of the system according to the loop presented in figure 5.24.

The first optimisation algorithm considered was the Nelder-Mead "simplex" described in [162]. This algorithm can be classified as a "direct search method".

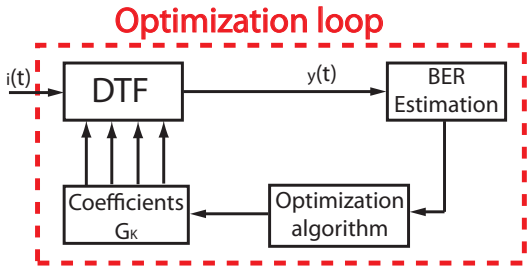

Figure 5.24: Optimisation loop of the gain coefficients.

This optimisation method is easy to program, does not require derivatives, and is often claimed to be robust for problems with discontinuities or where the function values are noisy [163]. However, Nelder-Mead "simplex" algorithm is susceptible to being trapped by local minima. This is particularly problematic in the optimisation of the transversal filter because this device is redundant in the sense that different gain coefficient combinations can give rise to the same output. This led the optimisation process to converge to a local minimum of the BER function.

In order to overcome this problem, Genetic Algorithms (GA) were chosen as the optimisation method. Genetic algorithms are known for exploring larger input variables combinations (larger spaces) and also for being less prone to converge to a local minimum [164].

The idea behind this algorithm is the survival of the fittest individuals. In nature, stronger individuals have higher probability of survival and reproduction, originating descendants. These are likely to be as well or better adapted to the environment than their parents, because they inherit their favourable genes. On the other hand, weaker individuals have lower probability to reproduce. Therefore, future generations are likely to be more adapted to the environment that the preceding ones. This process forms the base of natural selection introduced by Darwin and it is considered a central element in the modern theory of evolution.

The "survival of the fittest" concept is applied in genetic algorithms. First, a set of possible solutions is generated after which these solutions are recombined to obtain a new generation. Each solution is represented by an individual in the population, and their aptitude corresponds to their cost function values. An individual is more adapted than other if its cost function value is nearer the optimum. The goal is to create better solutions from generation to generation, in order to achieve the best fit individual (global optimum of the problem).

The main steps involved in the genetic algorithm are the formulation of the problem, creation of an initial population (initialisation), selection, reproduction and termination.

Problem formulation

Two types of simulations were considered in this section: one comprises the optimisation of the transversal filter gain stages and the second includes, apart from the gain stages, the interstage delay between adjacent transversal filter taps. In both cases, the delay between taps does not vary within the same device.

The simulation including temporal spacing is expected to give better results because it comprises an additional degree of freedom. However, this would require variable delays between taps in the DTF structure. With the current techniques, this is very difficult to achieve. The delay lines would have to include variable capacitors and lines with variable inductance to maintain their characteristic impedance. To the author's knowledge, a device with such characteristics has yet to be implemented for high speed operation (Gigabit per second applications).

On the other hand, simulations including solely the optimisation of gain stages may have practical applications by using existent distributed transversal filters such

as the ones described in chapter 3. In this case, simulations consider the total delay of the transversal filter to be equal to the chip time.

All stage gains span from zero to a maximum gain which, for simulation purposes, will be set to unity. Since the value of each individual tap gain only has significance in relation to the others, it is possible to define the central tap gain as one and optimise the remaining variables. Therefore, the optimisation problem has (N-1) variables for the optimisation without temporal spacing and N when temporal spacing is included. In genetic algorithms, each individual optimisation variable is called "gene", and the vector containing all optimisation variables is named "chromosome".

The problem can be described by the following expression:

$$\min(log_{10} BER_k). \tag{5.33}$$

The optimisation of the gain stages is subject to the following conditions:

$$G_j = \begin{cases} 1 \quad \text{for } j = \begin{cases} \frac{N_{stages}+1}{2} & \text{if } N_{stages} \text{ is odd} \\ \frac{N_{stages}}{2} & \text{if } N_{stages} \text{ is even} \end{cases} \\ [0,1] \quad \text{for any other j value} \end{cases} \tag{5.34}$$

$$T = \frac{T_{chip}}{N_{stages} - 1}. \tag{5.35}$$

For simulations including temporal spacing optimisation, T becomes an optimisation variable subject to the following limits:

$$T \in \left(0, 2\frac{T_{chip}}{N_{stages} - 1}\right]. \tag{5.36}$$

Initial population

The trade-off between algorithm efficiency and population diversity is the main factor to consider when selecting the population size. In fact, larger population sizes could give rise to extremely long simulation periods because the cost function of each individual has to be evaluated in each generation; on the other hand, small populations may reduce diversity and lead the algorithm towards a local solution. In this project each generation has a population of 25 individuals.

As usual in genetic algorithms, individuals of the initial population are generated randomly. This generation process is selected to assure diversity in the initial population and to avoid bias.

Selection

The selection of individuals that will pass for the next generation is an important operation because it defines the algorithm convergence. Roulette selection chooses parents by simulating a roulette wheel, in which the area of the wheel section corresponding to an individual is proportional to the individual's fitness. In other words, the algorithms randomly picks one individual with a probability proportional to its fitness.

Reproduction

Genetic Algorithms can generate children with three different methods described as follows:

1) Elite Children

The genetic algorithm allows to define a number of elements that are guaranteed to survive to the next generation. These are named "elite individuals" and are the elements with highest fitness. While this process guarantees that the best individuals stay in the next generation, it should be noted that it does not contribute for the diversity of future generations and this may lead the algorithm to a local minima. For this reason, only two elite children were chosen in the optimisation process.

2) Crossover

Crossover is the operation that, from two parents selected by roulette wheel, generates a new child for the next generation. Several methods for crossover are described in the literature; this project employs a scattered function. This method creates a random binary vector with a length equal to the number of optimisation variables. The child takes genes from parent 1 in the positions corresponding to "0" and genes from parent 2 where the binary vector takes value "1". For example, if p1 and p2 are the parents

p1 = [a b c d]

p2 = [e f g h]

and the binary vector is [0 1 1 0], the "chromosome" of the child is:

child = [a f g d]

3) Mutation

Mutation provides genetic diversity and enables the genetic algorithm to search

broader spaces. The main purpose is to avoid local minima by preventing individuals from becoming too similar to each other, thus slowing or even stopping evolution. The mutation is performed by adding a small random number to each entry of the selected individual "chromosome". The ratio crossover/mutation was selected to be 80:20; this is a common value and reflects the fact that crossover is generally considered more important for the genetic algorithm progression than mutation. For example, this is the default value for commercial software packages such as Matlab's "Genetic Algorithm and Direct Search Toolbox".

Termination by Local Search

The genetic algorithm stops after completing 30 generations. Because GAs normally show a very fast initial convergence, followed by progressively slower improvements it is effective to combine it with a local optimisation method. Therefore, a local search optimisation method based on gradients is used, taking the genetic algorithm solution as a seed. Figure 5.25 presents a block diagram of the genetic algorithm.

5.6 Compensation Results

The transversal filter compensator performance is analysed for different scenarios with constant time skewing between wavelength channels. The simulations were performed for a 40 GChip/s Optical CDMA system based on Bin Code and Prime-Hop Code, with pulse width of 12.5 ps. Each scenario is characterised by time skewing between wavelength channels and a number of simultaneous active users in the Optical CDMA network. All calculations include modelling of the bandwidth

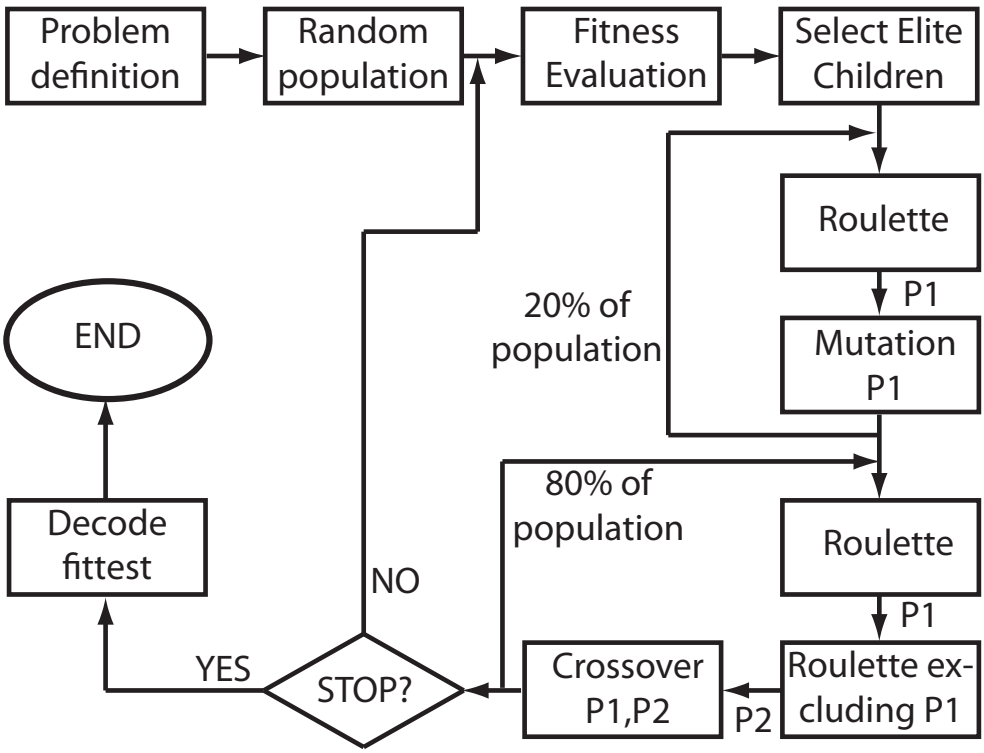

Figure 5.25: Genetic algorithm block diagram.

limitation of the electrical receiver with a 3rd order Bessel filter with 3dB cut-off frequency at 40 GHz.

5.6.1 Bin Code

In this section, the electronic compensation of Bin Code based Optical CDMA is analysed. Simulations are performed for a varying number of transversal filter stages.

Figure 5.26 provides an overview of the genetic algorithm performance. The graphs show the best and average values of $\log_{10}$(BER) for each genetic algorithm generation. The graphs show faster convergence for the final solution with lower number of transversal filter stages. Moreover, the convergence between the best individual's BER and the average value of the population tends to occur with lower

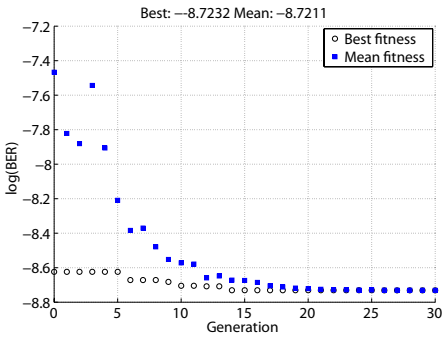

(a) 10 Users, 3 stages, $\Delta T = 1$ ps

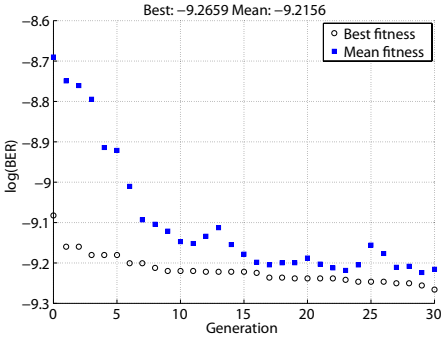

(b) 10 Users, 7 stages, $\Delta T = 1$ ps

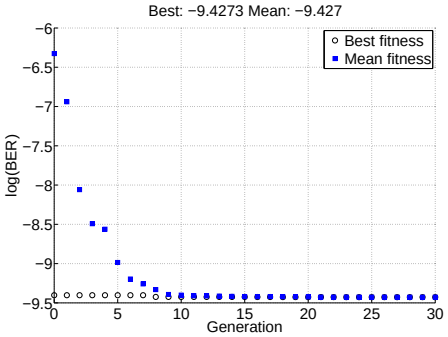

(c) 14 Users, 3 stages, $\Delta T = 0.6$ ps

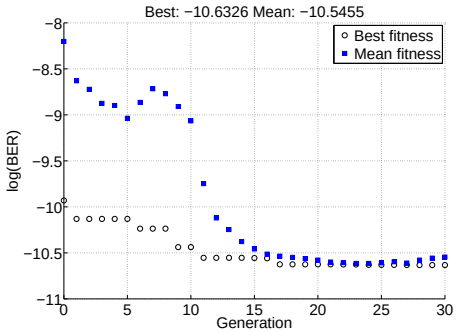

(d) 14 Users, 7 stages, $\Delta T = 0.6$ ps

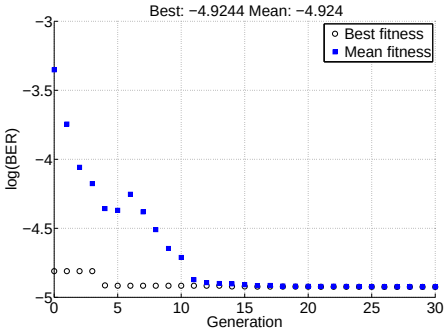

(e) 20 Users, 3 stages, $\Delta T = 0.6$ ps

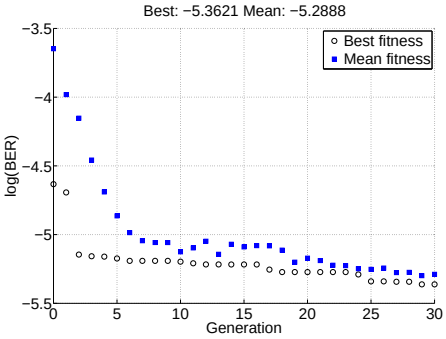

(f) 20 Users, 7 stages, $\Delta T = 0.6$ ps

Figure 5.26: Bit Error Rate for each generation of genetic algorithm (best individual and population average). Note: ΔT = time skewing between adjacent wavelength channels.

number of generations for three stages than with seven. These results could be predicted because higher number of transversal filter stages corresponds to higher diversity in the genetic algorithm population.

Figure 5.27 shows the Optical CDMA Bit Error Rate (BER) as a function of the number of the transversal filter stages. Six plots are shown for 10, 12, 14, 16, 18 and 20 users with the constant time skewing between adjacent wavelength channels ranging from 0.4 ps to 1.4 ps, as indicated for each curve. For each scenario considered, two curves are plotted: the blue curves describe the optimisation results for the fractionally spaced transversal filter with total delay equal to T_{chip} (interstage delay given by the equation 5.35), while the red curve describes the case where the delay between adjacent taps is added as an optimisation variable. The figure shows very significant improvements in the system BER. For example, when 10 simultaneous users share the network and the time skewing is 1 ps between wavelength channels, the performance gain is about five orders of magnitude for a transversal filter with only four taps.

The first conclusion to extract from figure 5.27 is that the transversal filter achieves maximum performance enhancement with only four taps; all graphs clearly show that the BER has very limited or no improvement for more than four stages. This conclusion has important practical consequences since building high-speed distributed transversal filters with large number of taps is very difficult with current techniques.

Figure 5.27 also allows the comparison between the performance of the transversal filter with and without variable temporal spacing between taps. The main conclusion is that variable delay increases the performance when the number of stages is small (two or three) but provides no advantage for a number of stages of

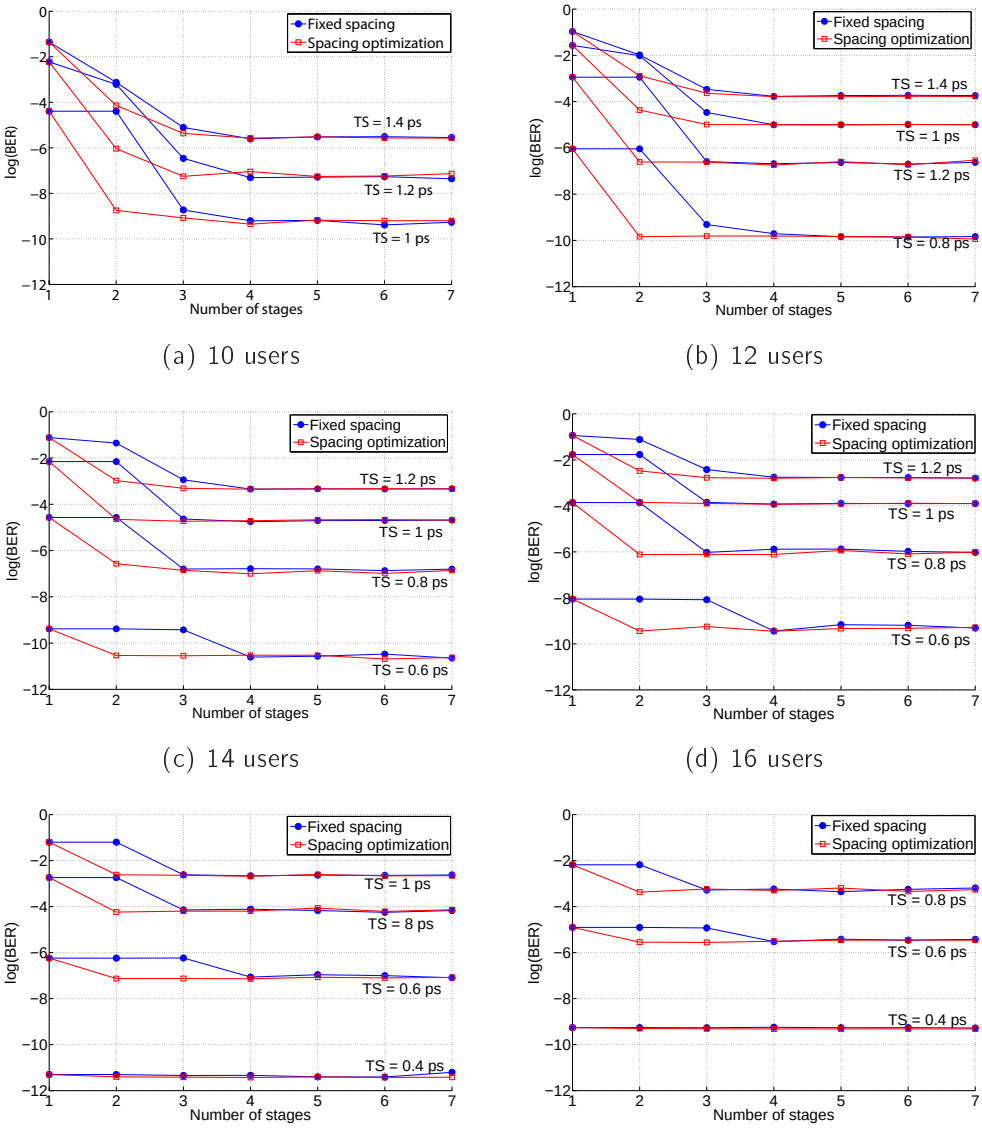

(a) 10 users

(b) 12 users

(c) 14 users

(d) 16 users

(e) 18 users

(f) 20 users

Figure 5.27: Bit Error Rate as a function of the number of transversal filter stages.

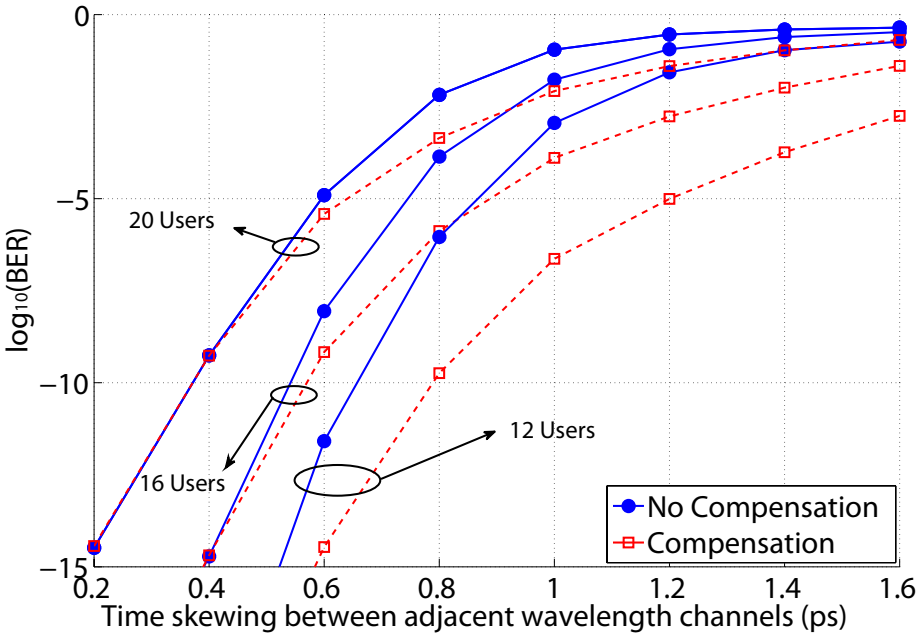

Figure 5.28: BER as a function of time skewing for compensated and uncompensated Optical CDMA system (20,16 and 12 users) - Bin Code.

four and beyond. As explained before, the implementation of distributed transversal filters with tunable delays presents many technological challenges with current techniques and processes. In practical terms, these simulations show that this feature is not necessary for transversal filters with a number of stages larger than four.

The transversal filter performance improvement as a function of the time skewing is shown figure 5.28 and 5.29 using a transversal filter with five stages and no tunable time delay between them. The results were divided in two separate graphs for clarity, with results concerning 12, 16 and 20 users in figure 5.28 and 10, 14 and 18 users in figure 5.29. For each scenario two curves are plotted: uncompensated (blue line) and compensated (red dashed line).

These graphs show that the performance improvement depends primarily on the time skewing regime. For all cases studied, there is no BER improvement for

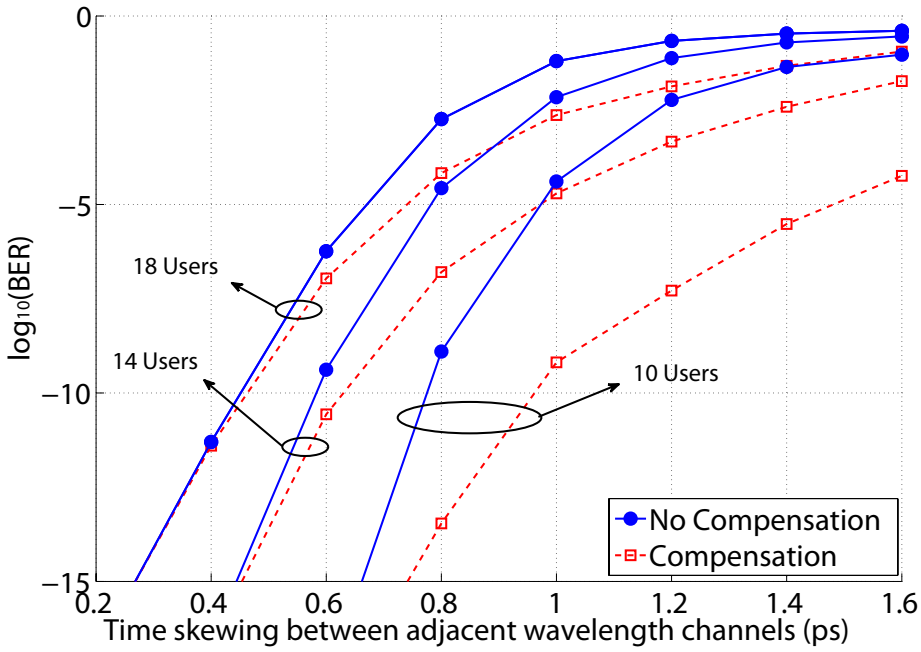

Figure 5.29: BER as a function of time skewing for compensated and uncompensated Optical CDMA system (18,14 and 10 users) - Bin Code.

time skewing regimes up to $\Delta T = 0.4$ ps. For higher values of time skewing, the transversal filter provides improvements in the BER up to five orders of magnitude for the analysed scenarios.

Table 5.7 shows the transversal filter gains for a particular scenario comprising 16 users and time skewing between adjacent wavelength channels of 1ps. The flexibility increases with the number of stages but it is clear that there is no advantage of using more than 4 stages, provided that the transversal filter gains can be tunned to any fraction of the maximum gain.

Table 5.8 shows the evolution of transversal filter gains with the time skewing for 10, 12, 14, 16, 18 and 20 users, considering a 5-stage device. The analysis of trends in this evolution aids understanding the operation of the transversal filter in the context of Optical CDMA networks.

Table 5.7: Transversal filter gains for 16 users and $\Delta T = 1$ps.

N_{stages}	G0	G1	G2	G3	G4	G5	G6	log_{10}BER
NTF*								-1.77
2	**1**	0	-	-	-	-	-	-1.77
3	0	**1**	0.90	-	-	-	-	-3.84
4	0	**1**	0.66	0.81	-	-	-	-3.91
5	0	0.92	**1**	0.59	0.97	-	-	-3.92
6	0	1	**1**	0.52	0.95	0.99	-	-3.91
7	0.01	0.99	0.31	**1**	0.05	0.99	0.13	-3.90

*NTF = No Transversal Filter/ No compensation

The first clear trend is the increase on the magnitude of transversal filter gains with time skewing. In fact, for the lowest time skewing regime analysed ($\Delta T = 0.2$ ps), the optimisation leads to only one non-zero gain which means that the transversal filter does not have effect on the system; it is effectively acting as a single stage device. Initially, as the time skewing increases, gains around the central stage (which has fixed gain at 1) start to increase. This corresponds to cases where the autocorrelation peak is moderately spread and therefore the total transversal filter delay required to compensate it is still low. For higher values of time skewing the spread in autocorrelation peak grows and the external stages (1 and 5) are switched on.

Apart from its effect in the autocorrelation peak, the transversal filter also has an impact on the Multi-Access Interference. In fact, when the transversal filter is present, the MAI comprises the linear combination of the cross-correlation functions of all users. Therefore, an increase in the transversal filter gains will have an negative impact on the system performance by increasing MAI. From the previous discussion, one can conclude that the optimum transversal filter gains provide an ideal balance between improvement in the autocorrelation peak and

(a) 10 Users

ΔT	G0	G1	G2	G3	G4
0.2	0	0	**1**	0	0
0.4	0	0	**1**	0.37	0
0.6	0	1	**1**	0	0
0.8	0	0	**1**	0.27	0.85
1	1	1	**1**	0.96	0.68
1.2	0.99	0.82	**1**	0.65	1
1.4	1	0.71	**1**	0.58	1
1.6	1	0.52	**1**	0.38	1

(b) 12 Users

ΔT	G0	G1	G2	G3	G4
0.2	0	0	**1**	0	0
0.4	0	0	**1**	0.35	0
0.6	0	0.97	**1**	0.32	0
0.8	1	0.50	**1**	0	0
1	1	0.99	**1**	0.99	0.02
1.2	0.99	0.84	**1**	0.68	0.99
1.4	1	0.66	**1**	0.52	0.99
1.6	1	0.45	**1**	0.28	1

(c) 14 Users

ΔT	G0	G1	G2	G3	G4
0.2	0	0	**1**	0	0
0.4	0	0	**1**	0.07	0
0.6	0	0	**1**	0.74	0.65
0.8	0.01	1	**1**	0.93	0
1	1	1	**1**	1	0
1.2	0.99	0.90	**1**	0.75	0.87
1.4	1	0.57	**1**	0.44	0.99
1.6	1	0.38	**1**	0.20	1

(d) 16 Users

ΔT	G0	G1	G2	G3	G4
0.2	0	0	**1**	0	0
0.4	0	0	**1**	0.05	0
0.6	0	0	**1**	0.94	0.57
0.8	0	1	**1**	0.86	0.01
1	0	0.92	**1**	0.59	0.97
1.2	1	1	**1**	0.91	0.92
1.4	1	0.59	**1**	0.43	1
1.6	1	0.27	**1**	0.13	1

(e) 18 Users

ΔT	G0	G1	G2	G3	G4
0.2	0	0	**1**	0	0
0.4	0	0	**1**	0.04	0
0.6	0	0	**1**	0.79	0
0.8	1	0.63	**1**	0	0
1	1	0.94	**1**	1	0
1.2	1	1	**1**	0.91	0.91
1.4	1	0.60	**1**	0.47	1
1.6	1	0.40	**1**	0.24	1

(f) 20 Users

ΔT	G0	G1	G2	G3	G4
0.2	0	0	**1**	0	0
0.4	0	0	**1**	0	0
0.6	0	0	**1**	0.78	0
0.8	0	0	**1**	0.30	0.83
1	0	0.98	**1**	0.63	1
1.2	0.99	1	**1**	0.93	0.87
1.4	1	0.70	**1**	0.52	1
1.6	1	0.50	**1**	0.32	1

Table 5.8: Transversal filter gains as a function of time skewing.

degradation in the MAI.

An important conclusion to derive from tables 5.8 is the dependence of the optimal gains with the number of users in the network. It is clear that the magnitude of the stage gains decreases with the number of users. Taking the time skewing regime of $\Delta T = 0.4$ ps as an example, the magnitude of $G3$ is one third of its maximum value with ten users and is consistently reduced until it reaches zero for 20 users. This trend is also clear for all other time skewing regimes.

In fact, more users in the network implies that MAI comprises higher number of cross-correlation function contributions in the same temporal period. Since the transversal filter provides a linear combination of delayed versions of this original MAI, higher density of cross-correlation functions means that higher gain coefficients will generate higher MAI peaks. This explains why the transversal filter coefficients tend to have lower values for high number of users in the network. Note that the impact of the transversal filter in the autocorrelation peak is independent of the number of users in the network.

The main conclusion to extract from this study is that the use of a post-detection transversal filter have a positive effect on the autocorrelation peak (and therefore in the threshold level of the system) and a detrimental effect on the Multi-Access Interference. However, through system optimisation, it is possible to find a balance so that the overall Optical CDMA system performance is improved.

In practice, a receiver similar to the one presented in figure 5.30 could be implemented. The system would monitor the number of simultaneous active users through a scheme such as the one proposed in [165]; this scheme uses a low pass filter to obtain information about the average optical power in the network. This information could be used by a simple microprocessor to estimate the number of

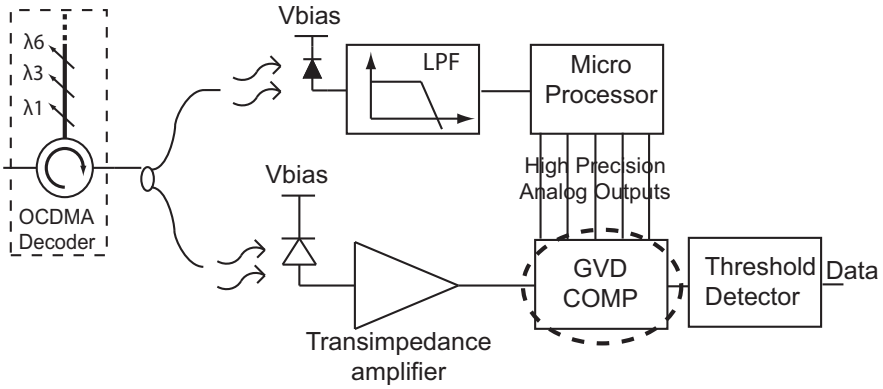

Figure 5.30: Possible Optical CDMA receiver with GVD compensation based on transversal filter.

users in the network. The microprocessor would maintain a lookup table with the optimum gains for each particular scenario comprising the number of users and the time skewing regime.

5.6.2 Prime-Hop Code

In the previous section, detailed analysis of the compensation of time skewing with Bin Code was provided. The conclusions obtained can be applied to Prime-Hop Code namely in terms of the performance of the genetic algorithm, number of stages necessary for compensation, and evolution of compensation coefficients with time skewing and number of users. Therefore, this section presents only the final BER results for Prime-Hop Code since the analysis and detailed results are analogous to those of the section 5.6.1.

Figure 5.31 and 5.32 show the BER improvement as a function of time skewing. The results were divided in two separate graphs for clarity, with results concerning 10, 14 and 18 users in figure 5.31 and 12 and 16 users in figure 5.32. For each scenario two curves are plotted: uncompensated (blue line) and compensated (red

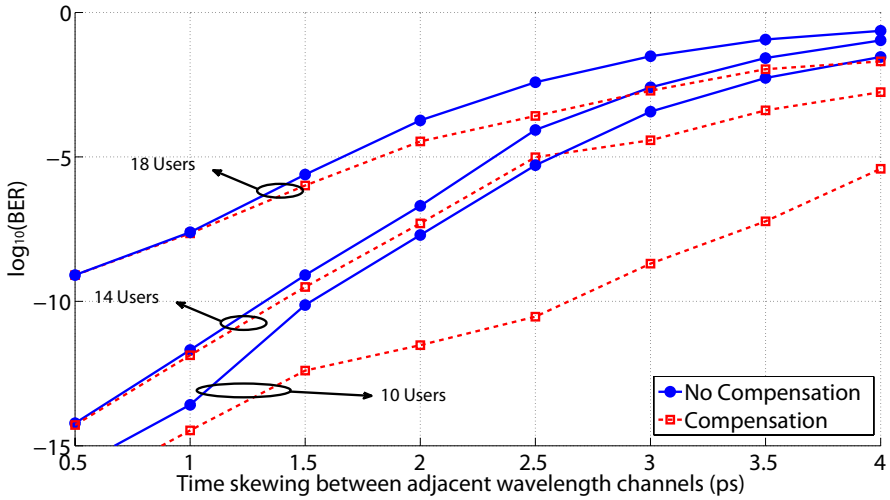

Figure 5.31: BER as a function of time skewing for compensated and uncompensated Optical CDMA system (18,14 and 10 users) - PH codes.

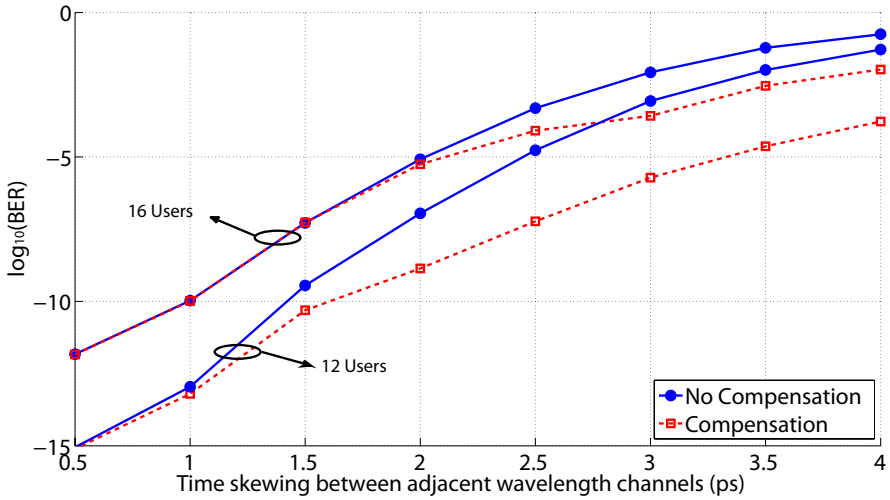

Figure 5.32: BER as a function of time skewing for compensated and uncompensated Optical CDMA system (16 and 12 users) - PH codes.

dashed line). Very significant improvements can be observed namely exceeding five orders of magnitude of BER.

5.7 Summary

In this chapter, the impact of time skewing due to Group Velocity Dispersion in Optical CDMA systems is analysed and a scheme for its compensation is proposed. A new semi-analytical model was developed to provide an accurate measure of the network performance while avoiding the use of pure Monte-Carlo simulations, which are inefficient in terms of simulation time. The model assumes Multi-Access Interference as the dominant source of errors as usual in most of the Optical CDMA literature. The work presented in this chapter gave rise to several publications in conference proceedings including regular papers [166] [167] [168] and an invited contribution [149].

For numerical comparison, two families of Optical CDMA codes were selected: Bin Code and Prime-Hop Code. These have similar dimensions but opposite balances between number of wavelengths and time slots. Numerical results clearly show that time skewing has a severe impact on multi-wavelength Optical CDMA. Results provide numerical evidence that Single Mode Fibre (SMF) is not a suitable medium for multi-wavelength Optical CDMA transmission. Moreover, results show strong degradation of the Bit Error Rate using Dispersion Shifted Fibres.

The main part of this chapter and the main purpose of the model is the assessment of the performance of the Optical CDMA network with an electrical compensation scheme. This scheme is based on a simple transversal filter structure that can be fabricated with commercial IC processes. Advantages of this

scheme include the flexibility to adapt the electrical characteristics of the filter by simply adjusting DC bias voltages, low-cost and the fact that the filter can be embedded in the electrical receiver avoiding the use of bulky all-optical solutions. The model also proposes a new optimisation method for estimation of the compensation parameters based on Genetic Algorithms. This method avoids problems encountered with gradient-based methods and "Simplex" algorithms, namely convergence for local minimum.

Results show that transversal filters with four stages and fixed delay between stages provide the best performance that can be achieved with a transversal filter using positive tap gains. In fact, from the modelling results one can conclude that a higher number of stages and/or variable delays between stages provides no advantage when compensating for time skewing. These conclusions are important because the fabrication of distributed transversal filters with a high number of stages and low dispersion is difficult with current techniques and achieving tunable delay between stages is considered impractical for high-speed applications.

Results also show that, apart from the time skewing regime, the compensation coefficients (stage gains of the transversal filter) are dependent on the number of simultaneous active users in the network. Therefore, an accurate compensation of the time skewing requires the use of a system that can estimate the number of users in the network. These have been proposed before and can be simply based on power measurements in the network.

The use of the transversal filter leads to very significant improvements in the network performance (up to five order of magnitude of BER). However, results show that the effectiveness of this approach is reduced as the number of active users in the network increases. In fact, results clearly show that the proposed

scheme is more effective for a scenario comprising a moderate number of users and a system affected by large values of time skewing.

This chapter provides an overview on the problem of time skewing in Optical CDMA. To the author's knowledge this is the first time that electronic compensation is considered in the context of Optical CDMA networks. It is hoped that this work contributes to the progression of the Optical CDMA field.

Chapter 6

Experimental Demonstration of Optical CDMA Group Velocity Difference Compensation

In the previous chapter, the performance degradation due to Group Velocity Difference induced time skewing was analysed in the context of multi-wavelength Optical CDMA systems. Modelling results were presented to study its effect on auto and cross-correlation characteristics, Multi Access Interference (MAI) and the Bit Error Rate (BER) of the system. Moreover, a potential solution based on electronic post-detection compensation was presented to alleviate this problem.

This chapter provides experimental demonstration of the principles presented in the previous chapter. The experimental setup is intended to show the impact of Group Velocity Difference induced time skewing in multi-wavelength Optical CDMA systems and to test the compensation scheme proposed. The aims of the work presented in this chapter include:

1. Analysis of the time skewing effect due to Group Velocity Dispersion in

Optical CDMA including its consequences in the auto and cross-correlation properties of the Optical CDMA system.

2. Explore the possibility of time skewing compensation in the electrical domain with a transversal filter and identify its practical limitations.

For such purpose, a Wavelength-Hopping Time-Spreading Optical CDMA system based on Fibre Bragg Grating encoding and decoding was designed and implemented. The system operates at 20 GChip/s and the wavelength spacing between channels was chosen to be 200 GHz. New optical orthogonal codes were created comprising five wavelength channels, four active chips and eight time slots. The system operates at 20/8 = 2.5 GBit/s [1].

6.1 Codes Design

The codes analysed in the previous chapter (Bin Code and Prime-Hop Code) were not suitable for this experimental demonstration due to practical limitations of the experimental setup. The selected family of Bin Code would require 29 wavelengths; a network based on such code was not possible to implement because there were not 29 tunable laser sources available and also due to the low number of phase masks for FBG printing. The selected family of Prime-Hop Code has only seven wavelengths but the number of temporal chips (49) would require FBG arrays with lengths exceeding 25 cm; the grating writing system could not accurately fabricate FBG arrays with such long spans. Therefore, there was a

[1] This work was done in collaboration with Instituto das Telecomunicacoes (IT), Aveiro, Portugal. The experimental setup and fabrication of Fibre Bragg Grating Arrays was done in the IT facilities in the University of Aveiro, Santiago campus. The FBG fabrication was performed by Mr. Carlos Marques.

need to search for other codes that, even with less practical interest, would fit the practical constraints of the experimental setup.

The first Optical CDMA codes considered for this experimental demonstration were proposed by Mendez and co-workers in [169], where an Optical CDMA network was successfully implemented in a laboratory environment. It should be noted that some problems have been reported with such codes, namely the fact that the cross-correlation constraint is not one for all the codewords, as it was implicit in the initial proposal of the codes [170]. Moreover, the majority of the codewords belonging to the "Mendez code" could not be used in this experiment because they include multiple pulses per temporal row or multiple pulses per wavelength column; these could not be implemented in the FBG writing facility available because a mechanism allowing the strict control of transmitted/reflected power in each FBG would be necessary. Nevertheless, "Mendez code" includes five codewords that could be used in our experimental demonstration; Mendez's five codewords form a sub-code with a cross-correlation constraint equal to one. Unfortunately, the aforementioned limitations in the experimental setup led to a further reduction of the total number of wavelengths in our experimental Optical CDMA system. For this reason, four WHTS Optical CDMA codewords were designed specifically for this experimental demonstration. The codewords developed for our experimental demonstration inherit some of the characteristics of the "Mendez code" such as the number of active chips (four), the number of total time slots (eight) and the use of guard-time [171]. The codewords were designed with zero off-peak auto-correlation and a normalised cross-correlation constraint equal to one. Note that, unlike in most of the Optical CDMA code design, no effort was put into the maximisation the code cardinality. The codewords are shown in figure 6.1.

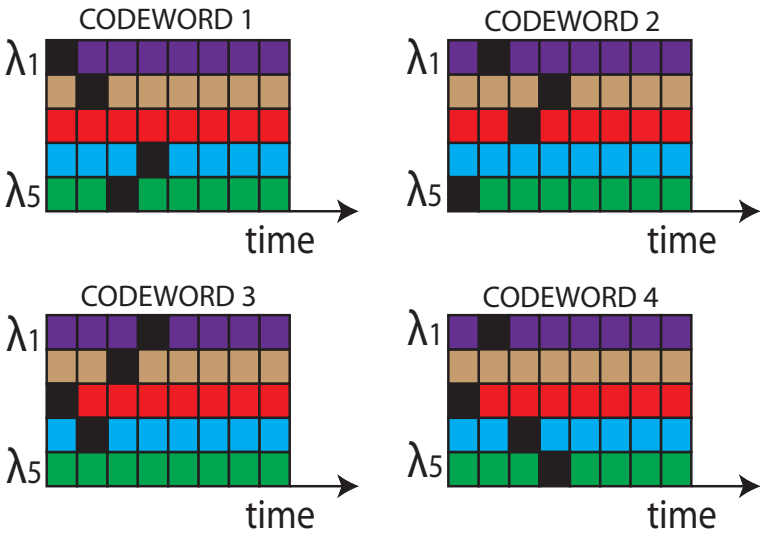

Figure 6.1: Optical Orthogonal Codewords designed for the experimental setup.

6.2 Design and Fabrication of Fibre Bragg Gratings Arrays

Arrays of Fibre Bragg Gratings were used to encode and decode the Optical CDMA codewords, as shown on figure 6.2. Since each codeword has four active chips, each array comprises four FBGs; the physical distance between adjacent FBGs is calculated so that the light round-trip delay is equal to the chip time (50 ps in this case). Therefore, the distance d can be calculated as follows:

$$d = \frac{c.T_{chip}}{2.n} \tag{6.1}$$

where c is the the speed of light in vacuum (2.99792×10^8 m/s), T_{chip} is the chip time of the Optical CDMA system (50 ps for 20 GChips/s) and n the effective refractive index of the fibre. Since the FBG arrays were printed in a germanium-doped photosensitive fibre with effective refractive index $n = 1.447$,

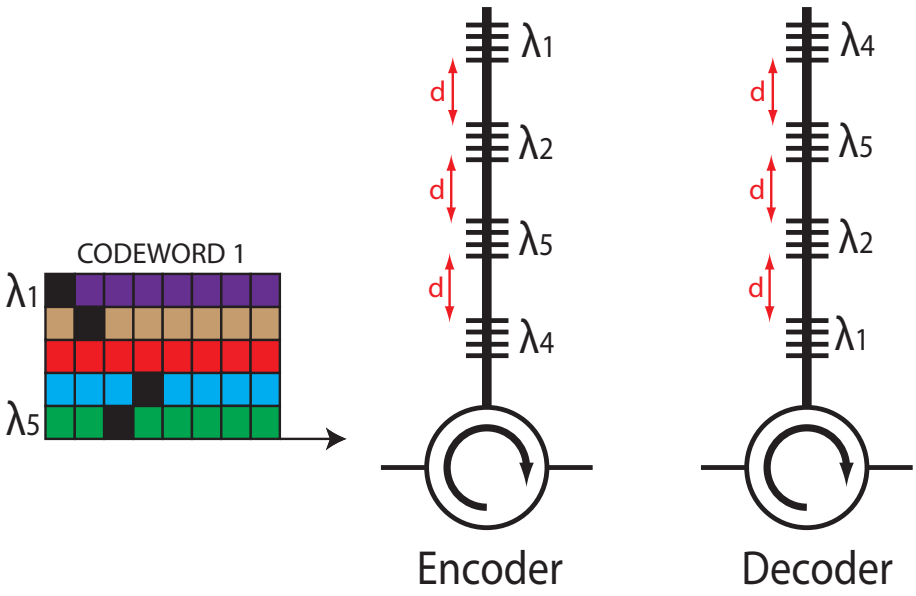

Figure 6.2: Fibre Bragg Grating array for encoding and decoding (codeword 1).

the distance d may be calculated as

$$d = \frac{2.99792 \times 10^{8} \times 50 \times 10^{-12}}{2 \times 1.447} = 5.183\text{mm}. \tag{6.2}$$

Note that a specific codeword may be encoded and decoded using the same FBG array according to which termination is connected to the circulator (figure 6.2). In the case of codeword 1, if the encoder is connected back-to-end with the circulator, wavelength 1 would be reflected in the first place while wavelength 4 in the last. It can be easily proved that, if the codeword 1 is applied in the input, this arrangement would lead to time coincidence of all four chips and therefore an autocorrelation peak would be generated.

Figure 6.3 shows the setup used to print the Fibre Bragg Grating arrays. The main components of this system include:

- "BraggStar" Industrial excimer laser transmitting at 248 nm.

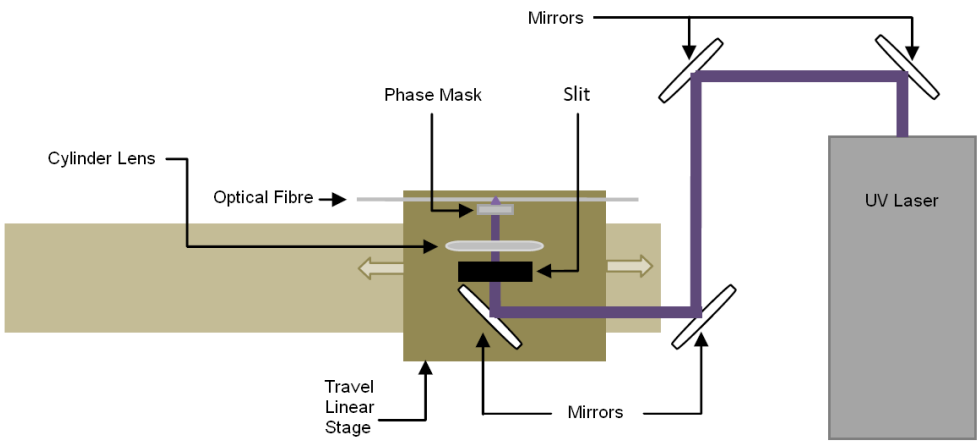

Figure 6.3: Setup used to write Fibre Bragg Grating arrays.

- Travel linear air-bearing stage with linear motor; its total length reach is 1 meter with minimum steps of 10 nm.
- Slit from "Melles Griot" with adjustable width from 0 to 4 mm and resolution of $1\mu m$.
- Optical Spectrum Analyser.
- Phase Masks with different periods.

The first step of the array fabrication process is the phase mask selection for the first FBG. According to the Fibre Bragg Grating theory [140], the central reflection of the grating is given by

$$\lambda_{Bragg} = 2n\Lambda \tag{6.3}$$

where n is the fibre effective refractive index and Λ is the grating period. Next, the fibre is connected to an Optical Network Analyser (ONA) to measure its reflection spectrum in real time, i.e., during the writing process. Magnetic holds are used to assure that the fibre is under tension during this process. In fact,

a grating with good reflection characteristics requires the fibre to be stretched; later in this section it will be shown that this represented a source of a set of problems. At this stage, the UV Laser is switched on and the printing process begins. The operator controls the exposition time (typically ranges from 2-3 minutes) by visualizing the Optical Network Analyser that repeatedly performs frequency sweeps. The exposition not only controls the FBG reflectivity but also increases the central frequency of the grating. This was used for fine tuning of the grating Bragg wavelength. Note that larger exposition times give rise to higher sidelobes in the reflection spectrum. After the first grating is written, the travel linear air-bearing stage is actuated to move exactly $d = 5.183$mm (as calculated in equation 6.2) and the phase mask is replaced according to the next wavelength to be written. This process is repeated for all four FBGs that form the array.

As mentioned, the main issue with the FBG fabrication was related to the tension applied to the fibre. In fact, because the fibre needs to be under tension at the moment of writing, the grating period Λ is reduced when the magnetic holds are removed and, consequently, the Bragg wavelength of all gratings is reduced by a constant value. The value was experimentally found to be around 1.5 nm but its exact value varies from grating to grating. This represents a problem in terms of reproducibility of the FBG arrays. This problem is due to be solved with a device that measures the tension applied to the fibre.

For such reason, a "trial and error" methodology was used for FBG array writing. After printing the first FBG array for codeword 1, several arrays were fabricated before obtaining one with similar characteristics. These two arrays were used as encoder and decoder in the experimental setup (note that an array that encodes a certain codeword can be used as decoder for that code by connecting it

front-to-back with the circulator - see figure 6.2). The third FBG array was built to encode user 2; the same "trial and error" methodology was used to achieve matching wavelengths. The fourth FBG array was allowed to have a constant wavelength shift of about 0.7 nm compared to the system wavelengths; a very precise fibre stretcher was used to align its Bragg wavelengths with the system wavelengths.

Figure 6.4 shows the spectral characteristics of the four FBG arrays used in the experimental setup. The peak reflectivity is about -4 to -5 dB for all gratings apart from the FBGs of the user 1 decoder where the peak reflectivity is about -7 dB. This difference is attributed to an artifact of manufacturing process associated with the variation of the gas pressure required for the excimer laser operation. Sidelobes 9dB below the reflectivity peaks were obtained. The figure also shows the group delay and confirms that the delay between adjacent FBGs is close to the predicted 50 ps. Note that the large variance of the delay outside the reflection peaks of the spectrum does not have impact on the system.

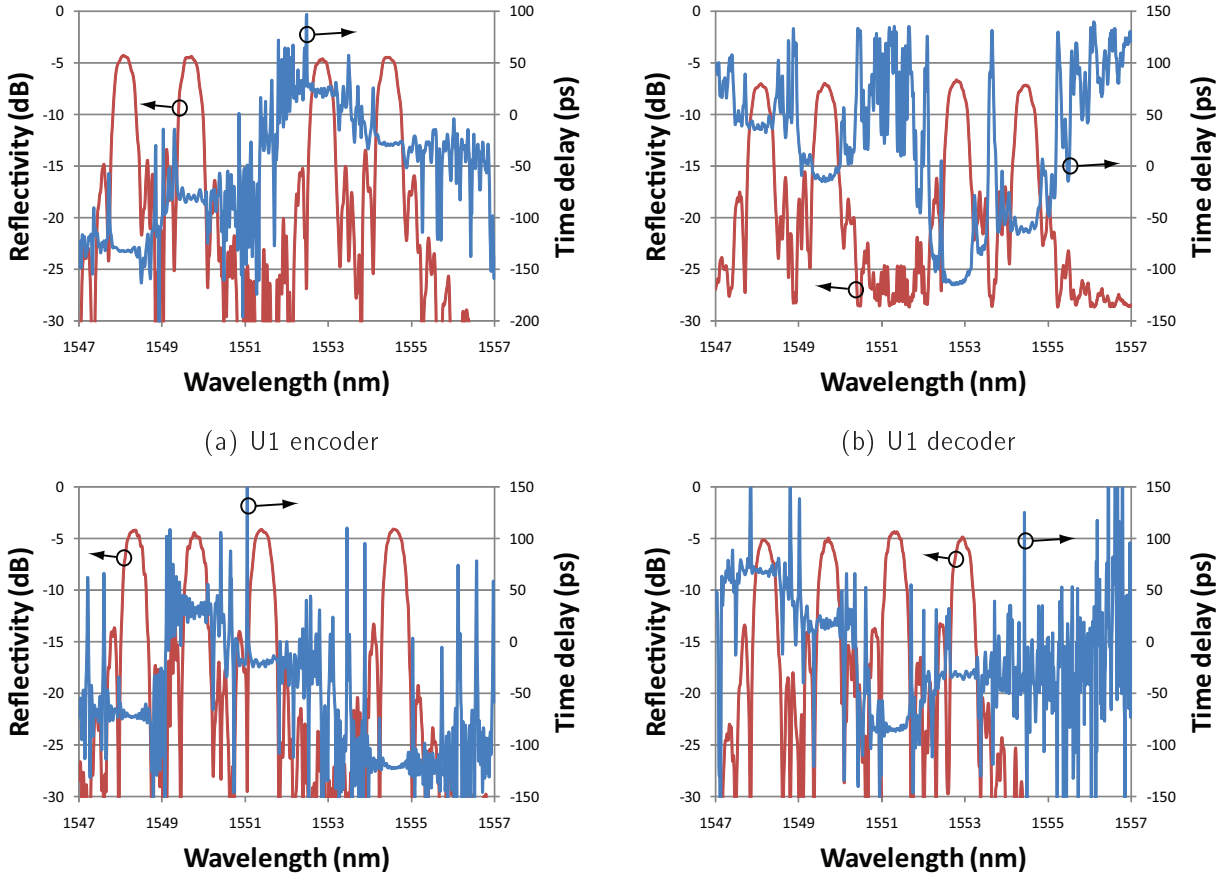

(a) U1 encoder

(b) U1 decoder

(c) U2 encoder

(d) U3 encoder (using fibre stretcher)

Figure 6.4: Reflectivity spectrum characteristics of the four FBG arrays (note the time reversal in subfigure (a) compared to (b).

Table 6.1: Fibre Bragg Gratings central wavelengths (nm).

	λ_1	λ_2	λ_3	λ_4	λ_5
User 1 - Encoder	1548.08	1549.70	-	1552.86	1554.46
User 2 - Encoder	1548.29	1549.77	1551.45	-	1554.56
User 3 - Encoder	1548.16	1549.71	1551.30	1552.94	-
User 1 - Decoder	1548.09	1549.62	-	1552.79	1554.43
Initial design	1547.71	1549.32	1550.92	1552.52	1554.12
Final	1548.20	1549.75	1551.42	1552.90	1554.50

Table 6.1 shows the Bragg wavelengths for each FBG array and the projected and final wavelengths of the system. Note that the projected central wavelength values were chosen to coincide with the ITU-grid value; however, because the lasers used in the experiment are tunable, the wavelengths were shifted to coincide with the FBG values. These final wavelength values used in the experiment are shown in the last row of the table.

6.3 Experimental Setup

Figure 6.5 shows the experimental setup. Five Semiconductor Distributed Feedback Lasers were chosen as light sources. Their central wavelengths were adjusted to coincide with the wavelengths in table 6.1. While many Optical CDMA implementations propose incoherent broad-band sources, due to cost considerations and robustness against beat noise [172], multi-laser sources are generally found to outperform broadband ones [173]. Polarisation controllers allow adjusting the polarisation between wavelength channels before modulation. The five wavelengths are multiplexed through a passive optical coupler.

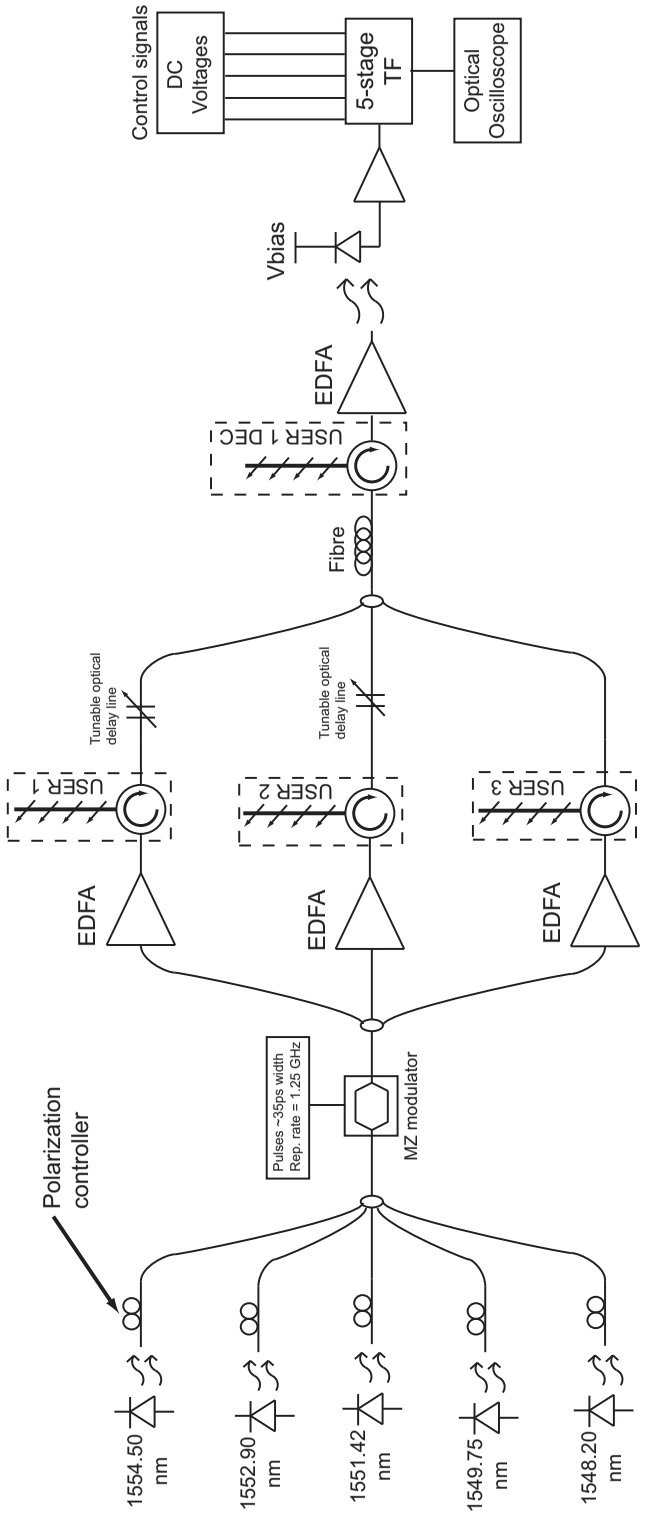

Figure 6.5: Experimental setup of the Optical CDMA system.

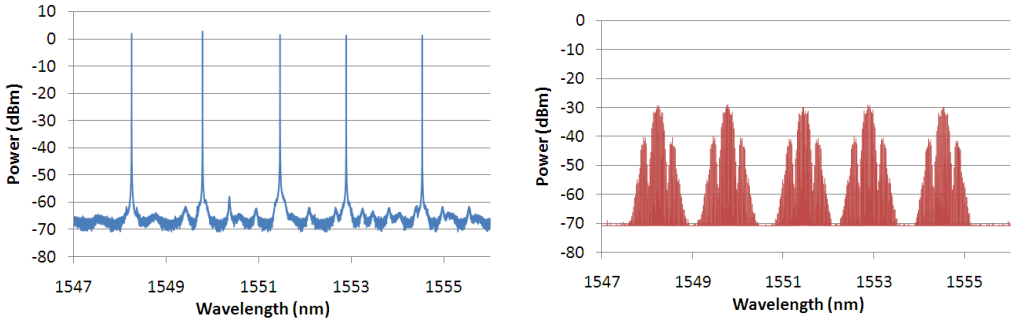

(a) Before modulation (b) After modulation

Figure 6.6: Spectrum of the system before and after modulation.

The signal modulation is performed with a Mach-Zehnder modulator. Because this type of modulation is sensitive to polarisation, it is essential to use five individual polarisation controllers for each wavelength channel. An external signal generator is used to generate 35 ps width pulses with repetition rate of 2.5 or 1.25 GHz, according with the requirements of the specific measurement. These correspond to an all ones sequence or an alternate sequence of zeros and ones, respectively.

The spectrum of the five lasers before and after modulation is presented in figure 6.6(a) and figure 6.6(b), respectively. The reduction of the peak power by nearly 30 dB can be explained with the modulation with a short pulse (35 ps) in a 400 ps period. Moreover, the modulator intrinsic losses were found to be about 10 dB.

The signal is then split in three and sent to three independent Erbium Doped Fibre Amplifiers (EDFAs). This topology was preferred over using a single EDFA to avoid saturation of the device. Each signal is then encoded after which tunable delay lines are used to allow the study of different patterns of interference between users. Figure 6.7 shows an oscilloscope screen shot of the encoder 1 output.

The Optical CDMA encoded signals are recombined with a passive coupler

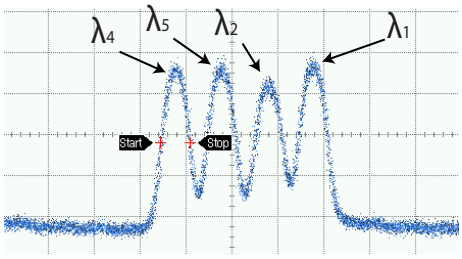

Figure 6.7: Oscilloscope screen shot of the encoder output of codeword 1 (Time: 50 ps/div; y axis: amplitude [a.u.]).

(emulating a star network) and launched into the optical fibre. At the receiver end, the signal is optically pre-amplified with an EDFA to adjust the optical levels to the range of the electrical receiver. The photoreceiver module comprises a photodiode and transimpedance amplifier with cut-off frequency of 34 GHz.

The transversal filter used was provided by the portuguese Instituto das Telecomunicacoes and was designed for multipurpose applications which include GVD and PMD compensation [90]. This device uses the distributed concept used in the design of the circuit presented in chapter 4. However, there are implementation differences. First, the DTF used for the experiment employs a modern version of the process used in the designs of chapter 4, the Phillips/OMMIC $0.13\mu m$ Gallium Arsenide process, called D01PH (PHEMT), has a cut-off frequency of $f_t = 100\text{GHz}$. Second, the gains stages are Gilbert cells instead of cascode configuration. Third, the interstage delays are constant and equal, and measured to be 18 ps.

The results were observed through an Optical Spectrum Analyser and an Electrical Sampling Oscilloscope with a bandwidth of 40 GHz.

6.4 Time Skewing Results

This section provides experimental analysis of the impact of GVDiff-induced time skewing in Optical CDMA networks. Where applicable, the experimental results are compared with theoretical predictions based on the model presented in the previous chapter. This includes the assumption that the pulses have a Gaussian shape and that the time skewing is the dominant source of performance degradation (as opposed to pulse broadening). Initially, the impact of the time skewing in the autocorrelation and cross-correlation of the system is analysed. In order to assess the system for progressively higher time skewing regimes, Single Mode Fibre segments were added to obtain the prescribed time skewing. The characteristics of the SMF were measured and the dispersion was found to be 16.6 ps/nm/km at 1550 nm and the dispersion slope 0.0585 ps/nm^2/km. Table 6.2 shows the time skewing between wavelength channels for the fibre lengths used in this section. The first column shows the length of Single Mode Fibre; in the second column (ΔT - zero slope (ps)) it is assumed that the time skewing between adjacent wavelength channels is constant, which is equivalent to consider that the dispersion slope is zero. In this case, the dispersion at central wavelength (λ_3 = 1551.42 nm) was assumed, which is 16.697 ps/nm/km. The remaining columns show the time skewing between wavelength channels between the first and second wavelengths and fourth and fifth wavelengths, respectively. One can conclude that it is possible to use the SMF to emulate constant time skewing between wavelength channels as this assumption leads to an error in the amount of time skewing smaller than 0.85 %.

In the last subsection (6.4.3), results concerning Optical CDMA propagation in Dispersion Shifted Fibre will be presented.

Table 6.2: Time skewing for different fibre lengths.

SMF length (m)	ΔT - zero slope (ps)	ΔT - λ_1 to λ_2 (ps)	ΔT - λ_4 to λ_5 (ps)
100	2.672	2.649	2.694
200	5.343	5.298	5.388
300	8.015	7.947	8.082
400	10.686	10.596	10.776
500	13.358	13.245	13.470
600	16.029	15.894	16.164
700	18.701	18.543	18.858
800	21.372	21.193	21.552
900	24.044	23.842	24.246
1000	26.715	26.491	26.940
1100	29.387	29.140	29.634
1200	32.058	31.789	32.328

6.4.1 Time Skewing Impact on Autocorrelation Peak

Firstly, the impact of GVD in the autocorrelation peak is studied. Figure 6.8 shows the degradation in the Optical CDMA autocorrelation peak due to time skewing. These oscilloscope screen shots were obtained with the experimental setup of figure 6.5, with the EDFAs corresponding to users 2 and 3 switched off. Single mode fibre segments of 100 meters were added to show the effect of time skewing (the equivalent value of time skewing can be found in table 6.2).

Figure 6.8 shows an initial pulse with 68 mV amplitude in the back-to-back case, being reduced to 12 mV after 800 meters of fibre. The amplitude of the signal is reduced to half with 500 meters of fibre [2].

Figure 6.9(a) compares the degradation in the autocorrelation peak amplitude

[2] In this case, the voltage values are given. However, these are mainly dependent on the gain of the front-end EDFA. For this reason, in the remaining part of this chapter, the amplitude will be presented in arbitrary units [a.u.].

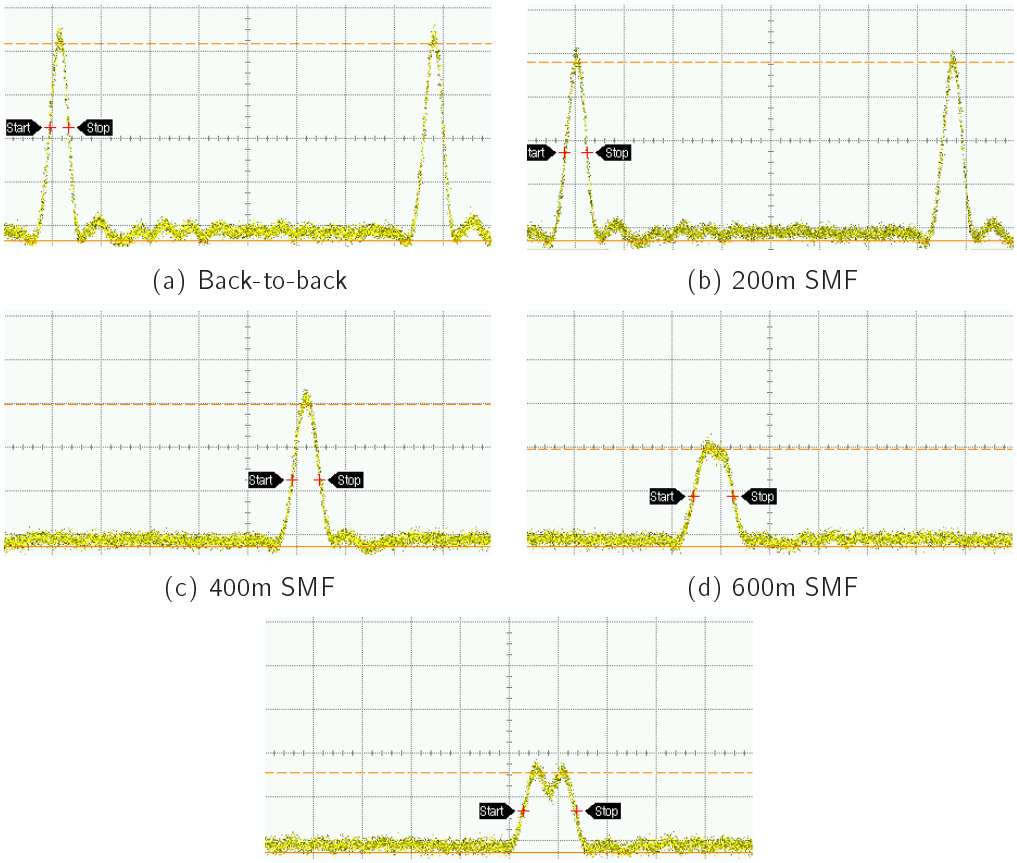

(a) Back-to-back (b) 200m SMF

(c) 400m SMF (d) 600m SMF

(e) 800m SMF

Figure 6.8: Autocorrelation peak degradation with SMF fibre lengths (time: 100 ps/div; y axis: amplitude [a.u.]).

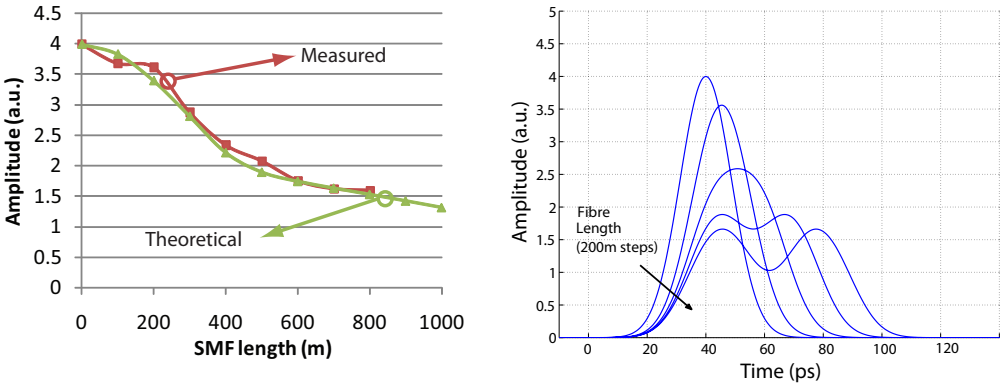

(a) Autocorrelation peak amplitude - experimental and simulated

(b) Autocorrelation peak degradation with fibre length

Figure 6.9: Impact of time skewing in the autocorrelation peak.

with the theoretical predictions using Gaussian pulses. The theoretical calculation assumes chips with 35 ps widths and a Single Mode Fibre with constant dispersion of 16.697 ps/nm/km in the wavelength window between 1548.20 nm and 1554.50nm. The results show that the model presented in the previous chapter is very accurate, with the differences between real and predicted amplitude values being less than 5%. Figure 6.9(b) shows the predicted autocorrelation peak degradation for the scenario analysed in 6.8. Once again, the pulse shape reproduces very closely the results obtained experimentally.

6.4.2 Time Skewing Impact on Cross-correlation

As seen in the previous chapter, time skewing does affect the performance of the Optical CDMA system by compromising the cross-correlation properties of the code.

Figures 6.10, 6.11 and 6.12 show the experimental results for three different cross-correlation functions:

1. Codeword 2 with decoder 1 (figure 6.10)
2. Codeword 3 with decoder 1 (figure 6.11)
3. Codeword 3 with decoder 2 (figure 6.12) - note that decoder 2 was obtained replacing the decoder 1 in figure 6.5 with the FBG array of encoder 2, connected back-to-front.

The illustration in each figure shows the expected cross-correlation and the effect of time skewing in each wavelength.

These figures clearly show that the time skewing impact on the cross-correlation properties of the code mainly depends on the specific chip arrangement of the

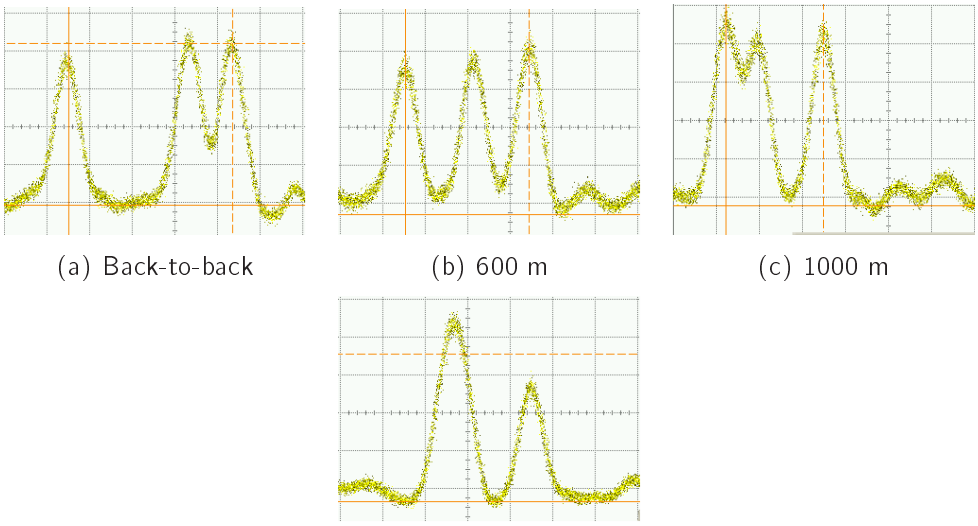

(a) Back-to-back (b) 600 m (c) 1000 m

(d) 1200 m

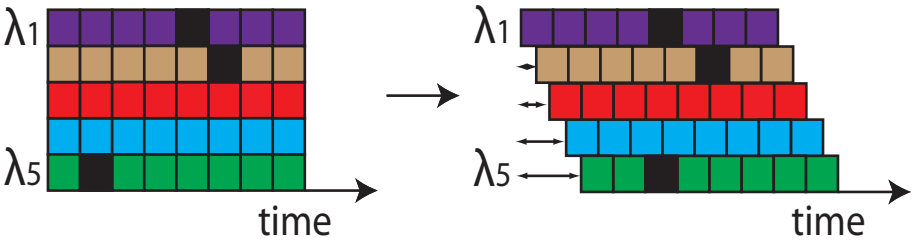

(e) Illustration of time skewing effect on the cross-correlation

Figure 6.10: Cross-correlation of codeword 2 with decoder of user 1 (time 100ps/div; y axis: amplitude [a.u.]).

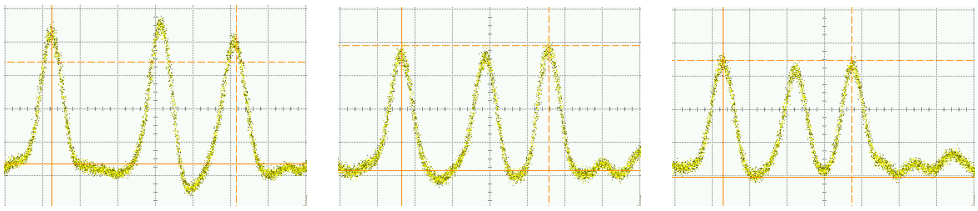

(a) Back-to-back (b) 600 m (c) 1000 m

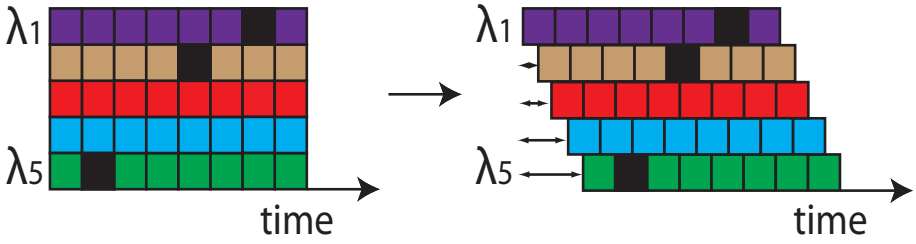

(d) Illustration of time skewing effect on the cross-correlation

Figure 6.11: Cross-correlation of codeword 3 with decoder of user 1 (time 100ps/div; y axis: amplitude [a.u.]).

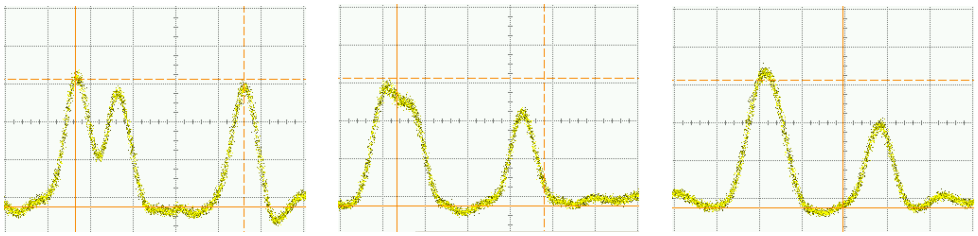

(a) Back-to-back (b) 600 m (c) 1000 m

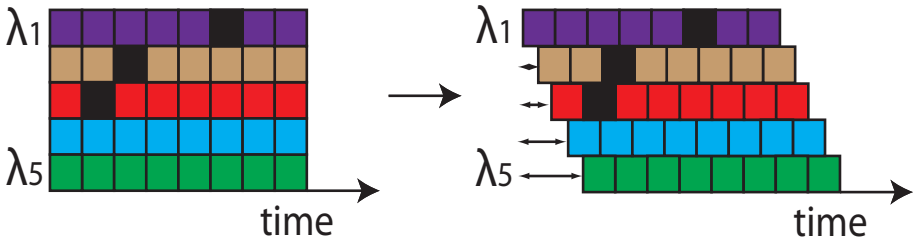

(d) Illustration of time skewing effect on the cross-correlation

Figure 6.12: Cross-correlation codeword 3 with decoder of user 2 (time 100ps/div; y axis: amplitude [a.u.]).

cross-correlation. In the case represented in figure 6.10, the cross-correlation characteristics of the code are destroyed after 1200m due to coincidence of the active pulses in wavelengths 1 and 5. For the scenario described in figure 6.11, the degradation of the cross-correlation properties never occur for SMF lengths up to 1200m. The third scenario (figure 6.12), is the least favorable because the degradation starts to occur at 600 m, due to coincidence between pulses transmitted on the second and third wavelengths.

Although the construction of codes for time-wavelength Optical CDMA is a highly active research topic, to the author's knowledge, there are no codes that take into account the time skewing effect on cross-correlation. In fact, it is possible to design codes so that scenarios such as the one represented in figure 6.12 could be avoided. This could be achieved by designing the codes according to the following condition: for each cross-correlation function of the system, let's consider all pairs of wavelengths with active chips i and j, with i being the fastest wavelength (i.e., facing a lower value of total time skewing). For each pair, if the wavelength i has its active chip in the chip position t_r, wavelength j should not have its active chip in the position t_{r-1}[3]. However, it should be noted that this recommendation would impose more restrictions to the code design which inevitably would reduce the code cardinality.

Comparing the impact of time skewing in the auto and cross-correlation of the Optical CDMA system, one can conclude that the impact is more severe in the former. This confirms the conclusion derived in the previous chapter. In fact, the autocorrelation peak is halved with 500 m (or 13.36 ps of time skewing between

[3]Note that the cross-correlation of the codeword three with the decoder of user two (scenario represented in figure 6.12) is not in conformity with this recommendation. In fact, the wavelength 2 is faster than wavelength 3 and their active chips are in positions three and two, respectively.

wavelength channels), an autocorrelation peak value that is clearly not suitable for Optical CDMA transmission. In the worst case analysed in this section, the degradation of cross-correlation function only starts occurring after 600 m of SMF (or 16.03 ps of time skewing between wavelength channels).

6.4.3 Dispersion Shifted Fibre

This section presents the propagation of the Optical CDMA signal over Dispersion Shifted Fibre. DSF is a propagation medium that was described as suitable for multi-wavelength Optical CDMA propagation [6]. Two DSF segments with the measured characteristics presented in table 6.3 were used. The group delay characteristics are presented in figure 6.13 for the individual fibre segments as well as the combined lengths. The five wavelengths of the system are marked with vertical dashed lines.

In this experiment we are mainly interested in assessing the degradation of the autocorrelation peak in this medium. For this reason, the encoder one was modulated with a data sequence of all ones. However, since the attenuation cannot be ignored in 17.3 km of DSF, a reference to compare the amplitude of the autocorrelation peak is required. For that purpose, the user 2 was included in the system. Note that, as seen in the previous section, the cross-correlation of user 2 with decoder 1 only starts to get degraded with more than 26 ps of time skewing between wavelength channels. As figure 6.13 clearly shows this value is never achieved with the DSF fibres considered (maximum time skewing is between wavelengths four and five and does not exceed 10 ps). This allows the comparison between the amplitude of the autocorrelation peak and the single chips that compose the cross-correlation function. The tunable delay line of user

Table 6.3: Dispersion Shifted Fibres characteristics.

	Length (km)	$\lambda_{ZD}(nm)$	**Slope (ps/nm^2/km)**
DSF 1	8.8	1547.34	0.0683
DSF 2	8.5	1550.8	0.0690
DSF 1 + DSF 2	17.3	1548.96	NA

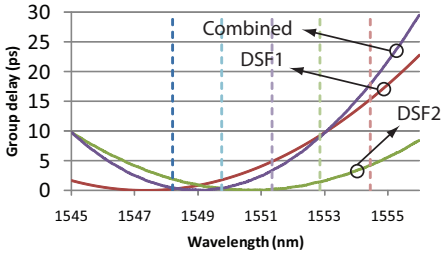

Figure 6.13: Dispersion Shifted Fibres group delay characteristics.

2 is actuated so that its cross-correlation does not coincide in time with the autocorrelation peak.

The distortion of autocorrelation peak obtained by simulation is shown in figure 6.14(c). It was obtained with the model presented in the previous chapter (comprising gaussian pulses) and considering the time skewing value for each wavelength as shown in line interceptions in graph 6.13. Figure 6.14(a) shows the experimental results for back-to-back case while figure 6.14(b) shows an oscilloscope screen shot of the Optical CDMA signal after propagation in the 17.3 km of Dispersion Shifted Fibre.

The modelling results shows that the amplitude of the autocorrelation peak

Table 6.4: Normalised amplitude of the autocorrelation peak.

	Simulated	Measured
Before	4	3.73
After	3.29	2.97
Ratio	0.82	0.80

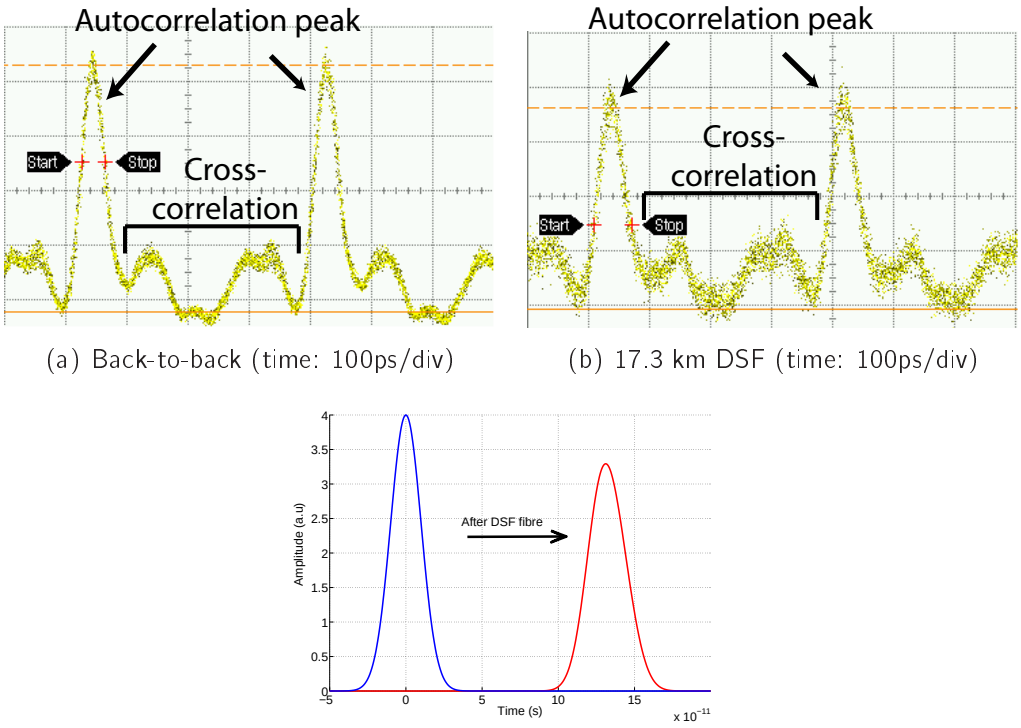

(a) Back-to-back (time: 100ps/div)

(b) 17.3 km DSF (time: 100ps/div)

(c) Theoretical

Figure 6.14: Dispersion Shifted Fibre theoretical and experimental results (y axis: amplitude [a.u.]).

is reduced from the ideal four (number of active chips) to 3.29. The measured value in the experimental setup was 3.73 for back-to-back; this small difference is attributed to non-ideal behavior of the photoreceiver. After propagation in the DSF fibre, the autocorrelation peak amplitude is reduced to 2.97. Table 6.4 shows the simulated and experimentally measured values of the autocorrelation peak amplitude, and the ratio between the autocorrelation peak before and after propagation. The predicted impact of the time skewing in the autocorrelation peak amplitude (ratio) is 0.82 while the experimental value was found to be 0.80. These results show excellent agreement between the experimental results and the theoretical predictions using the model described in the previous section.

Table 6.5: Measured fibre characteristics.

	Length (km)	Disp @ 1550 nm (ps/nm/km)	Slope (ps/nm^2.km)
SMF	39.94	16.6	0.0585
DCF	5.06	-133.4	-0.3745

6.5 Compensation Results

Unfortunately, due to experimental limitations, it was not possible to use an error detector for the experimental setup and, as consequence, it was impossible to calculate the system Bit Error Rate. Therefore, a figure of merit to show the system improvement due to the use of the transversal filter needs to be introduced. To measure quantitatively the performance improvement, we define the parameter auto-correlation intensity peak *to* the multi-access level ratio (P/M ratio) [4].

$$\text{P/M} = \frac{\text{Autocorrelation peak amplitude}}{\text{Maximum MAI level}}. \tag{6.4}$$

The assessment of the transversal filter performance requires the analysis of the Optical CDMA system for different time skewing scenarios. Moreover, a realistic situation should be tested to extract conclusions about the behavior of such solution in a practical scenario. The solution to fulfill these requirements was to consider a system based on standard Single Mode Fibre (SMF) and a segment of Dispersion Compensating Fibre (DCF). For verification purposes, short SMF segments were added to the system to emulate residual dispersion in the fibre. The measured characteristics of the SMF and DCF are shown in table 6.5 and in figure 6.15.

The experimental setup comprises three active users, where user "1" matches

[4] In papers [116] [168] we refer to this as P/C ratio (auto-correlation intensity peak *to* the cross-correlation level ratio) but P/M ratio is a more accurate description.

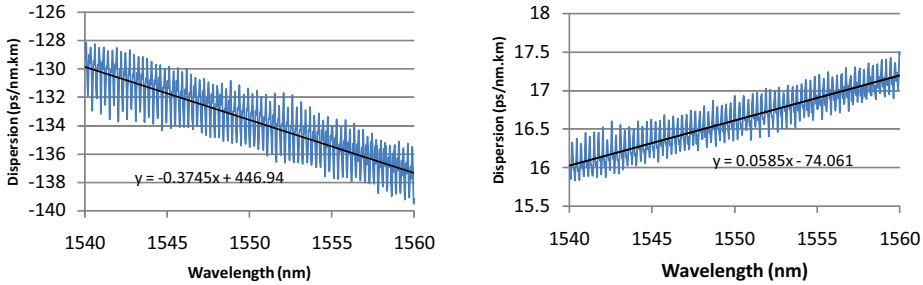

(a) Dispersion Compensating Fibre (b) Single Mode Fibre

Figure 6.15: Dispersion characteristics of the Single Mode Fibre and Dispersion Compensating Fibre.

the decoder and users "2" and "3" act as interferers. The modulator is set for an alternate sequence of zeros and ones (in practice, the frequency of the pulses was reduced by 50 %, i.e., to 1.25 GHz).

As discussed in section 5.2, an Optical CDMA error occurs when the Multi-Access Interference exceeds the threshold value. When multiple interferes exist at the receiver, the worst case scenario happens when there is time coincidence among the chips of the cross-correlation functions of these interferes. For our study we are limited by experimental facilities to two interferes in a three user network. The performance of the Distributed Transversal Filter is analysed for two extreme case scenarios. In the first scenario, the cross-correlation function from users "2" and "3" does not have any chip coincidence. This is done by adjusting the tunable optical delay lines after the encoder. For the second scenario, the cross-correlation functions are deliberately delayed so that they have chips coinciding in time. This corresponds to the worst case scenario because the cross-correlation peaks have their maximum value and the P/M ratio is minimum.

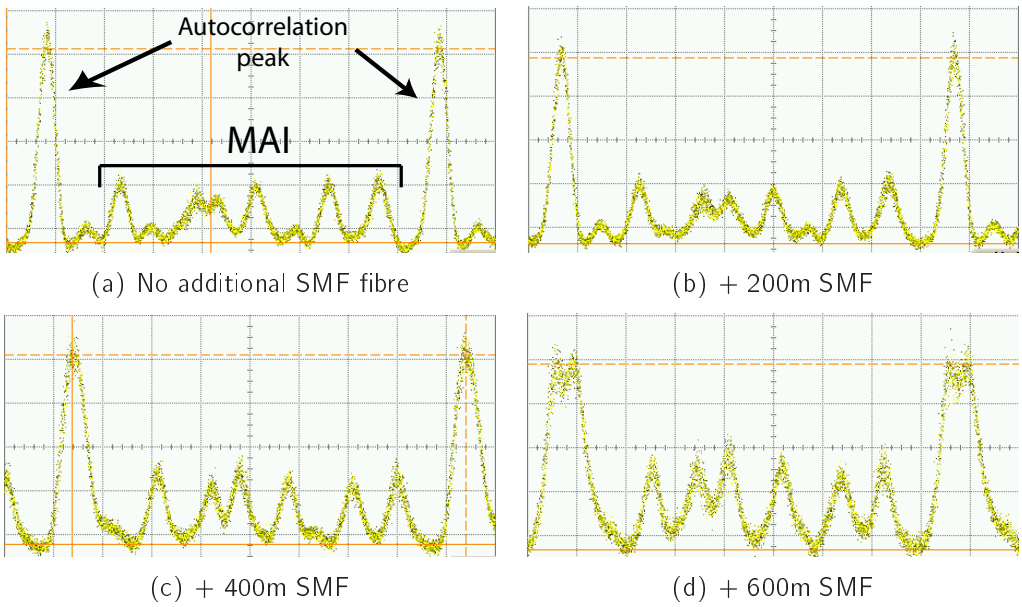

Figure 6.16: Oscilloscope screen shots of SMF+DCF, three users and no coincidence in cross-correlation functions (time: 100 ps/div; y axis: amplitude [a.u.]).

6.5.1 First Scenario

Figure 6.16 shows the experimental results for the Optical CDMA transmission over 40 km SMF fibre with DCF fibre; SMF segments of 200, 400 and 600 meters were added for figures 6.16(b), 6.16(c) and 6.16(d), respectively (for correspondent values of time skewing see table 6.2). The figure shows a clear reduction of the autocorrelation peak amplitude relative to the MAI.

Figure 6.17 shows the compensation results for the first scenario. The screen shots on the left represent the non-compensated Optical CDMA signal for 400 m and 600 m of additional SMF; on the right, the oscilloscope screen shots show the correspondent fibre lengths with DTF compensation. The transversal filter gains were set manually to maximise the P/M ratio.

Figure 6.18 summarises the P/M ratio of the first scenario. The graph shows a clear improvement in the performance especially in the case where the effect of time skewing is more intense (additional 600 m SMF). The improvement of

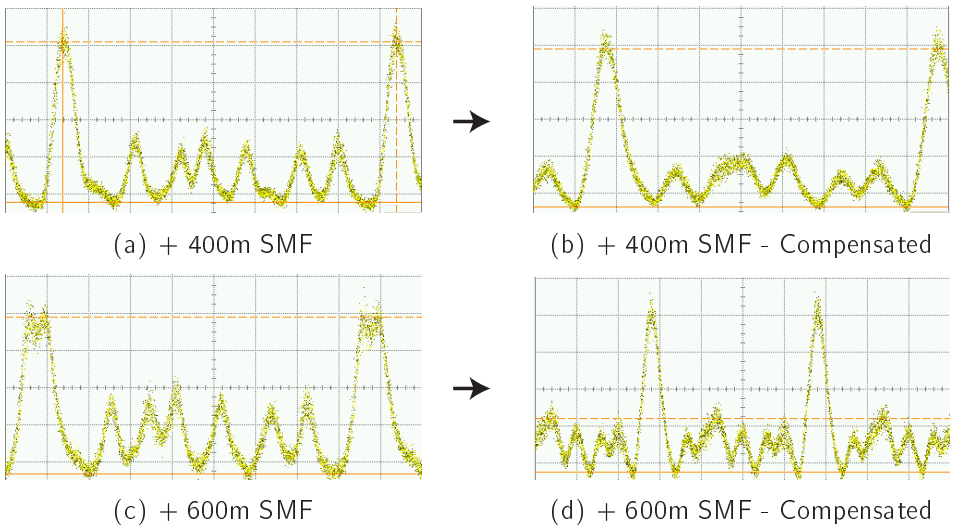

Figure 6.17: Compensation results for SMF+DCF, three users and no coincidence in cross-correlation functions (Time: 100 ps/div except fig. 6.17(d) with time: 200 ps/div; y axis: amplitude [a.u.]).

P/M ratio is 27% when 400m of additional fibre is used and 49% when the Optical CDMA signal is further degraded (600m SMF). The experiement also demonstrates that the transversal filter cannot fully compensate the time skewing effect. In fact, when the degradation due to time skewing is large (figures 6.17(c) and 6.17(d)), the ideal transversal filter coefficients give rise to a P/M ratio which, although offers 49% improvement, is 17% bellow initial (i.e., compared with the scenario comprising no time skewing). This confirms the conclusions of the previous chapter where the compensation obtained with the transverasl filter was found to be partial.

Table 6.6 shows relative values of transversal filter gains for additional SMF spans of 400 m and 600 m (where maximum gain is one and minimum in zero). The table confirms the predictions (see trends in tables 5.8) that higher transversal filter gains have to be used for higher values of time skewing.

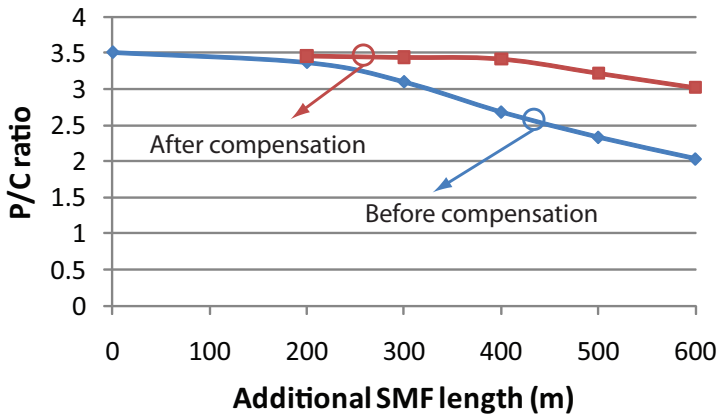

Figure 6.18: P/M ratio as function of additional SMF length for no coincidence in cross-correlations.

Table 6.6: Transversal Filter relative gains - scenario 1.

Additional SMF	G1	G2	G3	G4	G5
400 m	0.51	0.02	**1**	0.42	0
600 m	0.55	0.56	**1**	0.96	0.30

6.5.2 Second Scenario

The second scenario represents the worst case because the MAI peak is twice of a single chip amplitude. Figure 6.19 shows oscilloscope screen shots for the same fibre lengths analysed for the previous scenario. In this case, the ideal P/M ratio without dispersion is two. The Optical CDMA system degradation reaches an extreme point with additional SMF of 600m, where the MAI peak has the same value of the autocorrelation peak.

Figure 6.20 shows the compensation results for additional fibre spans of 400m and 600m. The improvement in P/M ratio is clear for both cases. Note that the extent of the autocorrelation peak compensation is ultimately limited by the interactions between the cross-correlation chips. This is particularly obvious in figure 6.20(d); if the gain coefficients continue to rise, the peak value of MAI will

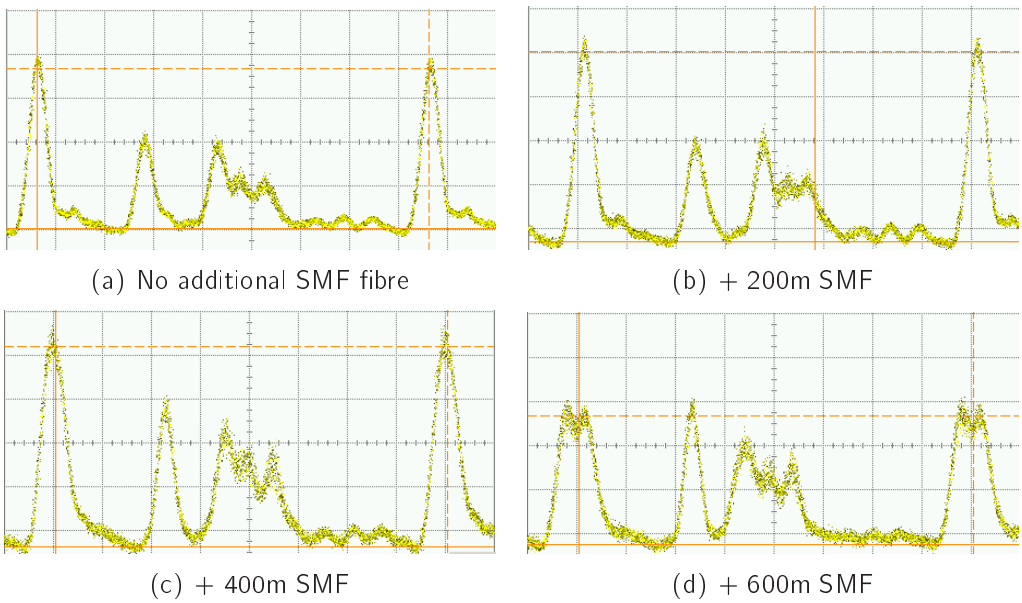

(a) No additional SMF fibre (b) + 200m SMF

(c) + 400m SMF (d) + 600m SMF

Figure 6.19: Oscilloscope screen shots of SMF+DCF, three users and coincidence in cross-correlation functions (Time: 100 ps/div; y axis: amplitude [a.u.]).

Table 6.7: Transversal Filter relative gains - scenario 2.

Additional SMF	G1	G2	G3	G4	G5
400 m	0.06	0.60	**1**	0.78	0
600 m	0.21	0.51	**1**	0.53	0.14

rise at faster pace than the autocorrelation peak. Therefore, the ideal coefficients provide the best balance between cross-correlation peak and the autocorrelation level. The graph 6.21 shows the P/M ratio without and with compensation for the analysed cases and table 6.7 shows the relative gains for both cases.

In this experimental work, the relative delay between cross correlation functions was adjusted in order to study the best case and worst case scenarios. In a real network, all users transmit information asynchronously and therefore the P/M ratio is expected to be between these extreme scenarios. Therefore, the transversal filter compensator is expected to provide performance improvement in all scenarios.

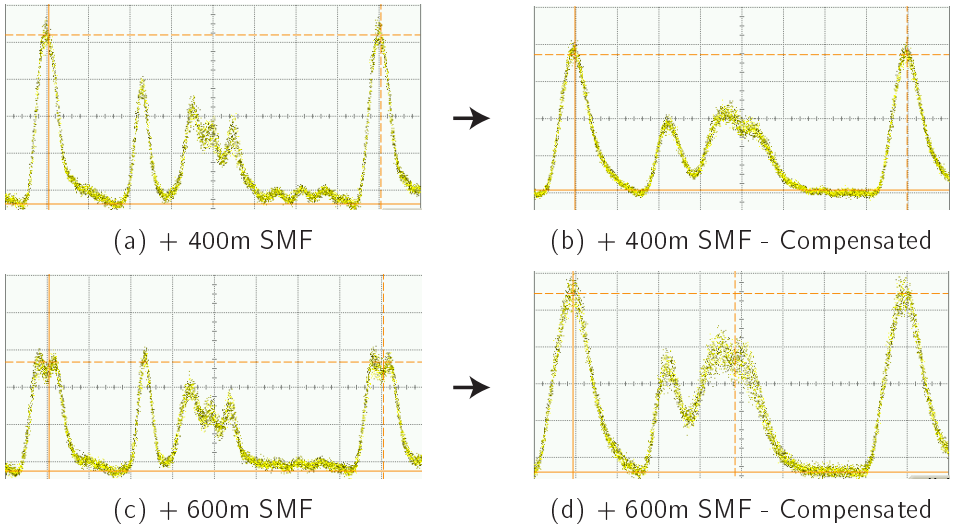

Figure 6.20: Compensation results for SMF+DCF, three users and coincidence in cross-correlation functions (Time: 100 ps/div; y axis: amplitude [a.u.]).

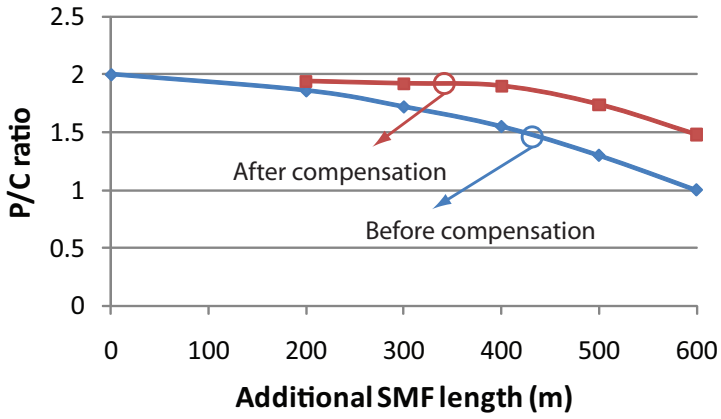

Figure 6.21: P/M ratio as function of additional SMF length for cross-correlations with chip coincidence.

6.5.3 Comparison Between Scenarios

Comparing tables 6.6 and 6.7, one can see that the magnitude of the optimum transversal filter gain coefficients is generally higher in the first scenario than in the second. Moreover, for the second scenario and considering 600m of added SMF fibre, the final value of the P/M ratio is 25 % below the initial value (note that this vale was 17 % in the first scenario). This result clearly shows that the effectiveness of the compensation is higher in the first scenario than in the second. This can be explained by the fact the MAI comprises linear combinations of delayed versions of the cross-correlation functions. The value of MAI depends on the temporal distance between the chips of different cross-correlations; "higher density" of chips correspond to higher MAI peaks, hence lower flexibility in the electronic post-compensation process.

In our experiment, "higher density" of chips was obtained by forcing the cross-correlation functions of interferes "2" and "3" to coincide in time (scenario 2). In a real network, the relative position of the cross-correlation function is a random process. Therefore, "higher density" of chips corresponds to a higher number of users in the network. Hence, the experimental results described in the previous paragraph confirm the conclusions of the previous chapter, namely that there is a trend of decreasing the transversal filter gain coefficients as the number of the users increases and that the compensation becomes less effective with higher number of users.

6.6 Summary

This chapter was dedicated to the experimental study of the effect of time skewing due to Group Velocity Dispersion in multi-wavelength Optical CDMA systems and its compensation. To the author's knowledge, this is the first Optical CDMA network implemented to study this effect. Moreover, this is the first time that analogue electrical signal processing is experimentally demonstrated in the context of Optical CDMA networks. The work presented in this chapter gave rise to publications in conference proceedings [174] [168].

The impact of time skewing in the auto and cross-correlation properties of the system is analysed. Results confirm that the impact is more severe in the autocorrelation peak than in the cross-correlation function. Note that the impact in the cross-correlation can be further attenuated by proper code design. The time skewing was also analysed with Dispersion Shifted Fibre as propagation medium. Experimental results show excellent agreement with the Optical CDMA model described in the previous chapter.

The main goal of the experimental system was to show the compensation of the time skewing effect with an electronic Distributed Transversal Filter. Results show that the compensation is more limited when the "density" of cross-correlation chips is higher. In this case, "higher density" of chips was reached by making the cross-correlation functions of the two users to coincide in time. In a real network, higher densities of cross-correlation chips result when higher number of users are sharing the network. In this sense, these results confirm the conclusion reached in the previous chapter, where the efficacy of compensation was found to be reduced as the number of interferes increases. Assuming that the second scenario emulates a situation with higher number of users, the magnitude of the

transversal filter gain coefficients confirm the trend found in the previous chapter, i.e., that higher number of user leads to lower filter gain coefficients.

Although no BER capture was possible, results show that using the transversal filter led to P/M ratio improvements up to 50%. This effectivelly shows that it is possible to have an electronic compensator that is cost effective and flexible for use in receivers of WHTS Optical CDMA systems. This provides a major advantage over the use of optical compensation techniques which are based on AWG and therefore bulky, expensive and do not afford flexibility.

Chapter 7

Concluding Remarks

In this thesis the use of electronic circuits for generation, detection and post-detection processing in Optical CDMA networks is studied. The research comprised two clearly distinguishable parts sharing the use of electronics and Optical CDMA networks as a common ground. The first part deals with electronic generation and detection of CDMA signals for optical fibre applications whilst the second is concerned with post-detection signal processing for compensation of GVDiff-induced time skewing in multi-wavelength Optical CDMA networks.

This thesis provided an overview of incoherent Optical CDMA networks (chapter 2). It is shown that this technique possesses significant advantages when compared with other multi-access schemes. A detailed review of temporal encoding and multi-wavelength encoding is provided, and the main drawbacks of Optical CDMA are highlighted, namely the crosstalk between users (Multi-Access Interference), the low spectral efficiency and the impact of beat noise. Significant work related to Optical CDMA proposals and laboratory implementations was also outlined.

Chapter 3 provided a brief introduction to distributed circuit design, where the

main principles were described and a review of recent work on distributed transversal filters for high-speed equalisation was presented. The review clearly showed that many groups worldwide are realising the potential of distributed topologies for compensation of various optical fibre impairments.

The first part of the research deals with circuit design for encoding and decoding high-speed CDMA signals. For such purpose, a new concept that aims to minimise the circuit complexity is proposed. This concept comprises the use of a distributed transversal filter where the number of stages is equal to the number of positive chips in the Optical CDMA codeword, as opposed to being equal to the total number of chips. Full integrated circuit layout and electromagnetic simulation shows the adequacy of the techniques for 40 GChip/s operation (using a 60 GHz MMIC process), with very close agreement between simulation results and theoretical predictions. In addition, several improvements were explored including the use of switchable delays to provide tunability across a range of codewords and the modification of the structure so that multi-wavelength CDMA signals could be encoded and decoded.

The time-domain structure presents main problems that may compromise its practical use. One of such problems is inherent to time-domain unipolar CDMA systems. In fact, these systems require long codewords and have very low spectral efficiency. Although providing very significant advantages in terms of circuit design, the use of unipolar codes presents main disadvantages in terms of system performance as it was made clear from the comparison between Gold codes (bipolar) and Prime codes (unipolar) presented in the discussion of chapter 4 (section 4.8). The time-domain structure was designed to implement a codeword with 10 chips; the implementation of longer codewords would require LC-delay lines with

lower attenuation and broader frequency characteristics. Moreover, the fact that the proposed design does not have tunability across a range of codewords is a limitation. In order to solve this problem, a section was dedicated to the study of structures with switchable delays in which delays between stages may be tuned to multiples of the chip time. The use of pHEMT switches was considered and it was concluded that devices with superior characteristics would be required, namely lower transmission losses in the "ON" state and better isolation in "OFF" state.

Considering the drawbacks of the time-domain approach, this project moved towards the investigation of structures that could encode/decode the more spectrally efficient multi-dimensional Optical CDMA codewords. The results presented are preliminary since it was not possible to implement the delays within practically allowed circuit dimensions. The effective realisation of such circuits depends upon the implementation of more compact delay lines and possibly the use of multi-dimensional circuit implementation such as MEMS and LTCC.

The research moved towards identifying areas where electronic signal processing could be employed as a complement to all-Optical CDMA networks. GVDiff-induced time skewing is an important impairment in multi-wavelength Optical CDMA networks and where the utilisation of simple analogue electronic signal processing to overcome it had never been addressed. In this work, a fully asynchronous (both chip and bit asynchronous) system was required to describe accurately the Optical CDMA network behaviour. The model proposed avoids the use of pure Monte-Carlo simulations because these are computationally inefficient and would lead to unrealistic simulation periods. Instead, we proved mathematically that the central limit theorem applies and an approximation could be used so that it is possible to predict the behaviour in regimes of low BER with a reasonable

number of simulation samples. Numerical results were obtained for Prime-Hop code and Bin code considering constant time skewing between wavelength channels and propagation in DSF fibre. Although the main goal of this model was to test the system with electrical post-detection compensation, some important conclusions of the impact of time skewing in the Optical CDMA system were derived. Namely, it was found that its impact on the autocorrelation peak is more significant than that on the cross-correlation function of the system. This information is important to assess the need for Optical CDMA codes that are more robust against the impact of time skewing in the cross-correlation characteristics of the code. It was concluded that time skewing is a serious impairment in WHTS Optical CDMA systems even when dispersion shifted fibre is employed. Therefore, flexible and low cost compensation schemes are required.

The second part of chapter 5 explores the compensation scheme for time skewing in Optical CDMA networks. Modifications on the previous model are described to accommodate the DTF model. Initial issues with optimisation convergence were solved using Genetic Algorithms to obtain the ideal filter coefficients. Results show very significant improvements in the system performance with BER improvements up to five orders of magnitude.

From the compensation results important conclusions about the practicability of such filter were derived:

1. This application does not require distributed transversal filters with more than four stages. In fact, results clearly showed that the flexibility provided by additional stages does not have any impact on the BER. This is an important conclusion because the fabrication of distributed transversal filters with a high number of stages is technologically challenging.

2. Provided that the transversal filter has (at least) four stages, results proved that there is no advantage in using devices with variable/tunable delays between stages. This is important as no distributed transversal filter with such characteristics has been built and the author believes that this is not achievable with current technology.

3. The efficacy of the post-detection compensation depends, apart from the amount of time skewing, on the number of simultaneous users in the network. In fact, results clearly indicated that the compensation is more efficient for network scenarios comprising a moderate number of users and high time skewing regime as opposed to scenarios where the number of users is high and the network is affected by moderate to high values of time skewing.

Chapter 6 provides experimental evidence of compensation of GVDiff-induced time skewing in multi-wavelength Optical CDMA networks using electronic post-detection signal processing. Results here presented are limited by the difficulties of using an error detector which prevents us from showing BER plots. An alternative method to show the detectability of the autocorrelation peak in presence of multi-access interference was used, specifically the use of auto-correlation intensity peak *to* the multi-access level ratio (P/M ratio). The system was first tested without compensation and the results are found to be very close to those of the model presented in the chapter 5 that comprised Gaussian input pulse and time skewing as the dominant source of system degradation. Results were shown for standard SMF propagation as well as for Dispersion Shifted Fibre.

The most important part of the chapter deals with compensation results. It is clearly proved that the detectability of the autocorrelation peak in the presence of multi-access interference can be improved by adjusting the coefficients of the

front-end distributed transversal filter. Significant improvements of the P/M ratio were achieved (up to 50%). Due to limitations in the experiemental setup, only a two user network was used. However, it is known that in a real network higher densities of cross-correlations result when higher number of users share the network. Therefore, we tuned the location of the cross-correlation function in the receiver so that conclusions may be extended for a high number of users (when the cross-correltion functions coincide) and a low number of users (when the cross-correlation functions do *not* coincide). Conclusions derived in chapter 5 were confirmed, namely that the efficacy of compensation is reduced as the number of interferes increases.

7.1 Suggestions for further Work

The areas of future research comprise practical and theoretical work that may be categorised in two main areas, as follows.

Generation and detection of CDMA signals for optical fibre applications

1. The practical assessment of the transversal filter structure proposed is essential for further research. In fact, simulations of circuits such as this (operating at microwave frequencies and relying on passive components) are very sensitive to the accuracy of the passive components modelling. Hence, building a prototype and measuring its performance would lead to a better understanding of the circuit behaviour and may well lead to improved designs.

2. The design of distributed transversal filters with switchable delays lines would be a major improvement to the structure presented in chapter 4. In fact, for

concept verification, the time-domain DTF encoder/decoder relies on fixed delays between stages. Ideally, these delays should be switchable to multiples of the chip time, so that the circuit could be tuned to encode/decode different CDMA codewords by simple adjustments. In this thesis, the possibility of using MEMS switches was mentioned, however in-depth analysis was not performed. An IC process that integrates MEMS switches with pHEMT devices would be ideal for this purpose but, to the author's knowledge, no such process is commercially available.

3. The large size occupied by the CDMA encoding/decoding Distributed Transversal Filter suggests that passive delay lines might not be the most appropriate form to implement the required delays. In fact, active delay lines have been proposed and implemented with much smaller areas per time delay than passive approaches. The main drawback is that the active delay lines are generally found to have reduced bandwidth when compared with passive ones. This area is worthy of further investigation, especially if appropriate technologies are available.

4. In order to obtain more compact and less expensive circuits, studies of the implementation of the design ideas described in this thesis in CMOS processes instead of Gallium Arsenide would be required. This requires CMOS processes that have the appropriate passive structures such as inductors, and are capable of operating in the 10s of GHz regime.

Compensation of time skewing in multi-wavelength Optical CDMA

1. The system analysis presented in this work was limited to distributed transversal filters with positive tap gains. As discussed in [100], controlling the polarity of the gains improves the flexibility in the definition of the receiver's transfer function. Note however, that the analysis of an Optical CDMA network with DTF comprising positive and negative gains would require very significant changes in the system model. Specifically, the assumption that the system threshold is equal to the amplitude of the autocorrelation peak would no longer be valid. In fact, the assumption that the Optical CDMA system is a positive system, implies that the Multi-Access Interference does not have a negative impact on the amplitude of the autocorrelation peak. This will no longer be the case if the DTF has negative gains because the MAI multiplied by a negative coefficient would result in a reduction of the value of the autocorrelation peak. It is worthwhile exploring this area by generating appropriate modelling techniques.

2. The experimental demonstration presented in chapter 6 was limited by several setup constraints. Improvements could include the use of more practical codes and testing the system with higher number of simultaneous active users. Perhaps more importantly, it would be essential to assess the system performance with a BER detector instead of measuring the detectability of the autocorrelation peak through P/C ratio improvement.

3. The design of Optical CDMA codes that take into account the effect of time skewing on the cross-correlation function may be an interesting area of research in the mathematics/information theory fields. This would re-

quire rigorous assessment of the cross-correlation functions of the system, so that the recommendation addressed in chapter 6 would be fulfilled. Unfortunately, these additional conditions outlined in the section 6.4.2 would inevitably reduce the cardinality of the codes and therefore the maximum number of the network subscribers would be reduced.

In summary, it is hoped that the work presented in this thesis will lead to good appreciation of the role that electronic circuits can play in this fast developing field and potentially new areas of associated research that may be developed.

Appendix A

Kullback-Leibler Divergence for Gaussian Approximation

The discussion in chapter 5 provides mathematical proof (following the Central Limit Theorem) that the probability density function (PDF) of the Multi-Access Interference may be approximated by a Gaussian distribution and that this approximation accuracy is improved as the number of simultaneous active users in the network increases. Comparing Prime-Hop and Bin codes, it was found that the Gaussian approximation fits better the later than the former, for a comparable number of users. These conclusions may be confirmed through observation of the histograms. However, all consideration and comments in chapter 5 were qualitative. This appendix describes an attempt to quantitatively assess the the "goodness" of the approximation and its improvement with the number of users. Results here presented were briefly referred to in [167].

Kullback-Leibler divergence was employed to test the accuracy of approximating the MAI PDF with a Gaussian distribution. Kullback-Leibler (KL) divergence is a statistical technique commonly used to measure the similarity between two

PDFs [175] [157]. In the present case, histograms with MAI values were constructed from the modelling results and these may be seen as step functions that will be named *f(x)*; the Gaussian approximation, with mean (μ) and standard deviation (σ) extracted from the modelling data, has the following expression:

$$g(x) = \frac{1}{\sigma\sqrt{2\pi}} \exp\left(-\frac{(x-\mu)^2}{2\sigma^2}\right). \tag{A.1}$$

By definition, Kullback-Leibler (KL) divergence is given by the expression:

$$D(f||g) = \int f(x) \log\frac{f(x)}{g(x)}\, dx \tag{A.2}$$

where *f(x)* is the MAI PDF and *g(x)* is its Gaussian approximation. $D(f||g) = 0$ only if $f = g$, otherwise it is a positive value and it increases as f(x) and g(x) diverge from each other.

Through modeling of various scenarios we found that for $D(f||g) < 0.2$, the final BER changes by less than an order of magnitude. This was done by considering two Gaussian distributions and then randomly change their mean values and standard deviations so that $D(f||g)$ always remains below 0.2. It was concluded that for the error rates regimes of interest (around 10^{-9}) the BER changes by less than an order of magnitude. Therefore, $D(f||g) = 0.2$ may be taken as an upper bound for what can be considered an acceptable approximation.

Figure A.1 shows the variation of the KL divergence with the number of simultaneous active users in the Optical CDMA system. The function f(x) was obtained with histograms of 50 steps. It is clear that KL divergence never exceeds 0.2, for the cases studied in this thesis. Moreover, both curves monotonically decrease with the increase in the number of active users, which means that the Gaussian

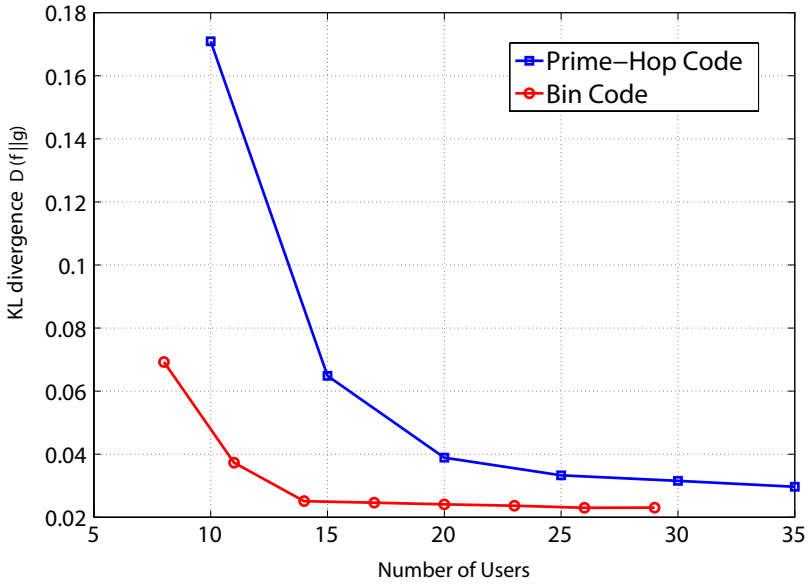

Figure A.1: Kullback-Leibler divergence values for Prime-Hop and Bin Code

approximation improves with the increase of the number of users in the network. Finally, it is confirmed that the Gaussian PDF provides a better approximation for Bin Code than for PH Code (for a comparable number of users), as it shows lower values of $D(f||g)$ for the same number of users.

Bibliography

[1] H. Fathallah, L. Rusch, and S. LaRochelle, "Passive optical fast frequency-hop CDMA communications system," *Journal of Ligthwave Technology*, vol. 17, no. 3, pp. 397–405, March 1999.

[2] V. Baby, I. Glesk, R. Runser, R. Fischer, Y.-K. Huang, C.-S. Bres, W. Kwong, T. Curtis, and P. Prucnal, "Experimental demonstration and scalability analysis of a four-node 102-Gchip/s fast frequency-hopping time-spreading optical CDMA network," *IEEE Photonics Technology Letters*, vol. 17, no. 1, pp. 253–255, Jan. 2005.

[3] J. Aguilar-Torrentera and I. Darwazeh, "Dual drain-line distributed cell design for multi-Gbit/s transversal filter implementations," in *IEEE International Symposium on Circuits and Systems ISCAS 2005.*, 23-26 May 2005, pp. 3958–3961.

[4] J. Aguilar-Torrentera, "Transversal Filter MMIC Design for Multi-Gbit/s Optical CDMA Systems," Ph.D. dissertation, University College London, 2004.

[5] P. Prucnal, *Optical Code Division Multiple Access: Fundamentals and Applications*, P. Prucnal, Ed. Taylor and Francis, 2005.

[6] C. Zuo, W. Ma, H. Pu, and J. Lin, "The impact of group velocity on frequency-hopping optical code division multiple access system," *Journal of Ligthwave Technology*, vol. 19, no. 10, pp. 1416–1419, Oct. 2001.

[7] X. Wang, "Keys towards practical OCDMA networks," in *Proc. PHOTONICS2004*, 2004.

[8] V. W. Fan Chung, Jawad Salehi, "Optical Orthogonal Codes: Design, Analysis and Applications," *IEEE Transactions on Information Theory*, vol. 35, pp. 595 – 604, 1989.

[9] C.-S. Bres, Y.-K. Huang, I. Glesk, and P. Prucnal, "Scalable asynchronous incoherent Optical CDMA," *Journal of Optical Networking*, vol. 6, pp. 599 – 615, June 2007.

[10] OMMIC, *ED02AH Design Manual*. Philips, 2005.

[11] H. Holma and A. Toskala, *WCDMA for UMTS: Radio Access for Third Generation Mobile Communications*, H. Holma, Ed. Wiley, 2001.

[12] P. Prucnal, M. Santoro, and T. R. Fan, "Spread Spectrum Fiber-Optic Local Area Netwrok Using Optical Processing," *Journal of Lightwave Technology*, vol. LT-4, pp. 547 – 554, 1986.

[13] J. Aguilar-Torrentera and I.Darwazeh, "A Transversal-Filter for High-Speed Fibre-Optic CDMA Receivers," in *Proc. of London Communication Symposium*, 2002.

[14] A. Viterbi, *CDMA: Principles of Spread Spectrum Communication*, A. Viterbi, Ed. Addison-Wesley, 1995.

[15] A. Stok and E. Sargent, "The Role of Optical CDMA in Access Networks," *IEEE Communications Magazine*, vol. September, pp. 83 – 87, 2002.

[16] T. Koonen, "Fiber to the Home/Fiber to the Premises: What, Where, and When?" *Proceedings of the IEEE*, vol. 94, no. 5, pp. 911–934, 2006.

[17] K. Fouli and M. Maier, "OCDMA and Optical Coding: Principles, Applications, and Challenges [Topics in Optical Communications]," *IEEE Communications Magazine*, vol. 45, no. 8, pp. 27–34, 2007.

[18] A. Stok and E. Sargent, "Lighting the local area: optical code-division multiple access and quality of service provisioning," *IEEE Network*, vol. 14, no. 6, pp. 42–46, 2000.

[19] R. Volner, "CATV-gateway between traditional video services and new multimedia applications," in *Proc. 22nd International Conference on Information Technology Interfaces ITI 2000*, 13–16 June 2000, pp. 253–260.

[20] A. M. Weiner, J. Heritage, and J. Salehi, "Encoding and Decoding of Femtosecond Pulses," *Optics Letters*, vol. 13, pp. 3000–3002, 1988.

[21] J. Shah, "Optical CDMA," *Optics and Photonics News*, vol. April, pp. 42 – 47, 1993.

[22] I. Sasase, "Optical code division multiple access," in *Proceedings of International Workshop on Optical and Electronic Device Technology for Access Network - Nano Photonics and Functional Device Technology*, 2005.

[23] J. Wu, F.-R. Gu, and H.-W. Tsao, "Jitter performance analysis of SOCDMA-based EPON using perfect difference codes," *Journal of Ligthwave Technology*, vol. 22, no. 5, pp. 1309–1319, 2004.

[24] H. Shalaby, "Synchronous fiber-optic CDMA systems with interference estimators," *Journal of Ligthwave Technology*, vol. 17, no. 11, pp. 2268–2275, 1999.

[25] H. Walle and U. Killat, "Combinatorial BER analysis of synchronous optical CDMA with prime sequences," *IEEE Transactions on Communications*, vol. 43, no. 12, pp. 2894–2895, 1995.

[26] M. Karbassian and H. Ghafouri-Shiraz, "Performance Analysis of Heterodyne-Detected Coherent Optical CDMA Using a Novel Prime Code Family," *Journal of Ligthwave Technology*, vol. 25, no. 10, pp. 3028–3034, 2007.

[27] J. Faucher, S. Ayotte, Z. A. El-Sahn, M. Y. Mukadam, L. A. Rusch, and D. V. Plant, "Receiver for 2D λ-t OCDMA with Quantizer, CDR and FEC," in *Proc. European Conference on Optical Communications ECOC 2006*, 2006, pp. 1–2.

[28] V. Baby, C.-S. Bres, L. Xu, I. Glesk, and P. Prucnal, "Demonstration of differentiated service provisioning with 4-node 253 Gchip/s fast frequency-hopping time-spreading OCDMA," *Electronics Letters*, vol. 40, no. 12, pp. 755–756, 2004.

[29] E. Inaty, P. Fortier, and L. Rusch, "SIR performance evaluation of a multirate OFFH-CDMA system," *IEEE Communication Letters*, vol. 5, no. 5, pp. 224–226, 2001.

[30] L. Tancevski, I. Andonovic, and J. Budin, "Secure Optical Network Architectures Utilizing Wavelength Hopping/Time Spreading Codes," *IEEE Photonics Technology Lettters*, vol. 7, pp. 573 – 575, 1995.

[31] S. Goldberg, R. C. Menendez, and P. R. Prucnal, "Towards a Cryptanalysis of Spectral-Phase Encoded Optical CDMA with Phase-Scrambling," in *Proc. Optical Fiber Conference OFC2007*, 2007.

[32] R. Scott, W. Cong, K. Li, V. Hernandez, B. Kolner, J. Heritage, and S. Yoo, "Demonstration of an error-free 4 &10 Gb/s multiuser SPECTS O-CDMA network testbed," *Photonics Technology Letters*, vol. 16, no. 9, pp. 2186–2188, Sept. 2004.

[33] Z. Jiang, D. Seo, S.-D. Yang, D. Leaird, R. Roussev, C. Langrock, M. Fejer, and A. Weiner, "Four-user, 2.5-Gb/s, spectrally coded OCDMA system demonstration using low-power nonlinear processing," *Journal of Ligthwave Technology*, vol. 23, no. 1, pp. 143–158, Jan. 2005.

[34] P. C. Teh, P. Petropoulos, M. Ibsen, and D. Richardson, "A comparative study of the performance of seven- and 63-chip optical code-division multiple-access encoders and decoders based on superstructured fiber Bragg gratings," *Journal of Ligthwave Technology*, vol. 19, no. 9, pp. 1352–1365, Sept. 2001.

[35] H. Sotobayashi, W. Chujo, and K. Kitayama, "1.6-b/s/Hz 6.4-Tb/s QPSK-OCDM/WDM (4 OCDM × 40 WDM × 40 Gb/s) transmission experiment using optical hard thresholding," *IEEE Photonics Technology Letters*, vol. 14, no. 4, pp. 555–557, April 2002.

[36] A. Mendez, J. Lambert, J.-M. Morookian, and R. Gagliardi, "Synthesis and demonstration of high speed, bandwidth efficient optical code division multiple access (CDMA) tested at 1 Gb/s throughput," *IEEE Photonics Technology Letters*, vol. 6, no. 9, pp. 1146–1149, 1994.

[37] Z. El-Sahn, M. Zeng, B. Shastri, N. Kheder, D. Plant, and L. Rusch, "Dual Architecture Uplink Demonstration of a 7622 Mbps SAC-OCDMA PON Using a Burst-Mode Receiver," in *Proc. Conference on Optical Fiber communication/National Fiber Optic Engineers Conference OFC/NFOEC 2008*, 2008, pp. 1–3.

[38] C.-S. Bres, I. Glesk, and P. Prucnal, "Demonstration of an eight-user 115-Gchip/s incoherent OCDMA system using supercontinuum generation and optical time gating," *IEEE Photonics Technology Letters*, vol. 18, no. 7, pp. 889–891, 2006.

[39] N. Kataoka, N. Wada, X. Wang, G. Cincotti, A. Sakamoto, Y. Terada, T. Miyazaki, and K. Kitayama, "Duplex, Fully-Asynchronous, 10Gbps x 8-User DPSK-OCDMA Field Trial Using a Multi-Port En/Decoder and SSFBG En/Decoders," in *Optical Fiber Communication Conference*, 2008.

[40] V. Hernandez, W. Cong, J. Hu, C. Yang, N. Fontaine, R. Scott, Z. Ding, B. Kolner, J. Heritage, and S. Yoo, "A 320-Gb/s Capacity (32-User x 10 Gb/s) SPECTS O-CDMA Network Testbed With Enhanced Spectral Efficiency Through Forward Error Correction," *Journal of Ligthwave Technology*, vol. 25, no. 1, pp. 79–86, 2007.

[41] M. Marhic, "Coherent Optical CDMA Networks," *Journal of Ligthwave Technology*, vol. 11, pp. 854 – 864, 1993.

[42] V. Hernandez, A. Mendez, C. Bennett, R. Gagliardi, and W. Lennon, "Bit-error-rate analysis of a 16-user gigabit ethernet optical-CDMA (O-CDMA) technology demonstrator using wavelength/time codes," *Photonics Technology Letters*, vol. 17, no. 12, pp. 2784–2786, Dec. 2005.

[43] Z. Jiang, D. Seo, S. Yang, D. Leaird, R. Roussev, C. Langrock, M. Fejer, and A. Weiner, "Four-user 10-Gb/s spectrally phase-coded O-CDMA system operating at 30 fJ/bit," *Photonics Technology Letters*, vol. 17, no. 3, pp. 705–707, March 2005.

[44] L. Kazovsky, S. Benedetto, and A. Willner, *Optical Fiber Communication Systems*, L. Kazovsky, Ed. Artech House, 1996.

[45] J. Salehi, "Code Division Multiple-Access Techniques in Optical Fiber Networks - Part I: Fundamental Principles," *IEEE Transactions on Communications*, vol. 37, pp. 824 – 833, 1989.

[46] R. Gold, "Optimal Binary Sequences for Spread Spectrum Multiplexing," *IEEE Transactions on Information Theory*, vol. 13, pp. 619–621, 1967.

[47] A. Holmes and R. Syms, "All-optical CDMA using 'quasi-prime' codes," *Journal of Ligthwave Technology*, vol. 10, no. 2, pp. 279–286, 1992.

[48] N. Karafolas and D. Uttamchandani, "Optical Code Division Multiple Access Netwroks: A Review," *Optical Fibre Technology*, vol. 2, pp. 149 – 186, 1996.

[49] S. Zahedi and J. Salehi, "Analytical comparison of various fiber-optic CDMA receiver structures," *Journal of Lightwave Technology*, vol. 18, no. 12, pp. 1718–1727, 2000.

[50] C. Iam, "To spread or not to spread: The myths of optical CDMA," in *IEEE Lasers and Electro-Optics Society Annual Meeting*, 2000, pp. 810–811.

[51] D. Zaccarin and M. Kavehrad, "An Optical CDMA System Based on Spectral Encoding of LED," *IEEE Photonics Technology Letters*, vol. 4, pp. 479 – 482, 1993.

[52] Z. Wei, H. Shalaby, and H. Ghafouti-Shiraz, "Modified Quadratic Congruence Codes for Fiber Bragg-Grating-Based Spectral-Amplitude-Coding Optical CDMA Systems," *Journal of Lightwave Technology*, vol. 19, pp. 1274 – 1281, 2001.

[53] S. Ayotte, M. Rochette, J. Magne, L. Rusch, and S. LaRochelle, "Experimental verification and capacity prediction of FE-OCDMA using superimposed FBG," *Journal of Ligthwave Technology*, vol. 23, no. 2, pp. 724–731, 2005.

[54] I. Djordjevic and B. Vasic, "Unipolar Codes for Spectral-Amplitude-Coding Optical CDMA Systems Based on Projective Geometries," *IEEE Photonics Technology Letters*, vol. 15, pp. 1318 – 1320, 2003.

[55] M. Kavehrad and D. Zaccarin, "Optical Code-Division-Multiplexed System Based on Spectral Encoding of Noncoherent Sources," *Journal of Lightwave Technology*, vol. 13, pp. 534 – 545, 1995.

[56] L. Tancevski and I. Andonovic, "Wavelength hopping/time spreading code division multiple acess systems," *Electronics Letters*, vol. 30, pp. 1388 – 1390, 1994.

[57] L. Bin, "One-Coincidence Sequences with Specified Distance Betwenn Adjacent Symbols for Frequency-Hopping Multiple Access," *IEEE Transactions on Communications*, vol. 45, pp. 408 – 410, 1997.

[58] A. Mendez, R. Gagliardi, V. Hernandez, C. Bennett, and W. Lennon, "Design and Performance Analysis of Wavelength/Time (W/T) Matriz Codes for Optical CDMA," *Journal of Ligthwave Technology*, vol. 21, pp. 2524 – 2533, 2003.

[59] E. Shivaleela, A. Selvarajan, and T. Srinivas, "Two-dimensional optical orthogonal codes for fiber-optic CDMA networks," *Journal of Ligthwave Technology*, vol. 23, no. 2, pp. 647–654, 2005.

[60] G.-C. Yang and W. C. Kwong, *Prime Codes with Applications to CDMA Optical and Wireless Networks*. Artech House, 2002.

[61] L. Tancevski and I. Andonovic, "Hybrid wavelength hopping/time spreading schemes for use in massive optical networks with increased security," *Journal of Lightwave Technology*, vol. 14, no. 12, pp. 2636–2647, 1996.

[62] J.-H. Wen, J.-Y. Lin, and C.-Y. Liu, "Modified prime-hop codes for optical CDMA systems," *IEE Proceedings-Communications*, vol. 150, no. 5, pp. 404–408, 2003.

[63] N. Wada, H. Sotobayashi, and K. Kitayama, "2.5 Gbit/s time-spread/wavelength-hop optical code division multiplexing using fibre Bragg grating with supercontinuum light source," *Electronics Letters*, vol. 36, no. 9, pp. 815–817, 2000.

[64] S. Lee and D. Green, "Performance analysis of optical orthogonal codes in CDMA LANs," *IEE Proceedings-Communications*, vol. 145, no. 4, pp. 265–271, 1998.

[65] H. Ben Jaafar, S. LaRochelle, P.-Y. Cortes, and H. Fathallah, "1.25 Gbit/s transmission of optical FFH-OCDMA signals over 80 km with 16 users," in *Proc. Optical Fiber Communication Conference and Exhibit OFC 2001*, vol. 2, 2001, pp. TuV3–.

[66] C.-K. Lee, J. Kim, and S.-W. Seo, "Generation and performance analysis of frequency-hopping optical orthogonal codes with arbitrary time blank patterns," in *Proc. IEEE International Conference on Communications ICC 2001*, J. Kim, Ed., vol. 4, 2001, pp. 1275–1279.

[67] M. Lequime, R. Parmentier, F. Lemarchand, and C. Amra, "Toward tunable thin-film filters for wavelength division multiplexing applications," *Applied Optics*, vol. 41, pp. 3277–3284, 2002.

[68] I. Glesk, V. Baby, C.-S. Bres, P. Prucnal, and W. Kwong, "A Design of a Wavelength-Hopping Time-Spreading Incoherent Optical Code Division Multiple Access System," *Acta Physica Slovaca*, vol. 55, pp. 211 – 227, 2005.

[69] K. Kravtsov, P. R. Prucnal, and M. M. Bubnov, "Simple nonlinear interferometer-based all-optical thresholder and its applications for optical CDMA," *Optics Express*, vol. 15, pp. 13 114–13 122, 2007.

[70] L. Xu, I. Glesk, V. Baby, and P. Prucnal, "Multiple access interference (MAI) noise reduction in a 2D optical CDMA system using ultrafast optical thresholding," in *Proc. 17th Annual Meeting of the IEEE Lasers and Electro-Optics Society LEOS 2004*, vol. 2, 7–11 Nov. 2004, pp. 591–592.

[71] T. Bazan, D. Harle, and I. Andonovic, "Performance analysis of 2-D time-wavelength OCDMA systems with coherent light sources: code design considerations," *Journal of Lightwave Technology*, vol. 24, no. 10, pp. 3583–3589, Oct. 2006.

[72] E. Ng, G. Weichenberg, and E. Sargent, "Dispersion in multiwavelength optical code-division multiple-access systems: impact and remedies," *IEEE Transactions on Communications*, vol. 50, no. 11, pp. 1811–1816, Nov. 2002.

[73] A. Sahin and A. Willner, "System limitations due to chromatic dispersion and receiver bandwidth for 2-D time-wavelength OCDMA systems," in *Proc. 16th Annual Meeting of the IEEE Lasers and Electro-Optics Society LEOS 2003*, A. Willner, Ed., vol. 2, 2003, pp. 551–552.

[74] W. Percival, "Improvements in and relating to thermionic valve circuits," *British Patent Specifications*, vol. 460, p. 562, 1936.

[75] R. Amaya, N. Tarr, and C. Plett, "A 27 GHz fully integrated CMOS distributed amplifier using coplanar waveguides," in *Proc. IEEE Radio Frequency Integrated Circuits (RFIC) Symposium*, 6–8 June 2004, pp. 193–196.

[76] M. A. M. Madureira, D. Fonseca, A. V. T. Cartaxo, R. L. Aguiar, and P. M. P. Monteiro, "Adjustable Electrical Dispersion Compensation in a 40-Gb/s Optical Single Sideband System," *Photonics Technology Letters*, vol. 18, no. 24, pp. 2689–2691, 2006.

[77] T. Wong, *Fundamentals of Distributed Amplification*, T. Wong, Ed. Artech House, 1993.

[78] D. M. Pozar, *Microwave Enginneering*, D. M. Pozar, Ed. John Wiley and Sons, 1998.

[79] A. Sedra and K. Smith, *Microelectronic Circuits*, A. Sedra, Ed. Oxford University Press, 1998.

[80] M. Golio, *Microwave MESFETs and HEMTs*, M. Golio, Ed. Artech House, 1991.

[81] S. Qureshi, "Adaptive Equalization," *IEEE Communications Magazine*, vol. March, pp. 9 – 16, 1982.

[82] A. Borjak, P. Monteiro, J. O'Reilly, and I. Darwazeh, "High-Speed Generalized Distributed-Amplifier Based Transversal-Filter Topology for Optical Communication Systems," *IEEE Transactions on Microwave Theory and Techniques*, vol. 45, pp. 1453 – 1457, 1997.

[83] Jutzi, "Microwave Bandwidth Active Transversal Filter Concept with MESFETs," *IEEE Transactions on Microwave Theory and Techniques*, vol. 19, pp. 760 – 767, 1971.

[84] C. Yuen, K. Laursen, D. Chu, and K. Mar, "50 GHz high output voltage distributed amplifiers for 40 Gb/s EO modulator driver application," in *Proc. IEEE MTT-S International Microwave Symposium Digest*, vol. 1, 2–7 June 2002, pp. 481–484.

[85] E. Kerherve, C. Moreira, P. Jarry, and L. Courcelle, "40-Gb/s wide-band MMIC pHEMT modulator driver amplifiers designed with the real frequency technique," *IEEE Transactions on Microwave Theory and Techniques*, vol. 53, no. 6, pp. 2145–2152, June 2005.

[86] I. Darwazeh, P. Moreira, A. Borjak, and J. O'Reilly, "A distributed optical receiver preamplifier with unequal gate/drain impedances," in *Microwave and Millimeter-Wave Monolithic Circuits Symposium, 1995. Digest of Papers., IEEE 1995*, 15-16 May 1995, pp. 199–202.

[87] B. Agarwal, A. Schmitz, J. Brown, M. Matloubian, M. Case, M. Le, M. Lui, and M. Rodwell, "112-GHz, 157-GHz, and 180-GHz InP HEMT traveling-wave amplifiers," *IEEE Transactions on Microwave Theory and Techniques*, vol. 46, no. 12, pp. 2553–2559, 1998.

[88] J.-D. Jin and S. Hsu, "A Miniaturized 70-GHz Broadband Amplifier in 0.13-μm CMOS Technology," *IEEE Journal on Microwave Theory and Techniques*, vol. 56, no. 12, pp. 3086–3092, 2008.

[89] C. Pelard, E. Gebara, A. Kim, M. Vrazel, F. Bien, Y. Hur, M. Maeng, S. Chandramouli, C. Chun, S. Bajekal, S. Ralph, B. Schmukler, V. Hietala, and J. Laskar, "Realization of multigigabit channel equalization and crosstalk cancellation integrated circuits," *IEEE Journal on Solid State Circuits*, vol. 39, no. 10, pp. 1659–1670, Oct. 2004.

[90] M. Madureira, D. Fonseca, R. Sousa, M. Violas, R. Aguiar, A. Cartaxo, and P. Monteiro, "Postdetection Adjustable Simultaneous Compensation of DGD and GVD in a 40-Gb/s Optical Single-Sideband System," *IEEE Photonics Technology Letters*, vol. 19, no. 18, pp. 1356–1358, 2007.

[91] M. Madureira, R. Aguiar, M. Violas, and P. Monteiro, "An electrically adjustable distributed pulse shaping filter for 40 Gbit/s optical links," in *Proc. IEEE International Symposium on Circuits and Systems ISCAS 2005*, vol. 2, 2005, pp. 1166–1169.

[92] J. Sewter and A. Carusone, "Electronic Equalization of Polarization-Mode Dispersion in 40-Gb/c Optical Systems," Master's thesis, University of Toronto, 2005.

[93] M. Nakamura, H. Nosaka, M. Ida, K. Kurishima, and M. Tokumitsu, "Electrical PMD equalizer ICs for a 40-Gbit/s transmission," in *Proc. Optical Fiber Communication Conference OFC 2004*, vol. 1, 23–27 Feb. 2004 2004.

[94] P. Pepeljugoski, J. Schaub, J. Tierno, J. Kash, S. Gowda, B. Wilson, H. Wu, and A. Hajimiri, "Improved performance of 10 Gb/s multimode fiber optic links using equalization," in *Proc. Optical Fiber Communications Conference OFC 2003*, 23–28 March 2003, pp. 472–474.

[95] M. Maeng, F. Bien, Y. Hur, H. Kim, S. Chandramouli, E. Gebara, and J. Laskar, "0.18 μm CMOS equalization techniques for 10-Gb/s fiber optical communication links," *IEEE Transaction of Microwave Threory and Techniques*, vol. 53, no. 11, pp. 3509–3519, 2005.

[96] P. Moreira, I. Darwazeh, and J. O'Reilly, "Distributed Amplifier Signal Shaping Strategy for Multigigabit Digital Optical Transmission," *Electronics Letters*, vol. 29, pp. 655 – 657, 1993.

[97] P. Monteiro, A. Borjak, F. da Rocha, J. O'Reilly, and I. Darwazeh, "Pulse shaping distributed based transversal filter for optical soliton system," in *26th European Microwave Conference*, vol. 1, Oct. 1996, pp. 409–412.

[98] P. Monteiro, A. Borjak, F. Rocha, J. O'Reilly, and I. Darwazeh, "10-Gb/s Pulse-Shaping Distributed-Based Transversal Filter for Optical Soliton Receivers," *IEEE Microwave and Guided Wave Letters*, vol. 8, pp. 4 – 6, 1998.

[99] Y. Jamani and A. Freundorfer, "An active transversal filter MMIC for very high speed lightwave systems," in *Proc. IEEE Antennas and Propagation Society International Symposium*, vol. 2, 13-18 July 1997, pp. 1232–1235.

[100] J. Lee and A. Freundorfer, "MMIC adaptive transversal filtering using Gilbert cells and is suitable for high-speed lightwave systems," *Photonics Technology Letters*, vol. 12, no. 2, pp. 196–198, Feb. 2000.

[101] A. Freundorfer, D. Choi, J. Lee, and Y. Jamani, "Electronic dispersion compensation ICs for high speed long haul lightwave systems," in *Canadian Conference on Electrical and Computer Engineering*, 1-4 May 2005, pp. 204–207.

[102] H. Wu, J. Tierno, P. Pepeljugoski, J. Schaub, S. Gowda, J. Kash, and A. Hajimiri, "Integrated transversal equalizers in high-speed fiber-optic systems," *IEEE Journal on Solid State Circuits*, vol. 38, no. 12, pp. 2131–2137, Dec 2003.

[103] ——, "Differential 4-tap and 7-tap transverse filters in SiGe for 10Gb/s multimode fiber optic link equalization," in *Proc. IEEE International Solid-State Circuits Conference ISSCC2003*, 2003, pp. 180–486.

[104] H. Kim, F. Bien, Y. Hur, S. Chandramouli, J. Cha, E. Gebara, and J. Laskar, "A 0.25 μm BiCMOS Feed Foward Equalizer Using Active Delay Line for Backplane Communication," in *Proc. IEEE International Symposium on Circuits and Systems ISCAS 2007*, 27–30 May 2007, pp. 193–196.

[105] A. Hazneci and S. Voinigescu, "49-Gb/s, 7-tap transversal filter in 0.18 μm SiGe BiCMOS for backplane equalization," in *Proc. IEEE Compound Semiconductor Integrated Circuit Symposium*, 24–27 Oct. 2004, pp. 101–104.

[106] J. Sewter and A. Carusone, "A 3-Tap FIR Filter With Cascaded Distributed Tap Amplifiers for Equalization Up to 40 Gb/s in 0.18 μm CMOS," *IEEE Journal on Solid State Circuits*, vol. 41, no. 8, pp. 1919–1929, 2006.

[107] ——, "A 40 Gb/s transversal filter in 0.18 μm CMOS using distributed amplifiers," in *Proc. IEEE Custom Integrated Circuits Conference*, 18–21 Sept. 2005, pp. 417–420.

[108] ——, "A CMOS finite impulse response filter with a crossover traveling wave topology for equalization up to 30 Gb/s," *IEEE Journal on Solid State Circuits*, vol. 41, no. 4, pp. 909–917, April 2006.

[109] P. Monteiro, M. Madureira, D. Fonseca, R. Aguiar, A. Cartaxo, R. Sousa, and M. Violas, "Optical Channel Impairments Mitigation on 40 Gb/s Systems Resorting to Post-Detection Adjustable Electrical Compensation," in *Proc. 9th International Conference on Transparent Optical Networks ICTON '07*, vol. 1, 1–5 July 2007, pp. 20–23.

[110] M. Madureira, D. Fonseca, P. Monteiro, A. Cartaxo, and R. Aguiar, "GVD and PMD Compensation Using a Linear Adjustable Filter Prototype in a 40 Gb/s OSSB System," in *Proc. IEEE International Symposium on Circuits and Systems ISCAS 2007*, 27–30 May 2007, pp. 1891–1894.

[111] G. Smith and D. Novak, "Broad-band millimeter-wave (38 GHz) fiber-wireless transmission system using electrical and optical SSB modulation to overcome dispersion effects," *IEEE Photonics Technology Letters*, vol. 10, no. 1, pp. 141–143, Jan. 1998.

[112] D. Fonseca, A. Cartaxo, and P. Monteiro, "Opto-electrical filter for 40 Gb/s optical single sideband signal generation," in *Proc. Optical Fiber Communication Conference OFC 2006*, 5–10 March 2006.

[113] P. Moreira, P. Lane, I. Darwazeh, and J. O'Reilly, "Time domain optimisation of high bit rate optical receivers," in *ASIC Conference and Exhibit, 1993. Proceedings., Sixth Annual IEEE International*, 27 Sept.-1 Oct. 1993, pp. 494–497.

[114] A. Borjak, L. Moura, J. O'Reilly, and I. Darwazeh, "Input noise current spectral density estimation for a distributed based optical receiver," in *Microwave Symposium Digest, 1997., IEEE MTT-S International*, vol. 3, 8-13 June 1997, pp. 1579–1582vol.3.

[115] M. Pimenta and I. Darwazeh, "Novel Encoder and Correlator for Optical Code Division Multiple Access Networks," in *Proc. IEEE Lasers and Electro-Optics Society Annual Meeting*, Oct. 2006, pp. 422–423.

[116] ——, "Electronic Processing for Generation and Detection of Multi GBit/s CDMA over fibre," in *Proc. 14th OptoElectronics and Communications Conference, Hong Kong*, 2009.

[117] S. Tamura, S. Nakano, and K. Okazaki, "Optical code-multiplex transmission by gold sequences," *Journal of Lightwave Technology*, vol. 3, pp. 121 – 127, February 1985.

[118] T.-W. Chang and E. Sargent, "Spectral efficiency limit of bipolar signaling in incoherent optical CDMA systems," in *Proc. IEEE Global Telecommunications Conference GLOBECOM '01*, vol. 3, 2001, pp. 1484–1486 vol.3.

[119] G. Gupta, M. Kashima, H. Iwamura, H. Tamai, T. Ushikubo, and T. Kamijoh, "Over 100km Bidirectional, Multi-channels COF-PON without Optical Amplifier," in *Proc. Optical Fiber Communication Conference OFC 2006*, 2006, pp. 1–3.

[120] ——, "A Simple One-System Solution COF-PON for Metro/Access Networks," *Journal of Lightwave Technology*, vol. 25, no. 1, pp. 193–200, 2007.

[121] H. Tamai, M. Sarashina, H. Iwamura, M. Kashima, G. Gupta, T. Ushikubo, T. Kamijoh, P. Chanclou, N. Genay, B. Landousies, A. Mosek, and M. Gredziak, "First Demonstration of Coexistence of Standard Gigabit TDM-PON and Code Division Multiplexed PON Architectures Toward Next Generation Access Network," *Journal of Lightwave Technology*, vol. 27, no. 3, pp. 292–298, 2009.

[122] H. Tamai, "Private communication," Oki Electric Industry Co., 2009.

[123] J. Rosas-Fernandez, J. Ingham, R. Penty, and I. White, "18 Gchips/s Electronic CDMA for Low-Cost Optical Access Networks," *Journal of Lightwave Technology*, vol. 27, no. 3, pp. 306–313, 2009.

[124] I. White, J. Ingham, J. Rosas-Fernandez, and R. Penty, "CDMA access networks using low-cost electronic techniques," in *Proc. 10th International Conference on Transparent Optical Networks ICTON 2008*, vol. 4, 2008, pp. 155–157.

[125] J. Rosas-Fernandez, J. Ingham, R. Penty, and I. White, "18 Gchips/s Error-Free OCDMA transmission with electronic processing for PON applications," in *Proc. 34th European Conference on Optical Communication ECOC 2008*, 2008.

[126] J. Ingham, "Private communication," University of Cambridge, 2009.

[127] Y. Ayasli, R. Mozzi, J. Vorhaus, L. Reynolds, and R. Pucel, "A monolithic GaAs 1 - 13-GHz traveling-wave amplifier," *IEEE Transactions on Microwave Theory and Techniques*, vol. 29, no. 7, pp. 1072–1077, Jul 1982.

[128] I. Robertson and S. Lucyszyn, *RFIC and MMIC design and technology*, I. Robertson, Ed. IEE, 2001.

[129] F. Ali, I. Bahl, and A. Gupta, *Microwave and Milimeter-Wave Heterostructure Transistors and Their Applications*, Norwood, Ed. Artech House, 1989.

[130] D. Pavlidis, "HBT vs. PHEMT vs. MESFET: What's best and why," in *Proc. International Conference on Compound Semiconductor Manufacturing Technology*, 1999.

[131] A. Iqbal and I. Z. Darwazeh, "A 23 GHz Baseband HBT Distributed Amplifier for Optical Communication Systems," in *Proc. 28th European Microwave Conference*, vol. 1, Oct. 1998, pp. 6–11.

[132] B. Razavi, *Design of Analog CMOS Integrated Circuits*. McGraw-Hill, 2001.

[133] Y. Ayasli, S. W. Miller, R. Mozzi, and H. L. K., "Capacitively Coupled Traveling-Wave Power Amplifier," *IEEE Transactions on Microwave Theory and Techniques*, vol. MTT-32, pp. 1704 – 1709, 1984.

[134] J. Pusl, B. Agarwal, R. Pullela, L. Nguyen, M. Le, M. Rodwell, L. Larson, J. Jensen, R. Yu, and M. Case, "Capacitive-division traveling-wave amplifier with 340 GHz gain/bandwidth product," in *Proc. IEEE Microwave and Millimeter-Wave Monolithic Circuits Symposium*, 1995, pp. 175–178.

[135] O. Siddiqui, S. Erickson, G. Eleftheriades, and M. Mojahedi, "Time-domain measurement of negative group delay in negative-refractive-index transmission-line metamaterials," *IEEE Transactions on Microwave Theory and Techniques*, vol. 52, no. 5, pp. 1449–1454, 2004.

[136] O. Siddiqui, M. Mojahedi, and G. Eleftheriades, "Periodically loaded transmission line with effective negative refractive index and negative group velocity," *IEEE Transactions on Antennas and Propagation*, vol. 51, no. 10, pp. 2619–2625, 2003.

[137] M. R. Brozel and G. E. Stillman, *Properties of Gallium Arsenide*. IEE Inspec, 1996.

[138] L. Moura, P. Monteiro, and I. Darwazeh, "Generalized noise analysis technique for four-port linear networks," *IEEE Transactions on Circuits and Systems I: Regular Papers*, vol. 52, no. 3, pp. 631–640, 2005.

[139] G. Wolf, S. Demichel, R. Leblanc, F. Blache, R. Lefevre, G. Dambrine, and H. Happy, "A metamorphic GaAs HEMT distributed amplifier with 50 GHz bandwidth and low noise for 40 Gbits/s optical receivers," in *Proc. European Gallium Arsenide and Other Semiconductor Application Symposium EGAAS 2005*, 2005, pp. 93–95.

[140] G. Keiser, *Optical Fiber Communications*, M.-H. I. Editions, Ed. Keiser, Gerd, 2000.

[141] R. Mihalovich, M. Kim, J. Hacker, A. Sovero, J. Stunder, J. Higgins, and J. DeNatale, "MEM Relay for Reconfigurable RF Circuits," *IEEE Microwave and Wireless Componets Letters*, vol. 11, pp. 53 – 55, February 2001.

[142] M. Kim, J. Hacker, R. Mihailovich, and J. DeNatale, "A DC-to-40 GHz four-bit RF MEMS true-time delay network," *IEEE Microwave Wireless Components Letters*, vol. 11, no. 2, pp. 56–58, 2001.

[143] J. Hacker, M. Kim, R. Mihailovich, and J. DeNatale, "Monolithic GaAs PHEMT MMICs integrated with RF MEMS switches," in *Proc. IEEE Compound Semiconductor Integrated Circuit Symposium*, 2004, pp. 229–232.

[144] E. Sovero, R. Mihailovich, D. Deakin, J. Higgins, J. Yao, J. DeNatale, and J. Hong, "Monolithic GaAs PHEMT MMICs integrated with high performance MEMS microrelays," in *Proc. International Microwave and Optoelectronics Conference IMOC'99*, vol. 1, 1999, pp. 257–260 vol. 1.

[145] M. Pimenta and I. Darwazeh, "Distributed Transversal Filter for Encoding and Decoding unipolar CDMA signals," in *Proc. Digest of the London Communications Symposium*, 2006.

[146] ——, "Circuit Design Proposal for Multi-Gbit/s CDMA over Fibre using Distributed Topologies," in *Proc. of the 9th International Symposium on Communications and Information Technology*, 2009.

[147] ——, "Optical fibre CDMA for access and optical networks," in *Proc. 6th International Conference on Information, Communications & Signal Processing*, 2007, pp. 1–4.

[148] ——, "System and Circuit Design for Time-Wavelength Optical CDMA Networks," in *Proc. 9th International Conference on Transparent Optical Networks ICTON '07*, vol. 1, 2007, pp. 126–126.

[149] ——, "Electronic signal processing for Optical Code Division Multiple Access Networks," in *Proc. 6th International Symposium on Communication Systems, Networks and Digital Signal Processing CNSDSP 2008*, 2008, pp. 740–742.

[150] H. Jantunen, T. Kangasvieri, J. Vhkangas, and S. Leppvuori, "Design aspects of microwave components with LTCC technique," *Journal of the European Ceramic Society*, vol. 23, pp. 2541–2548, 2003.

[151] G. Agrawal, *Fiber-Optic Communication Systems*, K. Chang, Ed. John Wiley and Sons, 1997.

[152] K. Takiguchi, S. Kawanishi, H. Takara, A. Himeno, and K. Hattori, "Dispersion slope equalizer for dispersion shifted fiber using a lattice-form programmable optical filter on a planar lightwave circuit," *Journal of Ligthwave Technology*, vol. 16, no. 9, pp. 1647–1656, Sept. 1998.

[153] M. Loeb and J. Stilwell, G.R., "High-speed data transmission on an optical fiber using a byte-wide WDM system," *Journal of Lightwave Technology*, vol. 6, no. 8, pp. 1306–1311, Aug. 1988.

[154] M. Vieira Segatto, R. Kashyap, G. Maxwell, J. Taylor, V. Bhagavatula, G. Berkey, and A. Evans, "Multi Gbit/s bit parallel WDM transmission using dispersion managed fibers," *IEEE Photonics Technology Lettters*, vol. 12, no. 8, pp. 995–997, 2000.

[155] S. Mashhadi and J. Salehi, "Optimum code structures for positive optical CDMA using normalized divergence maximization criterion," *IEEE Journal on Communications*, vol. 56, no. 9, pp. 1414–1421, 2008.

[156] L. Tancevski, I. Andonovic, M. Tur, and J. Budin, "Hybrid wavelength hopping/time spreading code division multiple access systems," *IEE Proceedings -Optoelectronics*, vol. 143, no. 3, pp. 161–166, 1996.

[157] D. Mackay, *Information Theory, Inference and Learning Algorithms*. Cambridge University Press, 2005.

[158] D. Shea and J. Mitchell, "A 10-Gb/s 1024-Way-Split 100-km Long-Reach Optical-Access Network," *Journal of Ligthwave Technology*, vol. 25, no. 3, pp. 685–693, 2007.

[159] R. Lus, A. Teixeira, and P. Monteiro, "Design of optical filter for increased efficiency of wavelength converters based on fiber XPM," *Optics Communications*, vol. 271, pp. 100 – 104, 2006.

[160] S. Pavan, "Continuous-time integrated FIR filters at microwave frequencies," *IEEE Transactions on Circuits and Systems II: Express Briefs*, vol. 51, no. 1, pp. 15–20, 2004.

[161] S. Pavan and S. Shivappa, "Analysis of traveling wave and transversal analog adaptive equalizers," in *Proc. IEEE International Symposium on Circuits and Systems ISCAS 2005*, vol. 6, 2005, pp. 5962–5965.

[162] J. Lagarias, J. Reeds, M. Wright, and P. Wright, "Convergence Properties of the Nelder-Mead Simplex Method in Low Dimensions," *SIAM Journal of Optimization*, vol. 9, p. 112147, 1998.

[163] K. I. M. Mckinnon, "Convergence of the Nelder-Mead simplex method to a nonstationary point," *SIAM Journal on Optimization*, vol. 9, p. 148158, 1998.

[164] M. Mitchell, *An Introduction to Genetic Algorithms*, M. Mitchell, Ed. MIT Press, 1998.

[165] E. Ng and E. Sargent, "Optimum threshold detection in real-time scalable high-speed multi-wavelength optical code-division multiple-access LANs," *IEEE Journal on Communications*, vol. 50, no. 5, pp. 778–784, 2002.

[166] M. Pimenta and I. Darwazeh, "Mitigation of Group Velocity Dispersion in optical CDMA networks using electronics," in *Proc. Digest of the IEEE/LEOS Summer Topical Meetings*, 2008, pp. 157–158.

[167] ——, "Performance Modeling of Optical Code Division Multiple Access Networks Impaired by Group Velocity Dispersion," in *Proc. IEEE Global Telecommunications Conference IEEE GLOBECOM 2008*, 2008, pp. 1–5.

[168] ——, "Distributed Transversal Filters for GVD Compensation in Multi-Wavelength Optical CDMA Networks," in *Proc. of the London Communications Symposium*, 2009.

[169] A. Mendez, R. Gagliardi, V. Hernandez, C. Bennett, and W. Lennon, "High-performance optical CDMA system based on 2-D optical orthogonal codes," *Journal of Ligthwave Technology*, vol. 22, no. 11, pp. 2409–2419, 2004.

[170] C.-C. Yang, J.-F. Huang, and Y.-H. Wang, "Comments on "Design and Performance Analysis of Wavelength/Time (W/T) Matrix Codes for Optical CDMA," *Journal of Lightwave Technology*, vol. 25, no. 10, pp. 3210–3210, 2007.

[171] A. Mendez and R. Gagliardi, "Combined effectiveness of optical hard-limiting and guard-time in optical CDMA systems," in *Proc. 15th Annual Meeting of the IEEE Lasers and Electro-Optics Society LEOS 2002*, vol. 2, 2002, pp. 857–858 vol.2.

[172] M. Rad, L. Rusch, and J.-Y. Chouinard, "Source Matching in Optical CDMA in the Presence of Multiple Access Interference and Phase-Induced Intensity Noise," in *Proc. 10th Canadian Workshop on Information Theory CWIT '07*, 2007, pp. 176–179.

[173] S. Ayotte and L. Rusch, "Experimental comparison of coherent versus incoherent sources in a four-user λ-t OCDMA system at 1.25 Gb/s," *IEEE Photonics Technology Letters*, vol. 17, no. 11, pp. 2493–2495, 2005.

[174] M. Pimenta and I. Darwazeh, "Experimental Demonstration of Electronic Compensation in Optical CDMA Networks," in *Proc. Digest of the IEEE/LEOS Summer Topical Meetings*, 2009.

[175] J. Hershey and P. Olsen, "Approximating the Kullback Leibler Divergence Between Gaussian Mixture Models," in *Proc. IEEE International Conference on Acoustics, Speech and Signal Processing ICASSP 2007*, vol. 4, 2007, pp. 317 – 320.